Appendix A

Periodic functions and their spectra

A.1 Introduction

According to the Fourier theory, any periodic function (which satisfies certain conditions; see Sec. C.12 in Appendix C) can be represented by means of a Fourier series, and moreover, its Fourier series expansion is *unique*. In this appendix we briefly review periodic functions in one or two variables, along with their Fourier series expansions and their spectral representations. The main purpose of this appendix is to put together, using our own nomenclature, the main results that we need about periodic functions and their spectra, results which are normally scattered in literature among several different domains. Some of these results can be found in standard mathematic textbooks, while others are treated in textbooks on optics or crystallography (see the cited references). Some aspects of our approach are, however, original (notably Sec. A.6).

It should be emphasized here that the Fourier series expansion of a periodic function $p(x)$ is just an alternative representation of that function in the image domain. The importance of this representation is in that it explicitly gives the spectral decomposition of $p(x)$, i.e., the frequencies and the amplitudes of the impulses which make up the spectrum of $p(x)$. The Fourier series expansion of a periodic function will serve us therefore as a link between the original function $p(x)$ in the image domain and its spectrum $P(u)$ in the frequency domain.

A.2 Periodic functions, their Fourier series and their spectra in the 1D case

A function $p(x)$ is called *periodic* if there exists a number $T \neq 0$ such that for all $x \in \mathbb{R}$:

$$p(x+T) = p(x)$$

The number T is called a *period* of the function $p(x)$; note however that T is not unique, since if T is a period of $p(x)$, so is nT for any integer n. The smallest period $T > 0$ is called the *fundamental period* of $p(x)$, and its reciprocal value, $f = 1/T$, is called the *fundamental frequency* of $p(x)$.[1] Note that the set of all periods of $p(x)$, i.e., the set of all integer multiples of the fundamental period of $p(x)$, forms a lattice in $\mathbb{R}$: $L_T = \{nT \mid n \in \mathbb{Z}\}$, whose basis is the fundamental period of $p(x)$.[2] Similarly, the set of all integer multiples of the fundamental frequency, i.e., all the harmonics of f, forms a lattice in the spectral domain:

---

[1] When no risk of confusion arises it is customary to omit the word "fundamental", and to use the terms *period* and *frequency* of $p(x)$ as abbreviations for the *fundamental period* and the *fundamental frequency* of $p(x)$.

[2] For the definition of a lattice, see Sec. 5.2.

$L_f = \{nf \mid n \in \mathbb{Z}\} = \{n/T \mid n \in \mathbb{Z}\}$, whose basis is the fundamental frequency of $p(x)$. As we will see later in this section, L_f is the support of the spectrum of $p(x)$ in the frequency domain. We will also see below (in Sec. A.4) that the lattices L_T in the image domain and L_f in the frequency domain are said to be *reciprocal*; note, however, that the only member of L_T whose reciprocal value is found in L_f is the fundamental period itself. (For instance, although $2T$ is a period of $p(x)$, there is no corresponding reciprocal frequency $\frac{1}{2T} = \frac{f}{2}$ in L_f).

Suppose that $p(x)$ is a periodic function of period T which satisfies the required convergence conditions (see Sec. C.12 in Appendix C). Then $p(x)$ can be expanded (or *developed*, or *decomposed*) into the form of a Fourier series, i.e., an infinite series of weighted cosine and sine functions at the fundamental frequency $f = 1/T$ and its harmonics $nf = n/T$ [Bracewell86 p. 205]:[3]

$$p(x) = a_0 + 2\sum_{n=1}^{\infty} a_n \cos(2\pi nx/T) + 2\sum_{n=1}^{\infty} b_n \sin(2\pi nx/T) \tag{A.1}$$

where the weighting coefficients a_n and b_n, which are called the *Fourier series coefficients* of $p(x)$, are real numbers given by:[4]

$$a_n = \frac{1}{T}\int_T p(x) \cos(2\pi nx/T)\, dx \qquad b_n = \frac{1}{T}\int_T p(x) \sin(2\pi nx/T)\, dx \tag{A.2}$$

$\int_T$ means here that the integration may be done over any full period of $p(x)$, i.e., from x_0 to x_0+T where x_0 is arbitrary; depending on the case it may be more convenient to integrate between 0...T, between $-T/2$...$T/2$, etc.

We notice from (A.2) that for negative n we have:

$$a_{-n} = a_n, \qquad b_{-n} = -b_n \qquad (n = 1,2,\ldots)$$

and $b_0 = 0$. Therefore the Fourier series of $p(x)$ can be rewritten as a two-sided series, in a *symmetric* way, as follows (putting also $f = 1/T$):

$$p(x) = \sum_{n=-\infty}^{\infty} a_n \cos(2\pi nfx) + \sum_{n=-\infty}^{\infty} b_n \sin(2\pi nfx) \tag{A.3}$$

with:
$$a_n = \frac{1}{T}\int_T p(x) \cos(2\pi nfx)\, dx \qquad b_n = \frac{1}{T}\int_T p(x) \sin(2\pi nfx)\, dx \tag{A.4}$$

Note that if $p(x)$ is symmetric about the origin there are no sine components, and $b_n = 0$ for all n.

However, although in Chapter 2 we adopt, for didactic reasons, this trigonometric form of the Fourier series, in more advanced chapters we will usually prefer the *exponential* (or

---

[3] Note that depending on $p(x)$ some or even most of the weighting coefficients a_n and b_n may be zero, so that the Fourier series expansion may include only a finite number of non-zero terms; a trivial example of this type is the function $p(x) = \cos(2\pi x/T)$.

[4] Note that in most textbooks the factors 2 appear within the Fourier coefficients a_n and b_n. We prefer, however, to put them before the summations in (A.1), in order to emphasize the correspondence between the Fourier series coefficients and the impulse amplitudes of the two-sided comb which extends to both directions in the spectrum.

complex) notation [Champeney73, p. 2], which is more compact and lends itself more easily to mathematical manipulations. This form is obtained from (A.3) and (A.4) by expressing the cosines and sines using the Euler identities: $2\cos\vartheta = e^{i\vartheta} + e^{-i\vartheta}$ and $2\sin\vartheta = -i(e^{i\vartheta} - e^{-i\vartheta})$, grouping the terms $e^{i2\pi nfx}$ and $e^{-i2\pi nfx}$ separately, and combining them into a single series. In the exponential notation the Fourier series expansion of $p(x)$ becomes:

$$p(x) = \sum_{n=-\infty}^{\infty} c_n \, e^{i2\pi nfx} \tag{A.5}$$

where the n-th Fourier series coefficient c_n is given (as a single complex number instead of a pair of real numbers a_n, b_n as in (A.4)) by:

$$c_n = \frac{1}{T}\int_T p(x) \, e^{-i2\pi nfx} \, dx \tag{A.6}$$

Note that the trigonometric and the exponential forms of the Fourier series are equivalent; by comparing expressions (A.5), (A.6) with expressions (A.3), (A.4) the following relations between their coefficients are obtained:

$$\begin{aligned} &c_0 = a_0 \\ &c_n = a_n - ib_n, \qquad c_{-n} = a_n + ib_n \qquad (n \geq 1) \\ &2a_n = (c_n + c_{-n}), \qquad 2b_n = i(c_n - c_{-n}) \qquad (n \geq 1) \end{aligned} \tag{A.7}$$

(see, for example, [Champeney73 p. 3], with the required adaptations to our notation conventions).

As already mentioned in Sec. A.1, the representation of a periodic function $p(x)$ in the form of its Fourier series expansion will serve us as a link between the original function $p(x)$ and its spectrum, $P(u)$. This is based on the fact that the Fourier transform (the spectrum) of $g(x) = e^{i2\pi fx}$ is $G(u) = \delta(u-f)$, namely: an impulse at the frequency f [Bracewell86 p. 101]. Consequently, the spectrum of each term in the Fourier series (A.5) consists of a single impulse at the frequency of nf, whose amplitude (real or complex) is given by the corresponding Fourier coefficient. It follows therefore (under the appropriate convergence conditions) that the spectrum $P(u)$ of the periodic function $p(x)$ is an impulse-comb of step f, whose n-th impulse is located at the frequency $u = nf$ and has the amplitude c_n. The general form of the spectrum of a periodic function $p(x)$ with period $T = 1/f$ is, therefore [Papoulis68 p. 107]:

$$P(u) = \sum_{n=-\infty}^{\infty} c_n \, \delta(u - n/T) = \sum_{n=-\infty}^{\infty} c_n \, \delta(u - nf) \tag{A.8}$$

where $\delta(u)$ is the impulse symbol (see Chapter 5 in [Bracewell86]). As we can see, the support of this spectrum is the lattice L_f, which contains all the integer multiples of the fundamental frequency f. Moreover, the converse is also true: given a spectrum $P(u)$ whose support is a lattice L_f, it follows that the original function $p(x)$ in the image domain, which can be represented by (A.5), is periodic with period $T = 1/f$ (of course, this is only meaningful if the convergence conditions on the Fourier series (A.5) are satisfied). We have, therefore, the following result, under the appropriate convergence conditions:

Proposition A.1: A function $p(x)$ in the image domain is periodic *iff* its spectrum support in the frequency domain is a lattice. ■

Finally, note that since we restrict ourselves to *real* functions $p(x)$ in the image domain, it follows from Eq. (A.7) that c_{-n} is the complex conjugate of c_n, namely: $\mathrm{Re}(c_{-n}) = \mathrm{Re}(c_n)$ and $\mathrm{Im}(c_{-n}) = -\mathrm{Im}(c_n)$. This means that our impulse-comb in the spectrum is always *Hermitian*: its real part is symmetric while its imaginary part is antisymmetric. This is also in agreement with the properties of Fourier transforms of real functions; see [Bracewell86 pp. 14–15]. Note also that depending on $p(x)$ some or even most of the comb impulses may have amplitudes $c_n = 0$, as in the case of $p(x) = \cos(2\pi fx)$, where only the fundamental impulse pair, with indices $n = \pm 1$, has a non-zero amplitude.

A.3 Periodic functions, their Fourier series and their spectra in the 2D case

The case of periodic functions with two variables is more diversified than the 1D case, and it can be divided into 4 subcases. A periodic function $p(x,y)$ may be either 1-fold periodic[5] (like a grating or a cosine over the plane) or 2-fold periodic (such as a dot-screen); and in each of these cases it may be periodic either in the direction of the main axes, or in any other direction. In the following subsections we briefly review each of these 4 subcases. The most general case of 2D periodicity is reviewed last, in Sec. A.3.4.

A.3.1 1-fold periodic functions in the *x* or *y* direction

The simplest case of 2D periodic functions is that of a 1-fold periodic function $p(x,y)$ whose fundamental period (smallest period>0) is in the direction of one of the axes, say, in the x direction. In this case $p(x,y)$ can be considered as a 1D periodic function $p(x)$, since it is constant in the y direction, and its Fourier series expansion is identical to (A.5). The 2D spectrum of $p(x,y)$ consists in this case of a 1D impulse-comb, identical to the spectrum (A.8) of the 1D function $p(x)$, which is located in the u,v plane on top of the u axis.

A.3.2 2-fold periodic functions in the *x* and *y* directions

Let us proceed now to the case of a 2-fold periodic function $p(x,y)$ which is periodic in the x and in the y directions with periods T_x and T_y, namely: $p(x+T_x,y) = p(x,y)$ and $p(x,y+T_y) = p(x,y)$ for all $(x,y) \in \mathbb{R}^2$. If $p(x,y)$ satisfies certain convergence conditions (see Sec. C.12 in Appendix C), then it can be expanded into a 2D Fourier series as follows:

$$p(x,y) = \sum_{m=-\infty}^{\infty} \sum_{n=-\infty}^{\infty} a_{m,n} \cos 2\pi(mx/T_x + ny/T_y) + \sum_{m=-\infty}^{\infty} \sum_{n=-\infty}^{\infty} b_{m,n} \sin 2\pi(mx/T_x + ny/T_y) \quad \text{(A.9)}$$

[5] By the term *1-fold periodic* we understand that the function $p(x,y)$ is *constant* in the direction perpendicular to the direction of periodicity. Otherwise the Fourier development of $p(x,y)$ is no longer a pure 1D Fourier series, and it may even be a hybrid case having Fourier series in one direction and Fourier transform in the other [Korn68 p. 143].

where:
$$a_{m,n} = \frac{1}{T_x T_y}\iint_{T_x T_y} p(x,y)\cos 2\pi(mx/T_x + ny/T_y)\,dxdy$$
$$b_{m,n} = \frac{1}{T_x T_y}\iint_{T_x T_y} p(x,y)\sin 2\pi(mx/T_x + ny/T_y)\,dxdy \qquad (A.10)$$

$\iint_{T_x T_y}$ means an integration over any full period of $p(x,y)$, i.e., over a rectangle of sides T_x and T_y defined by the points (x_0,y_0), (x_0+T_x,y_0), (x_0,y_0+T_y) and (x_0+T_x,y_0+T_y) where x_0 and y_0 are arbitrary. Clearly, this is a 2D extension of the 1D trigonometric expressions (A.3) and (A.4). Note that here, too, if $p(x,y)$ is symmetric about the origin then there are no sine components, and $b_{m,n} = 0$ for all m,n.

However, for the sake of convenience and conciseness we will adopt here, too, as in the 1D case, the exponential form of the Fourier series, which is obtained from the trigonometric form by the Euler identities. In the exponential notation the 2D Fourier series expansions of $p(x,y)$ becomes (using also $u_0 = 1/T_x$ and $v_0 = 1/T_y$):

$$p(x,y) = \sum_{m=-\infty}^{\infty}\sum_{n=-\infty}^{\infty} c_{m,n}\, e^{i2\pi(mu_0 x + nv_0 y)} \qquad (A.11)$$

where the Fourier coefficients $c_{m,n}$ are given by:

$$c_{m,n} = \frac{1}{T_x T_y}\iint_{T_x T_y} p(x,y)\, e^{-i2\pi(mu_0 x + nv_0 y)}\,dxdy \qquad (A.12)$$

Expressions (A.11) and (A.12) are clearly 2D extensions of (A.5) and (A.6). These 2D expressions can be rendered more compact by using the vector notation:

$$p(\mathbf{x}) = \sum_{m=-\infty}^{\infty}\sum_{n=-\infty}^{\infty} c_{m,n}\, e^{i2\pi \mathbf{f}_{m,n}\cdot\mathbf{x}} \qquad (A.13)$$

with the Fourier series coefficients:

$$c_{m,n} = \frac{1}{T_x T_y}\iint_{T_x T_y} p(\mathbf{x})\, e^{-i2\pi \mathbf{f}_{m,n}\cdot\mathbf{x}}\,d\mathbf{x} \qquad (A.14)$$

where $\mathbf{x} = (x,y)$, $\mathbf{f}_{m,n} = (mu_0,nv_0)$ is the (m,n)-th frequency harmonic, and $\mathbf{f}_{m,n}\cdot\mathbf{x}$ denotes the scalar product of the vectors $\mathbf{f}_{m,n}$ and $\mathbf{x}$. Note that an even more compact notation can be obtained by substituting $\mathbf{n}$ for (m,n) in the indices:

$$p(\mathbf{x}) = \sum_{\mathbf{n}} c_{\mathbf{n}}\, e^{i2\pi \mathbf{f}_{\mathbf{n}}\cdot\mathbf{x}} \qquad (A.15)$$

However, for the sake of clarity we will usually prefer the more explicit form of (A.13).

Like in the 1D case, the spectrum of the 2-fold periodic function $p(x,y)$ is readily obtained from the Fourier series representation of $p(x,y)$, (A.11): it is an impulse-nailbed, whose (m,n)-th impulse is located in the u,v plane at the point $\mathbf{f}_{m,n} = (mu_0,nv_0)$ and has the amplitude $c_{m,n}$ (see Fig. 2.12(f)). Using the 2D impulse symbol $\delta(u,v)$ the spectrum of $p(x,y)$ is, therefore [Papoulis68 p. 114]:

$$P(u,v) = \sum_{m=-\infty}^{\infty}\sum_{n=-\infty}^{\infty} c_{m,n}\,\delta(u-mu_0, v-nv_0) \qquad (A.16)$$

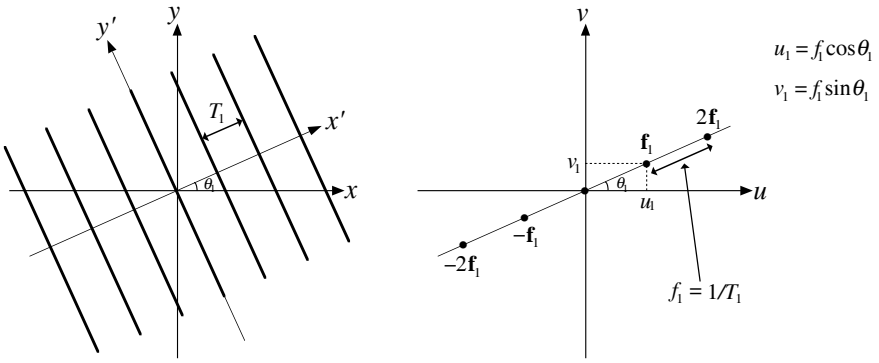

(a) (b)

Figure A.1: A schematic plot of the 1-fold periodic function $p_1(x,y)$ in the image domain (a), and its impulse-comb in the spectral domain (b).

or in a vector form, where $\mathbf{f} = (u,v)$ and $\mathbf{f}_{m,n} = (mu_0, nv_0)$:

$$P(\mathbf{f}) = \sum_{m=-\infty}^{\infty} \sum_{n=-\infty}^{\infty} c_{m,n}\, \delta(\mathbf{f} - \mathbf{f}_{m,n}) \tag{A.17}$$

This means that the support of the spectrum of $p(x,y)$ is the 2D lattice, oriented in the axes directions, which is spanned by the fundamental frequencies $\mathbf{f}_{1,0} = (u_0,0)$ and $\mathbf{f}_{0,1} = (0,v_0)$. Moreover, like in the 1D case we have the following result (under the appropriate convergence conditions):

Proposition A.2: A function $p(x,y)$ in the image domain is periodic in the x and y directions *iff* its spectrum support in the frequency domain is a 2D lattice in the axes directions. ■

A.3.3 1-fold periodic functions in an arbitrary direction

Unlike in the 1D case, in functions of two variables periodicity is not necessarily limited to the direction of the main axes. Let us consider first the case of a 1-fold periodic function, $p_1(x,y)$, whose fundamental period (i.e., smallest period > 0) is $T_1 = 1/f_1$ in the direction θ_1 (for example: a rotated grating). This is, in fact, a function of the single variable x' in the rotated coordinate system x',y', and along the y' direction it is constant (see Fig. A.1). Therefore its Fourier series expansion is given in the rotated coordinate system x',y' by expressions (A.5) and (A.6) of the 1D case:

$$p_1(x',y') = \sum_{n=-\infty}^{\infty} c_n\, e^{i2\pi n f_1 x'} \qquad \text{where:} \qquad c_n = \frac{1}{T_1}\int_{T_1} p_1(x',y')\, e^{-i2\pi n f_1 x'}\, dx' \tag{A.18}$$

Changing back to the x,y coordinate system by putting: $x' = x\cos\theta_1 + y\sin\theta_1$ [Spiegel68 p. 36] and hence: $f_1 x' = u_1 x + v_1 y$ (see Fig. A.1(b)) we obtain:

$$p_1(x,y) = \sum_{n=-\infty}^{\infty} c_n \, e^{i2\pi n(u_1 x + v_1 y)} \tag{A.19}$$

Note that (u_1,v_1) are the Cartesian coordinates, in the u,v plane, of the *frequency vector* $\mathbf{f}_1$ in the spectrum of $p_1(x,y)$, whose polar coordinates are (f_1,θ_1). Therefore the expression $(u_1x + v_1y)$ in the exponential part of (A.19) can be rewritten in a more compact vector form as the scalar product $\mathbf{f}_1 \cdot \mathbf{x}$ of the two vectors $\mathbf{f}_1 = (u_1,v_1)$ and $\mathbf{x} = (x,y)$, and the Fourier series becomes:

$$p_1(\mathbf{x}) = \sum_{n=-\infty}^{\infty} c_n \, e^{i2\pi n \mathbf{f}_1 \cdot \mathbf{x}} \tag{A.20}$$

The 2D spectrum of $p_1(x,y)$ consists of a 1D impulse-comb, identical to the comb (A.8) of the 1D case, which is rotated in the u,v plane by the angle of θ_1. Using the 2D impulse symbol $\delta(u,v)$ the spectrum of $p_1(x,y)$ is given by (see Fig. A.1(b)):

$$P_1(u,v) = \sum_{n=-\infty}^{\infty} c_n \, \delta(u - nu_1, v - nv_1) \tag{A.21}$$

or in a vector form, where $\mathbf{f} = (u,v)$ and $\mathbf{f}_1 = (u_1,v_1)$:

$$P_1(\mathbf{f}) = \sum_{n=-\infty}^{\infty} c_n \, \delta(\mathbf{f} - n\mathbf{f}_1) \tag{A.22}$$

The support of the spectrum $P_1(u,v)$ is a 1D lattice in the θ_1 direction, which contains all the integer multiples of the fundamental frequency $\mathbf{f}_1$. And moreover, under the appropriate convergence conditions we obtain, here too:

Proposition A.3: A function $p_1(x,y)$ is 1-fold periodic in the θ_1 direction *iff* its spectrum support in the frequency domain is a 1D lattice in the θ_1 direction. ■

A.3.4 2-fold periodic functions in arbitrary directions (skew-periodic functions)

Let us proceed now to the most general 2D case: that of a 2-fold periodic function having two arbitrary periods, which are not necessarily oriented in the x,y directions, not necessarily orthogonal to each other, and do not necessarily have the same period length in both directions. Such functions are called *2-fold periodic* or *skew-periodic* functions [Papoulis68 p. 116]. An example of such a function is shown in Fig. A.2(a).

Formally, a function $p(x,y)$ is called skew-periodic if there exist two non-zero and non-collinear vectors $\mathbf{P}_1 = (x_1,y_1)$ and $\mathbf{P}_2 = (x_2,y_2)$ so that for all $(x,y) \in \mathbb{R}^2$:

$$p(x+x_1,y+y_1) = p(x,y) \quad \text{and} \quad p(x+x_2,y+y_2) = p(x,y).^6$$

The vectors $\mathbf{P}_1$ and $\mathbf{P}_2$ are called *periods* or *period-vectors* of $p(x,y)$;[7] note however that they are not unique, since for any integers m,n the vector $m\mathbf{P}_1+n\mathbf{P}_2$ is also a period of $p(x,y)$ (in vector notation: $p(\mathbf{x}+m\mathbf{P}_1+n\mathbf{P}_2) = p(\mathbf{x})$ for all $\mathbf{x} \in \mathbb{R}^2$; see Fig. A.2(a)). Note that $p(x,y)$ is completely determined from its values in the period-parallelogram A defined by

[6] An alternative definition, based on the *period-parallelogram* of $p(x,y)$ rather than on its *period-vectors*, is given in the Glossary (see under the term "period").

[7] Like in the case of frequency-vectors, we always consider period-vectors as radius-vectors emanating from the origin (and hence, the period-parallelograms which they define are attached to the origin).

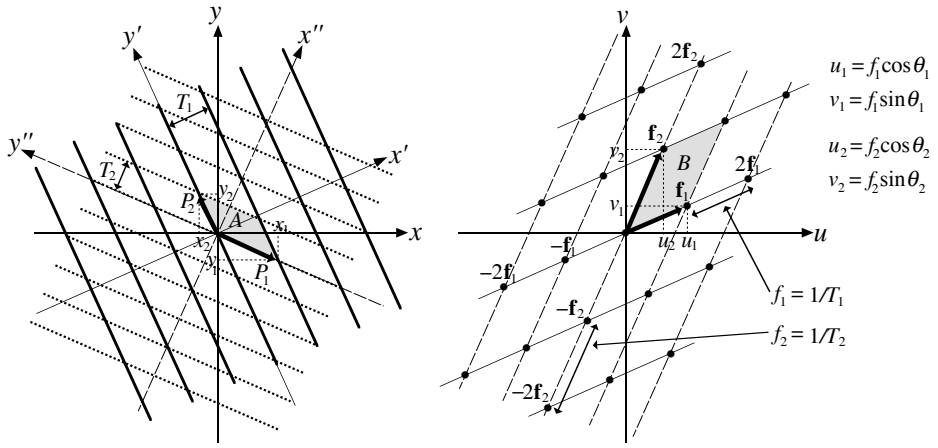

Figure A.2: A schematic plot of the 2-fold periodic (skew-periodic) function $p(x,y)$ in the image domain (a), and its skewed impulse-nailbed in the spectral domain (b). The gray parallelogram A in the image domain represents a one-period element (tile) of $p(x,y)$. P_1 and P_2 are segments of this parallelogram which coincide with the period-vectors $\mathbf{P}_1$ and $\mathbf{P}_2$.

$\mathbf{P}_1$ and $\mathbf{P}_2$, which repeats itself throughout the x,y plane. Clearly, each pair of non-zero and non-collinear period-vectors of $p(x,y)$ defines a different period-parallelogram A. A period parallelogram is called a *fundamental period-parallelogram* of $p(x,y)$ if it has the smallest area > 0 (the area of the smallest period). However, unlike in the 1D case in which there existed a single shortest period $T > 0$ attached to the origin, in the 2D case there exist infinitely many different period-parallelograms attached to the origin which all have the smallest period area (see, for example, parallelograms A in Fig. A.2 and A' in Fig. A.4). Each of these parallelograms is a fundamental period-parallelogram of $p(x,y)$, and each pair of period-vectors $\mathbf{P}_1$ and $\mathbf{P}_2$ of $p(x,y)$ which defines such a fundamental period-parallelogram is called a pair of *fundamental period-vectors* of $p(x,y)$. Their reciprocal vector pair (in a sense to be defined below in Sec. A.4) in the spectral domain, $\mathbf{f}_1$ and $\mathbf{f}_2$, is called a pair of *fundamental frequency-vectors* of $p(x,y)$ (see Fig. A.2(b)). For now, we just mention that $\mathbf{f}_1$ and $\mathbf{f}_2$ are oriented perpendicularly to the corresponding period-vectors $\mathbf{P}_2$ and $\mathbf{P}_1$, respectively: $\mathbf{f}_1 \perp \mathbf{P}_2$ and $\mathbf{f}_2 \perp \mathbf{P}_1$. Since each of the different fundamental period-parallelograms fully defines $p(x,y)$, we may freely choose one of them as a representative fundamental period-parallelogram, and consider its associated period-vectors $\mathbf{P}_1$, $\mathbf{P}_2$ and frequency vectors $\mathbf{f}_1$, $\mathbf{f}_2$ as the representative period and frequency vectors of $p(x,y)$.

Note that the set of all the periods of $p(x,y)$, i.e., the set of all integer linear combinations of the fundamental period-vectors $\mathbf{P}_1$ and $\mathbf{P}_2$, forms a skewed (=oblique) 2D lattice in the x,y plane: $L_{\mathbf{P}} = \{m\mathbf{P}_1 + n\mathbf{P}_2 \mid m,n \in \mathbb{Z}\}$. And similarly, the set of all integer linear combinations of the fundamental frequency-vectors $\mathbf{f}_1$ and $\mathbf{f}_2$ forms a skewed 2D lattice in the

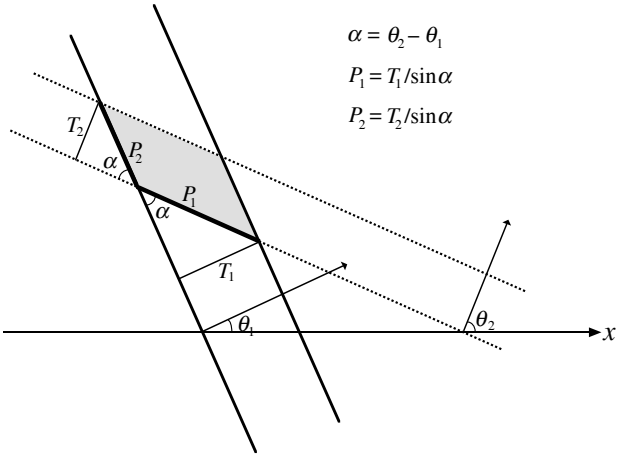

Figure A.3: A magnified view of a single period-parallelogram from Fig. A.2(a), showing the relations between P_i and T_i.

spectral u,v plane: $L_{\mathbf{f}} = \{m\mathbf{f}_1 + n\mathbf{f}_2 \mid m,n \in \mathbb{Z}\}$. Both of these lattices are spanned by any of the possible fundamental vector pairs $\mathbf{P}_1$, $\mathbf{P}_2$ (or $\mathbf{f}_1$, $\mathbf{f}_2$) of $p(x,y)$. We will see later in this section that like in the 1D case the lattice $L_{\mathbf{f}}$ is the support of the spectrum of $p(x,y)$ in the frequency domain. The lattice $L_{\mathbf{P}}$ in the image domain and the lattice $L_{\mathbf{f}}$ in the frequency domain are said to be *reciprocal* (in a sense to be defined below, in Sec. A.4).

It would be instructive at this point to illustrate the case of a skew-periodic function $p(x,y)$ by an example:

Example A.1: Let $p_1(x,y)$ be a 1-fold periodic function in the θ_1 direction as in Sec. A.3.3 above (see Fig. A.1, or the solid grating in Fig. A.2(a)), and let $p_2(x,y)$ be a similar 1-fold periodic function with the period $T_2 = 1/f_2$ in the θ_2 direction (see the dotted grating in Fig. A.2(a)). Then, the superposed function $p(x,y) = p_1(x,y)\,p_2(x,y)$ is skew-periodic. However, as it can be seen in Fig. A.2, the periodicity of $p(x,y)$ is *not* given by the periods T_1 and T_2 of the original functions $p_1(x,y)$ and $p_2(x,y)$, but rather by the periods P_1 and P_2, where $P_1 \perp T_2$, $P_2 \perp T_1$. This fact, although surprising at first sight, is explained as follows:

Consider the original function $p_1(x,y)$ (Fig. A.1). Clearly, this function is periodic in the direction of x' with the period T_1; but at the same time it is also periodic in the direction of x (with the period $T_1/\cos\theta_1$), in the direction of y (with the period $T_1/\sin\theta_1$), or in any other direction in the plane — *with only one exception*: the direction perpendicular to x', i.e., the direction of y', in which the function $p_1(x,y)$ is *constant*.

Similarly, $p_2(x,y)$ is periodic in all directions in the plane, except for the direction of y'', in which it is constant. Now, when $p_1(x,y)$ and $p_2(x,y)$ are superposed, their periodicities are destroyed in all directions — except in the directions in which $p_1(x,y)$ or $p_2(x,y)$ are constant and do not intervene, namely: except in the directions of y' and y''. And indeed, in

the direction of y' (in which $p_1(x,y)$ is constant) $p(x,y)$ behaves like $p_2(x,y)$ and has the period P_2, and in the direction of y'' (in which $p_2(x,y)$ is constant) $p(x,y)$ behaves like $p_1(x,y)$ and has the period P_1. These two exceptional directions define therefore the periodicity of the composite function $p(x,y)$. If we denote the angle difference $\theta_2-\theta_1$ between the two gratings by α (see Fig. A.3), we find that $P_1 = T_1/\sin\alpha$ and $P_2 = T_2/\sin\alpha$.

In the frequency domain, however, there are no such "surprises", and the spectrum of $p(x,y)$ is indeed the convolution of the 1D comb of $p_1(x,y)$ in the θ_1 direction and the 1D comb of $p_2(x,y)$ in the θ_2 direction (see Fig. A.2(b)). The result of this convolution is a skewed nailbed whose support is spanned by $\mathbf{f}_1$ and $\mathbf{f}_2$, the fundamental frequencies of the two original combs. Note that only when the directions θ_1 and θ_2 are perpendicular to each other ($\alpha = \pm 90°$) do P_1 and P_2 coincide with T_1 and T_2, respectively, and $\mathbf{f}_1 \perp \mathbf{P}_2$ and $\mathbf{f}_2 \perp \mathbf{P}_1$ mean, then, as we would expect: $\mathbf{f}_1 \| \mathbf{P}_1$ and $\mathbf{f}_2 \| \mathbf{P}_2$.

Note that Example A.1 illustrates also another typical phenomenon which is related to non-orthogonal lattices: Let $L_{\mathbf{f}}$ be the 2D frequency lattice of $p(x,y)$; this lattice is obtained in the spectrum by the convolution of the two 1D lattices (combs) of the superposed 1-fold periodic functions $p_1(x,y)$ and $p_2(x,y)$. Clearly, $L_{\mathbf{f}}$ is spanned by the vectors $\mathbf{f}_1$ and $\mathbf{f}_2$, the fundamental frequency vectors of $p_1(x,y)$ and $p_2(x,y)$; but unless these two functions are superposed perpendicularly, $\mathbf{f}_1$ and $\mathbf{f}_2$ are not necessarily the *shortest* frequency vectors which span $L_{\mathbf{f}}$. In the case of Fig. A.2(b), for example, the shortest fundamental frequency vectors which span $L_{\mathbf{f}}$ are $\mathbf{f}'_1 = \mathbf{f}_1$ and $\mathbf{f}'_2 = \mathbf{f}_2 - \mathbf{f}_1$, and not $\mathbf{f}_1$ and $\mathbf{f}_2$. This is clearly shown in Fig. A.4(b). Similarly, in the image domain (Fig. A.2(a)) the period-vectors $\mathbf{P}_1$ and $\mathbf{P}_2$ (the reciprocal vector pair of $\mathbf{f}_1$, $\mathbf{f}_2$) are not the shortest fundamental period-vectors of the 2-fold periodic function $p(x,y)$: the shortest period-vectors are $\mathbf{P}'_1 = \mathbf{P}_1 + \mathbf{P}_2$ and $\mathbf{P}'_2 = \mathbf{P}_2$, the reciprocal vector pair of $\mathbf{f}'_1$ and $\mathbf{f}'_2$ (see Fig. A.4(a)).

It is interesting to note that the question of finding the shortest basis vectors of a given lattice of dimension $n > 1$ is not trivial, and it is one of the subjects which are dealt in geometry of numbers [Kannan87 pp. 4*ff*, Gruber93 pp. 742, 751*ff*]. However, in our study of the moiré effect we will always choose the fundamental frequency vectors $\mathbf{f}_i$ of the superposition to be the fundamental frequency vectors of the superposed layers, like in Fig. A.2, even when they are not the shortest possible frequency vectors in the superposition. ■

Suppose now that $p(x,y)$ is a skew-periodic function which satisfies the required convergence conditions, and suppose that $\mathbf{P}_1$, $\mathbf{P}_2$ and $\mathbf{f}_1$, $\mathbf{f}_2$ are representative fundamental period and frequency vectors of $p(x,y)$ (see Fig. A.2). Then its Fourier series expansion in terms of the x' and x'' coordinates is given by:

$$p(x',x'') = \sum_{m=-\infty}^{\infty} \sum_{n=-\infty}^{\infty} c_{m,n}\, e^{i2\pi[mf_1x' + nf_2x'']}$$

Changing back to the x,y coordinate system by putting: $x' = x\cos\theta_1 + y\sin\theta_1$, $x'' = x\cos\theta_2 + y\sin\theta_2$ [Spiegel68 p. 36] and hence: $f_1x' = u_1x + v_1y$, $f_2x' = u_2x + v_2y$ (see Fig. A.2(b)) we obtain:

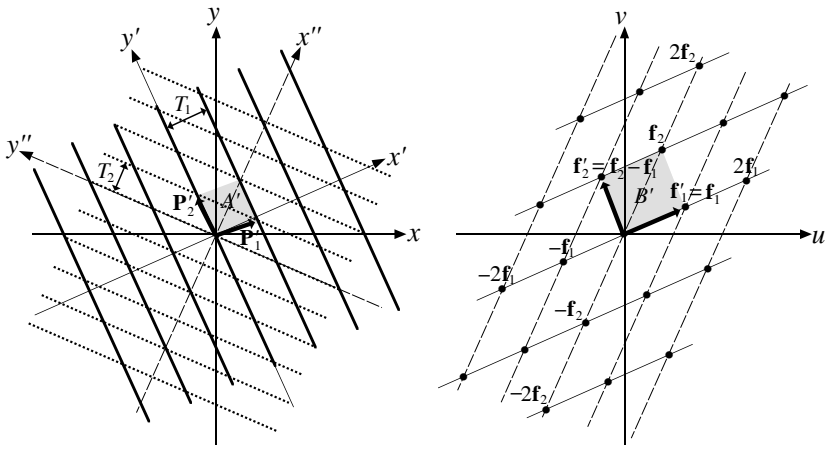

(a) (b)

Figure A.4: A different set of fundamental period-vectors $\mathbf{P}'_1$, $\mathbf{P}'_2$ and fundamental frequency vectors $\mathbf{f}'_1$, $\mathbf{f}'_2$ which span the same period-lattice $L_\mathbf{P}$ and frequency-lattice $L_\mathbf{f}$ as in Fig. A.2. Note that $\mathbf{P}'_1$, $\mathbf{P}'_2$ and $\mathbf{f}'_1$, $\mathbf{f}'_2$ are the shortest vector pairs which span the lattices $L_\mathbf{P}$ and $L_\mathbf{f}$; the parallelograms A' and B' they define have the same respective areas as the parallelograms A and B in Fig. A.2, but they are almost square.

$$p(x,y) = \sum_{m=-\infty}^{\infty} \sum_{n=-\infty}^{\infty} c_{m,n}\, e^{i2\pi[m(u_1x + v_1y) + n(u_2x + v_2y)]}$$

(compare with the 1D case of Eq. (A.19)), or in other words [Papoulis68 p. 117]:

$$p(x,y) = \sum_{m=-\infty}^{\infty} \sum_{n=-\infty}^{\infty} c_{m,n}\, e^{i2\pi[(mu_1 + nu_2)x + (mv_1 + nv_2)y]} \tag{A.23}$$

where u_1, u_2, v_1, v_2 are defined in Fig. A.2, and the Fourier coefficients $c_{m,n}$ are:

$$c_{m,n} = \frac{1}{\overline{A}} \iint_A p(x,y)\, e^{-i2\pi[(mu_1 + nu_2)x + (mv_1 + nv_2)y]}\, dxdy \tag{A.24}$$

$\iint_A$ means here an integration over the parallelogram A defined by $\mathbf{P}_1$ and $\mathbf{P}_2$ (see Fig. A.2(a)), whose area $\overline{A}$ is given by the cross product:

$$\overline{A} = \mathbf{P}_1 \times \mathbf{P}_2 = x_1y_2 - y_1x_2 \tag{A.25}$$

This can be expressed more compactly in the vector notation:

$$p(\mathbf{x}) = \sum_{m=-\infty}^{\infty} \sum_{n=-\infty}^{\infty} c_{m,n}\, e^{i2\pi(m\mathbf{f}_1 + n\mathbf{f}_2)\cdot\mathbf{x}} \tag{A.26}$$

with the Fourier series coefficients:

$$c_{m,n} = \frac{1}{\overline{A}} \iint_A p(\mathbf{x})\, e^{-i2\pi(m\mathbf{f}_1 + n\mathbf{f}_2)\cdot\mathbf{x}}\, d\mathbf{x} \tag{A.27}$$

where $\mathbf{f}_1 = (u_1,v_1)$ and $\mathbf{f}_2 = (u_2,v_2)$ are the corresponding fundamental frequency vectors, and $\mathbf{x} = (x,y)$.

Note that Eqs. (A.26) and (A.27) can be further simplified into the vector form of Eqs. (A.13) and (A.14) (with the integration being done over a parallelogram A rather than over a rectangle T_xT_y) if we take:

$$\mathbf{f}_{m,n} = m\mathbf{f}_1 + n\mathbf{f}_2 = (mu_1+nu_2,\ mv_1+nv_2) \tag{A.28}$$

as the (m,n)-th frequency harmonic. In this notation each frequency vector takes the indices of its impulse in the spectrum convolution; for example, the fundamental frequency vectors $\mathbf{f}_1$ and $\mathbf{f}_2$ are denoted by $\mathbf{f}_{1,0}$ and $\mathbf{f}_{0,1}$, respectively.

The spectrum of the skew-periodic function $p(x,y)$ is a skewed impulse-nailbed (see Fig. A.2(b)), whose (m,n)-th impulse is located in the u,v plane at the point given by Eq. (A.28), and has the amplitude $c_{m,n}$. Using the 2D impulse symbol $\delta(u,v)$ the spectrum of $p(x,y)$ is given by [Papoulis68 p. 117]:

$$P(u,v) = \sum_{m=-\infty}^{\infty} \sum_{n=-\infty}^{\infty} c_{m,n}\, \delta(u-mu_1-nu_2,\ v-mv_1-nv_2) \tag{A.29}$$

or in a vector form, with $\mathbf{f} = (u,v)$:

$$P(\mathbf{f}) = \sum_{m=-\infty}^{\infty} \sum_{n=-\infty}^{\infty} c_{m,n}\, \delta\big(\mathbf{f}-(m\mathbf{f}_1+n\mathbf{f}_2)\big) \tag{A.30}$$

Note that using the notation of (A.28), the spectrum (A.30), too, can be further simplified, and it coincides with the vector form of (A.17).

As we can see, the support of the spectrum $P(u,v)$ is the skewed 2D lattice $L_{\mathbf{f}}$, which contains all the integer linear combinations of the fundamental frequency vectors $\mathbf{f}_1$ and $\mathbf{f}_2$.[8] Furthermore, under the appropriate convergence conditions we have the following result:

Proposition A.4: A function $p(x,y)$ in the image domain is 2-fold periodic (skew-periodic) *iff* its spectrum support in the frequency domain is a 2D lattice. ■

The relationship between the periodicity of $p(x,y)$ in the image domain and its spectrum support in the frequency domain is the subject of the following section.

A.4 The period-lattice and the frequency-lattice (= spectrum support)

In this section we summarize the reciprocity relationship between the fundamental period(s) of a periodic function in the image domain and the corresponding fundamental frequency(ies) in the spectral domain. We have seen above, both in the 1D and in the 2D

[8] Note that the lattice $L_{\mathbf{f}}$ is independent of the choice of the fundamental frequency vectors, as illustrated in Figs. A.2(b) and A.4(b).

cases, that the set of all the periods of a periodic function (i.e., the set of all integer linear combinations of its fundamental period(s)) is a lattice $L_{\mathbf{P}}$ in the image domain, while the set of all the integer linear combinations of the fundamental frequency(ies) of the periodic function forms a lattice $L_{\mathbf{f}}$ in the spectral domain. This last lattice, $L_{\mathbf{f}}$, is in fact the *support* of the spectrum of the periodic function, i.e., the set of the geometric locations of all the impulses of the comb or the nailbed in the spectrum of the periodic function (including those impulses whose amplitudes happen to be zero).

For example, in the 1-fold periodic case of Fig. A.1 the 1D period-lattice $L_{\mathbf{P}}$ in the image domain (left) is represented by all integer multiples of the fundamental period along the x' axis; and the 1D frequency-lattice $L_{\mathbf{f}}$ in the frequency domain (right) is the set of all the integer multiples of the fundamental frequency $\mathbf{f}_1$. Both lattices are oriented in the same direction, θ_1, but their steps are reciprocal: the step of the period-lattice is T_1, while the step of the frequency-lattice is $f_1 = 1/T_1$. In the 2-fold periodic case shown in Fig. A.2 the 2D period-lattice $L_{\mathbf{P}}$ in the image domain (left) is represented by all the integer linear combinations of the fundamental periods $\mathbf{P}_1$ and $\mathbf{P}_2$; and the 2D frequency-lattice $L_{\mathbf{f}}$ in the spectral domain (right) is represented by all the linear combinations of the fundamental frequencies $\mathbf{f}_1$ and $\mathbf{f}_2$ (marked by dots in the figure). However, while the reciprocity between the lattices $L_{\mathbf{P}}$ and $L_{\mathbf{f}}$ is straightforward in the 1D case, in the 2D case some further explanation is required.

Let us see what is the relationship in the 2D case between the fundamental periods $\mathbf{P}_1$ and $\mathbf{P}_2$ (which are a basis of the period-lattice $L_{\mathbf{P}}$ in the image domain) and the corresponding fundamental frequencies $\mathbf{f}_1$ and $\mathbf{f}_2$ (which are a basis of the frequency-lattice $L_{\mathbf{f}}$ in the spectrum). According to Fig. A.2 we have:

in the image domain:
$$\begin{aligned} \mathbf{P}_1 &= (x_1, y_1) \\ \mathbf{P}_2 &= (x_2, y_2) \end{aligned} \tag{A.31}$$

and in the spectrum:
$$\begin{aligned} \mathbf{f}_1 &= (u_1, v_1) \\ \mathbf{f}_2 &= (u_2, v_2) \end{aligned} \tag{A.32}$$

In order to find how $\mathbf{f}_1$ and $\mathbf{f}_2$ are related to $\mathbf{P}_1$ and $\mathbf{P}_2$ we would like to express the coordinates u_i and v_i in terms of x_i and y_i. And indeed, we have (see Fig. A.1(b)):

$$\begin{aligned} u_1 &= f_1 \cos\theta_1 \\ &= \tfrac{1}{T_1} \cos\theta_1 \\ &= \tfrac{y_2}{T_1 P_2} \qquad\qquad (\text{since } \cos\theta_1 = \tfrac{y_2}{P_2};\ \text{see Fig. A.2(a)}) \\ &= \tfrac{y_2}{\overline{A}} \end{aligned}$$

where $\overline{A}$ is the area of the parallelogram A, as given by Eq. (A.25): $\overline{A} = \mathbf{P}_1 \times \mathbf{P}_2 = x_1 y_2 - y_1 x_2$. We can also express in a similar way v_1, u_2 and v_2; and by substituting them into (A.32) we obtain, therefore, the required expressions for $\mathbf{f}_1$, $\mathbf{f}_2$ in terms of x_i and y_i:

$$\begin{aligned}\mathbf{f}_1 &= \tfrac{1}{\overline{A}}(y_2,-x_2)\\ \mathbf{f}_2 &= \tfrac{1}{\overline{A}}(-y_1,x_1)\end{aligned} \tag{A.33}$$

From Eqs. (A.31) and (A.33) we immediately obtain the following properties:

(1) As we have already seen above: $\mathbf{f}_1 \perp \mathbf{P}_2$ and $\mathbf{f}_2 \perp \mathbf{P}_1$.

(2) Concerning the vector lengths we obtain:

from Eq. (A.31): $|\mathbf{P}_1| = \sqrt{x_1^2 + y_1^2}$

$|\mathbf{P}_2| = \sqrt{x_2^2 + y_2^2}$

and from Eq. (A.33): $|\mathbf{f}_1| = \tfrac{1}{\overline{A}}\sqrt{x_2^2 + y_2^2} = \tfrac{1}{\overline{A}}|\mathbf{P}_2|$

$|\mathbf{f}_2| = \tfrac{1}{\overline{A}}\sqrt{x_1^2 + y_1^2} = \tfrac{1}{\overline{A}}|\mathbf{P}_1|$

In other words, the length ratio between the two pairs of fundamental vectors is preserved reciprocally:

$$\frac{|\mathbf{f}_1|}{|\mathbf{f}_2|} = \frac{|\mathbf{P}_2|}{|\mathbf{P}_1|}$$

(For example, if the length of $\mathbf{P}_1$ is twice the length of $\mathbf{P}_2$ in the image domain, then in the spectrum the length of $\mathbf{f}_1$ is half the length of $\mathbf{f}_2$).

(3) Another interesting result concerns the areas of the fundamental period-parallelogram A in the image domain and the fundamental frequency-parallelogram B in the spectrum:

$$\begin{aligned}\overline{A} &= \mathbf{P}_1 \times \mathbf{P}_2 = x_1 y_2 - y_1 x_2\\ \overline{B} &= \mathbf{f}_1 \times \mathbf{f}_2 = u_1 v_2 - v_1 u_2 = \tfrac{1}{\overline{A}^2}(x_1 y_2 - y_1 x_2) = \tfrac{1}{\overline{A}}\end{aligned}$$

This means that the areas of the parallelograms A and B are, indeed, reciprocal.

Due to these reciprocity relations which prevail between the period-lattice $L_{\mathbf{P}}$ and the frequency lattice $L_{\mathbf{f}}$ these two lattices are said to be *reciprocal*. Similarly, the vector pair $\mathbf{f}_1$, $\mathbf{f}_2$ which spans the lattice $L_{\mathbf{f}}$ is said to be reciprocal to the vector pair $\mathbf{P}_1$, $\mathbf{P}_2$ which spans the lattice $L_{\mathbf{P}}$.

Finally, it is interesting to mention the following relations regarding the mixed scalar products of the basis vectors of the 2D reciprocal lattices $L_{\mathbf{P}}$ and $L_{\mathbf{f}}$, which are also obtained from Eqs. (A.31) and (A.33):

$$\mathbf{P}_1 \cdot \mathbf{f}_1 = x_1 \tfrac{y_2}{\overline{A}} - y_1 \tfrac{x_2}{\overline{A}} = \tfrac{1}{\overline{A}}\overline{A} = 1 \qquad \mathbf{P}_1 \cdot \mathbf{f}_2 = -x_1 \tfrac{y_1}{\overline{A}} + y_1 \tfrac{x_1}{\overline{A}} = 0$$

$$\mathbf{P}_2 \cdot \mathbf{f}_1 = x_2 \tfrac{y_2}{\overline{A}} - y_2 \tfrac{x_2}{\overline{A}} = 0 \qquad \mathbf{P}_2 \cdot \mathbf{f}_2 = -x_2 \tfrac{y_1}{\overline{A}} + y_2 \tfrac{x_1}{\overline{A}} = \tfrac{1}{\overline{A}}\overline{A} = 1$$

This property of the two reciprocal lattices is most useful, since it can be readily generalized to lattices in 3D (such as in the case of crystallography) or any other dimension $n \geq 1$. In fact, this property is often used to define reciprocal lattices (see, for example, [Rosenfeld82 p. 75] or [Jarić89 p. 15]):

Definition A.1: Let L be an n-dimensional lattice and let the vectors $\mathbf{P}_1,...,\mathbf{P}_n \in \mathbb{R}^n$ be a basis of L. Then its reciprocal lattice L^* is a lattice of the same dimension, whose basis vectors $\mathbf{f}_1,...,\mathbf{f}_n \in \mathbb{R}^n$ are defined by:

$$\mathbf{P}_i \cdot \mathbf{f}_j = \begin{cases} 1 & \text{if } i = j \\ 0 & \text{if } i \neq j \end{cases} \quad \blacksquare \tag{A.34}$$

The geometric interpretation of this definition is as follows:

(a) The second condition in (A.34) means that the vector $\mathbf{f}_j$ is perpendicular to all the vectors $\mathbf{P}_i$ with $i \neq j$; this determines the direction of the line through the origin of $\mathbb{R}^n$ on which $\mathbf{f}_j$ is situated. (For example, in the 3D case $\mathbf{f}_1$ is situated on the line emanating from the origin of $\mathbb{R}^3$ perpendicularly to the plane spanned by $\mathbf{P}_2$ and $\mathbf{P}_3$).

(b) The first condition in (A.34) determines the precise length and direction of the vector $\mathbf{f}_j$ on the line defined in (a). $\mathbf{P}_j \cdot \mathbf{f}_j = 1$ means that the length of $\mathbf{f}_j$ on this line is reciprocal to the length of the projection of $\mathbf{P}_j$ on the same line: Since by [Vygodski73 p. 142] $\mathbf{P} \cdot \mathbf{f} = |\mathbf{f}|\,|\text{proj}(\mathbf{P})_{\mathbf{f}}|$ (where $\text{proj}(\mathbf{P})_{\mathbf{f}}$ denotes the projection of $\mathbf{P}$ on $\mathbf{f}$), and since we have here $\mathbf{P} \cdot \mathbf{f} = 1$, it follows that $|\mathbf{f}| = 1/|\text{proj}(\mathbf{P})_{\mathbf{f}}|$. And furthermore, since we have $\mathbf{P}_j \cdot \mathbf{f}_j = 1 > 0$ the direction of the vector $\mathbf{f}_j$ on the same line is determined such that the angle between $\mathbf{f}_j$ and $\mathbf{P}_j$ is sharp [*ibid.*].

Hence, the two conditions of (A.34) fully determine each of the n vectors $\mathbf{f}_j$.

Although for our present work we will only need the 2D or 1D cases, it is interesting to mention that this definition permits us to generalize Propositions A.1–A.4 above to the n-dimensional case (again, under the appropriate convergence conditions), as follows:

Proposition A.5: A function $p(\mathbf{x})$ in the n-dimensional image domain is periodic with period-lattice L *iff* its n-dimensional spectrum $P(\mathbf{u})$ has as its support in the frequency domain the reciprocal lattice L^*. $\blacksquare$

A.5 The matrix notation, its appeal, and its limitations for our needs

It is interesting to note that based on Eq. (A.34) the reciprocity between the vectors $\mathbf{P}_i$ (which are a basis of the period-lattice L) and the vectors $\mathbf{f}_i$ (which are a basis of the frequency-lattice L^*, i.e., of the spectrum support) can be also expressed in matrix notation. Since from (A.34) we have:[9]

$$\begin{pmatrix} \mathbf{P}_1 \\ \vdots \\ \mathbf{P}_n \end{pmatrix} (\mathbf{f}_1,...,\mathbf{f}_n) = \begin{pmatrix} \mathbf{P}_1 \cdot \mathbf{f}_1 & \cdots & \mathbf{P}_1 \cdot \mathbf{f}_n \\ \cdots & \cdots & \cdots \\ \mathbf{P}_n \cdot \mathbf{f}_1 & \cdots & \mathbf{P}_n \cdot \mathbf{f}_n \end{pmatrix} = \begin{pmatrix} 1 & & 0 \\ & \ddots & \\ 0 & & 1 \end{pmatrix}$$

[9] Note that each vector in the following expressions represents an n-tuple of coordinates, and therefore each entity in parentheses is, in fact, a *matrix*.

it follows that if the matrix $(\mathbf{f}_1,...,\mathbf{f}_n)$ is invertible, i.e., non-singular (which is true *iff* the vectors $\mathbf{f}_1,...,\mathbf{f}_n$ are linearly independent over $\mathbb{R}$ [Birkhoff77 pp. 237–238]), then:

$$\begin{pmatrix}\mathbf{P}_1\\ \vdots\\ \mathbf{P}_n\end{pmatrix} = (\mathbf{f}_1,...,\mathbf{f}_n)^{-1}$$

and by writing both sides as columns we obtain:

$$\begin{pmatrix}\mathbf{P}_1\\ \vdots\\ \mathbf{P}_n\end{pmatrix} = \begin{pmatrix}\mathbf{f}_1\\ \vdots\\ \mathbf{f}_n\end{pmatrix}^{-\mathrm{T}} \tag{A.35}$$

(where "–T" means the transpose of the inverse matrix). We will henceforth denote these two matrices in short by P and F, and hence Eq. (A.35) becomes: $\mathrm{P} = \mathrm{F}^{-\mathrm{T}}$.

For example, in the 2D case we have, indeed, by Eqs. (A.33) and (A.31):

$$\mathrm{F} = \begin{pmatrix}\mathbf{f}_1\\ \mathbf{f}_2\end{pmatrix} = \begin{pmatrix}u_1 & v_1\\ u_2 & v_2\end{pmatrix} = \frac{1}{x_1y_2 - y_1x_2}\begin{pmatrix}y_2 & -x_2\\ -y_1 & x_1\end{pmatrix} = \begin{pmatrix}x_1 & y_1\\ x_2 & y_2\end{pmatrix}^{-\mathrm{T}} = \begin{pmatrix}\mathbf{P}_1\\ \mathbf{P}_2\end{pmatrix}^{-\mathrm{T}} = \mathrm{P}^{-\mathrm{T}} \tag{A.36}$$

We note that $\bar{A} = x_1y_2 - y_1x_2$ is, in fact, the determinant of the matrix $\mathrm{P} = \begin{pmatrix}\mathbf{P}_1\\ \mathbf{P}_2\end{pmatrix} = \begin{pmatrix}x_1 & y_1\\ x_2 & y_2\end{pmatrix}$.

This matrix representation of (A.34) leads us also to a matrix notation for the periodic function $p(x,y)$ and for its spectrum (=Fourier transform) $P(u,v)$:

We start first with the spectrum $P(u,v)$. As we have seen earlier, $P(u,v)$ is given in vector notation by Eq. (A.30), as follows:

$$P(\mathbf{f}) = \sum_{m=-\infty}^{\infty}\sum_{n=-\infty}^{\infty} c_{m,n}\,\delta(\mathbf{f} - (m\mathbf{f}_1 + n\mathbf{f}_2))$$

We note that:

$$\begin{aligned} m\mathbf{f}_1 + n\mathbf{f}_2 &= m(u_1,v_1) + n(u_2,v_2)\\ &= (mu_1+nu_2,\ mv_1+nv_2)\\ &= (m,n)\begin{pmatrix}u_1 & v_1\\ u_2 & v_2\end{pmatrix}\\ &= \mathbf{n}\mathrm{F}\end{aligned}$$

where $\mathrm{F} = \begin{pmatrix}\mathbf{f}_1\\ \mathbf{f}_2\end{pmatrix} = \begin{pmatrix}u_1 & v_1\\ u_2 & v_2\end{pmatrix}$ and $\mathbf{n} = (m,n)$.

Hence we obtain the following matrix notation for the spectrum $P(u,v)$:

$$P(\mathbf{f}) = \sum_{\mathbf{n}} c_{\mathbf{n}}\,\delta(\mathbf{f} - \mathbf{n}\mathrm{F}) \tag{A.37}$$

We proceed now to the periodic function $p(x,y)$ itself, in the image domain: Let $\mathbf{P}_1$, $\mathbf{P}_2$ be the fundamental period-vectors of $p(x,y)$ and let $d(x,y)$ be its restriction to the fundamental period-parallelogram defined by $\mathbf{P}_1$, $\mathbf{P}_2$, i.e., a single period-element of $p(x,y)$. Therefore, we can rewrite $p(x,y)$ in vector notation as follows:

$$p(\mathbf{x}) = \sum_{m=-\infty}^{\infty} \sum_{n=-\infty}^{\infty} d\big(\mathbf{x} - (m\mathbf{P}_1 + n\mathbf{P}_2)\big) \tag{A.38}$$

Again, we note that:

$$\begin{aligned} m\mathbf{P}_1 + n\mathbf{P}_2 &= m(x_1,y_1) + n(x_2,y_2) \\ &= (mx_1+nx_2,\, my_1+ny_2) \\ &= (m,n)\begin{pmatrix} x_1 & y_1 \\ x_2 & y_2 \end{pmatrix} \\ &= \mathbf{n}\mathrm{P} \end{aligned}$$

where $\mathrm{P} = \begin{pmatrix} \mathbf{P}_1 \\ \mathbf{P}_2 \end{pmatrix} = \begin{pmatrix} x_1 & y_1 \\ x_2 & y_2 \end{pmatrix}$ and $\mathbf{n} = (m,n)$.

Hence we obtain the following matrix notation for the periodic function $p(x,y)$:

$$p(\mathbf{x}) = \sum_{\mathbf{n}} d(\mathbf{x} - \mathbf{n}\mathrm{P}) \tag{A.39}$$

where, as we have already seen in Eqs. (A.35) and (A.36): $\mathrm{P} = \mathrm{F}^{-\mathrm{T}}$. [10]

The matrix notation of Eqs. (A.37) and (A.39) is frequently used in literature, due to its concise and appealing form;[11] see, for example, [Ulichney88 pp. 17–19, 44–47] and [Cartwright90 pp. 123–126]. However, although useful for expressing 2D or multi-dimensional periodic functions and their spectra (=Fourier transforms), we will not make use of this notation in our study on the superposition of periodic functions, and this for two main reasons:

First, in spite of its concise, appealing form, the matrix notation tends to obscure the detailed structure of the spectrum support — while the explicit vector notations that we introduced earlier, like in Eqs. (A.26) or (A.30), clearly reflect this structure, and are therefore particularly well adapted for our needs (see also Sec. 6.7 in Chapter 6).

But even more importantly, it must be noted that Eq. (A.39) in the image domain, which is based on the matrix $\mathrm{P} = \mathrm{F}^{-\mathrm{T}}$, is valid only for non-singular cases, where the matrix F is invertible (i.e., where the frequency-vectors $\mathbf{f}_1,...,\mathbf{f}_n$ are linearly independent; see earlier in this section). However, in our present study not only do such singular cases occur, but they even constitute some of the most interesting cases of our research. In fact, there exist two possible types of failure due to the singularity of the matrix F:

(a) If the vectors $\mathbf{f}_1,...,\mathbf{f}_n$ have $\mathrm{rank}_{\mathbb{Z}}\,\mathrm{Md}(\mathbf{f}_1,...,\mathbf{f}_m) = \dim \mathrm{Sp}(\mathbf{f}_1,...,\mathbf{f}_m) = k$ where $k < n$, meaning that the spectrum support is still a *lattice* (see Proposition 5.1) — but of a lower dimension $k < n$, then the failure is curable and Eq. (A.39) can still be used, after a manual adaptation to the new, lower dimension k (based on a new basis of k rather than n vectors $\mathbf{f}_i$, and on new $k\times k$ matrices F and P). For instance, in the case of $n = 2$

[10] Note that the multiplication of the integer index-vector $\mathbf{n}\in\mathbb{Z}^2$ by the matrix F in Eq. (A.37) (or by the matrix P, in Eq. (A.39)) can be interpreted as an application of a linear mapping on the integer lattice $\mathbb{Z}^2$ which transforms it into the skewed frequency-lattice $L_{\mathbf{f}}$, like in Fig. A.2(b) (or, respectively, into the reciprocal skewed period-lattice $L_{\mathbf{P}}$ in the image domain).

[11] Note, for instance, the similarity between Eq. (A.37) and its 1D counterpart, Eq. (A.8).

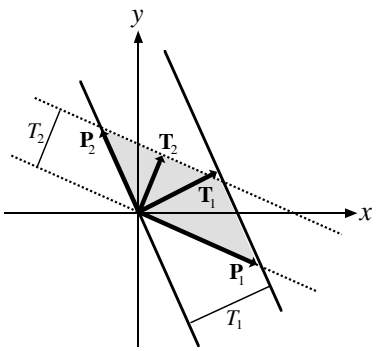

Figure A.5: A magnified view of the main period-parallelogram of Fig. A.2(a), showing the period-vectors $\mathbf{P}_i$ and the step-vectors $\mathbf{T}_i$.

this occurs when $\mathbf{f}_1$ and $\mathbf{f}_2$ are collinear and commensurable, i.e., linearly dependent over $\mathbb{R}$ and over $\mathbb{Z}$ (see Example 2 in Sec. 5.2).

(b) If, however, the vectors $\mathbf{f}_1,...,\mathbf{f}_n$ have $\text{rank}_{\mathbb{Z}}\, \text{Md}(\mathbf{f}_1,...,\mathbf{f}_m) > \dim \text{Sp}(\mathbf{f}_1,...,\mathbf{f}_m)$, meaning that the spectrum support is not a lattice but rather a *module* (so that our superposition in the image domain is an almost-periodic case; see Proposition 6.1), then there is no basis to the spectrum support (see Sec. 5.2) and therefore the singularity of matrix F cannot be remedied. In this case notation (A.39) fails altogether and cannot be used.

These reasons make the matrix notation unsuitable for our study of superposed layers and their spectra, and they favour, instead, our vector notation, based on the layer frequencies $\mathbf{f}_1,...,\mathbf{f}_n$.

A.6 The period-vectors $\mathbf{P}_i$ vs. the step-vectors $\mathbf{T}_i$

One further remark is due at this point. The failure of matrix P whenever matrix F is singular is, in fact, just an indication to a more fundamental failure: Since the period-vectors $\mathbf{P}_i$ in the image domain only exist when the frequency-vectors $\mathbf{f}_1,...,\mathbf{f}_n$ (the individual layer frequencies) in the spectrum are linearly independent over $\mathbb{R}$ (see Sec. A.5), the vectors $\mathbf{P}_i$ are inappropriate for our study of layer superpositions, because superpositions may well occur even when $\mathbf{f}_1,...,\mathbf{f}_n$ are linearly dependent. (And in fact, in the case of our 2D spectrum this necessarily occurs whenever $n > 2$). Therefore, instead of the vectors $\mathbf{P}_i$ we will only consider in the image domain the periods T_i of the n individual gratings (see Figs. A.2, A.3). And if a 2-fold periodic layer $p(x,y)$ appears in the superposition (say, a dot-screen), it will contribute *two* values T_i, which are the periods of the two *virtual gratings* defined by the borders of the fundamental period-parallelogram of that layer (see the solid and the dotted gratings in Fig. A.2(a) and the magnified view in

Fig. A.3).[12] And indeed, even the classical moiré formulas, such as Eqs. (2.9) – (2.11), are only based on the grating periods T_i. If we consider these grating periods as vectors $\mathbf{T}_i$ emanating from the origin of the image domain at the grating directions θ_i (see Fig. A.5), and call them *step-vectors*, we find that the relationship between each step-vector $\mathbf{T}_i$ and its counterpart $\mathbf{f}_i$ in the spectral domain is straightforward:

(1) The vectors $\mathbf{T}_i$ and $\mathbf{f}_i$ (for every i) are collinear, i.e., they have the same angle θ_i;

(2) Their lengths are reciprocal, namely: for every i, $|\mathbf{T}_i| = 1/|\mathbf{f}_i|$.

This means that for every i we have $\mathbf{T}_i = \frac{|\mathbf{T}_i|}{|\mathbf{f}_i|}\mathbf{f}_i = \frac{1}{|\mathbf{f}_i|^2}\mathbf{f}_i$. In other words, we obtain:

$$\begin{aligned} \mathbf{T}_1 &= \frac{1}{|\mathbf{f}_1|^2}\mathbf{f}_1 \\ &\vdots \\ \mathbf{T}_n &= \frac{1}{|\mathbf{f}_n|^2}\mathbf{f}_n \end{aligned} \tag{A.40}$$

As we can see, this relationship holds between any pair $\mathbf{T}_i$, $\mathbf{f}_i$, individually; and moreover, it exists in *all* cases and for any number n of superposed layers — even if $\mathbf{f}_1,\ldots,\mathbf{f}_n$ are linearly dependent.

In order to formulate better the relationship between the vector pair $\mathbf{T}_i$, $\mathbf{f}_i$ we introduce here the following definition:

Definition A.2: For any vector $\mathbf{v} \neq 0$, the *reciprocal vector* of $\mathbf{v}$ (with respect to scalar product) is defined as:

$$\mathbf{v}^{-1} = \frac{1}{|\mathbf{v}|^2}\mathbf{v} \qquad \blacksquare \tag{A.41}$$

This definition requires a short explanation. Although it is clear that the vector $\mathbf{v}^{-1}$ is reciprocal to $\mathbf{v}$ with respect to scalar product:

$$\mathbf{v}^{-1}\cdot\mathbf{v} = \mathbf{v}\cdot\mathbf{v}^{-1} = \frac{1}{|\mathbf{v}|^2}\mathbf{v}\cdot\mathbf{v} = 1 \tag{A.42}$$

$\mathbf{v}^{-1}$ is *not* the unique vector with this property. In fact, the locus of all the vectors $\mathbf{x}$ which satisfy $\mathbf{x}\cdot\mathbf{v} = 1$ contains (in the case of $\mathbb{R}^3$) the entire plane perpendicular to the vector $\mathbf{v}$, whose distance from the origin (along the line spanned by $\mathbf{v}$) is $\frac{1}{|\mathbf{v}|}$. Therefore, the uniqueness of $\mathbf{v}^{-1}$ in this definition is obtained only through the requirement, implicit in Eq. (A.41), that the reciprocal vector $\mathbf{v}^{-1}$ is collinear with the vector $\mathbf{v}$.

Using this definition and in view of (1), (2) and Eq. (A.40) above, we can now reformulate the relationship between the vector pair $\mathbf{T}_i$ and $\mathbf{f}_i$ as follows:

---

[12] Each of the different possible choices of fundamental frequency-vectors $\mathbf{f}_1,\mathbf{f}_2$ for $p(x,y)$ automatically determines a corresponding pair of fundamental period-vectors $\mathbf{P}_1,\mathbf{P}_2$ (by Eq. (A.34)), and hence it determines also the fundamental period-parallelogram they define, and the corresponding virtual-grating periods T_1,T_2. Note that all the different possible choices represent the same 2D lattices $L_\mathbf{f}$ and $L_\mathbf{P}$ of $p(x,y)$.

(3) For every i, the vector $\mathbf{T}_i$ in the image domain is the reciprocal vector (with respect to scalar product) of the frequency-vector $\mathbf{f}_i$ in the spectral domain:

$$\mathbf{T}_i = \frac{1}{|\mathbf{f}_i|^2}\,\mathbf{f}_i = \mathbf{f}_i^{-1} \tag{A.43}$$

This is, in fact, the 2D vectorial generalization of the relation $T = 1/f$ between period and frequency in the 1D case. This vector notation proves to be particularly useful in Chapter 7.

Returning now to our vector comparison, the main difference between the step-vectors $\mathbf{T}_i$ and the period-vectors $\mathbf{P}_i$ (all of which subsist in the image domain) is that each vector $\mathbf{T}_i$ depends only on a *single* frequency-vector $\mathbf{f}_i$, while as we have seen in Eqs. (A.34) and (A.35), each of the vectors $\mathbf{P}_i$ depends on *all* of the n frequency-vectors $\mathbf{f}_1,...,\mathbf{f}_n$. In the first case we speak about reciprocity (with respect to scalar product) between the individual vectors $\mathbf{T}_i$ and $\mathbf{f}_i$, but in the second case we speak about reciprocity between vector n-tuples, $\mathbf{P}_1,...,\mathbf{P}_n$ and $\mathbf{f}_1,...,\mathbf{f}_n$, or between the lattices $L_\mathbf{P}$ and $L_\mathbf{f}$ spanned by them. And while the vectors $\mathbf{P}_i$ exist only when the vectors $\mathbf{f}_1,...,\mathbf{f}_n$ are linearly independent, the vectors $\mathbf{T}_i$, on the contrary, exist for any vectors $\mathbf{f}_1,...,\mathbf{f}_n$ with no restrictions, since every vector $\mathbf{T}_i$ is only dependent on its own counterpart $\mathbf{f}_i$, and no matrix inversion is involved.[13]

Finally, it should be emphasized that in spite of the apparent symmetry between the frequency-lattice $L_\mathbf{f}$ and the period-lattice $L_\mathbf{P}$ (or between the frequency-vectors $\mathbf{f}_1,...,\mathbf{f}_n$ and the period-vectors $\mathbf{P}_1,...,\mathbf{P}_n$) due to Eqs. (A.34) and (A.35), there exists a substantial difference between them: While the spectrum support $L_\mathbf{f}$ is a fundamental property of any superposition of n periodic functions, the period-lattice $L_\mathbf{P}$ (and the period-vectors $\mathbf{P}_1,...,\mathbf{P}_n$) are only derived properties, and they exist only conditionally: *iff* the vectors $\mathbf{f}_1,...,\mathbf{f}_n$ are linearly independent (i.e., *iff* the superposition in the image domain is periodic in n dimensions).

[13] Note that when the vector frequencies $\mathbf{f}_1,...,\mathbf{f}_n$ are all orthogonal to each other (in the n-dimensional spectrum), the vectors $\mathbf{T}_i$ and $\mathbf{P}_i$ ($i = 1,...,n$) coincide in the image domain. The vectors $\mathbf{T}$ and $\mathbf{P}$ also coincide in any 1-fold periodic function.

Appendix B

Almost-periodic functions and their spectra

B.1 Introduction

Almost-periodic functions constitute an important generalization of the class of periodic functions. The theory of almost-periodic functions was founded in 1923 by the Danish mathematician Harald Bohr [Bohr23] and was further developed by A. S. Besicovitch and by others. The main importance of this theory is in the discovery of the tight relationship (or duality) between extensions of the structural concept of periodicity of functions on the one hand and generalizations of the analytic concept of the Fourier series representation of these functions on the other hand. This, in turn, further extends the scope of the reciprocity between functions in the image domain and their spectra in the frequency domain to a larger range of functions. In fact, this generalization introduces a new class of functions situated between periodic functions and aperiodic functions, whose spectral representation, too, is intermediate between the two: its spectrum is no longer composed of a comb or a nailbed of impulses, as in the periodic case, but it is not yet a continuous Fourier transform as in the aperiodic case, either. It is also distinct from the diffuse spectrum of random or pseudo-random functions. Rather, it is still composed of a denumerable set of impulses, but these impulses are freely located in the spectrum, and may be even everywhere dense.[1]

In this appendix we shortly review the concept of almost-periodic functions in one or two variables, along with their main properties. We mainly concentrate here on results which are needed for our purposes; additional details as well as a rigorous mathematic development of the subject can be found in the references cited throughout.

B.2 A simple illustrative example

Let $p_1(x)$ and $p_2(x)$ be periodic functions with periods T_1, T_2. What can be said about the functions $f(x) = p_1(x) + p_2(x)$, $g(x) = p_1(x)\, p_2(x)$? We must distinguish here between two cases:

---

[1] It is interesting to note that in 1984 almost-periodicity was brought to the center of scientific interest by a very remarkable discovery, made by Dan Shechtman *et al.* [Shechtman84]. They discovered solid materials with a new kind of microstructure, which is intermediate between the periodic structure of crystalline materials and the structure of amorphous solids. Further research of these materials, which were named *quasi-crystals*, has shown through spectral and other evidences that this new kind of physical structure corresponds to the mathematical properties of almost-periodicity [Nelson86], [Katz86]. This recent discovery, which has shaken the very foundations of the science of crystallography, shows that almost-periodic structures do not only belong to the wild imagination of mathematicians, but well to the contrary, they do correspond to the physical reality of our world.

(1) If the periods T_1 and T_2 are *commensurable*, i.e., if T_2/T_1 is rational, then there exist non-zero integers m, n such that $mT_1 = nT_2$. Since mT_1 is a period of $p_1(x)$ and nT_2 is a period of $p_2(x)$ it follows that $T = mT_1 = nT_2$ is a common period of both, and therefore also of their sum $f(x)$ and of their product $g(x)$. This means that the functions $f(x)$ and $g(x)$ are periodic with period T (obviously, $T \geq T_1, T_2$).

(2) If the periods T_1 and T_2 are *incommensurable*, i.e., if T_2/T_1 is irrational, then except at the origin the periods of the functions $p_1(x)$ and $p_2(x)$ never meet again after any integer numbers m, n of full periods T_1 and T_2. This means that there exists no common period to $p_1(x)$ and $p_2(x)$, and therefore $f(x)$ and $g(x)$ never exactly repeat themselves, and they are not periodic. As we will see below, $f(x)$ and $g(x)$ belong to a wider class of functions called: *almost-periodic functions*. This situation is illustrated in the following example.

Example B.1: Consider the functions $p_1(x) = \cos(2\pi x/20)$ and $p_2(x) = \frac{1}{4}\cos(2\pi x/\sqrt{2})$, whose periods are respectively $T_1 = 20$ and $T_2 = \sqrt{2}$. Since T_1 and T_2 are *incommensurable*, it is clear that except at the origin the periods of these two functions will never meet again after any integer numbers m, n of full periods T_1 and T_2. This means that the function $f(x) = \cos(2\pi x/20) + \frac{1}{4}\cos(2\pi x/\sqrt{2})$ is not periodic since no value of T, no matter how large it is, gives *exact* repetitions of $f(x)$ (see Fig. B.1). For instance, $f(x)$ gets its maximum value $f(x) = 1\frac{1}{4}$ only at $x = 0$, and for no other value of x. However, as it can be seen in the figure, $f(x)$ looks "almost" as a periodic function. And indeed, if we admit a certain small error ε, say $\varepsilon = 0.3$, then $\tau_\varepsilon = 20$ can be considered as an ε-almost-period of $f(x)$, which gives a repetition of $f(x)$ up to an error of ε. If we require a smaller error, such as $\varepsilon = 0.01$, then there can be found a larger number, such as $\tau_\varepsilon = 140$, which may be taken as an ε-almost-period. In fact, for any $\varepsilon > 0$ we can find an arbitrarily large ε-almost-period τ_ε for $f(x)$ such that for any $-\infty < x < \infty$, $|f(x+\tau_\varepsilon) - f(x)| < \varepsilon$ (this is demonstrated, for a similar function, in [Besicovitch32 p. ix]). A slightly stronger version of this property will serve as a basis for the definition of an almost-periodic function (see Sec. B.3). ■

As we will see below, any periodic function is almost-periodic, but clearly not every almost-periodic function is periodic. It should also be emphasized that not every non-periodic function is almost-periodic; an obvious counter-example would be $f(x) = x$. This means that almost-periodic functions form an intermediate class of functions between periodic functions and aperiodic functions (see Fig. B.3 in Sec. B.5 below).

B.3 Definitions and main properties

The definition of almost-periodic functions relies on the definition of the concept of ε-almost-period as a generalization of the concept of a period. Let us start by rephrasing the definitions of a period and of a periodic function which are given in Sec. A.2.

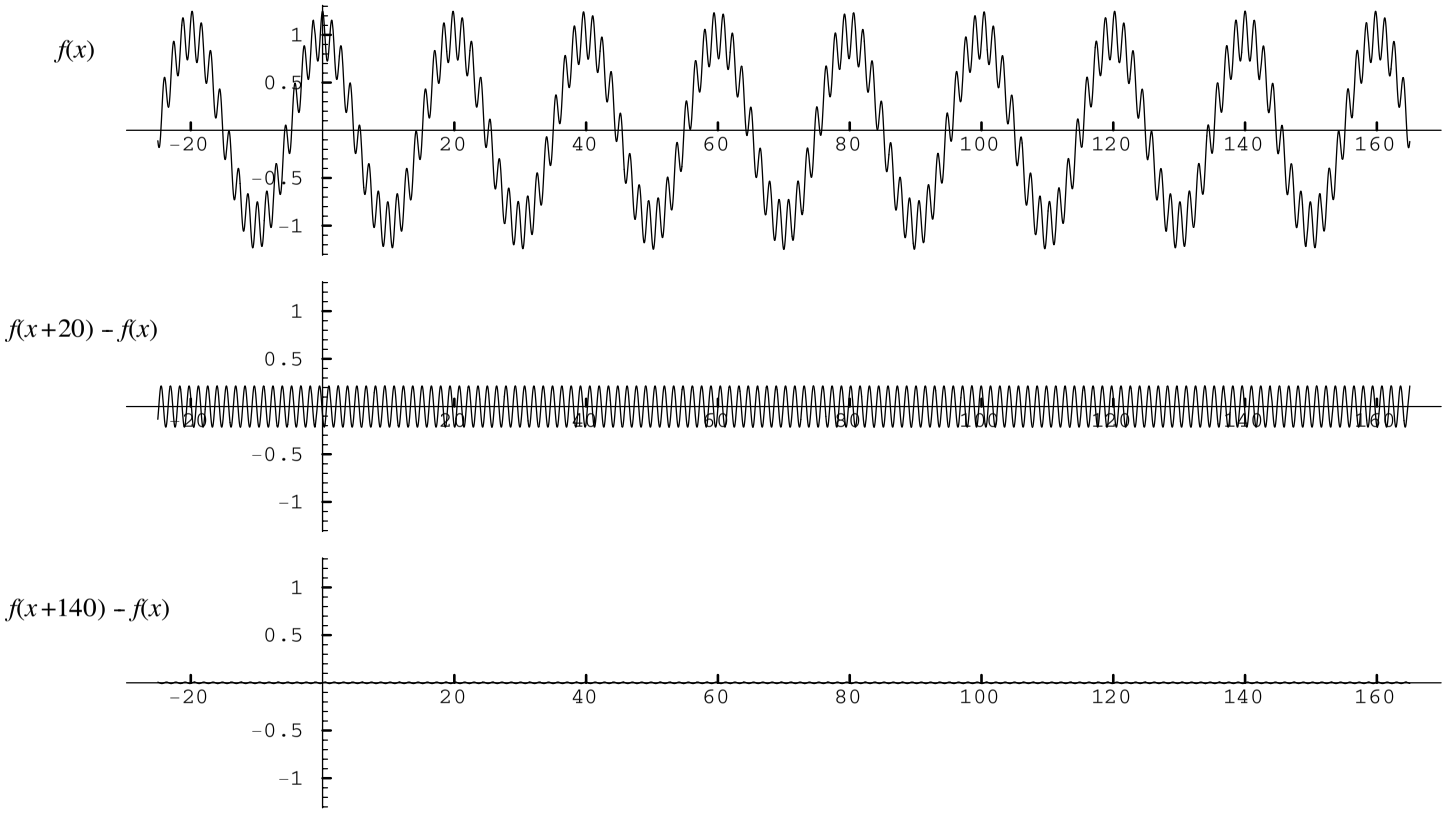

Figure B.1: Top: almost periodicity is clearly illustrated by the graphic plot of the function: $f(x) = \cos(2\pi x/20) + \frac{1}{4}\cos(2\pi x/\sqrt{2})$. In this case, a high-frequency oscillation (with period $T_2 = \sqrt{2}$) is added to a cosine with period of $T_1 = 20$. The resulting function $f(x)$ is not periodic, but still it "almost" repeats itself with $\tau = 20$, with just a tiny error; it repeats itself with an even smaller error if we take $\tau = 140$, and so forth. Center and bottom: the error $f(x+\tau) - f(x)$ for $\tau = 20$ and for $\tau = 140$, shown at the same scale as $f(x)$. Note that for $\tau = 20$ the error is smaller than 0.3 everywhere; for $\tau = 140$ the error is smaller than 0.01.

Definition B.1: A number T is called a *period* of $f(x)$ if for all $x \in \mathbb{R}$:

$$|f(x+T) - f(x)| = 0$$

If there exists such a number $T \neq 0$, then $f(x)$ is called *periodic*. As was noted in Sec. A.2 T is not unique, since if T is a period of $f(x)$, so is nT for any integer n. In fact, the set of all periods of $f(x)$ is denumerably infinite, and it forms a lattice in $\mathbb{R}$: $L_T = \{nT \mid n \in \mathbb{Z}\}$. Normally one considers the *fundamental period* of $f(x)$, i.e., the minimal positive number in L_T. ■

Using this definition for inspiration, we give now the following definitions [Bohr51 p. 32]:

Definition B.2: An infinite set S of real numbers τ is called *relatively dense* if there exists some number $l > 0$ (called *inclusion length*) such that every interval of length l, $(x, x+l) \subset \mathbb{R}$, contains at least one number τ of the set S. (This means that there are no arbitrarily large gaps between the numbers τ. As an example, the set L_T defined above is relatively dense since every interval $(x, x+2T)$ contains at least one number of L_T; but the set $\{n^2 \mid n \in \mathbb{Z}\}$ is not relatively dense.) ■

Definition B.3: Given $\varepsilon > 0$, a number τ_ε is called an *ε-almost-period*[2] of $f(x)$ if for all $x \in \mathbb{R}$:

$$|f(x+\tau_\varepsilon) - f(x)| < \varepsilon \tag{B.1}$$

A continuous function $f(x)$ is called *Bohr-almost-periodic*[3] (or *uniformly-almost-periodic*) if for *any* $\varepsilon > 0$, no matter how small, there exists a relatively dense set of ε-almost-periods.[4] ■

In other words, $f(x)$ is Bohr-almost-periodic if the equation $f(x+\tau_\varepsilon) = f(x)$ is satisfied with an arbitrary degree of accuracy $\varepsilon > 0$ by infinitely many values of τ_ε, these values being spread over the whole range from $-\infty$ to $+\infty$ in such a way as not to leave empty intervals of arbitrarily great length [Besicovitch32 p. x].

It should be noted that every periodic function is almost-periodic (since for any ε we may take the periods nT for all $n \in \mathbb{Z}$ as a relatively dense set of ε-almost-periods). But as we have seen in Example B.1 above there exist almost-periodic functions which are not periodic.

---

[2] This term is current in modern literature; the term originally used by Bohr (and still being used by others) is: "a translation number of $f(x)$ corresponding to ε" [Bohr51 p. 31].

[3] As we will see in Sec. B.5, this definition, initially given by Bohr, has been extended later in various different ways (for example, in order to lift the restriction of the continuity of $f(x)$). Each of these extensions defines a different class of almost-periodic functions, which is a superset of the class of Bohr-almost-periodic functions. We will use the general term "almost-periodic function" in the widest sense, and whenever a particular class of almost-periodic functions is intended we will refer to it specifically, such as: "Bohr-almost-periodic function" etc.

[4] As already pointed out in Example B.1 above, the property required by this definition is stronger than just having for any $\varepsilon > 0$ an arbitrarily large ε-almost-period τ_ε. The reasons for this choice are explained in [Bohr51 p. 32].

Almost-periodicity is not always as easy to identify visually as in Fig. B.1, and the graphic behaviour of an almost-periodic function may be quite complex. However, almost-periodic functions have the following structural properties:

(1) A (Bohr) almost-periodic function is bounded and uniformly continuous throughout $-\infty < x < \infty$ [Bohr51 pp. 33–35].

(2) A non-constant almost-periodic function does not tend to any limit when $x \to \pm\infty$; in fact, throughout $-\infty < x < \infty$ it oscillates irregularly between two finite extreme values without damping [Bass71 p. 345, 367].

Other important properties of almost-periodic functions include the following:

(3) If $f(x)$ is almost-periodic, so are $|f(x)|$, $cf(x)$ and $f(x+b)$ for any $a,b,c \in \mathbb{R}$, with the same almost-periods [Bass71 p. 344]. More generally, $cf(ax+b)$ is also almost-periodic [Corduneanu68 p. 11].

(4) If $f(x)$ and $g(x)$ are almost-periodic, so are $f(x) \pm g(x)$ and $f(x)g(x)$ [Bohr51 pp. 36–38]. If in addition $\inf_{-\infty<x<\infty} |g(x)| = m > 0$ then $1/g(x)$ and $f(x)/g(x)$ are also almost-periodic [Bohr51 pp. 34–35].

(5) Every almost-periodic function is representable as a generalized Fourier series and consequently has an impulsive spectrum.

This last property, which is probably the most remarkable of all, will be discussed in the following section.

B.4 The spectrum of almost-periodic functions

As we have seen in Appendix A, according to the Fourier theory if $p(x)$ is a periodic function of period T, then it can be uniquely developed into the form of a Fourier series:

$$p(x) \sim \sum_{n=-\infty}^{\infty} c_n \, e^{i2\pi nfx} \tag{B.2}$$

where the Fourier coefficients c_n are given by:

$$c_n = \frac{1}{T}\int_T p(x) \, e^{-i2\pi nfx} \, dx \tag{B.3}$$

(In all the above expressions $f = 1/T$ is the fundamental frequency of $p(x)$, and nf are its harmonics). Furthermore, if $p(x)$ satisfies certain convergence conditions (see Sec. C.12 in Appendix C), then the Fourier series indeed converges, and the '~' sign can be replaced by an equality: '='.

This implies that the spectrum of $p(x)$, $P(u)$, consists of impulses which are all included in a common impulse comb of step f, whose n-th impulse is located at the frequency $u = nf$

and its amplitude is c_n. Note that some, or even most, of the values c_n may be zero, as in the case of $p(x) = \cos(2\pi fx)$, where only the fundamental impulse pair, with indices $n = \pm 1$, has a non-zero amplitude.

One of the outstanding consequences of the theory of almost-periodic functions is that this result, namely, the correspondence between a periodic function and its Fourier series (and hence also with its spectrum), can be extended also to the case of almost-periodic functions [Bohr51 p. 50, 60]:

If $f(x)$ is an almost-periodic function then it can be uniquely[5] developed into the form of a *generalized Fourier series*:

$$f(x) \sim \sum_n c_n \, e^{i2\pi f_n x} \tag{B.4}$$

where f_n are arbitrary real numbers, called the *Fourier exponents* of $f(x)$, and the complex numbers c_n, called the *Fourier coefficients* of $f(x)$, are given by:

$$c_n = \lim_{T\to\infty} \frac{1}{T} \int_T f(x) \, e^{-i2\pi f_n x} \, dx \tag{B.5}$$

$\int_T$ means here an integration over any interval of length T, i.e., from x_0 to x_0+T where x_0 is arbitrary.[6]

Note that the infinite sum in (B.4) is a *generalized* Fourier series, in the sense that the frequencies f_n are no longer integer multiples (harmonics) of a fundamental frequency f, as was the case in the Fourier series (B.3) of a periodic function $p(x)$. In fact, the frequencies f_n may be here any denumerable set of arbitrary real numbers, which may have finite accumulation points or even be everywhere dense [EncMath88 Vol. 1 p. 155].

This means that the spectrum of an almost-periodic function consists of a denumerable set of impulses, which are located at the frequencies f_n and whose amplitudes are c_n:

$$P(u) = \sum_{n=-\infty}^{\infty} c_n \, \delta(u - f_n) \tag{B.6}$$

where $\delta(u)$ is the impulse symbol. In fact, almost-periodic functions are characterized by having *impulsive spectra* (also called *line-spectra*). This is a generalization of the spectrum of a periodic function: although it still consists of a denumerable set of impulses, it is no longer limited to a *comb* of impulses with a fixed step, as in Eq. (A.8), and it may consist of any set of impulses with arbitrary frequencies f_n, which may even be everywhere dense.

---

[5] Uniqueness is guaranteed for the Bohr-almost-periodic functions by the uniqueness theorem [Bohr51 p. 60]. In the case of generalized almost-periodic functions (see Sec. B.5 below) uniqueness is true up to a null function [Bohr51 p. 98].

[6] This integral is guaranteed to exist for every Bohr-almost-periodic function $f(x)$ by the mean value theorem [Bohr51 p. 39, 44]. However, it is interesting to note that the series (B.4) does not always converge to $f(x)$ in the sense of *uniform convergence* (not even in the case of Bohr-almost-periodic functions), but it does converge to $f(x)$ in the sense of *convergence in the square mean* (see, for example, [Bass71 p. 366]). In this sense, the symbol '~' can be replaced by an equality: '='.

The following converse statement is also true: if $\{f_n\}$ is a denumerable set of arbitrary real numbers and $\{c_n\}$ are complex numbers for which $\sum|c_n| < \infty$, then there exist a Bohr-almost-periodic function $f(x)$ which has (B.4) as its generalized Fourier series [Bohr51 p. 52].[7] Note that in contrast to the frequencies $\{f_n\}$, the amplitudes $\{c_n\}$ can not be completely arbitrary, and they must satisfy some conditions in order that the Fourier series (B.4) converge.

Example B.2: Consider the almost-periodic function $f(x)$ defined in Example B.1. Clearly, the spectrum of $f(x)$ is the sum of the spectra of its two terms, namely: it consists of a pair of impulses with amplitude 1/2 at the frequency of $\pm f_1 = 1/20$, and a pair of impulses with amplitude 1/8 at the frequency of $\pm f_2 = 1/\sqrt{2}$. And indeed, since f_1 and f_2 are incommensurable, these four impulses on the x axis are not located on any common comb. This is an almost-periodic case in which the number of impulses in the spectrum is finite. As we will see in Sec. B.5 below, this function belongs in fact to the subclass of quasi-periodic functions. ■

We conclude this section with one further remark concerning the connection between the almost-periods of an almost-periodic function and its Fourier exponents. In the periodic case, the fundamental period of a function $p(x)$ uniquely defines the set of its Fourier exponents: if $T > 0$ is the fundamental period of $p(x)$, then all its Fourier exponents are integer multiples of $f = 1/T$. It is interesting to note that there exists also a similar connection between the *almost-periods* of an almost-periodic function and its *Fourier exponents*, though it is not as simple as in the periodic case. More details on this subject can be found, for example, in [Levitan82 pp. 40–41].

B.5 The different classes of almost-periodic functions and their spectra

As we have seen in Sec. B.3, the definition of almost-periodic functions given by Bohr is only valid for *continuous* functions. This is however a severe restriction in our case, since it excludes all discontinuous functions such as square waves, gratings and their superpositions. Moreover, mathematically speaking, this class is, in a way, not fully complete, since it is only closed[8] under the strongest limiting process (uniform convergence for all $-\infty < x < \infty$), but not under other limiting processes. These considerations gave rise to many efforts to extend the definition of almost-periodic functions in various different ways (see: "Almost-periodic function", "Generalized almost-periodic functions" in [EncMath88]). A beautiful account on these different extensions and on the reciprocity between their definitions in terms of almost-periods and in terms of their Fourier series is given in [Bohr51 pp. 91–99]. Without going here into detail we will only mention that the widest (and most complete) class of almost-periodic

[7] For the wider class of Besicovitch-almost-periodic functions (see Sec. B.5 below) the weaker condition of $\sum|c_n|^2 < \infty$ is enough [Besicovitch32 p. xii].

[8] A set S is *closed* under a certain limiting process if it includes all the possible elements which can be obtained by applying this limiting process on sequences of members of S.

functions, known as the class of *Besicovitch almost-periodic functions*, contains all the Bohr almost-periodic functions plus other functions, including all "reasonably" discontinuous functions (and in particular all the discontinuous functions which may occur in our case, such as square waves, gratings, etc., and their superpositions; see Fig. B.2). In fact, in this class the requirement of continuity of $f(x)$ is replaced by the requirement of integrability in the Lebesgue sense [Bohr51 pp. 92–94].

It is interesting to note that the class of Bohr-almost-periodic functions (which is itself a subset of the Besicovitch class) contains, in turn, several subclasses of interest. These include:

(1) The subclass of *quasi-periodic functions* (also called *Bohl-almost-periodic functions*). This subclass contains all continuous functions which can be represented as:

$$\sum_{n_1=-\infty}^{\infty} \dots \sum_{n_m=-\infty}^{\infty} c_{n_1,\dots,n_m}\ e^{i2\pi(n_1 f_1+\dots+n_m f_m)x} \tag{B.7}$$

or in other words, all continuous almost-periodic functions whose Fourier exponents f_n in (B.4) are not completely arbitrary, but rather can be generated as a linear combination with integer coefficients of a finite number m of arbitrary (possibly incommensurable) frequencies $f_1,\dots,f_m$. Using our terminology, the Fourier exponents f_n in this case are simply the members of the module $\{n_1 f_1 + \dots + n_m f_m \mid n_i \in \mathbb{Z}\}$. It is said therefore that the support of the spectrum of $f(x)$ is *finitely generated*. Any sum or product of m continuous periodic functions belongs to this class [EncMath88 Vol. 1 p. 414]. And indeed, expression (B.7) has exactly the same form as Eqs. (6.3) and (6.5) that we obtained in Chapter 6 for the product of m periodic functions $p_1(x)\cdot\dots\cdot p_m(x)$ with periods $f_1,\dots,f_m$. The only detail which disqualifies the class of quasi-periodic functions for our needs in the treatment of layer superpositions is the fact that this class is restricted only to the case where $p_1(x),\dots,p_m(x)$ are *continuous* (which obviously excludes square waves, binary gratings etc.).

(2) The subclass of *limit-periodic functions* [Besicovitch32 pp. 32–34]. A function is called limit-periodic if it is the limit of a uniformly convergent sequence $\{f_n(x)\}$, $n = 1,2,\dots$ of continuous periodic functions. It can be shown [*ibid.*] that this subclass contains all the Bohr-almost-periodic functions whose Fourier exponents are rational multiples of one arbitrary number $f \in \mathbb{R}$, i.e., all functions which can be represented in the form:

$$f(x) \sim \sum_n c_n\, e^{i2\pi r_n f x} \qquad \text{where } r_n \in \mathbb{Q}. \tag{B.8}$$

(3) The subclass of periodic functions (which is a subclass of both the quasi-periodic and the limit-periodic classes).

Fig. B.3 gives a schematic description of the hierarchy of the different classes and subclasses of almost-periodic functions that are mentioned in this section.

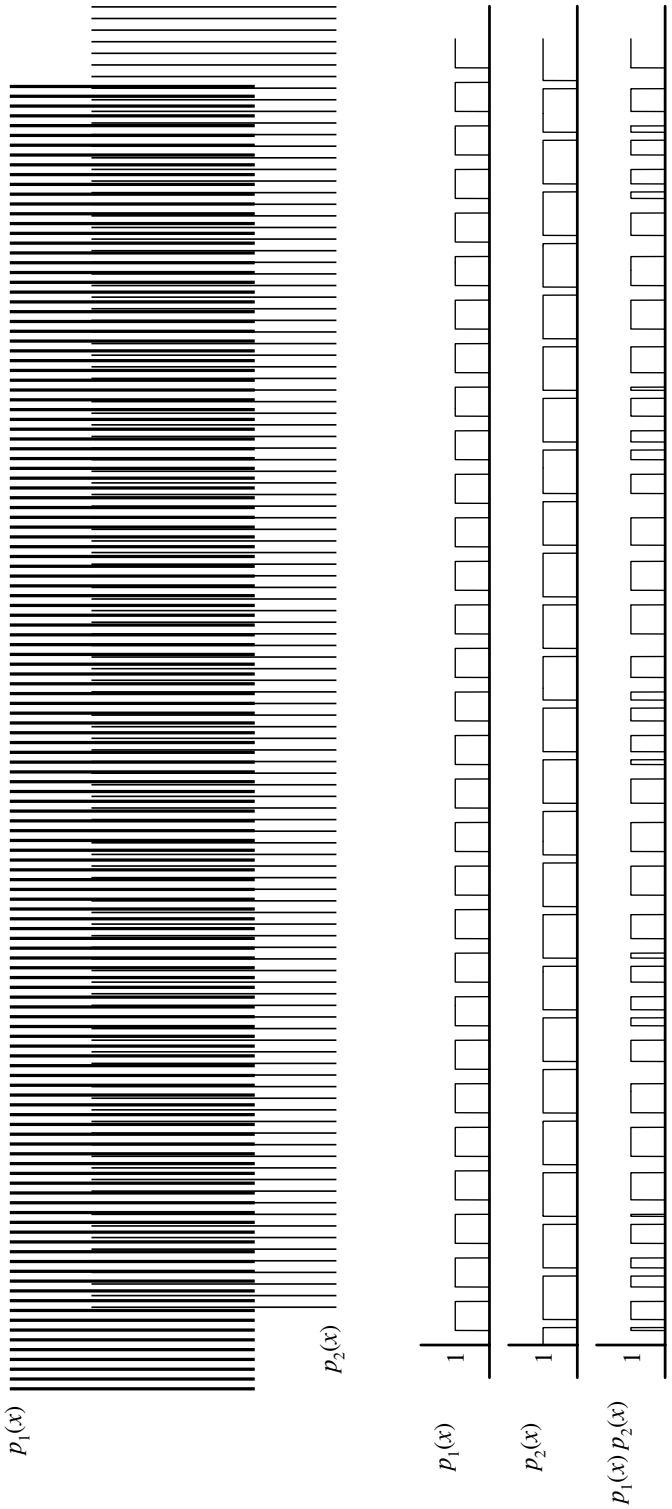

Figure B.2: Top: an example of a discontinuous (and hence non-Bohr) almost-periodic function, obtained as a superposition (= multiplication) of two periodic gratings with incommensurable frequencies f_1 and f_2. Bottom: a magnified section through the two gratings and their superposition (1 = white, 0 = black). Note the irregular microstructure of the superposition; both the pulse widths and their locations vary irregularly. Although the microstructure detail never repeats precisely, the global visual impression is that the superposition looks "almost" periodic with a low frequency of $f_2 - f_1$. In fact, the extracted intensity profile of this moiré, which eliminates all microstructure detail and only preserves the macrostructure of the moiré (see Fig. 4.2(a)), *is* indeed a periodic function with the frequency $f = f_2 - f_1$.

B.6 Characterization of functions according to their spectrum support

It will be interesting to conclude this discussion by a short review of the different classes of functions through the perspective of their spectral characteristics. Let us denote the support of the spectrum of the function $f(x)$ by F. Then:

(1) If $f(x)$ is a "pure vibration" [Bohr51 p. 2], namely: $\cos 2\pi fx$, $\sin 2\pi fx$, or more generally $a\cos(2\pi fx + b)$, then its spectrum simply consists of one pair of impulses:

$$F = \{\pm f\}$$

(2) If $f(x)$ is periodic with period $T = 1/f$, then its spectrum consists of a denumerable (finite or infinite) set of impulses, which are located on a common lattice (i.e., included in a common comb) with a fixed step of f:

$$F = \{nf \mid n \in \mathbb{Z}\}$$

(Note that some or even most of the impulses on the lattice may have a zero amplitude, as is case (1) above. But if $f(x)$ is discontinuous, like a square wave, then the number of non-zero impulses on the lattice is denumerably infinite.)

(3) If $f(x)$ is quasi-periodic, then its spectrum consists of a denumerable set of impulses which are located on a common module spanned by a finite number m of arbitrary (possibly incommensurable) frequencies $f_1,...,f_m$:

$$F = \{n_1 f_1 + ... + n_m f_m \mid n_i \in \mathbb{Z}\}$$

(Here, too, some or even most of the impulses may have a zero amplitude, as in the case of Example B.1, where $F = \{\pm f_1, \pm f_2\}$. However, if the number of non-zero impulses in F is infinite, then F may be everywhere dense.)

(4) If $f(x)$ is limit-periodic, then its spectrum consists of a finite or denumerable set of impulses which are located on rational multiples of one arbitrary frequency f:

$$F = \{r_n f \mid r_n \in \mathbb{Q}\}$$

Here, too, if the number of non-zero impulses is infinite, then F is everywhere dense.

(5) If $f(x)$ is almost-periodic (in the sense of Bohr, Besicovitch, etc.), then its spectrum consists of a denumerable set of impulses with any arbitrary frequencies:

$$F = \{f_n \in \mathbb{R} \mid n \in \mathbb{Z}\}$$

This is the most general case of impulsive spectrum, in which no restrictions exist on the values of the frequencies f_n, and they may have finite accumulation points, or even be everywhere dense.[9]

[9] Note that the inverse question of determining to which set of impulses in the spectrum there actually corresponds an almost-periodic function is more delicate, since it requires also conditions on the

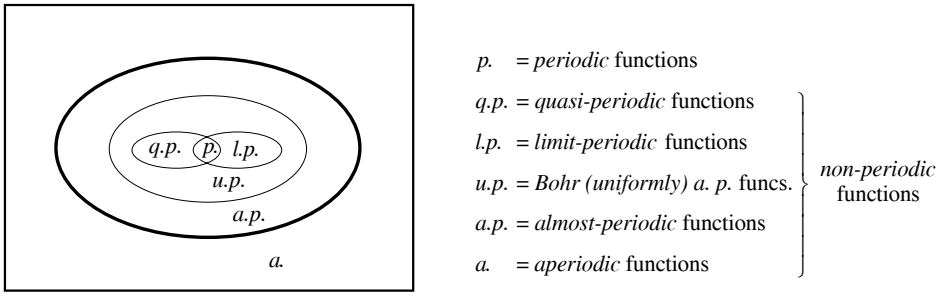

Figure B.3: A schematic diagram showing the classification of functions according to their periodicity properties, and the inclusion relationships between these different function-classes. The outside rectangle represents the universe of all functions; thin lines represent the borders of classes which are contained in each other, while thick borders separate between mutually exclusive classes.

It is interesting to note, just in order to complete the picture, that if we go one (big) step further and admit a non-denumerable set of frequencies f in the spectrum [Bohr51 pp. 2–3], then the summation in (B.4) is no longer denumerable and should be understood in the sense of integration. We arrive then to the realm of the functions $f(x)$ which are representable by:[10]

$$f(x) \sim \int_{-\infty}^{\infty} F(u)\, e^{i2\pi ux}\, du \tag{B.9}$$

rather than by (B.4): $f(x) \sim \sum_n c_n\, e^{i2\pi f_n x}$

$F(u)$ plays in (B.9) the same role as the Fourier coefficients c_n in (B.4), namely: assigning the proper amplitudes (weights) to the various frequencies. It can be said, therefore, that in this case the spectrum of the function $f(x)$ is a function of the continuous frequency u, which is given by:

$$F(u) \sim \int_{-\infty}^{\infty} f(x)\, e^{-i2\pi ux}\, dx \tag{B.10}$$

Visibly, this is the continuous counterpart of the impulsive spectrum of almost-periodic functions: as we have seen, in the almost-periodic case the spectrum is only defined on a denumerable set of frequencies $\{f_n\}$, and its impulse amplitudes at these frequencies are given by Eq. (B.5):

---

impulse amplitudes in order to guarantee that their Fourier series indeed converges and "makes sense" [Besicovitch32 p. xii–xiii]. The same is true also for the previous function classes having infinitely many impulses in their spectra, such as periodic functions, etc.

[10] By convention we use here the letter 'u' rather than 'f' to denote the frequency values.

$$c_n = \lim_{T\to\infty} \frac{1}{T}\int_T f(x)\, e^{-i2\pi f_n x}\, dx$$

Note, however, that these amplitudes can be also regarded as a function of the continuous frequency u $(-\infty < u < \infty)$:

$$c(u) = \lim_{T\to\infty} \frac{1}{T}\int_T f(x)\, e^{-2\pi u x}\, dx \tag{B.11}$$

And indeed, a fundamental theorem in the theory of almost-periodic functions states that for any almost-periodic function $f(x)$, the function (B.11) is zero for all values of u with the exception of an at most denumerable set of numbers $u = f_n$ [Bohr51 p. 48–50; the equivalent theorem for the periodic case is given on pp. 50–51]. These numbers $\{f_n\}$ are the Fourier exponents of $f(x)$, i.e., the frequencies which appear in the Fourier series (B.4), and the values of $c(u)$ at these points, $c_n = c(f_n)$, are the Fourier coefficients of $f(x)$.

We recognize, of course, that (B.10) and (B.9) above are simply the formulas of the (continuous) Fourier transform and inverse Fourier transform of the (aperiodic) function $f(x)$; $F(u)$ is the continuous-frequency spectrum of $f(x)$.

It can be said, therefore, roughly speaking, that making the step from denumerable to non-denumerable spectra is the spectral-domain equivalent of proceeding from almost-periodic to aperiodic functions in the image domain. More on the subject of impulsive and continuous spectra can be found in Chapter 11 of [Champeney87], especially on pp. 109–114.[11]

B.7 Almost-periodic functions in two variables

The theory of almost-periodic functions can be also extended to functions of two or more variables (see, for instance, [Besicovitch32 pp. 59–66]); for our needs, however, we are only concerned with the 2D case, i.e., the case of two variables.

The 2D generalized Fourier series representation of an almost-periodic function $f(x,y)$, namely, the 2D extension of (B.4), is given by:

$$f(x,y) \sim \sum_m \sum_n c_{m,n}\, e^{i2\pi(u_{m,n}x + v_{m,n}y)} \tag{B.12}$$

or in the more compact vector notation:

$$f(\mathbf{x}) \sim \sum_m \sum_n c_{m,n}\, e^{i2\pi \mathbf{f}_{m,n}\cdot\mathbf{x}} \tag{B.13}$$

---

[11] It should be noted, however, that many authors present the transition between impulsive and continuous spectra as a limiting process directly between the periodic and aperiodic cases, ignoring the intermediate case of almost-periodic functions. Such a transition from Fourier series to the Fourier transform as a limit case is given, for example, in [Cartwright90 pp. 101–103], [Bracewell86 pp. 208–209] and [Gaskill78 pp. 111–112]. For the inverse direction, i.e., obtaining the Fourier series as a limit case of the Fourier transform, see [Cartwright90 pp. 99–101]; [Bracewell86 pp. 205–208].

where $\mathbf{f}_{m,n} = (u_{m,n},v_{m,n})$, the (m,n)-th Fourier exponents, are arbitrary points in $\mathbb{R}^2$ (i.e., in the (u,v) frequency plane of the spectrum), and $\mathbf{x} = (x,y)$. Note that an even more compact notation can be obtained by substituting $\mathbf{n}$ for (m,n) in the indices:

$$f(\mathbf{x}) \sim \sum_{\mathbf{n}} c_{\mathbf{n}}\, e^{i2\pi \mathbf{f}_{\mathbf{n}}\cdot\mathbf{x}} \tag{B.14}$$

However, for the sake of clarity we will usually prefer the form of (B.13). The Fourier coefficients $c_{m,n}$ of $f(x,y)$, i.e., the 2D extension of (B.5), are given by:

$$c_{m,n} = \lim_{T\to\infty} \frac{1}{T^2} \iint_{TT} f(\mathbf{x})\, e^{-i2\pi \mathbf{f}_{m,n}\cdot\mathbf{x}}\, d\mathbf{x} \tag{B.15}$$

where $\iint_{TT}$ means an integration over any square interval of side T, i.e., over the area defined by the points (x_0,y_0), (x_0+T,y_0), (x_0,y_0+T) and (x_0+T,y_0+T) where x_0 and y_0 are arbitrary.

The spectrum of the 2D almost-periodic function (B.12) is given by:

$$P(u,v) = \sum_{m=-\infty}^{\infty} \sum_{n=-\infty}^{\infty} c_{m,n}\, \delta(u-u_{m,n}, v-v_{m,n}) \tag{B.16}$$

which is the 2D extension of Eq. (B.6).

Examples of 2D almost-periodic functions appear throughout this book; let us mention here, for instance, the superposition of three identical dot-screens with angle differences of 30° that is traditionally used in colour printing (see Example 5.13 in Sec. 5.7).

For the sake of comparison, we recall from Sec. A.3 in Appendix A that the Fourier series representation of the 2-fold periodic function $p(x,y)$ whose periods are $T_x = 1/u_0$ and $T_y = 1/v_0$ is given by (A.11):

$$p(x,y) \sim \sum_{m=-\infty}^{\infty} \sum_{n=-\infty}^{\infty} c_{m,n}\, e^{i2\pi(mu_0 x + nv_0 y)}$$

Note that the vector notation of this expression is identical to (B.13), with only $\mathbf{f}_{m,n} = (mu_0,nv_0)$ replacing the more general $\mathbf{f}_{m,n} = (u_{m,n},v_{m,n})$. The Fourier coefficients $c_{m,n}$ in the 2-fold periodic case are given by Eq. (A.14):

$$c_{m,n} = \frac{1}{T_x T_y} \iint_{T_x T_y} p(\mathbf{x})\, e^{-i2\pi \mathbf{f}_{m,n}\cdot\mathbf{x}}\, d\mathbf{x}$$

instead of Eq. (B.15) of the almost-periodic case; and the spectrum of the 2-fold periodic function $p(x,y)$ is given by Eq. (A.16):

$$P(u,v) = \sum_{m=-\infty}^{\infty} \sum_{n=-\infty}^{\infty} c_{m,n}\, \delta(u-mu_0, v-nv_0)$$

instead of the more general expression (B.16) in the almost-periodic case.

Note that there exist also "hybrid" functions which are periodic in one direction and almost-periodic in the other direction (see Sec. 6.2). These hybrid cases are still considered as almost-periodic functions.

Appendix C

Miscellaneous issues and derivations

C.1 Derivation of the classical moiré formula (2.9) of Sec. 2.4

We show here that the classical formula (2.9) is simply a special case of Eqs. (2.28) and (2.8), that is obtained when the number of superposed gratings is $m=2$, and the moiré in question is the (1,-1)-moiré, namely: $k_1=1$, $k_2=-1$. In this particular case (2.28) reduces to:

$$u = f_1 \cos\theta_1 - f_2 \cos\theta_2$$

$$v = f_1 \sin\theta_1 - f_2 \sin\theta_2$$

Therefore we have by Eq. (2.8):

$$\begin{aligned} f^2 &= u^2 + v^2 \\ &= f_1^2 \cos^2\theta_1 - 2f_1f_2 \cos\theta_1\cos\theta_2 + f_2^2 \cos^2\theta_2 \\ &\qquad + f_1^2 \sin^2\theta_1 - 2f_1f_2 \sin\theta_1\sin\theta_2 + f_2^2 \sin^2\theta_2 \\ &= f_1^2 (\cos^2\theta_1 + \sin^2\theta_1) - 2f_1f_2 (\cos\theta_1\cos\theta_2 + \sin\theta_1\sin\theta_2) + f_2^2 (\cos^2\theta_2 + \sin^2\theta_2) \\ &= f_1^2 - 2f_1f_2 \cos(\theta_2-\theta_1) + f_2^2 \end{aligned}$$

In terms of periods rather than frequencies we have, therefore (where $\alpha = \theta_2-\theta_1$):

$$\begin{aligned} \frac{1}{T_M^2} &= \frac{1}{T_1^2} - 2\frac{1}{T_1}\frac{1}{T_2}\cos\alpha + \frac{1}{T_2^2} \\ &= \frac{T_2^2 - 2T_1T_2\cos\alpha + T_1^2}{(T_1T_2)^2} \end{aligned}$$

which finally gives, indeed, the period T_M of the moiré, as predicted by formula (2.9):

$$T_M = \frac{T_1T_2}{\sqrt{T_1^2 + T_2^2 - 2T_1T_2\cos\alpha}}$$

As for the angle φ_M of the moiré, we obtain from Eqs. (2.8) and (2.28):

$$\varphi_M = \arctan(v/u) = \arctan\left(\frac{f_1\sin\theta_1 - f_2\sin\theta_2}{f_1\cos\theta_1 - f_2\cos\theta_2}\right)$$

$$= \arctan\left(\frac{\frac{\sin\theta_1}{T_1} - \frac{\sin\theta_2}{T_2}}{\frac{\cos\theta_1}{T_1} - \frac{\cos\theta_2}{T_2}}\right) = \arctan\left(\frac{T_2\sin\theta_1 - T_1\sin\theta_2}{T_2\cos\theta_1 - T_1\cos\theta_2}\right) \quad \blacksquare$$

C.2 Derivation of the first part of Proposition 2.1 of Sec. 2.5

We show in this section that if the values of the periodic function $p(x)$ are bounded between 0 and 1 then its Fourier series coefficients (impulse amplitudes) given by (A.2) satisfy: $0 \le a_0 \le 1$, and for any $n \neq 0$: $|a_n| \le 1/\pi$, $|b_n| \le 1/\pi$.

Proof: According to (A.4) we have:

$$a_0 = \frac{1}{T}\int_T p(x)\,dx$$

a_0 is, therefore, the average value of $p(x)$ on a single period; and since $0 \le p(x) \le 1$ it is obvious that $0 \le a_0 \le 1$.

Now, according to (A.4) we have for any $n \neq 0$:

$$a_n = \frac{1}{T}\int_T p(x)\cos(2\pi nx/T)\,dx \tag{C.1}$$

The function $\cos(2\pi nx/T)$ is periodic with the period T/n, and therefore it makes exactly n full cosinusoidal cycles (periods) within the interval T, oscillating between 1 and –1. Its total area within the interval T is therefore 0 (see Fig. C.1).

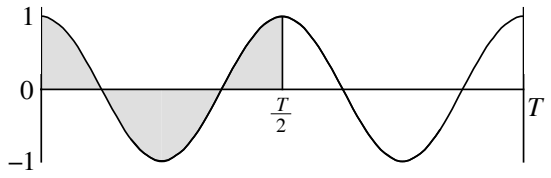

Figure C.1: The function $\cos(2\pi nx/T)$ for $n = 2$.

Now, since the value of the function $p(x)$ is bounded between 0 and 1, it is clear that the most it can do to increase the area defined by the integral (C.1) is to become 0 at all the negative areas of $\cos(2\pi nx/T)$ in order to mask them out. But even then, the maximum possible area left within the interval T is the positive area of $\cos(2\pi nx/T)$, which equals $2n$ times the area of half a lobe, namely:

$$2n\int_0^{\frac{T}{4n}} \cos(2\pi nx/T)\,dx = 2n\left[\frac{\sin(2\pi nx/T)}{2\pi n/T}\right]_0^{\frac{T}{4n}} = \frac{\sin(\pi/2)}{\pi/T} = \frac{T}{\pi}$$

which means by (C.1) that $a_n \le 1/\pi$. In a similar way, by masking out the positive areas we obtain $a_n \ge -1/\pi$, and hence, by combining both results we get, indeed, $|a_n| \le 1/\pi$.

$|b_n| \le 1/\pi$ is obtained in a similar way. ■

C.3 Invariance of the impulse amplitudes under rotations and x,y scalings

We used in Secs. 4.2 and 4.3 the fact that stretching and rotating a periodic (or doubly periodic) image does not affect the *impulse amplitudes* of its comb (or nailbed), but only their *impulse locations* in the spectrum. In this section we show how these properties can be derived, based on well-known results in the Fourier theory. We will use here the letters p and P to denote a periodic function and its spectrum, and the letters f and F to denote an arbitrary function (not necessarily periodic) and its spectrum.

C.3.1 Invariance of the 2D Fourier transform under rotations

The rotation-invariance property of the 2D Fourier transform means that a rotation of $f(x,y)$ in the image domain by angle θ has no effect on its spectrum $F(u,v)$ other than a rotation by the same angle θ. This property of the 2D Fourier transform, which is valid for any function, is guaranteed by the rotation theorem [Bracewell95 p. 157]. This invariance of the 2D Fourier transform under rotation is a special case of its more complex behaviour under a general linear transformation, which is given for instance in [Bracewell95 p. 160].

C.3.2 Invariance of the impulse amplitudes under x, y scalings

According to the similarity theorem [Bracewell86 p. 244], for any function $f(x,y)$ with Fourier transform $F(u,v)$ we have:

$$f(ax,by) \;\leftrightarrow\; \frac{1}{|ab|}F(u/a,v/b) \tag{C.2}$$

However, a special case of interest occurs with periodic functions, where the spectrum is impulsive. In this case, thanks to the particular scaling property of $\delta(u,v)$ [Bracewell86 p. 85]: $\delta(u/a,v/b) = |ab|\,\delta(u,v)$, the factor $1/|ab|$ in Eq. (C.2) is cancelled out, and we obtain [Bracewell86 p. 103]:

$$p(ax,by) \;\leftrightarrow\; P(u/a,v/b)$$

This is usually formulated in the following way (see, for example, the 1D equivalent in [Cartwright90 pp. 59–61]):

Let the function $p(x,y)$ be periodic with periods T_x, T_y and generate the Fourier series:

$$p(x,y) \;\sim \sum_{m=-\infty}^{\infty}\sum_{n=-\infty}^{\infty} a_{m,n}\cos 2\pi\left(\frac{mx}{T_x}+\frac{ny}{T_y}\right) \;+ \sum_{m=-\infty}^{\infty}\sum_{n=-\infty}^{\infty} b_{m,n}\sin 2\pi\left(\frac{mx}{T_x}+\frac{ny}{T_y}\right)$$

Then $p(ax,by)$ is periodic with periods T_x/a, T_y/b, and the Fourier series it generates preserves the original coefficients (impulse amplitudes) $a_{m,n}$ and $b_{m,n}$:

$$p(ax,by) \;\sim \sum_{m=-\infty}^{\infty}\sum_{n=-\infty}^{\infty} a_{m,n}\cos 2\pi\left(\frac{mx}{T_x/a}+\frac{ny}{T_y/b}\right) \;+ \sum_{m=-\infty}^{\infty}\sum_{n=-\infty}^{\infty} b_{m,n}\sin 2\pi\left(\frac{mx}{T_x/a}+\frac{ny}{T_y/b}\right)$$

C.4 Shift and phase

This section, which complements the introduction to Chapter 7, provides a more detailed explanation on the connection between the phase in the context of complex number theory and the phase in periodic functions.

C.4.1 The shift theorem

Let $f(x)$ be a 1D function (periodic or not) in the image domain, and let $F(u)$ be its spectrum. As already mentioned in Sec. 2.2, if $f(x)$ is symmetric about the origin then its spectrum $F(u)$ is purely real; and if $f(x)$ is non-symmetric or non-centered about the origin then $F(u)$ is complex-valued (its imaginary part is non-zero).

Assume now that we shift $f(x)$ in the image domain by a. The shift theorem [Bracewell86 p. 104] states that if the spectrum of $f(x)$ is $F(u)$, then the spectrum of the shifted function $f(x-a)$ is $F_a(u) = e^{-i2\pi ua} \cdot F(u)$. This means that a shift of a in the image domain multiplies the spectrum at each frequency u by the complex factor $e^{-i2\pi ua}$. Therefore, even if the spectrum $F(u)$ of the unshifted function $f(x)$ is purely real, the spectrum $F_a(u)$ of the shifted function $f(x-a)$ is a complex-valued function of the real variable u, namely: $F_a : \mathbb{R} \to \mathbb{C}$.

The situation in the 2D case is similar: Assume that $f(x,y)$ is a 2D function (periodic or not) in the image domain and that $F(u,v)$ is its spectrum. Then, according to the 2D shift theorem [Bracewell95 p. 156], the spectrum of the shifted function $f(x-a, y-b)$ is $F_{a,b}(u,v) = e^{-i2\pi(ua+vb)} \cdot F(u,v)$. In other words, a shift of $\mathbf{a} = (a,b)$ in the image domain multiplies the spectrum at each frequency $\mathbf{f} = (u,v)$ by the complex factor $e^{-i2\pi \mathbf{f}\cdot\mathbf{a}}$. We see, therefore, that as in the 1D case, even if the spectrum $F(u,v)$ of the unshifted function $f(x,y)$ is purely real, the spectrum $F_{a,b}(u,v)$ of the shifted function $f(x-a, y-b)$ is a complex-valued function of the real variables u,v, namely: $F_{a,b} : \mathbb{R}^2 \to \mathbb{C}$.

It may be in order, therefore, to review here some of the properties of complex-valued functions. We will do it here for complex-valued functions of two real variables, but the situation in the case of a single real variable is completely analogous.

A complex-valued function $F(u,v)$ can be represented either by its real and its imaginary parts:

$$F(u,v) = \mathrm{Re}[F(u,v)] + i\ \mathrm{Im}[F(u,v)]$$

or, using the polar notation, by its *magnitude* (also called *absolute value* or *modulus*) and its *phase* (also called *argument*):

$$F(u,v) = \mathrm{Abs}[F(u,v)] \cdot e^{i\ \mathrm{Arg}[F(u,v)]}$$

where:

$$\mathrm{Abs}[F(u,v)] = \sqrt{\mathrm{Re}[\mathrm{F}(u,v)]^2 + \mathrm{Im}[\mathrm{F}(u,v)]^2}$$

$$\mathrm{Arg}[F(u,v)] = \arctan \frac{\mathrm{Im}[\mathrm{F}(u,v)]}{\mathrm{Re}[\mathrm{F}(u,v)]}$$

Note that Re[$F(u,v)$], Im[$F(u,v)$], Abs[$F(u,v)$] and Arg[$F(u,v)$] are all real-valued functions of the real variables u,v. The functions Abs[$F(u,v)$] and Arg[$F(u,v)$] represent the local magnitude and the local phase of the complex-valued function $F(u,v)$ at the point (u,v). Therefore, by analogy with the polar notation of a complex number, the complex-valued function $F(u,v)$ can be interpreted as a phasor (a varying radius-vector) rotating in the complex plane, whose length and angle at any point (u,v) are given, respectively, by Abs[$F(u,v)$] and Arg[$F(u,v)$].[1] As Abs[$F(u,v)$] varies with u and v, the length of the vector varies, and as Arg[$F(u,v)$] varies with u and v, the direction of the vector varies. (A good, concise introduction on phasors can be found, for example, in [Gaskill78 pp. 18–29].) Therefore, in the context of complex number theory the term "the phase of the function $F(u,v)$" refers to the argument Arg[$F(u,v)$], which represents the angle of the phasor of $F(u,v)$ in the complex plane at each point (u,v) of the u,v plane.

Now, if $F(u,v)$ is the spectrum of $f(x,y)$, then according to the 2D shift theorem the spectrum of the shifted function $f(x-a, y-b)$ is $F_{a,b}(u,v) = e^{-i2\pi(ua+vb)} \cdot F(u,v)$, or, using the polar notation: $F_{a,b}(u,v) = \text{Abs}[F(u,v)] \cdot e^{i[\text{Arg}[F(u,v)] - 2\pi(ua+vb)]}$. We obtain, therefore, that:

$$\text{Abs}[F_{a,b}(u,v)] = \text{Abs}[F(u,v)]$$

$$\text{Arg}[F_{a,b}(u,v)] = \text{Arg}[F(u,v)] - 2\pi(ua + vb)$$

This means that a shift of (a,b) in $f(x,y)$ in the image domain does not influence the magnitude of the spectrum, but it does decrement its phase at any point (u,v) by $2\pi(ua + vb)$. We obtain, therefore, the following corollary:

Corollary of the 2D shift theorem: When a function $f(x,y)$ in the image domain is shifted by (a,b), its *magnitude-spectrum* (i.e., the magnitude of its complex spectrum) remains unchanged, but its *phase-spectrum* (i.e., the phase, or the argument, of its complex spectrum) is linearly decremented at any point (u,v) of the u,v plane by the linear function $2\pi(ua + vb)$. ■

We see, therefore, that the increment generated in the phase spectrum due to a shift of **a** in the image domain is a linear function of the frequency, i.e., it is a continuous linear plane through the origin, whose slopes are determined by $\mathbf{a} = (a,b)$.[2] Denoting this phase increment by φ we have, therefore:

$$\varphi(\mathbf{f}) = -2\pi\mathbf{f}\cdot\mathbf{a}$$

namely: $$\varphi(u,v) = -2\pi(ua + vb) \qquad \text{(C.3)}$$

Similarly, we can obtain from the 1D shift theorem the 1D counterpart of the above corollary:

---

[1] Note that the complex plane should not be confused here with the u,v plane: the complex-valued function $F(u,v)$ is defined on the u,v plane, but its image is located in the complex plane $\mathbb{C}$.

[2] Note that the converse is also true: it follows from the shift theorem that a linear increment occurs in the phase-spectrum *iff* the original function has undergone a shift in the image domain.

Corollary of the 1D shift theorem: When a function $f(x)$ in the image domain is shifted by a, its *magnitude-spectrum* remains unchanged, but its *phase-spectrum* is linearly decremented at any frequency u by $2\pi ua$. ■

As we can see, the 1D case is indeed a straightforward simplification of the 2D case: The increment generated in the phase spectrum due to a shift of a in the image domain is a linear function of the frequency u, i.e., it is a straight line through the origin, whose slope is determined by a. Denoting this phase increment by φ, the 1D equivalent of Eq. (C.3) is given therefore by:

$$\varphi(u) = -2\pi ua \tag{C.4}$$

C.4.2 The particular case of periodic functions

Let us return now from the general shift theorem to the particular case of periodic functions. Let $p(x,y)$ (or in short, $p(\mathbf{x})$) be a 2-fold periodic function with fundamental frequency vectors $\mathbf{f}_1 = (u_1,v_1)$, $\mathbf{f}_2 = (u_2,v_2)$ (see Sec. A.3.4 in Appendix A). As we have seen above, Eq. (C.3) says that for any given $f(x,y)$ the increment generated in the phase-spectrum due to a shift of $\mathbf{a}$ in the image domain is a linear function of the frequency, i.e., a continuous plane whose slopes are determined by $\mathbf{a} = (a,b)$. In our case, however, the spectrum of $p(\mathbf{x})$ is an impulse nailbed, whose (m,n)-th impulse has the frequency $\mathbf{f} = m\mathbf{f}_1+n\mathbf{f}_2$, or in other words: $(u,v) = m(u_1,v_1) + n(u_2,v_2) = (mu_1+nu_2\ ,\ mv_1+nv_2)$. This spectrum is given in vector form by Eq. (A.30) in Appendix A. The phase increment generated at the (m,n)-th impulse in the spectrum as a result of the shift of $\mathbf{a}$ in the image domain is, therefore:

$$\begin{aligned} &\varphi(m\mathbf{f}_1+n\mathbf{f}_2) = -2\pi(m\mathbf{f}_1+n\mathbf{f}_2)\cdot\mathbf{a} \\ \text{namely:}\quad &\varphi(mu_1+nu_2\ ,\ mv_1+nv_2) = -2\pi[(mu_1+nu_2)a + (mv_1+nv_2)b] \end{aligned} \tag{C.5}$$

which is simply the restriction of the linear plane (C.3) to the points of our nailbed. In other words, Eq. (C.5) samples the continuous plane (C.3) of the phase-spectrum increment, which is owed to the shift theorem, at all the impulse locations $m\mathbf{f}_1+n\mathbf{f}_2$. This is clearly seen in the spectrum of the shifted function $p(\mathbf{x}-\mathbf{a})$ (see Eq. (7.4)).

Similarly, in the case of a 1-fold periodic function $p(x)$, the spectrum is an impulse comb whose n-th impulse has the frequency $u = nf$ (this spectrum is given by Eq. (A.8) in Appendix A). The phase increment generated at the n-th impulse in the spectrum as a result of the shift of a in the image domain is, therefore:

$$\varphi(nf) = -2\pi nfa \tag{C.6}$$

which is simply the restriction of the straight line (C.4) to the points of our comb. In other words, Eq. (C.6) samples the continuous line (C.4) of the phase-spectrum increment, which is due to the shift theorem, at all the impulse locations nf.

C.4.3 The phase of a periodic function: the φ and the ϕ notations

We have seen until now how shifts of a function in the image domain are related to phase changes in the spectrum, where the term "phase" is understood as the argument of the complex spectrum.

However, in the particular case of periodic functions the term "phase" can be also used in a different sense, which is related, this time, to the image domain. Consider, as a simple example, the 1D periodic function $p(x) = \cos(2\pi fx)$, whose period is $T = 1/f$. Its counterpart that is shifted in the image domain by a is given by: $p(x-a) = \cos(2\pi f(x-a))$. As explained in detail in Sec. 7.3, an alternative way to specify the amount of shift in a periodic function is to state it as a fraction of the period T: $\phi = \frac{a}{T} = fa$. This value is often called in literature the *phase* of the shifted function $p(x-a)$; for example, when $\phi = n$, $n \in \mathbb{Z}$, it is said that $p(x)$ and $p(x-a)$ are "in phase", and when $\phi = n+\frac{1}{2}$ it is said that they are "in counter-phase". In order to avoid confusion between the two meanings of the term "phase" we prefer to call ϕ the *period-shift* of the periodic function; this name will clearly distinguish it from the phase $\text{Arg}[P_a(u)]$ and the phase increment φ which were defined in the context of complex number theory. Obviously, the period-shift ϕ is only meaningful in periodic functions, while the phase increment φ in the sense of complex numbers is meaningful in the spectrum of any function. Therefore, in the case of a periodic function both ϕ and φ can be used as a measure of its shifts in the image domain.

Let us first illustrate this for the case of a 1D periodic function $p(x)$ and its shifted copy $p(x-a)$. As we have seen above, the shift of a in the image domain is expressed, in terms of the phase increment of the complex spectrum, by the linear function (C.4):

$$\varphi(u) = -2\pi ua$$

But in our particular case in which the shifted function is periodic this continuous line is sampled (and is only meaningful) at the frequencies $u = nf$ ($n \in \mathbb{Z}$), since the impulsive spectrum is only defined at these points. The phase increment of the n-th impulse in the spectrum of $p(x-a)$ owed to the shift a is given, therefore, by:

$$\varphi(nf) = -2\pi nfa$$

or:

$$\varphi(nf) = -2\pi n\phi$$

where the period-shift $\phi = fa = \frac{a}{T}$ expresses the shift of the periodic function $p(x-a)$ in the image domain in terms of its period. This equation gives, indeed, the connection between φ and ϕ, which are both measures of the shift a in the periodic function $p(x)$: While ϕ describes the shift in terms of the period of $p(x)$, φ describes the shift as an angle difference in the complex plane (where for the n-th impulse, $\varphi = -2\pi n$ is equivalent to a shift of one full period, $\phi = 1$).

This connection between φ and ϕ can be also generalized to the case of a 2-fold periodic function $p(\mathbf{x})$. As explained in detail in Sec. 7.5.2, an alternative way to specify the amount

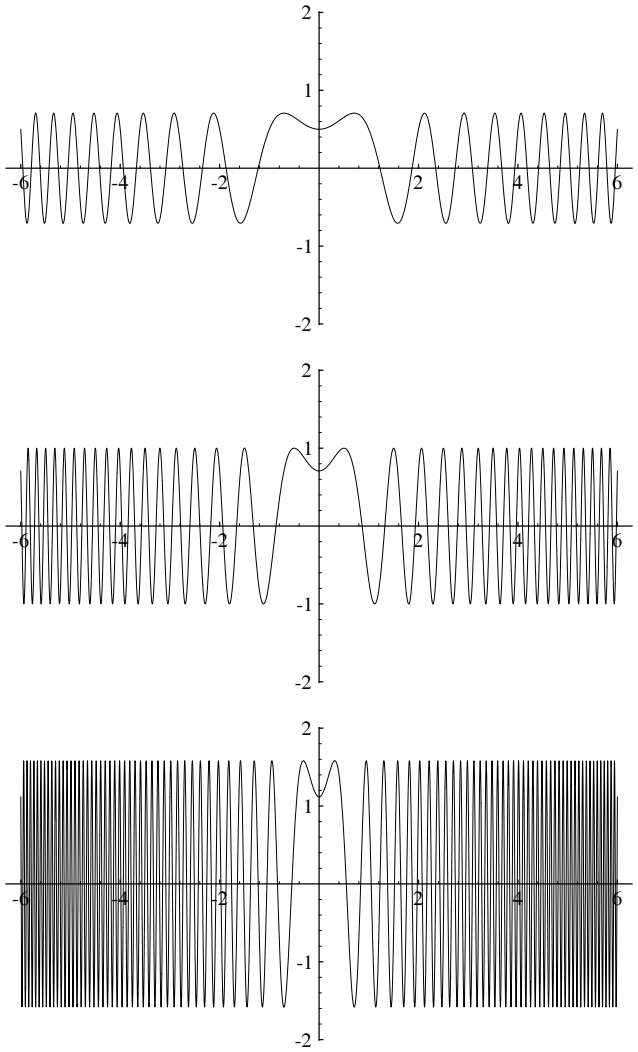

Figure C.2: The function $R_c(u) = \frac{1}{2\sqrt{fa}}(\cos(\frac{\pi}{2fa}u^2) + \sin(\frac{\pi}{2fa}u^2))$ with $f = 1$ and three different values of a: $a = 1$ (top), $a = 0.5$ (center) and $a = 0.2$ (bottom).

of shift in a 2-fold periodic function is to state it using the period-shifts ϕ_1 and ϕ_2, i.e., as fractions of the two periods $\mathbf{T}_1$ and $\mathbf{T}_2$. And indeed, as we can see in Eq. (7.12) at the end of Sec. 7.5.2, the phase increment of the (m,n)-th impulse in the spectrum of $p(\mathbf{x}-\mathbf{a})$ owing to the shift $\mathbf{a}$ can be expressed by:

$$\varphi(m\mathbf{f}_1+n\mathbf{f}_2) = -2\pi(m\phi_1+n\phi_2) \tag{C.7}$$

This equation is, indeed, the connection between φ and ϕ in the 2D case.

It should be noted, however, that in Chapters 7 and 8 we usually use the period-shifts ϕ, while the phase increment φ is only occasionally mentioned.

C.5 The function $R_c(u)$ converges to $\delta(u)$ as $a \to 0$

We derive here the rather surprising fact (see Sec. 10.4.1) that in spite of its undamped oscillatory nature, the function $R_c(u) = \frac{1}{2\sqrt{fa}}(\cos(\frac{\pi}{2fa}u^2) + \sin(\frac{\pi}{2fa}u^2))$ tends when $a \to 0$ to the impulse $\delta(u)$ (see Fig. C.2). Following [Gelfand64 pp. 36–38], we have to show for this end that: (a) the total area under $R_c(u)$ is 1 independently of a; and (b) the area under $R_c(u)$ in the ranges (u_1,u_2) and $(-u_2,-u_1)$ for any $u_2 > u_1 > 0$ tends to zero when $a \to 0$.

We start by showing part (a). Since we have [Spiegel68 p. 97]:

$$\int_0^\infty \sin cx^2\, dx = \int_0^\infty \cos cx^2\, dx = \tfrac{1}{2}\sqrt{\frac{\pi}{2c}}$$

it follows that:

$$\begin{aligned}\int_0^\infty R_c(u)\, du &= \frac{1}{2\sqrt{fa}}\int_0^\infty (\cos(\tfrac{\pi}{2fa}u^2) + \sin(\tfrac{\pi}{2fa}u^2))\, du \\ &= \frac{1}{2\sqrt{fa}}\left(\tfrac{1}{2}\sqrt{fa} + \tfrac{1}{2}\sqrt{fa}\right) = \tfrac{1}{2}\end{aligned}$$

and since $R_c(u)$ is symmetric we obtain, as required:

$$\int_{-\infty}^\infty R_c(u)\, du = 2\int_0^\infty R_c(u)\, du = 1.$$

Proceeding now to part (b), we wish to show that for any $u_2 > u_1 > 0$ we have:

$$\lim_{a \to \infty} \int_{u_1}^{u_2} R_c(u)\, du = 0.$$

And indeed, using the formulas [Gradshteyn94 pp. 178–179]:

$$\int \sin cx^2\, dx = \sqrt{\frac{\pi}{2c}}\, S(\sqrt{c}\, x)$$

$$\int \cos cx^2\, dx = \sqrt{\frac{\pi}{2c}}\, C(\sqrt{c}\, x)$$

where $S(x)$ and $C(x)$ are the Fresnel sine and cosine integrals, defined as:

$$S(x) = \sqrt{\frac{2}{\pi}}\int_0^x \sin t^2\, dt$$

$$C(x) = \sqrt{\frac{2}{\pi}}\int_0^x \cos t^2\, dt$$

we obtain:

$$\int_{u_1}^{u_2} R_c(u)\,du = \frac{1}{2\sqrt{fa}}\int_{u_1}^{u_2} \left(\cos(\tfrac{\pi}{2fa}u^2) + \sin(\tfrac{\pi}{2fa}u^2)\right) du$$

$$= \frac{1}{2\sqrt{fa}}\left(\left[\sqrt{fa}\; C(\sqrt{\tfrac{\pi}{2fa}}x)\right]_{u_1}^{u_2} + \left[\sqrt{fa}\; S(\sqrt{\tfrac{\pi}{2fa}}x)\right]_{u_1}^{u_2}\right)$$

$$= \tfrac{1}{2}\left([C(\sqrt{\tfrac{\pi}{2fa}}u_2) - C(\sqrt{\tfrac{\pi}{2fa}}u_1)] + [S(\sqrt{\tfrac{\pi}{2fa}}u_2) - S(\sqrt{\tfrac{\pi}{2fa}}u_1)]\right)$$

and hence, when $a \to 0$ we get:

$$\lim_{a\to\infty}\int_{u_1}^{u_2} R_c(u)\,du = \tfrac{1}{2}([C(\infty)-C(\infty)] + [S(\infty)-S(\infty)])$$

but since $S(\infty) = C(\infty) = \frac{1}{2}$ [Spiegel68 p. 184] we obtain, as required:

$$\lim_{a\to\infty}\int_{u_1}^{u_2} R_c(u)\,du = 0.$$

The proof of (b) for the range $(-u_2,-u_1)$ is similar. ■

C.6 The 2D spectrum of a cosinusoidal zone grating

As shown in Example 10.7 of Sec. 10.3, a cosinusoidal zone grating is defined by:

$$r^{+}(x,y) = p(x^2+y^2) = \cos(2\pi f(x^2+y^2))$$

and its hyperbolic counterpart is given by:

$$r^{-}(x,y) = p(x^2-y^2) = \cos(2\pi f(x^2-y^2))$$

We find now the spectra $R^{+}(u,v)$ and $R^{-}(u,v)$ of these two functions. According to the trigonometric identity $\cos(\alpha \pm \beta) = \cos\alpha\cos\beta \mp \sin\alpha\sin\beta$ we have:

$$r^{\pm}(x,y) = \cos(2\pi fax^2)\cos(2\pi fby^2) \mp \sin(2\pi fax^2)\sin(2\pi fby^2)$$

Thanks to the separable-product theorem [Bracewell95 p. 166] we obtain:

$$\cos(2\pi fax^2)\cos(2\pi fby^2) \leftrightarrow \frac{1}{2\sqrt{f}}(\cos(\tfrac{\pi}{2f}u^2) + \sin(\tfrac{\pi}{2f}u^2))\frac{1}{2\sqrt{f}}(\cos(\tfrac{\pi}{2f}v^2) + \sin(\tfrac{\pi}{2f}v^2))$$

$$= \frac{1}{4f}[\cos(\tfrac{\pi}{2f}u^2)\cos(\tfrac{\pi}{2f}v^2) + \sin(\tfrac{\pi}{2f}u^2)\cos(\tfrac{\pi}{2f}v^2)$$

$$+ \cos(\tfrac{\pi}{2f}u^2)\sin(\tfrac{\pi}{2f}v^2) + \sin(\tfrac{\pi}{2f}u^2)\sin(\tfrac{\pi}{2f}v^2)]$$

Now, using the trigonometric identities

$$\cos\alpha\cos\beta = \tfrac{1}{2}[\cos(\alpha-\beta) + \cos(\alpha+\beta)]$$

$$\sin\alpha\sin\beta = \tfrac{1}{2}[\cos(\alpha-\beta) - \cos(\alpha+\beta)]$$

$$\sin\alpha\cos\beta = \tfrac{1}{2}[\sin(\alpha-\beta) + \sin(\alpha+\beta)]$$

we obtain:

$$= \tfrac{1}{8f}[\cos\tfrac{\pi}{2f}(u^2-v^2) + \cos\tfrac{\pi}{2f}(u^2+v^2) + \sin\tfrac{\pi}{2f}(u^2-v^2) + \sin\tfrac{\pi}{2f}(u^2+v^2)$$
$$+ \sin\tfrac{\pi}{2f}(v^2-u^2) + \sin\tfrac{\pi}{2f}(u^2+v^2) + \cos\tfrac{\pi}{2f}(u^2-v^2) - \cos\tfrac{\pi}{2f}(u^2+v^2)]$$
$$= \tfrac{1}{4f}[\cos\tfrac{\pi}{2f}(u^2-v^2) + \sin\tfrac{\pi}{2f}(u^2+v^2)]$$

Similarly, thanks to the separable-product theorem we obtain:

$$\sin(2\pi fax^2)\sin(2\pi fby^2) \leftrightarrow \tfrac{1}{2\sqrt{f}}(\cos(\tfrac{\pi}{2f}u^2) - \sin(\tfrac{\pi}{2f}u^2))\tfrac{1}{2\sqrt{f}}(\cos(\tfrac{\pi}{2f}v^2) - \sin(\tfrac{\pi}{2f}v^2))$$
$$= \tfrac{1}{4f}[\cos(\tfrac{\pi}{2f}u^2)\cos(\tfrac{\pi}{2f}v^2) - \sin(\tfrac{\pi}{2f}u^2)\cos(\tfrac{\pi}{2f}v^2)$$
$$- \cos(\tfrac{\pi}{2f}u^2)\sin(\tfrac{\pi}{2f}v^2) + \sin(\tfrac{\pi}{2f}u^2)\sin(\tfrac{\pi}{2f}v^2)]$$
$$= \tfrac{1}{4f}[\cos\tfrac{\pi}{2f}(u^2-v^2) - \sin\tfrac{\pi}{2f}(u^2+v^2)]$$

We have, therefore:

$$R^{\pm}(u,v) = \tfrac{1}{4f}[\cos\tfrac{\pi}{2f}(u^2-v^2) + \sin\tfrac{\pi}{2f}(u^2+v^2) \mp \cos\tfrac{\pi}{2f}(u^2-v^2) \pm \sin\tfrac{\pi}{2f}(u^2+v^2)]$$

and hence:

$$R^{+}(u,v) = \tfrac{1}{2f}\sin(\tfrac{\pi}{2f}(u^2+v^2))$$
$$R^{-}(u,v) = \tfrac{1}{2f}\cos(\tfrac{\pi}{2f}(u^2-v^2)). \quad \blacksquare$$

C.7 The convolution of two orthogonal line-impulses

Suppose that we are given a horizontal line-impulse $f(x)\delta(y)$, whose amplitude is defined by $f(x)$, and a vertical 1D line-impulse $g(y)\delta(x)$, whose amplitude is defined by $g(y)$. We assume that both line-impulses are centered on the origin. We want to show (see Sec. 10.7.3) that their 2D convolution is given by the 2D function $f(x)g(y)$, namely:

$$f(x)\delta(y) \ast\ast g(y)\delta(x) = f(x)g(y)$$

And indeed, according to the definition of 2D convolution [Bracewell86 p. 243] we have:

$$f(x)\delta(y) \ast\ast g(y)\delta(x) = \int_{-\infty}^{\infty}\int_{-\infty}^{\infty} f(x')\delta(y')\, g(y-y')\delta(x-x')\, dx'\, dy'$$
$$= \int_{-\infty}^{\infty} f(x')\delta(x-x')\, dx' \int_{-\infty}^{\infty} \delta(y')g(y-y')\, dy'$$

but since each of these two integrals is simply a 1D convolution of two 1D functions:

$$= [f(x)*\delta(x)][g(y)*\delta(y)]$$
$$= f(x)g(y)$$

This is a 2D surface which is centered about the origin. Similarly, if the centers of the original line-impulses are shifted from the origin to the points (x_1,y_1) and (x_2,y_2), respectively, so that the line-impulses are given by $f(x-x_1)\delta(y-y_1)$ and $g(y-y_2)\delta(x-x_2)$, their 2D convolution gives:

$$f(x-x_1)\,\delta(y-y_1) \;**\; g(y-y_2)\,\delta(x-x_2) = f(x-x_1-x_2)\,g(y-y_1-y_2)$$

This is the same 2D surface as before, but as expected its center is shifted to the point (x_1+x_2, y_1+y_2). ■

C.8 The compound line-impulse of the singular (k_1,k_2)-line-impulse cluster

We have seen in Sec. 10.7.3 that a (k_1,k_2)-moiré in the superposition of a parabolic grating and a periodic straight grating becomes singular when the line-impulses of the (k_1,k_2)-cluster in the spectrum convolution fall on a single line through the spectrum origin. This gives us in the spectrum a compound line-impulse, whose amplitude is the sum of all the individual line-impulses of the (k_1,k_2)-cluster. Note that the collapsed line-impulses do not necessarily fall center-on-center: in the general case the distance between the centers of consecutive line-impulses of the collapsed (k_1,k_2)-cluster is not zero but some other constant, so that the individual line-impulses are summed up along the compound line-impulse with a constant shift between each other. We call this shift (the distance between the DC and the center of the first line-impulse of the collapsed cluster) the *internal discrepancy* of the compound line-impulse and we denote it by f_0; the distance between the DC and the n-th impulse center is therefore nf_0. The role of the internal discrepancy f_0 will become clear below; we will see that when $f_0 = 0$ (so that all the collapsed line-impulses are centered on the DC) the compound line-impulse corresponds in the image domain to a singular moiré which is centered on the origin, but when $f_0 \neq 0$ the center of the singular moiré is shifted away from the center of the image domain.

Let us now concentrate on the n-th line-impulse pair of the (k_1,k_2)-cluster. For the sake of simplicity we assume, like in Example 10.13, that the parabolic grating $r_1(x,y)$ is oriented horizontally, so that all the line-impulses in the spectrum are vertical and the (k_1,k_2)-cluster may only collapse on the vertical v axis. Since the shift f_0 in this case takes place vertically along the v axis, we prefer to denote it henceforth by v_0 (see Fig. C.3).

As a generalization of Eq. (10.23), the n-th line-impulse pair of the (k_1,k_2)-cluster, namely: the (nk_1,nk_2)- and $(-nk_1,-nk_2)$-line-impulses, are given (for $n \neq 0$) by:

$$a_{nk_1,nk_2}(u,v) = \tfrac{1}{2}[R_c(v-nv_0) + iR_s(v-nv_0)]\;\delta(u)\;a^{(1)}{}_{nk_1}\;a^{(2)}{}_{nk_2}$$

$$a_{-nk_1,-nk_2}(u,v) = \tfrac{1}{2}[R_c(v+nv_0) - iR_s(v+nv_0)]\;\delta(u)\;a^{(1)}{}_{-nk_1}\;a^{(2)}{}_{-nk_2}$$

with:

$$R_c(v) = \frac{1}{2\sqrt{nk_1f_1a}}\left(\cos\left(\frac{\pi}{2nk_1f_1a}v^2\right) + \sin\left(\frac{\pi}{2nk_1f_1a}v^2\right)\right)$$

$$R_s(v) = \frac{1}{2\sqrt{nk_1f_1a}}\left(\cos\left(\frac{\pi}{2nk_1f_1a}v^2\right) - \sin\left(\frac{\pi}{2nk_1f_1a}v^2\right)\right)$$

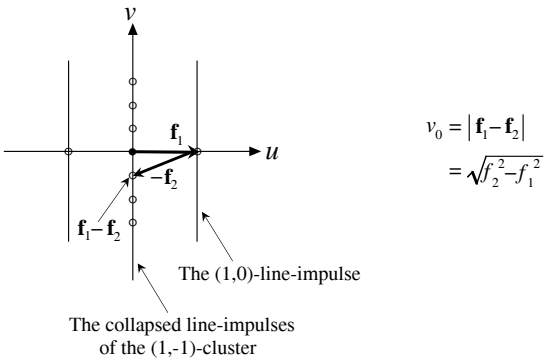

Figure C.3: The spectrum convolution showing the compound line-impulse of the singular (1,-1)-moiré, which is collapsed on the v axis, and its internal discrepancy v_0. Note that it is assumed here that $f_2 \geq f_1$. When $f_2 < f_1$ the line-impulses of the (1,-1)-cluster cannot fall on the v axis, and hence no rotation angle θ of $\mathbf{f}_2$ (i.e., of the straight grating $r_2(x,y)$) can bring the (1,-1)-moiré to a singular state.

(the terms $\delta(u)$ indicate that both line-impulses are located now on the vertical v axis).

We prefer to use here the exponential notation, which is more compact and easier to handle. We have, therefore:

$$R_c(v) + iR_s(v) = \frac{1}{2\sqrt{nk_1f_1a}}\left[\cos\left(\frac{\pi}{2nk_1f_1a}v^2\right) + \sin\left(\frac{\pi}{2nk_1f_1a}v^2\right) + i\cos\left(\frac{\pi}{2nk_1f_1a}v^2\right) - i\sin\left(\frac{\pi}{2nk_1f_1a}v^2\right)\right]$$

$$= \sqrt{\frac{c}{2\pi}}\left[e^{-icv^2} + ie^{-icv^2}\right]$$

where $c = \frac{\pi}{2nk_1f_1a}$; and similarly:

$$R_c(v) - iR_s(v) = \frac{1}{2\sqrt{nk_1f_1a}}\left[\cos\left(\frac{\pi}{2nk_1f_1a}v^2\right) + \sin\left(\frac{\pi}{2nk_1f_1a}v^2\right) - i\cos\left(\frac{\pi}{2nk_1f_1a}v^2\right) + i\sin\left(\frac{\pi}{2nk_1f_1a}v^2\right)\right]$$

$$= \sqrt{\frac{c}{2\pi}}\left[e^{icv^2} - ie^{icv^2}\right]$$

Therefore we can rewrite the line-impulses $a_{nk_1,nk_2}(u,v)$ and $a_{-nk_1,-nk_2}(u,v)$ using the exponential notation as follows:

$$a_{nk_1,nk_2}(u,v) = \tfrac{1}{2}\sqrt{\tfrac{c}{2\pi}}\left[e^{-ic(v-nv_0)^2} + ie^{-ic(v-nv_0)^2}\right]\,\delta(u)\,a^{(1)}{}_{nk_1}\,a^{(2)}{}_{nk_2}$$

$$a_{-nk_1,-nk_2}(u,v) = \tfrac{1}{2}\sqrt{\tfrac{c}{2\pi}}\left[e^{ic(v+nv_0)^2} - ie^{ic(v+nv_0)^2}\right]\,\delta(u)\,a^{(1)}{}_{-nk_1}\,a^{(2)}{}_{-nk_2}$$

Now, since at the singular state the amplitudes of these two line-impulses are summed together on the v axis we have (note that for the sake of simplicity we assume that the grating profiles are symmetric, so that $a^{(1)}{}_{-nk_1} = a^{(1)}{}_{nk_1}$ and $a^{(2)}{}_{-nk_2} = a^{(2)}{}_{nk_2}$):

$$a_{nk_1,nk_2}(u,v) + a_{-nk_1,-nk_2}(u,v) =$$

$$= \tfrac{1}{2}\sqrt{\tfrac{c}{2\pi}}\left[e^{-ic(v-nv_0)^2} + ie^{-ic(v-nv_0)^2} + e^{ic(v+nv_0)^2} - ie^{ic(v+nv_0)^2}\right]\delta(u)\, a^{(1)}{}_{nk_1}\, a^{(2)}{}_{nk_2}$$

$$= \tfrac{1}{2}\sqrt{\tfrac{c}{2\pi}}\left[e^{-ic(v^2-2nv_0v+n^2v_0^2)} + ie^{-ic(v^2-2nv_0v+n^2v_0^2)} + e^{ic(v^2+2nv_0v+n^2v_0^2)} - ie^{ic(v^2+2nv_0v+n^2v_0^2)}\right]\delta(u)\, a^{(1)}{}_{nk_1}\, a^{(2)}{}_{nk_2}$$

$$= \tfrac{1}{2}\sqrt{\tfrac{c}{2\pi}}\, e^{i2cnv_0v}\left[e^{-ic(v^2+n^2v_0^2)} + ie^{-ic(v^2+n^2v_0^2)} + e^{ic(v^2+n^2v_0^2)} - ie^{ic(v^2+n^2v_0^2)}\right]\delta(u)\, a^{(1)}{}_{nk_1}\, a^{(2)}{}_{nk_2}$$

$$= \sqrt{\tfrac{c}{2\pi}}\, e^{i2cnv_0v}\left[\cos(c(v^2 + n^2v_0^2)) + \sin(c(v^2 + n^2v_0^2))\right]\delta(u)\, a^{(1)}{}_{nk_1}\, a^{(2)}{}_{nk_2}$$

and using the trigonometric identity $\cos\alpha + \sin\alpha = \sqrt{2}\cos(\alpha - \frac{\pi}{4})$:

$$= \sqrt{\tfrac{c}{\pi}}\, e^{i2cnv_0v}\left[\cos(cv^2 + cn^2v_0^2 - \tfrac{\pi}{4})\right]\delta(u)\, a^{(1)}{}_{nk_1}\, a^{(2)}{}_{nk_2} \qquad \text{(C.8)}$$

Now, using the 1D Fourier transform pair (see Sec. C.9 below):

$$\cos(ax^2 - b) \;\leftrightarrow\; \sqrt{\tfrac{\pi}{a}}\cos(\tfrac{\pi^2}{a}u^2 + b - \tfrac{\pi}{4})$$

or rather its vertical 2D counterpart:

$$\cos(ay^2 - b) \;\leftrightarrow\; \sqrt{\tfrac{\pi}{a}}\cos(\tfrac{\pi^2}{a}v^2 + b - \tfrac{\pi}{4})\,\delta(u)$$

we find that:

$$\cos(\tfrac{\pi^2}{c}y^2 - cn^2v_0^2) \;\leftrightarrow\; \sqrt{\tfrac{c}{\pi}}\cos(cv^2 + cn^2v_0^2 - \tfrac{\pi}{4})\,\delta(u)$$

Denoting this 2D Fourier pair by $h_n(x,y) \leftrightarrow H_n(u,v)$, we see that expression (C.8) is simply $e^{i2cnv_0v}H_n(u,v)$ (multiplied by the constants $a^{(1)}{}_{nk_1}$ and $a^{(2)}{}_{nk_2}$). Therefore, according to the 2D shift theorem [Bracewell86 p. 244], expression (C.8) is the Fourier transform of a vertically shifted version of $h_n(x,y)$, where $h_n(x,y)$ is a centered, horizontal linear zone grating.[3] Denoting this vertical shift by y_0, we have by the shift theorem:

$$y_0 = \frac{v_0}{2k_1f_1a}$$

We see, therefore, that the internal discrepancy v_0 of the collapsed (k_1,k_2)-cluster in the spectrum convolution causes a vertical shift of $y_0 = \frac{v_0}{2k_1f_1a}$ in the horizontal linear zone grating of the singular (k_1,k_2)-moiré in the image domain. And indeed, if $v_0 = 0$ (so that all the collapsed line-impulses of the (k_1,k_2)-cluster are centered on the DC) then $y_0 = 0$ and the singular moiré linear zone grating is centered on the x axis, i.e., unshifted; this occurs in the (1,-1)-moiré when $f_1 = f_2$ and $\theta = 0$ (see Fig. C.3).[4]

---

[3] Note that although the 2D functions $\cos(ay^2 - b)$ and $\cos ay^2$ differ in their vertical relative phase at any value of y, both of them are horizontal, cosinusoidal linear zone gratings which are centered along the x axis.

[4] Note that when the shifted singular (k_1,k_2)-moiré slightly moves away from its singular state, for example when the grating $r_2(x,y)$ is slightly rotated on top of the parabolic grating $r_1(x,y)$, then the shifted horizontal linear zone grating of the singular moiré turns into a parabolic moiré grating with the same shift y_0. Only when the moiré is getting farther away from its singular state, the shift of the parabolic moiré grating visibly diverges from y_0. As we have seen in Sec. 10.7.3, the shift of the parabolic moiré grating in the superposition can be explained by the shear theorem.

As we can see, the amount of the shift y_0 in the image domain is independent of n and hence it is identical for all harmonics of the (k_1,k_2)-moiré. This means that all harmonics build up together a moiré grating (in the form of a horizontal linear zone grating) which is vertically shifted by y_0 from the x axis.

Finally, it is important to emphasize that in contrast to the moiré shifts in the periodic case, which were discussed in Chapter 7, we are dealing here with moiré shifts of a different type, namely: shifts of the *singular locus* of the moiré. Moreover, the moiré shifts in the present case are *not* generated by shifting the original layers in the superposition, and they are even *invariant* under such shifts. In fact, shifts of the original layers in the present case will only cause relative phase shifts in the moiré bands which surround the singular locus of the moiré, but they will not influence the *location* of the singular locus of the moiré in the superposition.

C.9 The 1D Fourier transform of the chirp $\cos(ax^2 + b)$

Knowing that for $a > 0$ we have (see Example 10.5 in Sec. 10.3):

$$\cos ax^2 \;\leftrightarrow\; \sqrt{\tfrac{\pi}{a}}\cos(\tfrac{\pi^2}{a}u^2 - \tfrac{\pi}{4}) = \sqrt{\tfrac{\pi}{2a}}(\cos\tfrac{\pi^2}{a}u^2 + \sin\tfrac{\pi^2}{a}v^2)$$

$$\sin ax^2 \;\leftrightarrow\; \sqrt{\tfrac{\pi}{a}}\sin(\tfrac{\pi^2}{a}u^2 + \tfrac{\pi}{4}) = \sqrt{\tfrac{\pi}{2a}}(\cos\tfrac{\pi^2}{a}u^2 - \sin\tfrac{\pi^2}{a}v^2)$$

we show here that:

$$\cos(ax^2 + b) \;\leftrightarrow\; \sqrt{\tfrac{\pi}{a}}\cos(\tfrac{\pi^2}{a}u^2 - b - \tfrac{\pi}{4})$$

(Note that although $\cos(ax^2 + b)$ and $\cos ax^2$ differ in their relative phase at any value of x, both of them, as well as their spectra, are centered on the origin.)

Using the trigonometric identity $\cos(\alpha+\beta) = \cos\alpha\cos\beta - \sin\alpha\sin\beta$ we have:

$$\cos(ax^2 + b) = \cos ax^2 \cos b - \sin ax^2 \sin b$$

and therefore:

$$\cos(ax^2 + b) \;\leftrightarrow\; \cos b\sqrt{\tfrac{\pi}{2a}}(\cos\tfrac{\pi^2}{a}u^2 + \sin\tfrac{\pi^2}{a}v^2) - \sin b\sqrt{\tfrac{\pi}{2a}}(\cos\tfrac{\pi^2}{a}u^2 - \sin\tfrac{\pi^2}{a}v^2)$$

$$= \sqrt{\tfrac{\pi}{2a}}\,[(\cos b - \sin b)\cos\tfrac{\pi^2}{a}u^2 + (\cos b + \sin b)\sin\tfrac{\pi^2}{a}u^2]$$

and using the known trigonometric identity for $c_1\sin\alpha + c_2\cos\alpha$ [Bronstein p. 273]:

$$= \sqrt{\tfrac{\pi}{2a}}\sqrt{(\cos b + \sin b)^2 + (\cos b - \sin b)^2}\cos(\tfrac{\pi^2}{a}u^2 - \varphi)$$

where: $$\varphi = \operatorname{arctg}\frac{\cos b + \sin b}{\cos b - \sin b} = \operatorname{arctg}\frac{\sqrt{2}\,\sin(b+\pi/4)}{\sqrt{2}\,\cos(b+\pi/4)} = b + \frac{\pi}{4}$$

and: $$\sqrt{(\cos b + \sin b)^2 + (\cos b - \sin b)^2} = \sqrt{2}$$

so that we obtain, as required:

$$= \sqrt{\frac{\pi}{a}}\cos(\frac{\pi^2}{a}u^2 - b - \frac{\pi}{4}) \quad \blacksquare$$

C.10 The 2D Fourier transform of the 2D chirp $\cos(ax^2 + by^2 + c)$

Knowing that for $a,b > 0$ we have (see Example 10.7 in Sec. 10.3):

$$\cos(ax^2 + by^2) \;\leftrightarrow\; \frac{\pi}{\sqrt{ab}}\sin(\frac{\pi^2}{a}u^2 + \frac{\pi^2}{b}v^2)$$

and hence also (by reading the same Fourier pair the other way around):

$$\sin(ax^2 + by^2) \;\leftrightarrow\; \frac{\pi}{\sqrt{ab}}\cos(\frac{\pi^2}{a}u^2 + \frac{\pi^2}{b}v^2)$$

we show here that:

$$\cos(ax^2 + by^2 + c) \;\leftrightarrow\; \frac{\pi}{\sqrt{ab}}\sin(\frac{\pi^2}{a}u^2 + \frac{\pi^2}{b}v^2 - c - \frac{\pi}{2})$$

and also that: $$\sin(ax^2 + by^2 + c) \;\leftrightarrow\; \frac{\pi}{\sqrt{ab}}\cos(\frac{\pi^2}{a}u^2 + \frac{\pi^2}{b}v^2 - c - \frac{\pi}{2})$$

(Note that although $\cos(ax^2 + by^2 + c)$ and $\cos(ax^2 + by^2)$ differ in their relative phase at any point (x,y), both of them, as well as their spectra, are centered on the origin. The same goes also for their sine counterparts.)

Using the trigonometric identity $\cos(\alpha+\beta) = \cos\alpha\cos\beta - \sin\alpha\sin\beta$ we have:

$$\cos(ax^2 + by^2 + c) = \cos(ax^2 + by^2)\cos c - \sin(ax^2 + by^2)\sin c$$

and therefore:

$$\cos(ax^2 + by^2 + c) \;\leftrightarrow\; \cos c\,\frac{\pi}{\sqrt{ab}}\sin(\frac{\pi^2}{a}u^2 + \frac{\pi^2}{b}v^2) - \sin c\,\frac{\pi}{\sqrt{ab}}\cos(\frac{\pi^2}{a}u^2 + \frac{\pi^2}{b}v^2)$$

Using the known trigonometric identity for $c_1\sin\alpha + c_2\cos\alpha$ [Bronstein p. 273]:

$$= \frac{\pi}{\sqrt{ab}}\sqrt{\cos^2 c + \sin^2 c}\,\sin(\frac{\pi^2}{a}u^2 + \frac{\pi^2}{b}v^2 - \varphi)$$

where: $$\varphi = \frac{\pi}{2} - \operatorname{arctg}\frac{-\sin c}{\cos c} = \frac{\pi}{2} + c$$

and: $$\sqrt{\cos^2 c + \sin^2 c} = 1$$

so that we obtain, as required:

$$= \frac{\pi}{\sqrt{ab}}\sin(\frac{\pi^2}{a}u^2 + \frac{\pi^2}{b}v^2 - c - \frac{\pi}{2})$$

Furthermore, if we denote $a' = \frac{\pi^2}{a}$, $b' = \frac{\pi^2}{b}$ and $c' = -c - \frac{\pi}{2}$ we obtain, by reading the same Fourier pair the other way around:

$$\sin(a'u^2 + b'v^2 + c') \;\leftrightarrow\; \frac{\pi}{\sqrt{a'b'}}\cos(\frac{\pi^2}{a'}x^2 + \frac{\pi^2}{b'}y^2 - c' - \frac{\pi}{2})$$

and by renaming the variables we obtain:

$$\sin(ax^2 + by^2 + c) \;\leftrightarrow\; \frac{\pi}{\sqrt{ab}}\cos(\frac{\pi^2}{a}u^2 + \frac{\pi^2}{b}v^2 - c - \frac{\pi}{2}) \quad \blacksquare$$

C.11 The spectrum of screen gradations

A screen gradation is a profile-transformed dot-screen (see Sec. 10.2) in which the "period" remains constant throughout the image, but the dot size and/or the dot shape within each such "period" (or cell) vary smoothly according to a certain given rule. Halftoned images (printed with a clustered dot halftoning method) are in fact screen gradations in which the dot size varies according to the tone values in the original, continuous-tone image to be reproduced (see Sec. 3.2). A halftoned image can be seen therefore as a *surface-area modulation* of an underlying dot-screen (the "*carrier*") by the tone values of the original image (the "*modulator*"). This is in fact a 2D extension of the modulation method known in communication theory as *pulse-width modulation*, in which a train of square pulses with period T is modulated by varying the duration τ of each of its pulses within the limits permitted by the period T [Black53 pp. 32, 263–281].

The influence of surface-area modulation on the nailbed spectrum of the underlying periodic dot-screen (the carrier) is quite complex. It is therefore instructive to start by studying the simplest case, in which the modulating function is a raised cosine function so that its spectrum contains only the DC and the fundamental impulse pair at the cosine frequency. Since in this case both of the functions involved (the carrier and the modulator) are periodic, the modulated function is either periodic or almost-periodic (see Appendix B), depending on whether their periods are commensurable or not. This means that the spectrum of the modulated screen is impulsive; in fact, its impulses are located:

(1) At the fundamental frequency f_c of the underlying dot-screen and all its harmonics (i.e., at the impulse locations of the nailbed spectrum of the unmodulated screen);

(2) At the frequency f_m of the modulating cosine and all its harmonics; and

(3) In all their sums and differences (the intermodulation frequencies).

More formally speaking, the impulse locations in the resulting spectrum form the module $\{mf_c + nf_m \mid m,n \in \mathbb{Z}\}$. In the 1D case this spectrum looks as if a decaying comb of period f_m has been placed on top of each of the impulses of the comb of the underlying square wave, all the combs being intermingled together (see Fig. C.4). In the 2D case all the above mentioned frequencies become frequency-vectors (which represent the impulse locations in the 2D spectrum), and the combs are replaced by nailbeds. The explicit expression for the impulse amplitudes is quite complicated; an example for the 1D case is given in [Black53 p. 275].[5] In general, the strongest impulses in the spectrum are those of

[5] The formula given there is in fact the Fourier series development of the modulated function, from which the impulse frequencies and amplitudes can be readily found. This formula was developed there for the case of a modulating function with a triangular profile.

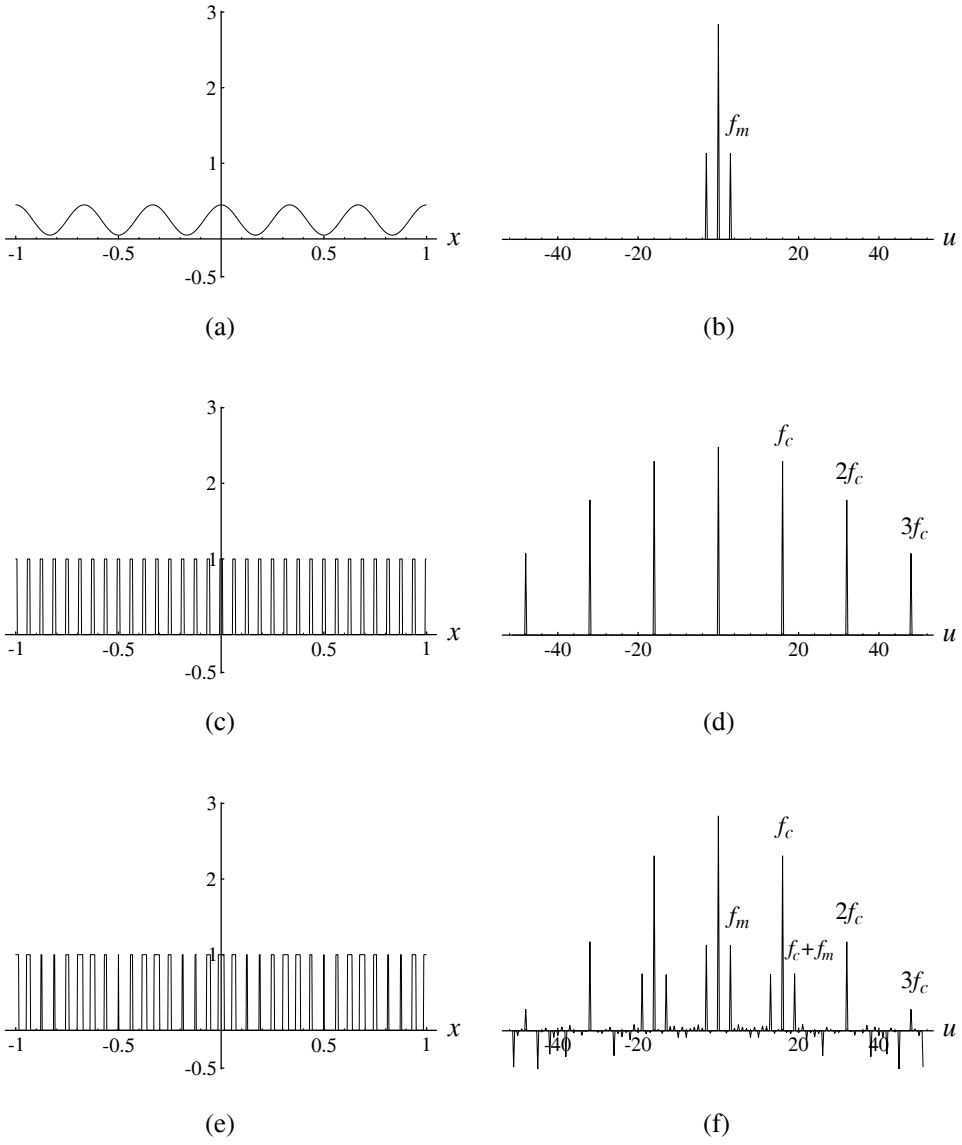

Figure C.4: A simple case of 1D pulse-width modulation. The modulating function (a) is a raised cosine $0.2\cos(2\pi f_m x) + 0.25$ with frequency $f_m = 3$; its spectrum is shown in (b). The carrier (c) is a pulse-train of frequency $f_c = 16$; its spectrum is shown in (d). The result of the pulse-width modulation is shown in (e), and its spectrum is shown in (f). Note that all the spectra have been obtained by FFT, which explains the slightly visible noise.

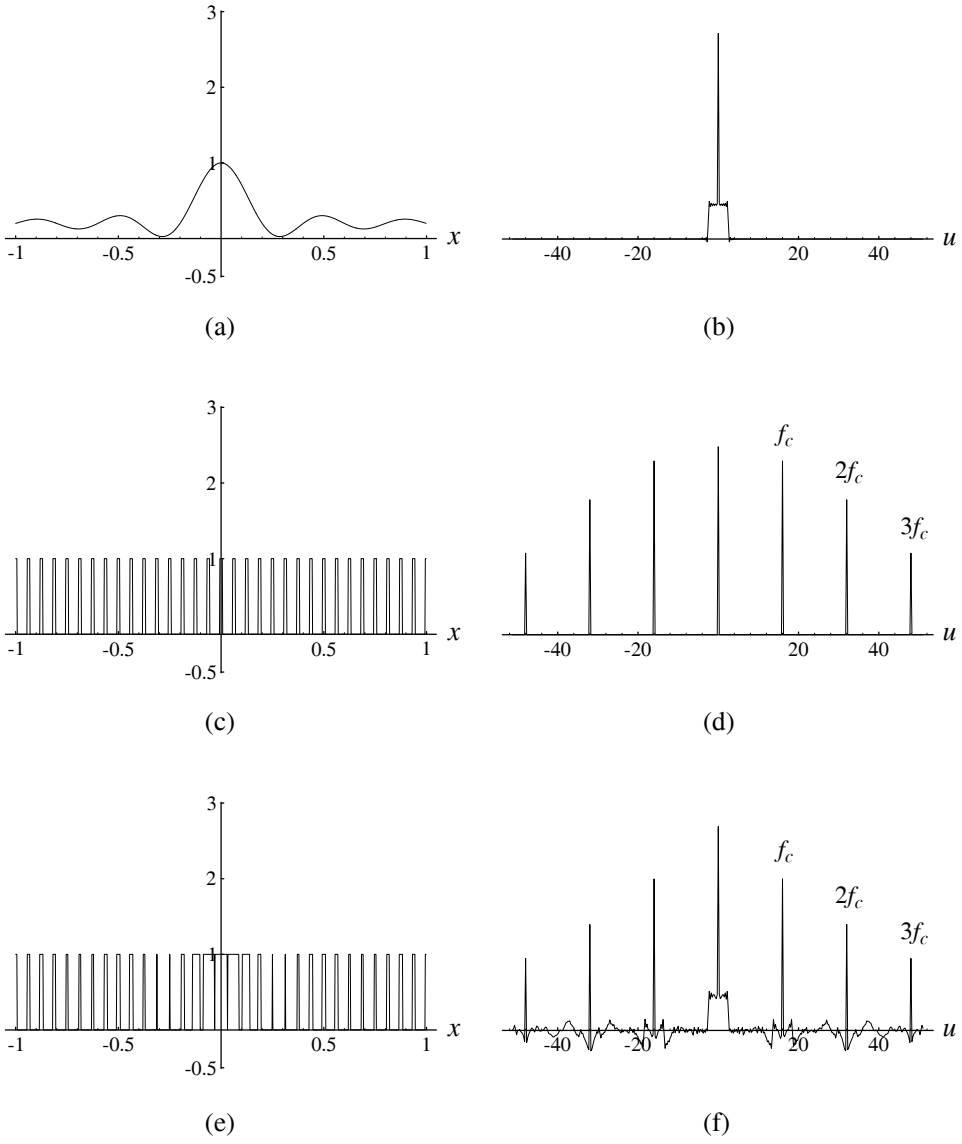

Figure C.5: A 1D pulse-width modulation simulating a halftoned image and its spectral interpretation. The original continuous-tone image (a), i.e., the modulating function, is $0.8\text{sinc}(5x) + 0.2$; its spectrum (b) is a square pulse of width 5 (plus a DC impulse). The carrier (c) is a pulse-train of frequency $f_c = 16$; its spectrum is shown in (d). The result of the pulse-width modulation is shown in (e), and its spectrum in (f). It is clearly seen that the spectrum (f) contains around its DC a faithful replica of the spectrum (b) of the original image; farther away it contains also the impulses of the carrier at the halftoning frequency f_c and its harmonics nf_c, as well as the distorted replicas of (b) around each of them (the *intermodulation distortions*).

the DC, the underlying dot lattice frequency f_c and its first few higher harmonics, and the modulation frequency f_m; the impulses at higher harmonics and at intermodulation frequencies die out quite rapidly. Note that f_c is in fact the frequency of the halftone cells which constitute the halftone image; it is therefore often called the *halftone frequency*.

Now, if the modulating function is not a pure cosine but rather consists of several frequencies, then all of these frequencies are present in the spectrum, and they participate in the generation of the new intermodulation impulses. The same principle is also true for the general case where the modulating function is a real-world image, whose original spectrum may consist of infinitely many frequencies f_m of various amplitudes (obviously, $f_m < f_c$). It has been shown in [Kermisch75 p. 723] that even in this case the spectrum of the modulated function (the halftoned image) can be written in the form of a series, where the first term represents the spectrum of the original continuous tone image, and the other terms represent the distortions introduced by the halftoning process. Similar results have been obtained in [Allebach79] for the case of discrete images. In general, the spectrum of a halftoned image contains a replica of the spectrum of the original continuous tone image (the modulating function), which is centered on the DC, as well as distorted replicas which are centered on each of the carrier's harmonic frequencies nf_c. This is illustrated in Fig. C.5, where the modulating function is sinc(5x), a function whose own spectrum (a square pulse of width 5) is easily recognizable. As we can see in the figure, the spectrum of the modulated function (the halftoned image) shows a clear replica of this square pulse around the DC, as well as distorted replicas of this pulse which surround the halftone frequency f_c and its harmonics nf_c.[6]

However, in our case here we are not interested in general halftoned images, but rather in the particular case of uniform screen gradations ("wedges") which are modulated by a uniform slope. We use such gradations for demonstrating within a single image the moirés which are generated at various possible tone levels of each of the superposed screens (see, for example, Figs. 4.1, 4.4, etc.). In the 1D case the modulating function of the gradation is $f(x) = ax + b$, whose Fourier transform is $F(u) = (ai/2\pi)\delta'(u) + b\delta(u)$ [Champeney87 p. 138], where $\delta'(u)$ is the first derivative of the impulse $\delta(u)$ (see [Bracewell86 p. 80–82]). Therefore the spectrum of the modulating function $f(x)$ consists of a single impulsive entity at the spectrum origin; this guarantees that no new frequencies appear in the spectrum of a dot-screen when it is modulated by this function. A similar result is obtained in the 2D case, where the modulating function is $f(x,y) = ax + by + c$. This confirms that the profile-transformation which transforms the original dot-screen into such a screen gradation only affects the amplitudes and the nature of the impulses in the spectrum of the original dot-screen, but it does not modify the impulse locations nor does it introduce any new impulses. In other words: The spectrum support of such a screen

[6] Note that when looking at the halftoned image from a normal viewing distance the halftone frequency f_c and its harmonics nf_c are already beyond the border of the visibility circle, and only the frequencies of the main replica of the spectrum of the original image around the DC are still located within the visibility circle. This explains why when looking at a halftoned image the eye normally perceives an almost identical version of the original, continuous-tone image.

gradation remains the same lattice as in the spectrum of the underlying dot-screen and it corresponds to the cell periodicity of the gradation.

As a consequence, the moiré effects in the superposition of such screen gradations vary locally in their *profiles* according to the profile variations in the superposed layers; but their angles and "periods" remain unchanged throughout the superposition (see Figs. 4.1, 4.4, etc.).

C.12 Convergence issues related to Fourier series

In this section we briefly review questions concerning the convergence of Fourier series (proper and generalized), and the order of summation in multiple Fourier series. Additional details as well as more rigorous mathematical development of the subjects may be found in the cited references.

C.12.1 On the convergence of Fourier series

Suppose that $p(x)$ is a periodic function of period T; $p(x)$ is therefore fully defined by any 1-period interval of length T, such as $0...T$.[7] If $p(x)$ is integrable on a 1-period interval, then a set of complex numbers c_n for $n = 0, \pm1, \pm2,...$ may be defined by:

$$c_n = \frac{1}{T}\int_T p(x)\, e^{-i2\pi nfx}\, dx \tag{C.9}$$

where $f = 1/T$, and $\int_T$ means integration over any full period of $p(x)$, i.e., from x_0 to x_0+T where x_0 is arbitrary. The complex numbers c_n are called the *Fourier series coefficients* of $p(x)$, and their values are independent of the choice of x_0.

The following series, involving the Fourier series coefficients c_n of the function $p(x)$, is called the *(formal) Fourier series belonging to* $p(x)$:

$$p(x) \sim \sum_{n=-\infty}^{\infty} c_n\, e^{i2\pi nfx} \tag{C.10}$$

(where the symbol '~' is used to denote the relation "belongs to"). Note that at any value of x the formal Fourier series in (C.10) may or may not converge, depending on the choice of $p(x)$ and of x. Many periodic functions $p(x)$ possess a Fourier series that converges to the function $p(x)$ itself at all x; in such cases the symbol '~' in (C.10) can be replaced by an equality '=', and the term "formal Fourier series belonging to $p(x)$" can be replaced by the term "*Fourier series expansion of* $p(x)$". But in other cases the formal Fourier series may fail to converge at some or even all values of x (see for example [Zygmund68 pp. 298–315]). One of the main aims of the theory of Fourier series has been to determine

[7] If $f(x)$ is not periodic (e.g., $f(x) = x^2$) but its behaviour is of interest only within a given interval of x, it can still be artificially made periodic by simply defining $p(x) = f(x)$ within this interval, and redefining $p(x)$ outside this interval to be a periodic repetition of its values within the interval.

in what sense (what type of convergence) and under what conditions the formal Fourier series tends to $p(x)$; see, for instance, [Zygmund68; Katzenelson68].

Several convergence criteria for Fourier series can be stated, depending on the class of functions considered and on the way "convergence" is understood (see, for example, [Champeney87 pp. 156–164], [Gaskill78 pp. 107–108]). Some convergence criteria are also known for the case of almost-periodic functions, i.e., for generalized Fourier series (see [EncMath88 Vol. 1 pp. 154–156: "Almost-periodic functions"; Vol. 4 p. 79: "Fourier series of an almost-periodic function"]). However, this problem is more difficult than its periodic counterpart and is still far from a complete solution [Corduneanu68 pp. 31–38].

It is beyond the scope of this work to define rigorously the precise class of periodic or almost-periodic functions which satisfy the required convergence conditions for our needs. Instead, we simply restrict ourselves to those functions which do satisfy these conditions. It should be noted that practically all functions which represent real physical quantities satisfy the convergence conditions [Gaskill78 p. 108]. Therefore we may adopt for our purposes the pragmatic approach which says, roughly speaking: if a function describes a physically realizable phenomenon (e.g., if a theoretic reflectance function can be realized and demonstrated, for instance reproduced on film[8]), then the required convergence conditions are mathematically met. In particular, common functions such as square waves, gratings, etc. present no convergence problems, and their Fourier series developments can be found tabulated in literature.

C.12.2 Multiplication of infinite series

As we have seen in Sec. 2.2, the superposition of periodic layers in the image domain means, mathematically, their multiplication. Therefore, the Fourier series of the superposition is the product of the Fourier series of each of the individual layers. Intuitively, as an extension of the finite case, the product of infinite series $\sum a_n$ and $\sum b_k$ should be given by the infinite series $\sum\sum a_n b_k$. However, handling infinite series must be done with care, since even simple operations which are obvious in the finite case, such as reordering the terms within the series, may affect its convergence.

If we are lucky to have original functions (individual layers in the superposition) whose Fourier series are absolutely convergent,[9] then we are in a happy situation, thanks to the following theorem:

Theorem 1: If the infinite series $\sum a_n = A$ and $\sum b_k = B$ are *absolutely convergent*, then the double series $\sum\sum a_n b_k$ is absolutely convergent, and has the sum AB *however the terms are arranged* [Hardy73 pp. 227–228]. ■

---

[8] Unlike various "pathological" functions such as $\sin(1/x)$, the Cantor function, etc.

[9] An infinite series $\sum a_n$ is *absolutely convergent* if $\sum|a_n|$ is convergent (this implies that $\sum a_n$ is also convergent).

This means that the double series is indeed the product of the two given series, and furthermore, any order of summation in this double series is permitted.

The most familiar multiplication rule (order of terms) is Cauchy's, in which the double series is summed "diagonally", by associating together the terms in which $n+k$ has a fixed value. We then define the product series $C = AB$ as:

$$C = \sum_{m=0}^{\infty} \sum_{n+k=m} a_n b_k = \sum_{m=0}^{\infty} \sum_{n=0}^{m} a_n b_{m-n} = \sum_{m=0}^{\infty} \sum_{k=0}^{m} a_{m-k} b_k \qquad \text{(C.11)}$$

However, this diagonal summation is by no means the only possible summation order for the double series. In fact, by the above theorem, if the series being multiplied are absolutely convergent, any arrangement of the terms is permitted (provided that it is exhaustive, and that no term is taken more than once). This can be generalized to the multiplication of any number of absolutely convergent series, i.e., to the ordering of the terms in any such multiple series.

The above theorem for absolutely convergent series stands unchanged, for any rule of multiplication, also for two-sided series (i.e., series infinite in both directions); for example, if $\sum_{n=-\infty}^{\infty} a_n = A$ and $\sum_{k=-\infty}^{\infty} b_k = B$, then Cauchy's diagonal summation:

$$C = \sum_{m=-\infty}^{\infty} \sum_{n+k=m} a_n b_k = \sum_{m=-\infty}^{\infty} \sum_{n=-\infty}^{\infty} a_n b_{m-n} = \sum_{m=-\infty}^{\infty} \sum_{k=-\infty}^{\infty} a_{m-k} b_k$$

satisfies $C = AB$ [Hardy73 pp. 239–241].

If, however, the Fourier series of our superposed functions are not absolutely convergent, the following theorem (Abel's product theorem) may come to the rescue:

Theorem 2: If the series $\sum a_n = A$, $\sum b_k = B$ and (C.11) are all convergent, then $AB = C$ [Hardy73 p. 228]. ■

In other words, if we know in advance that the original series $\sum a_n = A$, $\sum b_k = B$ and also their Cauchy series (C.11) are all convergent, then the Cauchy series (C.11) is indeed the product of the original series.[10] It can be shown that other linear variants of the Cauchy diagonal ordering are also permitted, such as: $\sum_{m=0}^{\infty} \sum_{qn+pk=m} a_n b_k = C$, where p and q are constant integers (see, for example, Fig. 5.1(a)).

Clearly, this is not as general as in the case of Theorem 1, where virtually any order of summation is permitted. But for our needs, when our original superposed functions do not have absolutely convergent Fourier series as required by Theorem 1, Theorem 2 will also do: since we do know — due to the physical realizability of the superposition — that its Fourier series is indeed convergent.

---

[10] Note that Abel's theorem is not always true for two-sided series [Hardy73 p. 244]; however, since in our case the Fourier series is symmetric (or Hermitian, in the complex case), we have no problem to represent the two-sided Fourier series as a one-sided infinite series, i.e., in the form (A.1) rather than (A.3).

C.13 Moiré effects in image reproduction

Undesired moiré patterns may appear in the printing process for several possible reasons, which can be classified into the following main categories:

(a) *Screening moirés*. These are moiré patterns which occur as an interaction between repetitive patterns in the original image (such as striped clothes, fences, etc.) and the halftone screen which is used to print the image. An example containing such moirés is shown in [Bann90 p. 65]. Screening moirés are also called *subject* or *content moirés*, since they depend on the details of the original image [Blatner98 p. 282].

(b) *Auto moirés*. These are moiré patterns which occur owing to an interaction between the halftone screen and the pixel grid of the output device [Jones94 pp. 267–268]. These moirés are also called *internal moiré artifacts* [Levien93] because they are generated internally to the screening process, and do not depend on an "external" source.

(c) *Superposition moirés*. These are moiré patterns which occur in the superposition of two or more repetitive structures, such as the halftone screens of the different process colours which are used in colour printing [Blatner98 p. 279]. See Chapter 3.

(d) *Sampling moirés*. These are moiré patterns which occur in the analog to digital conversion of an image between the sampling grid (the device resolution) and repetitive patterns in the original image. Sampling moirés most frequently occur when attempting to scan an already halftoned image (such as a photo from a book or a newspaper), or an image which includes repetitive patterns (see also Sec. 2.13, and several of the problems at the end of Chapter 3).

All of these types of moiré are generated as interactions between repetitive structures (which may be, depending on the case, the halftone screen, the pixel grid of the input or output device, or repetitive details within the original image). These different types of moirés are all included within the framework of our superposition moiré theory if we consider sampling grids, pixel grids, etc., as particular cases of dot-screens.

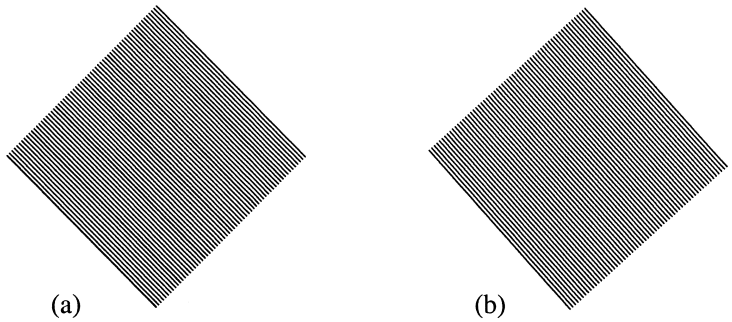

Figure C.6: (a) An auto moiré may occur when printing a single line-grating (or dot-screen) on a PostScript printer, owing to periodic pixel rounding errors. Is this really a *single layer moiré*? (b) This printer artifact may disappear by slightly changing the angle or the frequency of the grating (or dot-screen).

C.14 Hybrid (1,-1)-moiré effects whose moiré bands have 2D intensity profiles

In this section we describe an interesting moiré effect which may carry 2D information although it is based on the 1D case of the (1,-1)-moiré between two line gratings. This 1D moiré effect could be also considered, therefore, as a "$1\frac{1}{2}$D case". This phenomenon was known to Joe Huck who used it in his artistic work [Huck03], but it was first investigated in depth and fully explored in [Hersch04] and in [Chosson06]. Interesting applications of this phenomenon to the field of document protection have been described in detail in [Hersch04a], [Hersch06], [Hersch06a] and [Schilling06].

It should be noted that the terminology, the notations and the conventions used in the above mentioned references differ from the ones that we use throughout this book. But for the sake of consistensy and uniformity within this volume we will use here the same conventions and notation standards as in the rest of the book. Note also that although the original publications were only based on geometric considerations and on the indicial equations approach, we will base our discussion here on the Fourier-based approach, which provides a much deeper insight into this phenomenon. In particular, the Fourier-based approach can also explain the intensity profiles of the phenomena in question, and it is not only limited to their planar geometric properties as the other approaches.

C.14.1 Preliminary considerations

Suppose that we are given a (1,-1)-moiré between two periodic line gratings, as shown in Figs. 1.1 or 2.5. The period and the angle of the moiré bands are given, as we have seen in Chapter 2, by Eq. (2.9) or by its particular cases, Eqs. (2.10) or (2.11).

Assume, now, that we replace the simple black lines of the first grating by lines that incorporate along their main direction some predefined information (such as tiny letters, digits or symbols), while the other grating is replaced by a series of linear slits (narrow white or rather transparent lines) on a black background (see Fig. C.7). The resulting effect may remind us of the 2D case that we have already studied in Sec. 4.3 (see, for example, Figs. 4.4 or C.23). In that 2D case, when the first layer is a periodic dot screen whose individual dots have some predefined dot shapes and the second layer is a periodic pinhole screen having similar periods, we obtain in the superposition a moiré effect whose intensity profile is a largely magnified (and possibly rotated) version of the information that is incorporated in the dot shapes of the first screen. And indeed, as we can see in Fig. C.7, a similar phenomenon occurs also in our 1D case: The superposition of our two line gratings gives moiré bands whose intensity profile is a largely magnified (and possibly slanted) version of the information that is incorporated along the lines of the first grating. However, the periodicity and the magnification of this moiré effect only occur along *one* direction, and not along two directions as in the 2D case (compare Figs. C.7 and C.23). The same goes also for the dynamic behaviour of the moiré effect under layer shifts.

Obviously, because the baseline direction of the incorporated text coincides with the line direction of our grating, the period and the orientation of the baselines of our moiré bands

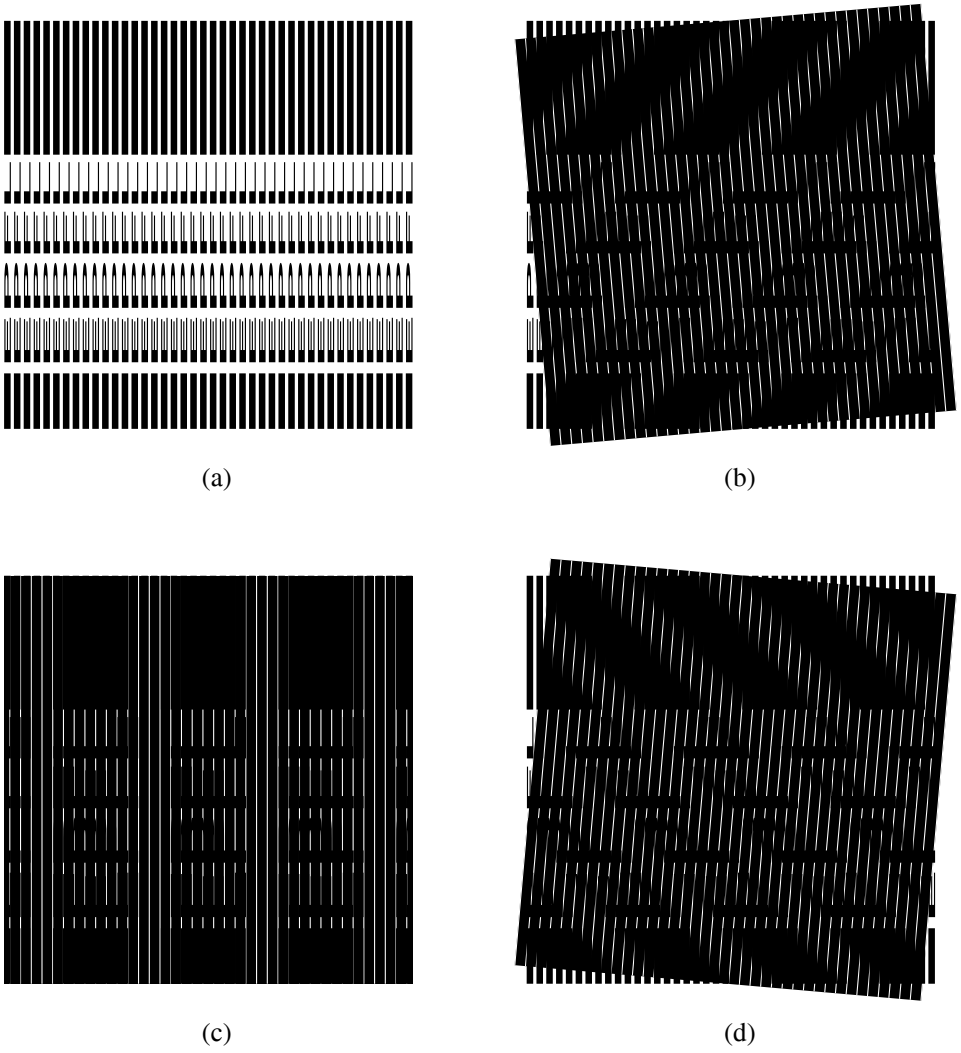

(a) (b)

(c) (d)

Figure C.7: (a) A periodic line grating whose individual lines contain a flattened version of the letters "EPFL". (b)–(d) The superposition of this line grating with a second periodic line grating having a slightly larger period $T_2 > T_1$, which consists of narrow slits on a black background. The angle difference between the two superposed gratings is 5° in (b), 0° in (c) and –5° in (d). Each of these superpositions gives a periodic (1,-1)-moiré effect whose individual bands contain a largely stretched-out (and possibly sheared) version of the 2D information that is embedded in the individual lines of the first grating. Note that we have intentionally left the upper and the lower parts of the grating (a) non-modulated; this allows us to compare in each of the superpositions our modulated moiré bands with the simple moiré bands that are obtained in the classical, non-modulated case.

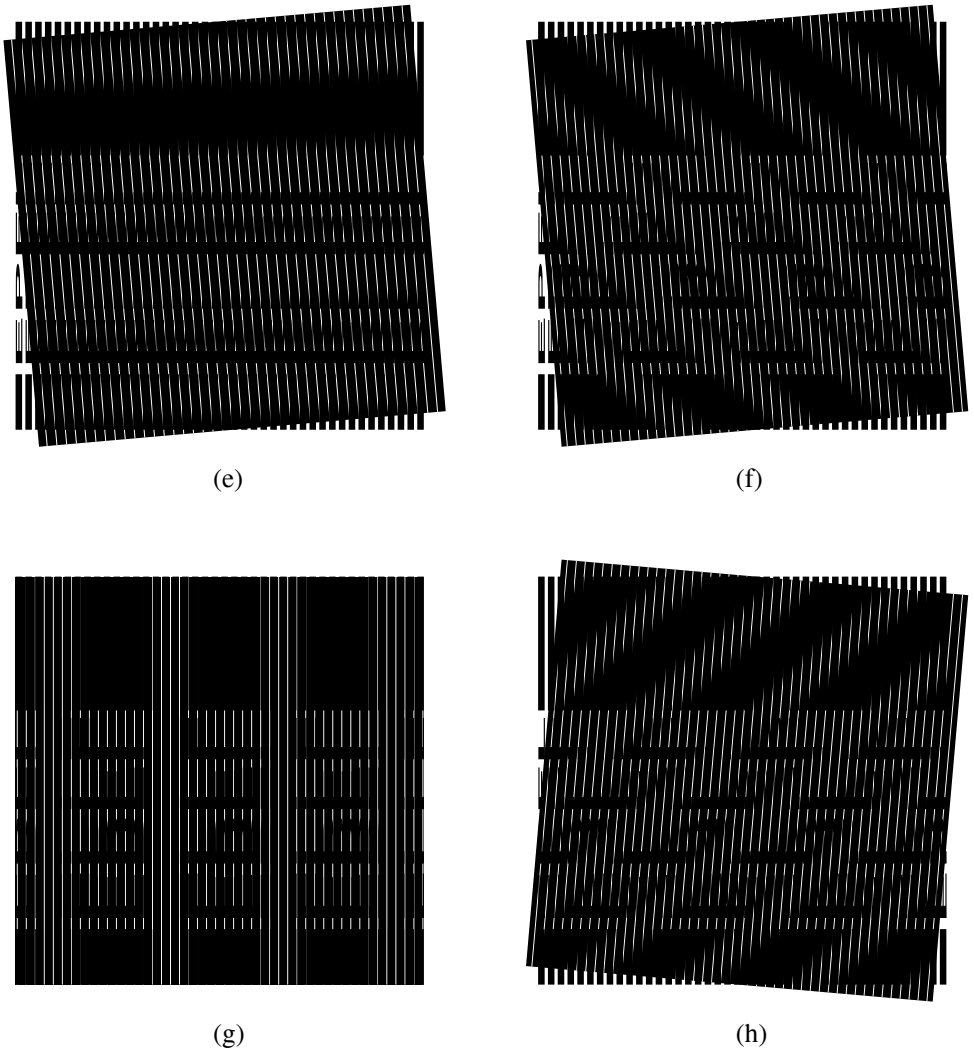

(e) (f)

(g) (h)

Figure C.7: (*continued*.) (e) Same as in (b), but with periods $T_2 = T_1$; this case is explained in greater detail in Fig. C.8. (f)–(h) Same as in (b)–(d), but this time with periods $T_2 < T_1$; in this case the letters "EPFL" appear in the moiré bands mirror-imaged, and under layer shifts they move in the opposite direction than in (b)–(d), respectively.

are still given by the same equations as in the case consisting of simple, black lines (Eqs. (2.9)–(2.11)). However, as we can see in Fig. C.7(b), this periodicity does not correspond to the periodicity of the moiré text that is incorporated within the moiré bands. The reason is that unlike in the simple case of black lines, in our present case two of the three structures involved — the first grating and the resulting moiré bands — also have a

secondary orientation, i.e. the height direction of the letters.[11] And indeed, it turns out that the secondary direction of the moiré letters is not necessarily orthogonal to their baseline direction. For instance, in the case shown in Fig. C.7 the height direction of the moiré letters remains horizontal, like in the original text of the first grating, so that the resulting moiré text can be significantly slanted, depending on the direction of the moiré bands.

This interesting phenomenon can be explained using geometric considerations, as done, indeed, in the original publications mentioned above. However, by also considering the intensity information, i.e. the intensity profiles of the two given gratings and the intensity profile of the resulting moiré effect, in addition to their planar geometric layouts, we can obtain a much deeper understanding of this phenomenon. This deeper insight is provided by the Fourier-based approach, as we will see below.

In fact, the (1,-1)-moiré that we discuss here differs from the classical case that is shown in Fig. 2.5 in that it is based on lines having 2D profile variations rather than on lines having only 1D profile variations across the line width, as in the classical case. This type of moiré will be called here a *hybrid* (1,-1)-moiré, due to the fact that it still carries 2D information although it is based on line gratings and not on dot screens. As shown in the references mentioned above, the hybrid (1,-1)-moiré has some nice properties which make it very useful in applications. These include, notably, the larger amount of light that passes through a grating made of line slits (as compared to a 2D pinhole screen), which makes the resulting moiré more easily visible than its 2D counterpart even in difficult light conditions; and the fact that it can carry along its moiré bands information of practically any desired length. But on the other hand, the hybrid (1,-1)-moiré only provides 1D rather than 2D magnification (compare Figs. C.7(a),(c) with Fig. C.24(a)). Moreover, the hybrid (1,-1)-moiré is more sensitive to layer rotations than its 2D counterpart, since such rotations do not cause a *rotation* of the resulting moiré as in the 2D case (as shown, for example, in Fig. C.23(a)) but rather a strong *shearing* effect (as shown in Figs. C.7(b) or C.8), which may distort the carried information and make it harder to recognize.

C.14.2 The Fourier-based approach

Let us start with the familiar superposition of two simple straight periodic gratings having similar periods and angles, as already described in Chapters 2 and 4 (see Fig. 2.5). This time, however, we allow each individual line of our first grating $r_1(x,y)$ to carry some given information, not necessarily periodic, along its main direction. In other words, the intensity of each of the lines of our grating $r_1(x,y)$ may be modulated by any given information, such as letters, digits or symbols, provided that these objects are sufficiently narrow or flattened to fit within each individual line. For example, in the case shown in Fig. C.9(a) each of the grating lines contains a very flattened version of the letters "EPFL". Because the line grating $r_1(x,y)$ is periodic along its main direction (in our figure, along the x axis),[12] it is clear that its Fourier spectrum $R_1(u,v)$ is impulsive.

[11] The *height direction* of the letters is understood here as the direction defined by letters such as "I".
[12] Note that the main direction of a line grating is perpendicular to its individual lines.

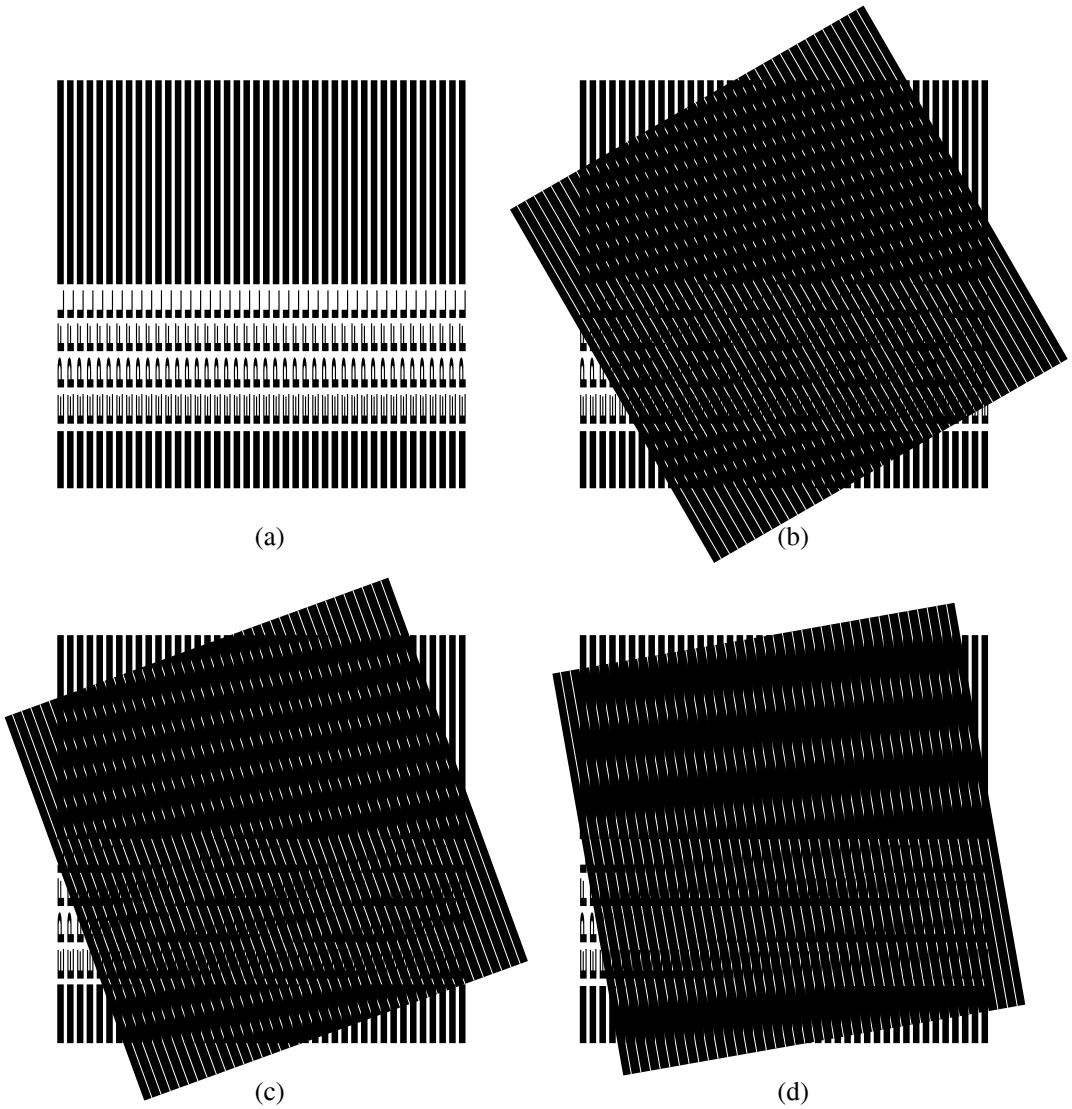

Figure C.8: A more detailed explanation of the case shown in Fig. C.7(e), in which both of the superposed gratings have identical periods, $T_2 = T_1$. (a) A periodic line grating whose individual lines contain a flattened version of the letters "EPFL". Note that the black, unmodulated part of the individual lines at the top of this grating is intentionally left longer than in Fig. C.7(a), in order to leave more room for the black, unmodulated moiré bands at the top of the resulting superpositions. (b)–(d) The superposition of this line grating with a second periodic line grating which consists of narrow slits on a black background. The periods of the two superposed gratings are identical, and the angle difference between them is 30° in (b), 20° in (c) and 10° in (d). As we can clearly see, the letters "EPFL" are still present within each of the moiré bands even though $T_2 = T_1$. But in this case, when the angle difference between the gratings is lower than about 20°, the letter shapes become so elongated and slanted that they are no longer recognizable.

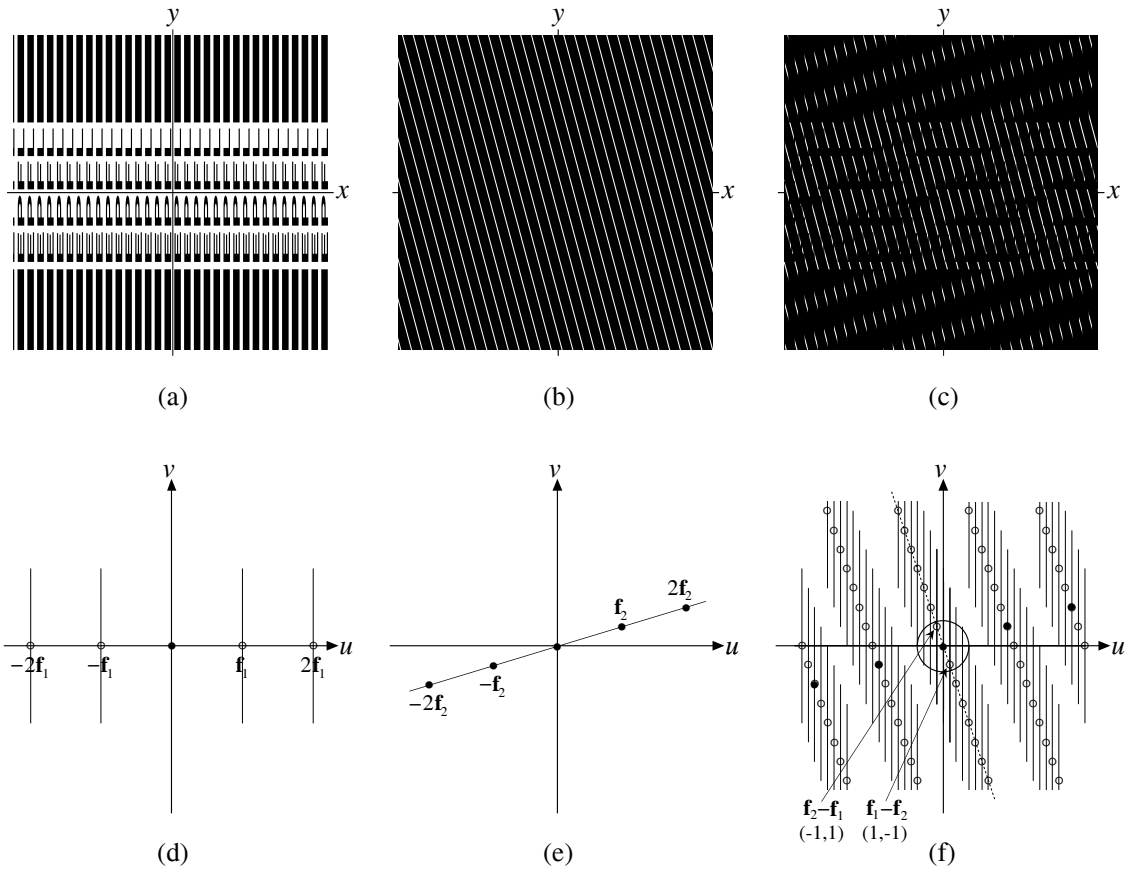

Figure C.9: Periodic grating (a) whose individual lines are modulated by the flattened letters "EPFL", periodic line grating (b), and their superposition (c) in the image domain. Their respective spectra are the infinite line-impulse comb (d), the infinite impulse comb (e) and their convolution (f). Black dots in the spectra represent impulses, while open dots indicate the skeleton locations of the line-impulses. Notice the hybrid (1,-1)-moiré which appears in the superposition. Compare with the classical (1,-1)-moiré shown in Fig. 2.5. (Note that for the sake of clarity the periods in the upper row of the present figure have been magnified with respect to those shown in Fig. 2.5.)

However, unlike the simple non-modulated line gratings that we considered so far, the intensity along each line within our grating $r_1(x,y)$ is not constant, and it needs not even be periodic. Therefore the Fourier spectrum of such a grating is no longer an impulse comb like in Fig. 2.5(d), but rather a line-impulse comb, i.e. a sequence of equispaced parallel line impulses that are orthogonal to the grating's main direction (see Fig. C.9(d) and the illustrative explanation that is provided in Fig. C.11). These continuous line impulses are centered about their *skeleton locations*, which are the locations of the corresponding

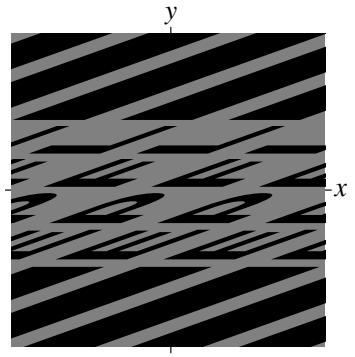

(a)

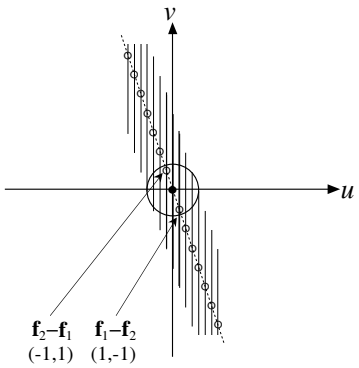

(b)

Figure C.10: Extraction of the (1,-1)-moiré of Fig. C.9: (b) shows the isolated line-impulse comb of the (1,-1)-moiré after its extraction from the full spectrum of Fig. C.9(f). (a) shows the image domain function which corresponds to the spectrum (b). This is the intensity profile of the modulated (1,-1)-moiré shown in Fig. C.9(c); note that it only contains the extracted moiré (i.e., its isolated contribution to the superposition), but not the microstructure details of the original gratings and of the superposition. The orientation of the *skeleton* of the line-impulse comb corresponds to the direction of the 1-fold periodicity of the non-modulated moiré bands, while the *shearing* of this line-impulse comb with respect to the original line-impulse comb of the first grating (Fig. C.9(d)) determines the slanting angle of the letters within each moiré band (see Fig. C.12 below). Compare with the classical (1,-1)-moiré shown in Fig. 4.2.

impulses in the spectrum of the equivalent non-modulated line grating (see Fig. 2.5(d)), i.e. the points $n\mathbf{f}_1$, $n \in \mathbb{Z}$, where $\mathbf{f}_1$ is the frequency vector of our grating. The information that is modulated along each of the grating lines is encoded in the spectrum by the

$r(x,y)$ $\mathrm{Re}[R(u,v)]$ $\mathrm{Im}[R(u,v)]$

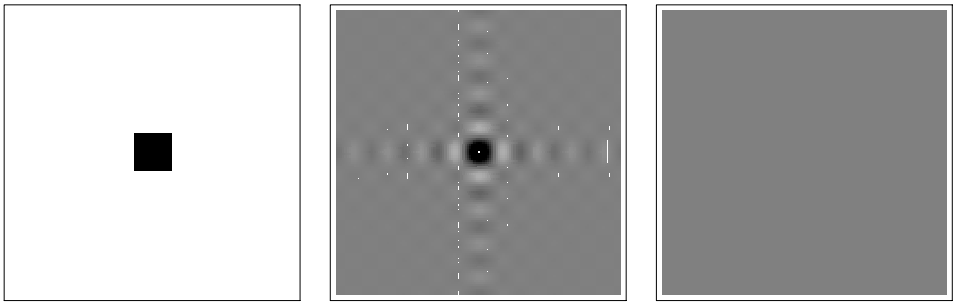

(a)

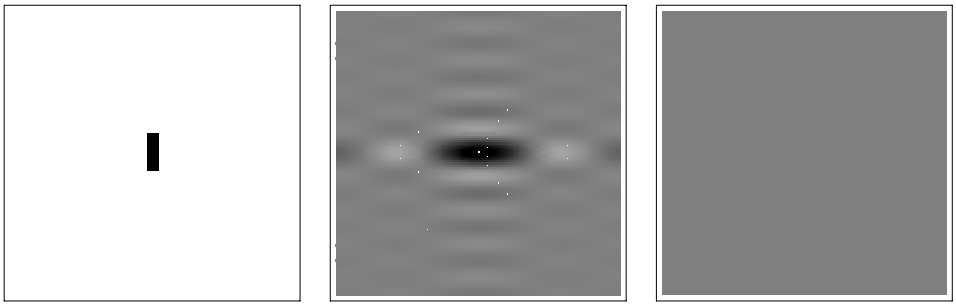

(b)

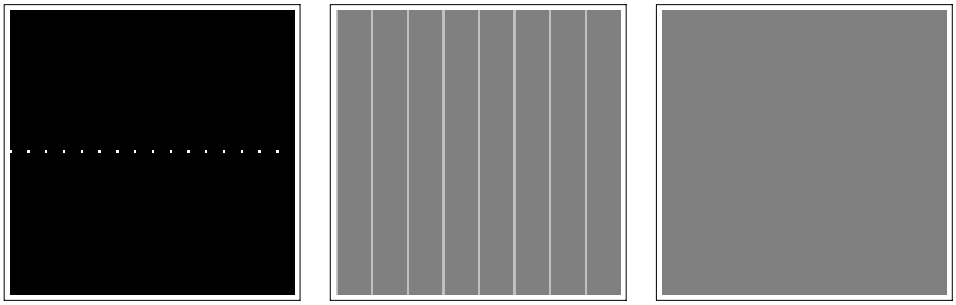

(c)

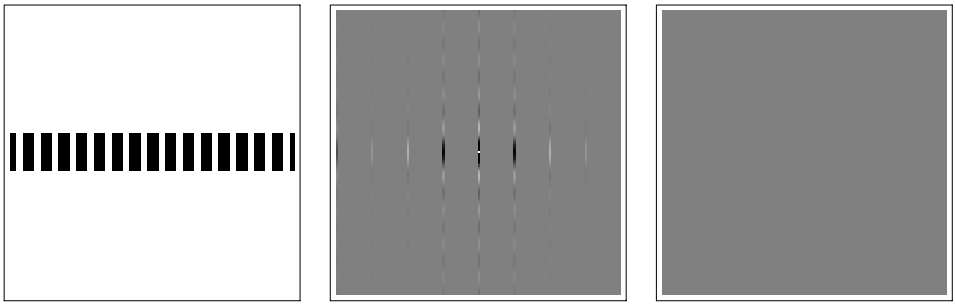

(d)

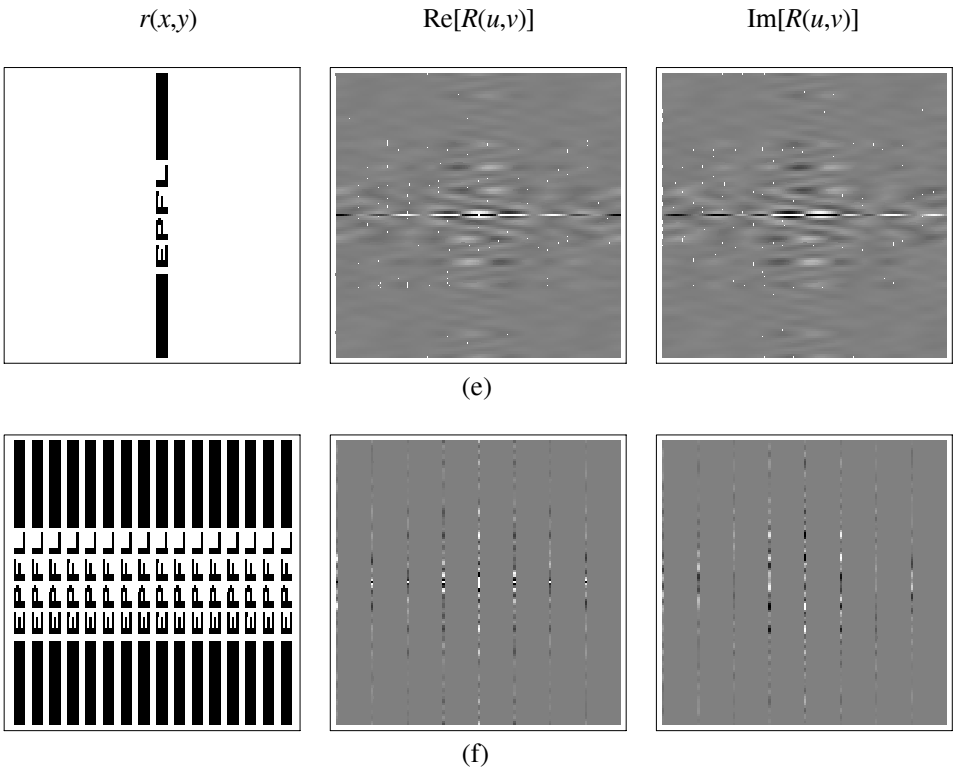

Figure C.11: Explanation of the spectrum of a line grating whose individual lines are modulated by 2D information; two simple examples are shown in (d) and (f). For each image $r(x,y)$ in this figure, $\mathrm{Re}[R(u,v)]$ and $\mathrm{Im}[R(u,v)]$ show the real and the imaginary parts of the spectrum $R(u,v)$ as obtained on computer by 2D DFT. We start with the simple modulated line grating shown in (d): (a) Since the Fourier spectrum of a centered white square of width τ on black background, $d(x,y) = \mathrm{rect}(x/\tau, y/\tau)$, is given by $D(u,v) = \tau^2 \,\mathrm{sinc}(\tau u)\,\mathrm{sinc}(\tau v)$ [Bracewell95 p. 150], it follows that the Fourier spectrum of a centered *black* square of width τ on *white* background, $1 - d(x,y)$, is given by $\mathcal{F}[1 - d(x,y)] = \mathcal{F}[1] - \mathcal{F}[d(x,y)] = \delta(u,v) - D(u,v)$, where $\delta(u,v)$ is an impulse at the origin (note that this impulse is clearly visible in the center of the spectrum). (b) Compressing the black square (a) horizontally results in a horizontal expansion of its spectrum (due to the similarity theorem [Bracewell86 p. 244]). (c) A horizontal impulse comb of constant amplitude; its spectrum is a comb of constant vertical line impulses [Bracewell86 p. 246]). (d) Periodic repetition of the line segment (b) (i.e. its convolution with the constant horizontal impulse comb (c)) gives in the spectral domain, according to the convolution theorem, the product of the spectrum of (b) with the spectrum of (c), namely, a line-impulse comb which is a sequence of vertical slices through the spectrum of (b). The spectrum of the modulated line grating (f) is obtained in the same way: (e) A single modulated line and its spectrum. (f) A periodic repetition of the modulated line (e) gives in the spectral domain a line-impulse comb which is a sequence of vertical slices through the spectrum of (e). Note that the spectra in (e) and (f) are complex-valued.

amplitude variations along the line impulses.[13] It is interesting to note, however, that if the grating lines are only modulated across the line width and their profile remains constant along the line, then the spectrum of the grating reduces into a simple impulse comb in the grating's main direction, as described in Sec. 4.2 and in Fig. 2.5. Another interesting special case occurs when the information that is modulated within each of the lines *is* periodic along the line's direction. In this case each of the parallel continuous line impulses in the spectrum reduces into an impulse comb (which is a discrete subset of the continuous line impulse), and the entire spectrum turns into a 2D nailbed, reflecting the fact that our grating is now a 2-fold periodic structure. Note, however, that in the discussions which follow we do not require periodicity along the grating's individual lines.

Let us now consider the second line grating, $r_2(x,y)$, that is superposed on top of our modulated grating. In the most general case this grating may be modulated by some given information, just as the first grating. However, in our case of interest (see Fig. C.7) the lines of the second grating are only modulated in one direction, across the line widths; typically, our second grating consists of black lines on a white background, or of white lines (or transparent slits) on a black background. The spectrum $R_2(u,v)$ of this grating (see Fig. C.9(e)) is, therefore, a classical impulse comb whose impulses are located in the u,v plane at integer multiples of the grating frequency $\mathbf{f}_2$, exactly as in Fig. 2.5(e).

What happens, now, when we superpose both of our gratings on top of each other with a small angle difference? As we already know, the superposition of the two layers $r_1(x,y)$ and $r_2(x,y)$ is given in the image domain by the product of the two individual layers, $r_1(x,y)r_2(x,y)$; therefore, according to the convolution theorem, the spectrum of the layer superposition is given by the convolution of the two individual spectra, $R_1(u,v)**R_2(u,v)$. In the simple case where none of the grating lines contains information, which is shown in Fig. 2.5, this convolution gives an oblique impulse nailbed (see Fig. 2.5(f)). However, in our present case the spectrum $R_1(u,v)$ of the first grating is no longer an impulse comb but rather a line-impulse comb. And indeed, as already shown in Sec. 10.7.3 for a similar case (see Figs. 10.9(d)–(f)), the convolution of such a line-impulse comb with the impulse comb $R_2(u,v)$ of the second spectrum consists of an infinite number of replicas of the spectrum $R_1(u,v)$, each of which being centered on top of an impulse of the comb $R_2(u,v)$.[14] The resulting spectrum convolution $R_1(u,v)**R_2(u,v)$ is shown in Fig. C.9(f).

At this point it may be helpful to recall the intuitive reasoning that we have presented in Sec. 10.7.3, and to momentarily think of $R_1(u,v)$ as a comb of impulses that "leaked out" perpendicularly to the comb direction to form our parallel continuous line-impulses. Before the impulses "leak out", i.e., when our first grating is still a non-modulated periodic grating $p_1(x,y)$, its spectrum $P_1(u,v)$ is an impulse comb, just like $R_2(u,v)$, and

[13] Obviously, if our grating is not symmetric about the origin, then each of the line impulses in the spectrum may have a complex-valued amplitude. But even in this case the spectrum still remains Hermitian (because our grating is always real valued; see [Bracewell86 pp. 14–15]).

[14] Remember that the convolution of any object with a comb of impulses places a centered replica of that object on top of each impulse of the comb (after properly scaling its amplitude).

therefore the convolution $P_1(u,v)**R_2(u,v)$ is an oblique lattice of impulses like in Fig. 2.5(f). We call this oblique lattice the *skeleton* of our line-impulse spectrum $R_1(u,v)**R_2(u,v)$. As the first grating starts being modulated, all the impulses of this skeleton lattice (except for the impulses of the comb $R_2(u,v)$) start "leaking out" to both directions, forming the line-impulse spectrum of Fig. C.9(d). This point of view allows us to identify each line-impulse in the spectrum of the superposition with the corresponding impulse in the skeleton lattice. Each line-impulse may thus "inherit" the properties of its original skeleton-impulse; the *skeleton location* (or the *center*) of a line-impulse in the spectrum will be defined as the location of its skeleton-impulse, and the *index* of a line-impulse will be defined as the index of its skeleton impulse. This allows us to carry over the important notions of *impulse location* and *impulse index* to the case of continuous line-impulses, too. Hence, a (k_1,k_2)-moiré in the superposition is the moiré which is caused by the (k_1,k_2)-line-impulse in the spectrum convolution (or, in fact, by the (k_1,k_2)-comb of line-impulses). This moiré becomes visible if the center of the (k_1,k_2)-line-impulse is located inside the visibility circle, close to the spectrum origin.

Using this terminology we can say, therefore, that the visible moiré effect in our case is represented in the spectrum convolution (Fig. C.9(f)) by the (1,-1)-line-impulse (whose center is located inside the visibility circle), or, rather, by the entire (1,-1)-comb of line-impulses that it spans.

Thus, by extracting from the spectrum convolution only this line-impulse comb (see Fig. C.10(b)) and taking its inverse Fourier transform, we obtain, back in the image domain, the isolated contribution of the (1,-1)-moiré in question to the image superposition. And indeed, as shown in Fig. C.10(a), this gives us precisely the macroscopic intensity profile of the moiré bands. Note that although this moiré is visible both in the layer superposition (Fig. C.9(c)) and in the extracted moiré intensity profile (Fig. C.10(a)), the latter does not contain the fine structure of the original layers $r_1(x,y)$ and $r_2(x,y)$ but only the pure contribution of the extracted moiré itself.

Now, following the same reasoning as in Sec. 4.2, we may ask ourselves how the intensity profile of the resulting (1,-1)-moiré (Fig. C.10(a)) is related to the gratings $r_1(x,y)$ and $r_2(x,y)$ themselves, in terms of image domain considerations only. To see this, let us first briefly review the simpler case that we have already studied in Chapter 4, in which none of the superposed line gratings contains modulated information.

In the case of Chapter 4 no line combs are involved in the spectral domain, and the spectra of the two given gratings as well as the spectrum of the extracted (1,-1)-moiré are all simple impulse combs. As we have seen in Sec. 4.2, the n-th impulse of the resulting moiré-comb is located in the spectrum at the point:

$$\mathbf{f}_{n,-n} = n\mathbf{f}_1 - n\mathbf{f}_2 \tag{C.12}$$

and its amplitude is given by:

$$d_n = a^{(1)}{}_n \, a^{(2)}{}_{-n} \tag{C.13}$$

where $a^{(1)}_i$ and $a^{(2)}_i$ are the amplitudes of the i-th impulses in the combs of the first and of the second line gratings, respectively. This means, as we have seen in Proposition 4.1, that the impulse amplitudes of the comb of the (1,-1)-moiré in the spectrum convolution are obtained by a term-by-term multiplication of the combs of the original superposed gratings, one of which is being inverted (rotated by 180°) before the multiplication.

Proceeding with this simple non-modulated case we see, therefore, that the moiré comb (Fig. 4.2(b)) can be considered in the spectral domain as a product of the two original combs (Figs. 2.5(d) and 2.5(e)), after they have been normalized (rotated and stretched) to fit the impulse locations of the resulting moiré comb. However, thanks to the 1D T-convolution theorem (see Sec. 4.2), this term-by-term multiplication of the original combs, as defined by Eq. (C.13), can be also represented as a 1D convolution in the image domain. Thus, the (normalized) 1D intensity profile of the extracted (1,-1)-moiré bands is simply the 1D T-convolution of the (normalized) 1D intensity profiles of the two original gratings (see Proposition 4.2 for a more detailed formulation). For example, if one of the superposed gratings (say, the second one) consists of narrow slits on a black background, the 1D intensity profile $p_2(x)$ of its period may be approximated by the 1D impulse $\delta(x)$, and therefore, the normalized 1D intensity profile of the resulting (1,-1)-moiré bands is almost identical to the normalized 1D intensity profile of the first grating.[15] In other words, the 1D intensity profile of the resulting (1,-1)-moiré is simply a magnified and rotated version of the 1D intensity profile of the first grating, where the magnification rate is controlled by the periods of the individual gratings and their angle difference, according to Eqs. (2.9). As we have seen in Sec. 4.3, this reasoning extends easily to the 2D case, too, where both of the superposed layers are dot screens.

Let us now return to our present case, the superposition of a *modulated* line grating with a simple line grating. In this case the situation is slightly different, since the spectra of the first grating and of the resulting (1,-1)-moiré consist of line-impulses, and are no longer simple impulse combs. And indeed, in this case the line-impulse comb in the spectrum convolution that corresponds to our modulated (1,-1)-moiré bands is not a term-by-term product of the (normalized) line-impulse comb of $R_1(u,v)$ with the (normalized) impulse comb of $R_2(u,v)$, since such a term-by-term product would yield a simple *impulse comb* rather than the expected *line-impulse comb*. So how is the line-impulse spectrum of our (1,-1)-moiré effect related to the spectra of the two original gratings? Since the spectrum of Fig. C.9(f) is obtained as a convolution of the line-impulse comb $R_1(u,v)$ with a simple impulse comb, $R_2(u,v)$, it follows from the properties of a convolution with an impulse comb that the line-impulse comb of the (1,-1)-moiré that is generated in the spectrum convolution of Fig. C.9(f) still consists of the same line impulses as the spectrum $R_1(u,v)$ of the modulated grating, where the amplitude of each of these continuous line impulses has only been scaled (during the convolution process) by the amplitude of the corresponding impulse of the simple impulse comb $R_2(u,v)$. Thus, the line-impulse comb of our modulated (1,-1)-moiré is not a normalized term-by-term product of the line-impulse

[15] Remember that the convolution of any object with an impulse $\delta(x)$ simply gives the original object.

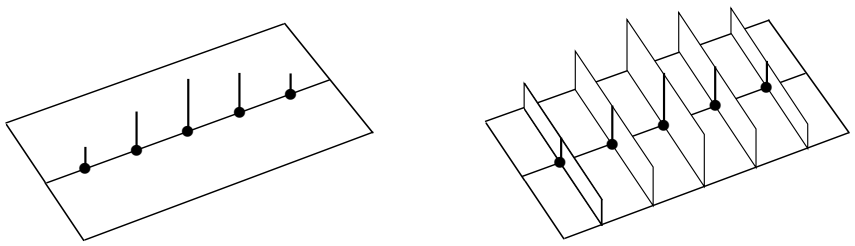

(a) (b)

Figure C.12: (a) The original impulse comb $R_2(u,v)$ of Fig. C.9(e). (b) The line-impulse comb $V_2(u,v)$ which is the constant perpendicular extension of $R_2(u,v)$.

comb $R_1(u,v)$ with the impulse comb $R_2(u,v)$, but rather a normalized term-by-term product of the line-impulse comb $R_1(u,v)$ with the new *line-impulse comb* $V_2(u,v)$ that results from the constant perpendicular extension of the simple impulse comb $R_2(u,v)$ (see Fig. C.12), after having inversed its elements order, as required by Eq. (C.13). The normalization step, which consists of rotation, scaling and *shearing*, guarantees that both of the line-impulse combs being multiplied have the same line-impulse locations and orientations.

Now, returning to the image domain, what is the inverse Fourier transform of the new line-impulse comb $V_2(u,v)$? It turns out that this inverse Fourier transform is simply the 1D section through our second grating along its main direction.[16] Therefore, we may distinguish here between 3 possible cases, just as we did in Sec. 4.4.1 for the classical 2D (1,0,-1,0)-moiré (for the effects of *shearing* in the normalization see Remark C.1 below):

Case 1: If our second grating consists of narrow slits on a black background, as in Fig. C.9(b), its spectrum $R_2(u,v)$ consists of a 1D impulse comb along the grating direction. In this case the inverse Fourier transform of the corresponding extended line-impulse comb

[16] Because the horizontal line impulse $\delta(y)$ over the x,y plane and the vertical line impulse $\delta(u)$ over the u,v plane are a 2D Fourier pair (see [Bracewell86p. 247] or [Bracewell95 pp. 152–153]), it follows from the 2D convolution theorem that if $f(x,y)$ and $F(u,v)$ are a 2D Fourier pair, then the horizontal slice $f(x,y)\delta(y)$ and the vertical extension $F(u,v)**\delta(u)$ are also a 2D Fourier pair [Gaskill78 pp. 307–308]. Note that this result is not limited to horizontal and vertical line impulses, and it can be generalized using the rotation theorem [Bracewell95 p. 157] to perpendicular pairs of line impulses at any other directions. Some graphical examples that may illustrate this rule are shown in [Bracewell86 pp. 246–247]. For example, because the 2D spectrum of a vertical cosinusoidal grating $p(x,y) = \cos(2\pi fx)$ consists of two impulses that are located along the u axis at $u = f$ and $u = -f$, it follows that the 2D spectrum of the horizontal section through this cosinusoidal grating, $p(x,y)\delta(y)$, consists of two vertical line impulses having a constant amplitude, that cross the u axis at the points $u = f$ and $u = -f$. These line impulses are the constant perpendicular extension of the original impulse pair. Note that $\delta(x)$ and $\delta(y)$ are considered here as 2D functions of the two variables x,y, just like the function $p(x,y) = \cos(2\pi fx)$, and they denote here, therefore, the vertical and horizontal line impulses over the x,y plane through its origin [Gaskill78 pp. 85–86]; they should not be confused with the simple impulse $\delta(x)$ in the 1D case.

$V_2(u,v)$ gives back in the image domain a 1D section through our grating's slits, i.e. a train of 1D narrow pulses which can be closely approximated as a simple impulse comb. Therefore, the profile of the resulting (1,-1)-moiré bands in the image domain is simply a 2D *T*-convolution of one period of the modulated grating $r_1(x,y)$ (i.e. an entire 2D modulated line of the grating $r_1(x,y)$) with a simple impulse. This means that the 2D intensity profile of the resulting modulated (1,-1)-moiré band is basically a magnified and rotated (or rather *sheared*, as explained in Remark C.1 below) version of the modulated lines of our first grating $r_1(x,y)$.[17] But because our slits and their 1D section are not really perfect impulses the moiré shapes obtained in the convolution are slightly blurred and rounded, just like in Fig. 4.5(a).

Case 2: Similarly, if our second grating consists of narrow black lines on a white (or rather transparent) background, the profile of the resulting (1,-1)-moiré bands is simply a 2D *T*-convolution of a modulated line of the grating $r_1(x,y)$ with an "inverse" 1D pulse of 0-amplitude on a constant background of amplitude 1. This gives, just as in Case 2 of Sec. 4.4.1, an *inverse-video* version of the moiré bands that are obtained in Case 1. However, for reasons similar to those given in Case 2 of Sec. 4.4.1, the perceived contrast of the moiré in Case 2 appears to the eye much weaker than in Case 1.

Case 3: If our second grating consists of lines having any other profile, the profile form of the resulting (1,-1)-moiré is still a magnified version of the *T*-convolution between a modulated line of the grating $r_1(x,y)$ and a period of the 1D section through the grating $r_2(x,y)$. This *T*-convolution gives, again, some kind of blending between the two original profile shapes, but this time the resulting shape has a rather blurred or smoothed-out appearance and the moiré looks less attractive to the eye. This explains, in particular, the triangular or trapezoidal profile shape of the (1,-1)-moiré bands in the superposition of two simple line gratings as shown, for example, in Fig. 2.5(c) or in Fig. 2.9.

Note that in all of these cases the direction and the frequency of the line-comb of our modulated (1,-1)-moiré, i.e., the direction and the frequency of its (1,-1)-skeleton comb, are given by the direction φ_M and the frequency f_M of the vector $\mathbf{f}_1 - \mathbf{f}_2$; see Eqs. (2.9)–(2.11).

Remark C.1: As we can see in Figs. C.9(f) and C.10(b), the line-impulse comb of our modulated (1,-1)-moiré differs from the spectrum of a modulated grating (Fig. C.9(d)) in that its parallel line-impulses are not orthogonal to the comb direction. Let us try to understand the meaning of this fact.

---

[17] Remember that the inverse Fourier transform of the impulse comb $R_2(u,v)$ gives the entire 2D grating $r_2(x,y)$, while the inverse Fourier transform of $V_2(u,v)$, the constant perpendicular extension of the impulse comb $R_2(u,v)$, gives the 1D section through the 2D grating $r_2(x,y)$ along its main direction. Therefore, if we "forget" to take the constant perpendicular extension of the impulse comb $R_2(u,v)$, the 2D *T*-convolution in the image domain would be performed with the 2D profile of an entire slit of the grating $r_2(x,y)$, i.e. with a *line impulse* rather than with a simple impulse. This, however, does not give the expected result, since the convolution of any given object with a line impulse gives a blurred, continuous replication (or averaging) of the given object along the entire line impulse (see [Gaskill78 p. 308]).

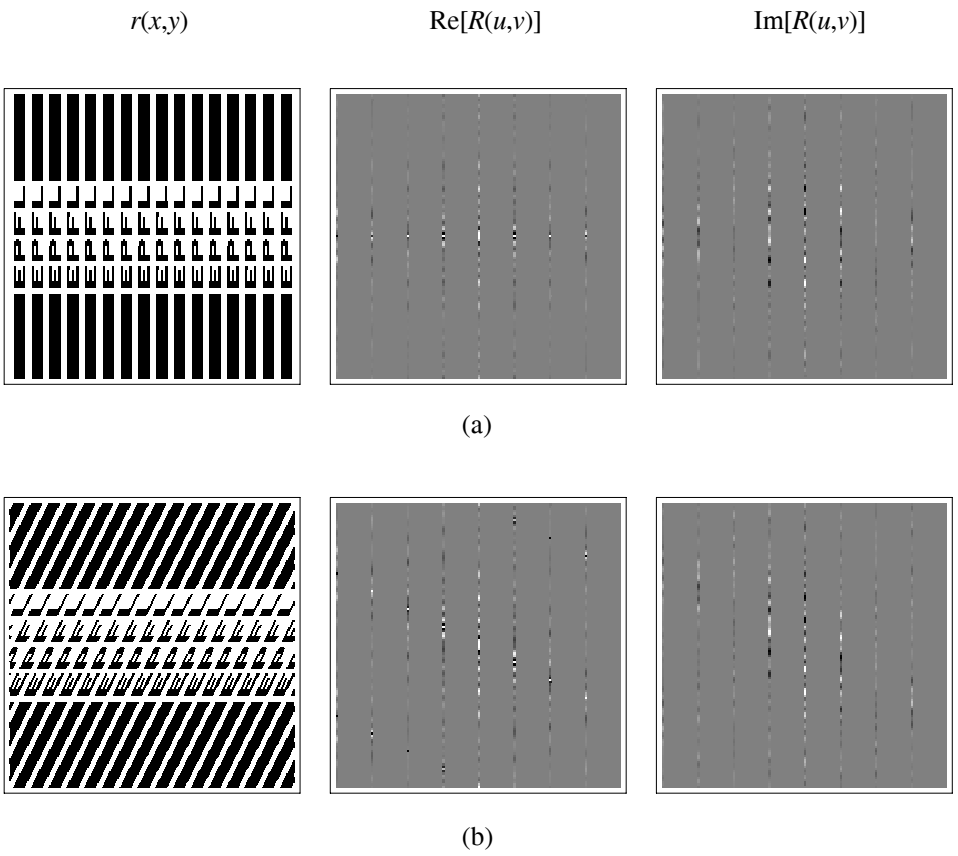

Figure C.13: A vertical shear transformation in the spectrum causes a horizontal shear transformation in the image domain, and vice versa. This is explained by the shear theorem [Bracewell95 p. 158].

As shown in Fig. C.13 (and as we have already seen in Sec. 10.7.3), the non-orthogonal line-impulse comb of Fig. C.10(b) can be obtained from an orthogonal line-impulse comb whose skeleton is located on the u axis by applying a vertical shear transformation, namely, by replacing the vertical coordinate v with $v+bu$ (where the coefficient b, in our case negative, is given by $b = \tan\varphi_M$, φ_M being the direction of the skeleton comb). Now, according to the well-known shear theorem (see, for example, [Bracewell95 p. 158]), a vertical shear in the spectral domain corresponds to a horizontal shear in the image domain, namely: if $f(x,y) \leftrightarrow F(u,v)$ then $f(x+by,y) \leftrightarrow F(u,v-bu)$. This means that our vertically sheared (1,-1)-line-impulse comb corresponds in the image domain to a horizontally sheared modulated moiré-grating. And indeed, as it can be seen in Figs. C.9(c) and C.10(a), the (1,-1)-moiré that we obtain in the present example forms a horizontally sheared periodic grating pattern.

We see, therefore, that while in the simple superposition of non-modulated line gratings (Fig. 2.5) the resulting moiré effect is a magnified and rotated version of the lines of the original grating, in our present case the resulting moiré effect is a magnified and *sheared* version of the modulated lines of the original grating. The reason is, in fact, that the rotation is applied here only to one dimension of the moiré bands (the baseline direction of the modulated text), while the other direction of the modulated text, the letter's height, remains unchanged. This results in a *shearing* effect on the modulated moiré text rather than a *rotation* effect (that would have influenced *both* directions of the text). But when the moiré bands are not modulated and they contain no text (see, for example, the upper or the lower parts of Fig. C.7) this shearing effect can be also considered as a rotation of the moiré bands (with an appropriate scaling of their periods), and both interpretations are in fact equivalent and give the same results. ■

Remark C.2: If the letters that are embedded (or modulated) within the individual lines of the grating $r_1(x,y)$ are not upright but rather slanted (i.e. sheared), while they still keep their original baseline direction, the resulting text within the moiré bands will also be sheared, without affecting its baseline direction. The resulting shear transformation of the moiré text (and hence, its slanting angle, too) can be determined by using the shear theorem. We will return to this point in Remark C.4 at the end of Sec. C.14.4. ■

Remark C.3: It is interesting to note that just like in the similar case discussed in Sec. 10.7.3, when $f_2 > f_1$ (i.e. when the period of the slit grating is smaller than the period of the modulated grating), there exists a critical superposition angle at which all the vertical line impulses of the line-impulse comb of the hybrid (1,-1)-moiré collapse into a single vertical line impulse that coincides with the y axis. This is a particularly interesting situation, because in this case the hybrid (1,-1)-moiré is singular, while its simple (1,-1)-moiré counterpart between non-modulated gratings is not. This singularity of the hybrid moiré can be easily understood in the image domain, too: at this particular superposition angle the resulting moiré bands are perfectly horizontal, which means that the letters embedded in them become infinitely elongated and slanted and hence they are no longer visible. An analogous spectral situation is depicted, for the case described in Sec. 10.7.3, in Fig. 10.12. Note that just like in that analogous case, such a singular state can only occur when $f_2 \geq f_1$, i.e. when $T_2 \leq T_1$; the equality here corresponds to the trivial singular case in which the two superposed layers have identical periods and angles. ■

Finally, it should be noted that just as in Sec. 4.2, our reasoning here can be also generalized to any (k_1,k_2)-moiré. However, the reason we have limited ourselves here to the simplest substractive case, the (1,-1)-moiré, is that this is the only case in which the resulting moiré effect can clearly preserve the letter shapes that are embedded in the individual lines of our first grating. As we have already seen in Chapter 4 (both in the 1D case of line gratings and in the 2D case of dot screens), when higher order moirés are considered the T-convolution theorem is no longer applicable in the image domain, and the relationship between the intensity profile of the resulting moiré and the intensity profiles of the two original layers becomes much more complex.

C.14.3 Generalization to curvilinear gratings

As we have seen in Chapter 10, the results obtained by the Fourier-based approach can be also generalized to cases in which the original periodic layers undergo geometric transformations, either linear or non-linear. The fundamental moiré theorem for the superposition of two curved gratings (see Sec. 10.9.1) determines the effects of such layer transformations on the resulting profile and geometric layout of the (k_1,k_2)-moiré between two gratings. Similarly, the fundamental moiré theorem for the superposition of two curved screens (see Sec. 10.9.2) determines the effects of such layer transformations on the resulting profile and geometric layout of the (k_1,k_2,k_3,k_4)-moiré between two screens. It may be asked, therefore, if a similar rule can be also formulated for our hybrid case, allowing us to see how the application of linear or non-linear transformations to the original gratings will affect the resulting modulated moiré bands.

Because we are only interested here in the simplest, subtractive first-order moiré, let us first reformulate the two fundamental moiré theorems of Chapter 10 specifically for such first-order moirés (see Propositions 10.2 and 10.5):

The fundamental (1,-1)-moiré theorem for line gratings: Let $r_1(x,y)$ and $r_2(x,y)$ be two curvilinear line gratings that are obtained by applying the bending functions (linear or not) $g_1(x,y)$ and $g_2(x,y)$, respectively, to two periodic line gratings having the intensity profiles $p_1(x')$ and $p_2(x')$:

$$r_1(x,y) = p_1(g_1(x,y)), \qquad r_2(x,y) = p_2(g_2(x,y))$$

Then, the (1,-1)-moiré $m(x,y)$ in the superposition of $r_1(x,y)$ and $r_2(x,y)$ is given by:

$$m(x,y) = p(g(x,y))$$

where:

(1) $p(x')$, the normalized intensity profile of the (1,-1)-moiré, is the 1D T-convolution of the normalized intensity profiles of the original gratings:

$$p(x') = p_1(x') * p_2(-x') \tag{C.13}$$

(2) $g(x,y)$, the bending function which brings $p(x')$ back into the actual moiré pattern $m(x,y)$ as it appears in the superposition of the two *transformed* layers, is given by:

$$g(x,y) = g_1(x,y) - g_2(x,y) \quad \blacksquare \tag{C.14}$$

The fundamental (1,0,-1,0)-moiré theorem for dot screens: Let $r_1(\mathbf{x})$ and $r_2(\mathbf{x})$ be two curvilinear screens that are obtained by applying the mappings (linear or not) $\mathbf{g}_1(\mathbf{x})$ and $\mathbf{g}_2(\mathbf{x})$, respectively, to two periodic screens having the intensity profiles $p_1(\mathbf{x}')$ and $p_2(\mathbf{x}')$:

$$r_1(\mathbf{x}) = p_1(\mathbf{g}_1(\mathbf{x})), \qquad r_2(\mathbf{x}) = p_2(\mathbf{g}_2(\mathbf{x}))$$

Then, the (1,0,-1,0)-moiré $m(\mathbf{x})$ in the superposition of $r_1(\mathbf{x})$ and $r_2(\mathbf{x})$ is given by:

$$m(\mathbf{x}) = p(\mathbf{g}(\mathbf{x}))$$

where:

(1) $p(\mathbf{x}')$, the normalized intensity profile of the (1,0,-1,0)-moiré, is the 2D *T*-convolution of the normalized intensity profiles of the original, untransformed screens:

$$p(\mathbf{x}') = p_1(\mathbf{x}') \ast\ast\ p_2(-\mathbf{x}') \tag{C.15}$$

(2) $\mathbf{g}(\mathbf{x})$, the transformation which brings $p(\mathbf{x}')$ back into the actual moiré pattern $m(\mathbf{x})$ as it appears in the superposition of the two *transformed* layers, is given by:

$$\mathbf{g}(\mathbf{x}) = \mathbf{g}_1(\mathbf{x}) - \mathbf{g}_2(\mathbf{x}) \quad \blacksquare \tag{C.16}$$

We now return to the new moiré theorem that we wish to establish for our hybrid case. We have already seen in Sec. C.14.2 above how to formulate its first part, which concerns the intensity profiles: The intensity profile of our hybrid (1,-1)-moiré is the 2D *T*-convolution of the profile of the first, modulated grating with a section through the second, unmodulated grating along its main direction. How can we now formulate the second part of the theorem, which concerns the geometric transformations?

To see this, consider the full componentwise notation of the two layer transformations $\mathbf{g}_1(\mathbf{x})$ and $\mathbf{g}_2(\mathbf{x})$ and of the moiré transformation $\mathbf{g}(\mathbf{x})$:

$$\mathbf{g}_1(\mathbf{x}) = \begin{pmatrix} g_{1,1}(x,y) \\ g_{1,2}(x,y) \end{pmatrix}, \qquad \mathbf{g}_2(\mathbf{x}) = \begin{pmatrix} g_{2,1}(x,y) \\ g_{2,2}(x,y) \end{pmatrix}, \qquad \mathbf{g}(\mathbf{x}) = \begin{pmatrix} g_1(x,y) \\ g_2(x,y) \end{pmatrix}$$

According to Eq. (C.16) of the fundamental (1,0,-1,0)-moiré theorem, the transformation $\mathbf{g}(\mathbf{x})$ undergone by the moiré is given by $\mathbf{g}(\mathbf{x}) = \mathbf{g}_1(\mathbf{x}) - \mathbf{g}_2(\mathbf{x})$. And indeed, in the 2D case, where both of the original, untransformed layers are dot screens, this simply means:

$$\begin{pmatrix} g_1(x,y) \\ g_2(x,y) \end{pmatrix} = \begin{pmatrix} g_{1,1}(x,y) \\ g_{1,2}(x,y) \end{pmatrix} - \begin{pmatrix} g_{2,1}(x,y) \\ g_{2,2}(x,y) \end{pmatrix} \tag{C.17}$$

Now, what happens in the 1D case, i.e. when both of the original, untransformed layers consist of vertical lines with a purely 1D profile? In this case the second component in each of the above transformations becomes irrelevant, and we obtain:

$$\mathbf{g}_1(\mathbf{x}) = \begin{pmatrix} g_{1,1}(x,y) \\ 0 \end{pmatrix}, \qquad \mathbf{g}_2(\mathbf{x}) = \begin{pmatrix} g_{2,1}(x,y) \\ 0 \end{pmatrix}, \qquad \mathbf{g}(\mathbf{x}) = \begin{pmatrix} g_1(x,y) \\ 0 \end{pmatrix}$$

or, more simply, by dropping the unused components and indices:

$$\mathbf{g}_1(\mathbf{x}) = g_1(x,y), \qquad \mathbf{g}_2(\mathbf{x}) = g_2(x,y), \qquad \mathbf{g}(\mathbf{x}) = g(x,y)$$

Therefore in this case Eq. (C.16) reduces into its single-component counterpart:

$$g(x,y) = g_1(x,y) - g_2(x,y) \tag{C.18}$$

which is, indeed, Eq. (C.14) of the fundamental moiré theorem for *line gratings*.

We now return to our present hybrid case. In this case, only one of the two original, untransformed gratings (the second one) has a purely 1D profile, and therefore we have:

$$\mathbf{g}_1(\mathbf{x}) = \begin{pmatrix} g_{1,1}(x,y) \\ g_{1,2}(x,y) \end{pmatrix}, \qquad \mathbf{g}_2(\mathbf{x}) = \begin{pmatrix} g_{2,1}(x,y) \\ 0 \end{pmatrix}, \qquad \mathbf{g}(\mathbf{x}) = \begin{pmatrix} g_1(x,y) \\ g_2(x,y) \end{pmatrix}$$

Hence, Eq. (C.16) of the fundamental moiré theorem simply becomes here:[18]

$$\begin{pmatrix} g_1(x,y) \\ g_2(x,y) \end{pmatrix} = \begin{pmatrix} g_{1,1}(x,y) \\ g_{1,2}(x,y) \end{pmatrix} - \begin{pmatrix} g_{2,1}(x,y) \\ 0 \end{pmatrix} \tag{C.19}$$

which is, indeed, intermediate between the 2D case of Eq. (C.17) and the 1D case of Eq. (C.18). This suggests, once again, that our hybrid superposition could be considered in fact as a "$1\frac{1}{2}$D case". Our new fundamental moiré theorem for the (1,-1)-hybrid case can be therefore formulated as follows:[19]

The fundamental moiré theorem for the hybrid (1,-1)-moiré: Let $r_1(\mathbf{x})$ and $r_2(\mathbf{x})$ be two curvilinear gratings that are obtained by applying the mappings (linear or not) $\mathbf{g}_1(\mathbf{x})$ and $\mathbf{g}_2(\mathbf{x})$, respectively, to a first, modulated periodic grating having the 2D intensity profile $p_1(\mathbf{x}')$, and to a second, unmodulated periodic grating having the intensity profile $p_2(\mathbf{x}')$:

$$r_1\begin{pmatrix} x \\ y \end{pmatrix} = p_1\begin{pmatrix} g_{1,1}(x,y) \\ g_{1,2}(x,y) \end{pmatrix}, \qquad r_2\begin{pmatrix} x \\ y \end{pmatrix} = p_2\begin{pmatrix} g_{2,1}(x,y) \\ g_{2,2}(x,y) \end{pmatrix}$$

Then, the hybrid (1,-1)-moiré $m(\mathbf{x})$ in the superposition of $r_1(\mathbf{x})$ and $r_2(\mathbf{x})$ is given by:

$$m\begin{pmatrix} x \\ y \end{pmatrix} = p\begin{pmatrix} g_1(x,y) \\ g_2(x,y) \end{pmatrix}$$

where:

(1) $p(\mathbf{x}')$, the normalized intensity profile of our hybrid (1,-1)-moiré, is the 2D T-convolution of the normalized intensity profile of the first, original modulated (but untransformed) grating, with a 1D section through the normalized intensity profile of the second, unmodulated grating along its main direction:

$$p\begin{pmatrix} x' \\ y' \end{pmatrix} = p_1\begin{pmatrix} x' \\ y' \end{pmatrix} ** \; p_2\begin{pmatrix} -x' \\ 0 \end{pmatrix} \tag{C.20}$$

(2) $\mathbf{g}(\mathbf{x})$, the transformation which brings $p(\mathbf{x}')$ back into the actual moiré pattern $m(\mathbf{x})$ as it appears in the superposition of the two *transformed* layers, is given by:

$$\begin{pmatrix} g_1(x,y) \\ g_2(x,y) \end{pmatrix} = \begin{pmatrix} g_{1,1}(x,y) \\ g_{1,2}(x,y) \end{pmatrix} - \begin{pmatrix} g_{2,1}(x,y) \\ 0 \end{pmatrix} \quad \blacksquare \tag{C.21}$$

---

[18] The fact that we have chosen here the *second* component of $\mathbf{g}_2(\mathbf{x})$ to be zero is just a matter of convention. We could equally well start our discussion on the hybrid (1,-1)-moiré with gratings made of horizontal rather than vertical lines, in which case the *first* component of $\mathbf{g}_2(\mathbf{x})$ would have been zero. We have chosen to present the hybrid (1,-1)-moiré using vertical gratings in order to remain consistent with our discussions in Chapter 2 (see, for example, Fig. 2.5).

[19] Note that the mathematical development that leads to this result is basically the same as in Sec. 10.9.2, except that $g_4(x,y) = 0$. The slight difference between the indexing conventions that are used here and in Sec. 10.9.2 for the components of the transformations is just a matter of convenience in the notations.

Example C.1: As a simple illustration to this theorem consider, once again, the hybrid (1,-1)-moiré shown in Fig. C.7(c). In this case, the normalized intensity profile of the moiré effect is, indeed, equal to the normalized intensity profile of the first layer, as predicted by the first part of the theorem (see Case 1 in Sec. C.14.2). In order to see how the second part of the theorem works, we start with three normalized vertical gratings having identical periods, which represent the initial, untransformed version of the two original gratings and of the resulting moiré bands. The transformations $\mathbf{g}_1$, $\mathbf{g}_2$ and $\mathbf{g}$ are given, with respect to these initial gratings, as follows: The first grating (the modulated one) does not undergo any layer transformations, so that $\mathbf{g}_1(x,y) = (x,y)$. The second, 1D grating undergoes the 1D transformation $\mathbf{g}_2(x,y) = (0.9x, 0)$, meaning that its horizontal period is slightly stretched out by 1/0.9 = 1.111. Consequently, according to the second part of our theorem, the moiré bands are determined by the transformation:

$$\mathbf{g}\begin{pmatrix} x \\ y \end{pmatrix} = \begin{pmatrix} x \\ y \end{pmatrix} - \begin{pmatrix} 0.9x \\ 0 \end{pmatrix} = \begin{pmatrix} 0.1x \\ y \end{pmatrix} \tag{C.22}$$

meaning that the modulated moiré bands are horizontally stretched by the factor 1/0.1 = 10, while in the vertical direction they remain unchanged.[20] Note that both the first layer and the moiré effect are 2D entities (because they carry 2D information), while the second layer is only of 1D nature, so that the second component of the transformation $\mathbf{g}_2(x,y) = (g_1(x,y),g_2(x,y))$ is $g_2(x,y) = 0$.

As a second simple example, consider the hybrid (1,-1)-moiré shown in Fig. C.7(b). In this case the first part of the theorem remains exactly as in the previous case, but in the second part of the theorem we have:

$$\mathbf{g}\begin{pmatrix} x \\ y \end{pmatrix} = \begin{pmatrix} x \\ y \end{pmatrix} - \begin{pmatrix} x\cos\theta + y\sin\theta \\ 0 \end{pmatrix} = \begin{pmatrix} (1-\cos\theta)x - \sin\theta y \\ y \end{pmatrix} \tag{C.23}$$

This means that the moiré bands have been horizontally stretched out by the factor $1/(1-\cos\theta)$ and horizontally sheared by $\sin\theta y$.[21] ■

Finally, it should be always remembered that the transformations $\mathbf{g}_1$, $\mathbf{g}_2$ and $\mathbf{g}$ are applied to the initially normalized and untransformed layers as *domain* (and hence, *inverse*) transformations. For example, $\mathbf{g}(x,y) = (0.1x, y)$ corresponds to a 10-fold *magnification* in the x direction, and $\mathbf{g}(x,y) = (x - ay, y)$ represents a horizontal shearing effect to the *right*.

---

[20] In fact, if the three original normalized gratings have the period 1, then after the application of the transformations $\mathbf{g}_1$, $\mathbf{g}_2$ and $\mathbf{g}$ the horizontal periods of the two superposed gratings and of the resulting moiré bands are given, respectively, by 1, 1/0.9 = 1.111 and 1/0.1 = 10.

[21] It is interesting to note that $\mathbf{g}_2(x,y)$ only consists here of the first component of the rotation transformation $\mathbf{f}(x,y) = (x\cos\theta + y\sin\theta, -x\sin\theta + y\cos\theta)$, since its second component has no influence on our vertical slit grating and is set to zero (see also Fig. 10.1(b) in Chapter 10). But if the rotation transformation were applied to the *first* layer (the 2D modulated line grating), then $\mathbf{g}_1(x,y)$ would consist of both components of $\mathbf{f}(x,y)$, and the second component of the resulting moiré transformation $\mathbf{g}(x,y)$ would no longer be simply y. And indeed, in this case the resulting moiré text would not only be horizontally scaled and sheared, as in Fig. C.7(b), but also rotated (by the same angle θ as the first, modulated grating).

C.14.4 Synthesis of hybrid (1,-1)-moiré effects

The fundamental moiré theorem for the hybrid (1,-1) case tells us also how we can design layers that will give in their superposition a hybrid (1,-1)-moiré effect having any desired geometric layout, and any predefined information running along each of its moiré bands. In order to obtain hybrid moiré bands whose intensity profiles are modulated by some predefined information, we simply need to embed a flattened version of the information in question inside each of the lines of the first grating, while the second grating should consist of linear slits on a black background. Then, in order to impose on the resulting moiré bands a certain desired geometric layout, we simply have to apply to our original straight gratings transformations $\mathbf{g}_1(\mathbf{x})$ and $\mathbf{g}_2(\mathbf{x})$ whose difference gives the desired moiré-band transformation $\mathbf{g}(\mathbf{x})$, in accordance with Eq. (C.21). Note that $\mathbf{g}_1(\mathbf{x})$, $\mathbf{g}_2(\mathbf{x})$ and $\mathbf{g}(\mathbf{x})$ are understood here as domain transformations that are applied to three untransformed, normalized periodic structures, all of which have the same initial periods and orientations; after the application of these domain transformations the first two structures give the geometric layouts of the two transformed layers, and the third one gives the geometric layout of the resulting moiré pattern.

To illustrate the synthesis of such a hybrid (1,-1)-moiré, let us consider the following interesting example which involves non-linear transformations.

Example C.2: Suppose we wish to generate two layers that give in their superposition a circular moiré effect whose intensity profile consists of repeated occurrences of the digit "1". For didactic reasons we will do this exercise twice, once using the approach based on the fundamental (1,0,-1,0)-moiré theorem for dot screens (as described in Sec. 10.9.2), and then using our new approach based on the fundamental moiré theorem for the hybrid (1,-1) case. Note that in the latter case we could have incorporated into the moiré bands any aperiodic text, but we have chosen to use here the same repetitive pattern of "1"s in order to be able to compare the two approaches using the very same underlying data.

In order to obtain our desired moiré effect using the first approach, as described in Sec. 10.9.2, we start with two original periodic dot screens having identical frequencies and orientations, one of which consists of dots having the shape of tiny "1"s, while the other consists of tiny pinholes on a black background. In order to obtain the desired moiré geometric layout, we may define the moiré transformation $\mathbf{g}(\mathbf{x})$ as follows:

$$\mathbf{g}\begin{pmatrix} x \\ y \end{pmatrix} = \begin{pmatrix} \varepsilon \log(\sqrt{x^2+y^2}) \\ \varepsilon \arctan(y/x) \end{pmatrix} \tag{C.24}$$

where ε is a small positive constant. Note that by using here the logarithm of the radius rather than the radius itself we obtain gradually increasing elements along the radial direction, which is more visually pleasing than keeping fixed sized elements along the radial direction.

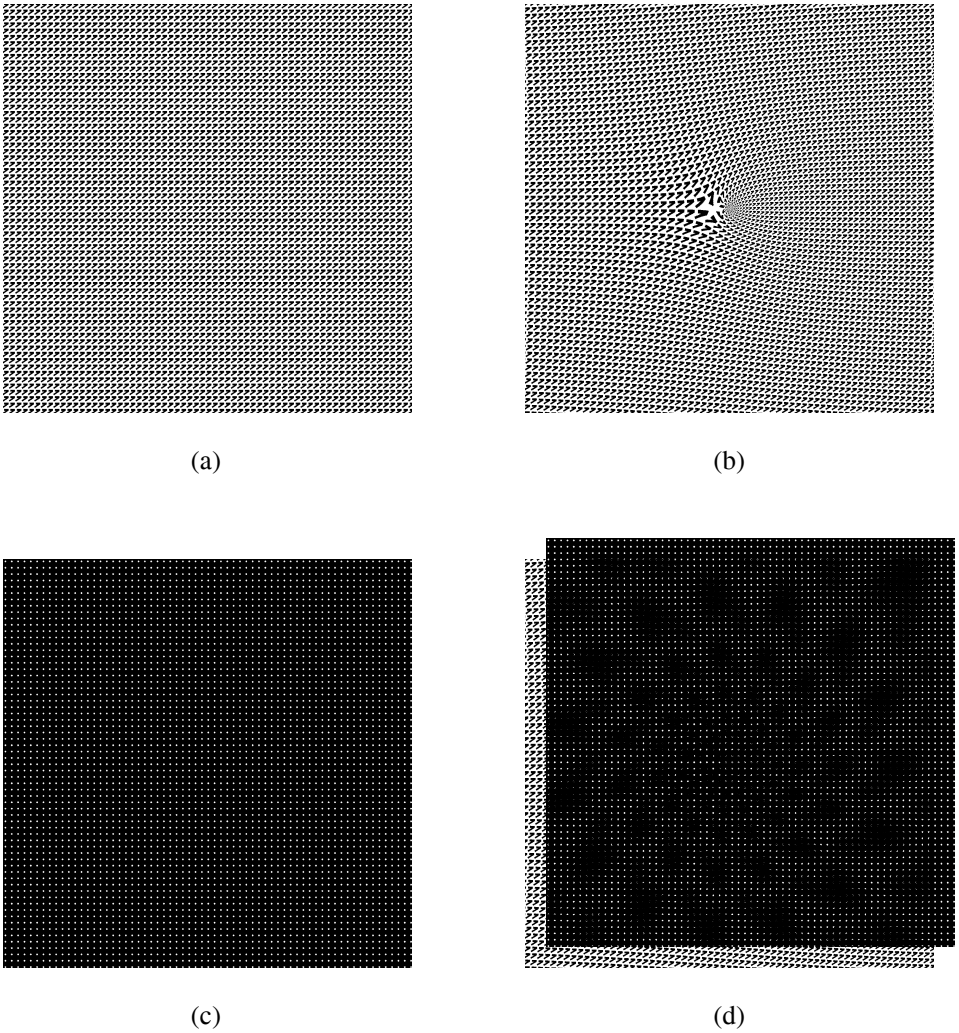

Figure C.14: Synthesis of a circular moiré effect whose intensity profile consists of repeated "1"s using the fundamental (1,0,-1,0)-moiré theorem (see Example C.2). (a) A periodic dot screen whose individual dots have the shape of "1". (b) The same dot screen after having undergone the transformation $\mathbf{g}_1(x,y)$ of Eq. (C.25). (c) A periodic pinhole screen having the same periodicity as the screen (a). (d) The superposition of the screens (b) and (c) gives the desired moiré effect. Note that shifting the second layer horizontally causes the moiré effect to move in the radial direction, while shifting it vertically causes the moiré effect to rotate clockwise or counterclockwise. The dynamics of the moiré effect can be best appreciated by using transparencies of the layers (b) and (c) and sliding them on top of each other.

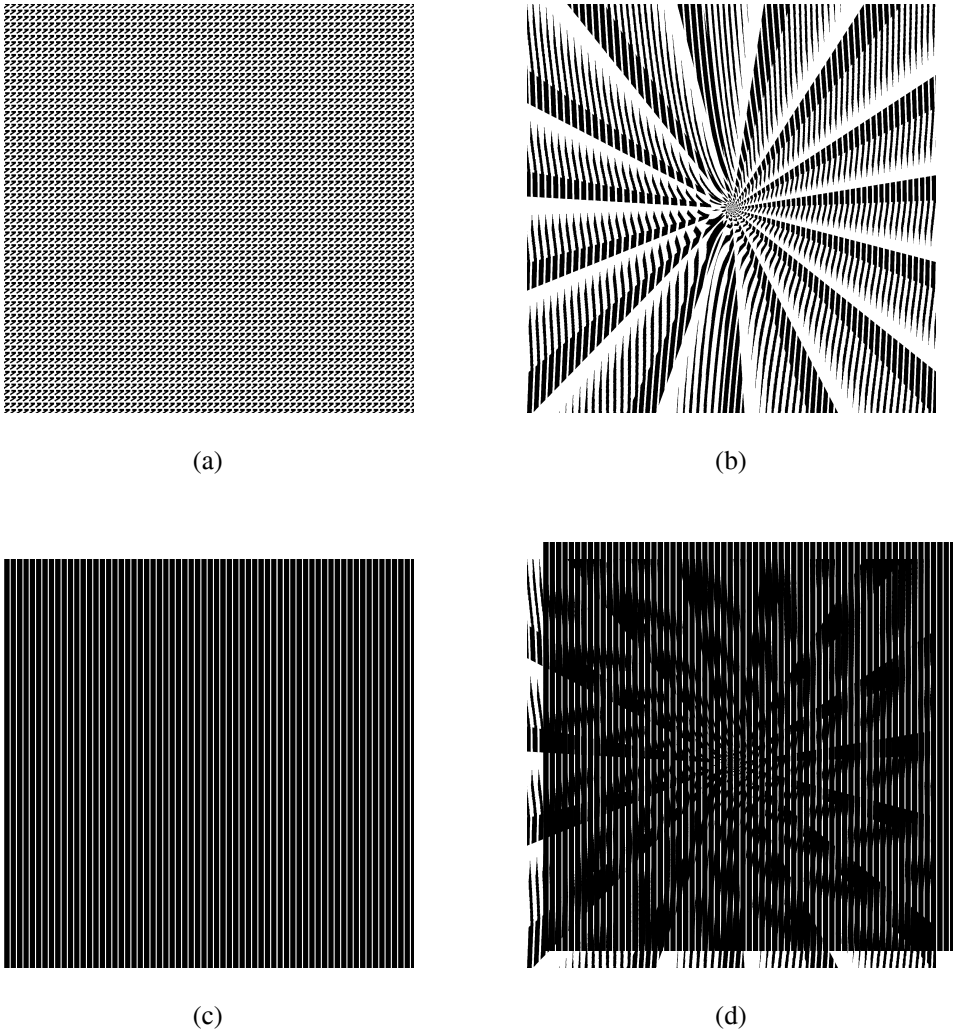

(a) (b)

(c) (d)

Figure C.15: Synthesis of the same macroscopic moiré effect as in Fig. C.14 using, this time, the fundamental moiré theorem for the hybrid (1,-1)-moiré (see Example C.2). (a) The same periodic dot screen as in Fig. C.14(a). (b) The same dot screen after having undergone the transformation $\mathbf{g}_1(x,y)$ of Eq. (C.26). (c) A periodic grating consisting of vertical slits having the same horizontal periodicity as the screen (a). (d) The superposition of the screens (b) and (c) gives the desired moiré effect. Note that shifting the second layer horizontally causes the moiré effect to move in the radial direction, but unlike in Fig. C.14, shifting it vertically has no effect on the resulting moiré. The dynamics of the moiré effect can be best appreciated by using transparencies of the layers (b) and (c) and sliding them on top of each other.

Now, according to Eq. (C.16), all that we have to do is to apply to our original periodic layers two layer transformations $\mathbf{g}_1(\mathbf{x})$ and $\mathbf{g}_2(\mathbf{x})$ such that $\mathbf{g}(\mathbf{x}) = \mathbf{g}_1(\mathbf{x}) - \mathbf{g}_2(\mathbf{x})$. Obviously, there exist infinitely many ways to define transformations $\mathbf{g}_1(\mathbf{x})$ and $\mathbf{g}_2(\mathbf{x})$ that satisfy this condition, but if we wish to transform only one of the two original layers, say, the first one, we may choose the transformations:

$$\mathbf{g}_1\begin{pmatrix} x \\ y \end{pmatrix} = \begin{pmatrix} x \\ y \end{pmatrix} + \begin{pmatrix} \varepsilon\log(\sqrt{x^2+y^2}) \\ \varepsilon\arctan(y/x) \end{pmatrix}, \qquad \mathbf{g}_2\begin{pmatrix} x \\ y \end{pmatrix} = \begin{pmatrix} x \\ y \end{pmatrix} \tag{C.25}$$

And indeed, as shown in Fig. C.14, this choice of layers and geometric transformations gives us in the superposition the desired moiré effect, using the first approach.

Now, if we wish to obtain a similar result using the second approach, i.e. using the hybrid (1,-1)-moiré effect, we have to start with two original periodic line gratings having identical frequencies and orientations: One of the gratings incorporates along each of its lines a sequence of tiny "1"s (which, in principle, could be replaced, if we so desired, by any aperiodic text running along the line), while the other grating consists of straight narrow slits on a black background.[22] Assuming that we want to obtain precisely the same moiré transformation, as given by Eq. (C.24), all that we have to do now is to apply to our two original periodic gratings two layer transformations $\mathbf{g}_1(\mathbf{x})$ and $\mathbf{g}_2(\mathbf{x})$ that satisfy Eq. (C.21) (rather than Eq. (C.16) in the first approach). If, once again, we wish to transform only one of the two original layers, we may choose this time the following layer transformations:[23]

$$\mathbf{g}_1\begin{pmatrix} x \\ y \end{pmatrix} = \begin{pmatrix} x \\ 0 \end{pmatrix} + \begin{pmatrix} \varepsilon\log(\sqrt{x^2+y^2}) \\ \varepsilon\arctan(y/x) \end{pmatrix}, \qquad \mathbf{g}_2\begin{pmatrix} x \\ y \end{pmatrix} = \begin{pmatrix} x \\ 0 \end{pmatrix} \tag{C.26}$$

Note that the only difference between the geometric transformations (C.25) and (C.26) that we apply to the layers in our two approaches is that in the latter approach the second component of $\mathbf{g}_2$ remains zero, so that we must replace the term (x,y) in both $\mathbf{g}_1(\mathbf{x})$ and $\mathbf{g}_2(\mathbf{x})$ by $(x,0)$. And indeed, as shown in Fig. C.15, this choice of layers and geometric transformations gives us in the superposition a moiré effect having the same intensity profile as in Fig. C.14, but, this time using the hybrid (1,-1)-moiré effect. Note, however, that only the macroscopic properties of the moiré (its intensity profile, its geometric layout, etc.) are common to both cases; the microstructure details, on their part, are obviously different.

Finally, it is interesting to note that the two similar moiré effects shown in Figs. C.14 and C.15 also have a similar dynamic behaviour: In Fig. C.14, when the second layer is slowly shifted on top of the first layer horizontally, the resulting moiré effect moves

---

[22] Note that in practice we can use here the same first layer as in the first approach, since a dot screen consisting of periodic "1"s can be also viewed as a grating composed of lines that consist of a periodic sequence of "1"s.

[23] Note that in this case the *second* component of our desired transformation (C.24) must be entirely taken care of by $\mathbf{g}_1(\mathbf{x})$, since the second component of $\mathbf{g}_2(\mathbf{x})$ has no influence and is set to zero. However, the *first* component of our desired transformation (C.24) can be distributed between the two layer transformations $\mathbf{g}_1(\mathbf{x})$ and $\mathbf{g}_2(\mathbf{x})$ as we may wish.

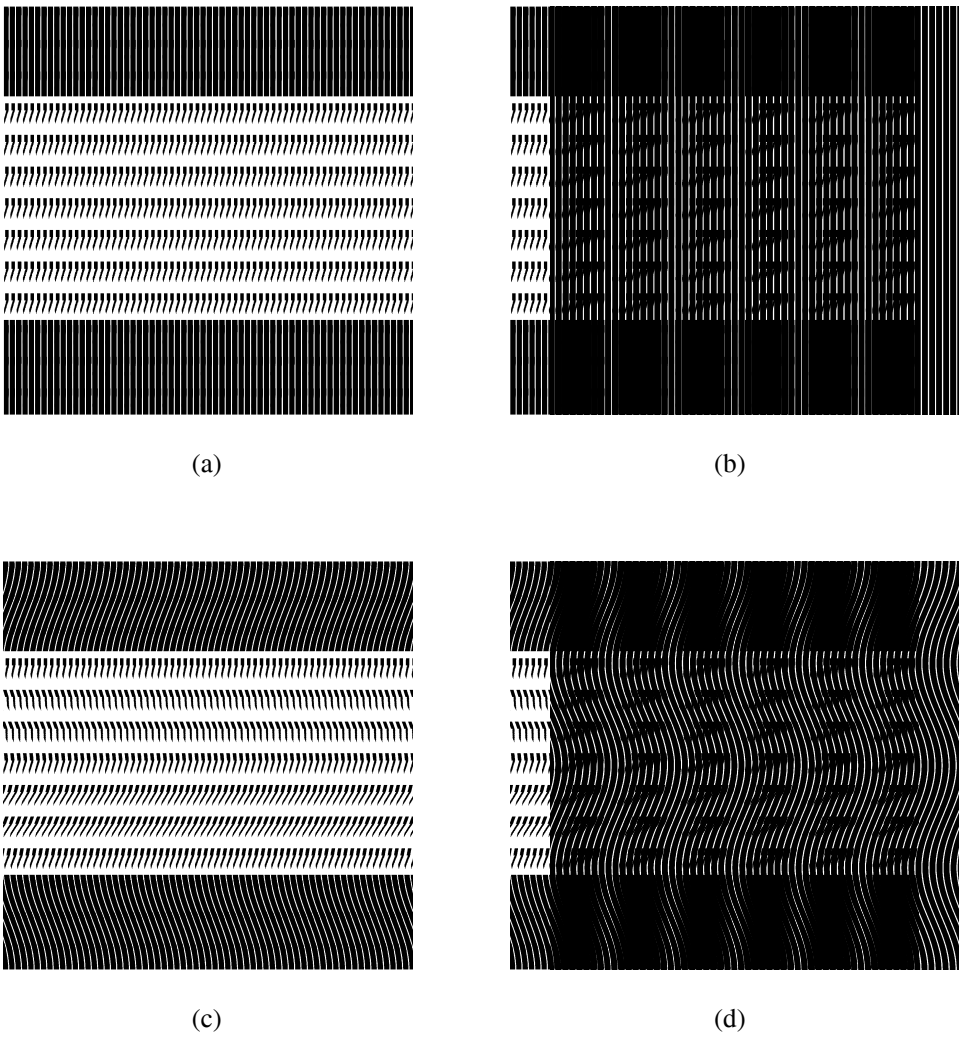

Figure C.16: (a),(b) A hybrid (1,-1)-moiré giving vertical moiré bands like in Fig. C.7(c). (c),(d) If the first, modulated grating undergoes a horizontal transformation $\mathbf{g}_1(x,y) = (g_{1,1}(x,y), y)$, it is still possible to apply to the second, slit grating a compensating transformation $\mathbf{g}_2(x,y)$ such that the resulting moiré remains unchanged (see Example C.3). Note that the information embedded along each of the vertical lines of the first grating needs not necessarily be periodic like in (a) and (c), and it may include any aperiodic text.

rapidly in the radial direction outward or inward, depending on the direction of the horizontal shift; and when applying a vertical shift, the resulting moiré effect rotates clockwise or counterclockwise, depending on the direction of the vertical shift. The hybrid

case of Fig. C.15, however, only inherits the dynamic behaviour of Fig. C.14 in the *horizontal* direction, giving a radial motion of the moiré, while vertical shifts have no effect on the resulting moiré. Can you think of a similar hybrid (1,-1)-moiré that only inherits the dynamic behaviour of Fig. C.14 in the *vertical* direction, giving a circular motion of the moiré, while horizontal shifts have no effect on the resulting moiré? (*Hint*: in Eqs. (C.25), zero the x components rather than the y components as we did in Eqs. (C.26).) Note that the dynamic effects of the moiré can be best observed by printing the two layers in question on transparencies and shifting them on top of each other. ■

Example C.3: Suppose that we are given a vertical hybrid (1,-1)-moiré like in Fig. C.7(c) (see Figs. C.16(a),(b)), and that we apply to its first, modulated grating (Fig. C.16(a)) a geometric transformation $\mathbf{g}_1(x,y)$. For example, we may bend the straight vertical lines of this grating into cosinusoidal lines, as shown in Fig. C.16(c), by using the transformation:

$$\mathbf{g}_1\begin{pmatrix} x \\ y \end{pmatrix} = \begin{pmatrix} x - \varepsilon\cos(2\pi f y) \\ y \end{pmatrix} \tag{C.27}$$

where ε is a small positive constant. What geometric transformation $\mathbf{g}_2(x,y)$ should be applied to the second layer, the slit grating, in order to keep the moiré bands straight as before?

Following the same reasoning as in Sec. 10.9 (see, for instance, Eqs. (10.35) and (10.44) and Examples 10.20–10.23), it is easy to see that vertical, periodic moiré bands occur in our superposition *iff* the moiré transformation has the form:

$$\mathbf{g}\begin{pmatrix} x \\ y \end{pmatrix} = \begin{pmatrix} x/T_x + c \\ y \end{pmatrix}$$

where T_x is the desired horizontal magnification of the vertical moiré bands,[24] and c is their horizontal displacement (that we assume here to be zero).

Now, since the transformations $\mathbf{g}_1(x,y)$ and $\mathbf{g}(x,y)$ are already known, it follows from Eq. (C.21) that the transformation $\mathbf{g}_2(x,y)$ is given by their difference:

$$\mathbf{g}_2\begin{pmatrix} x \\ y \end{pmatrix} = \mathbf{g}_1\begin{pmatrix} x \\ y \end{pmatrix} - \mathbf{g}\begin{pmatrix} x \\ y \end{pmatrix} = \begin{pmatrix} (1 - 1/T_x)x - \varepsilon\cos(2\pi f y) \\ 0 \end{pmatrix}$$

And indeed, as illustrated in Fig. C.16(d), the application of this transformation to our slit grating gives in the superposition exactly the same straight moiré bands as in Fig. C.16(b).

Now, is it also possible to expand the resulting moiré text vertically, say, by a factor of two? In order to obtain this result, the moiré transformation should obviously be:

$$\mathbf{g}\begin{pmatrix} x \\ y \end{pmatrix} = \begin{pmatrix} x/T_x \\ y/2 \end{pmatrix}$$

[24] In fact, if the original gratings are normalized and have the period 1, then T_x simply indicates the horizontal period of the moiré bands.

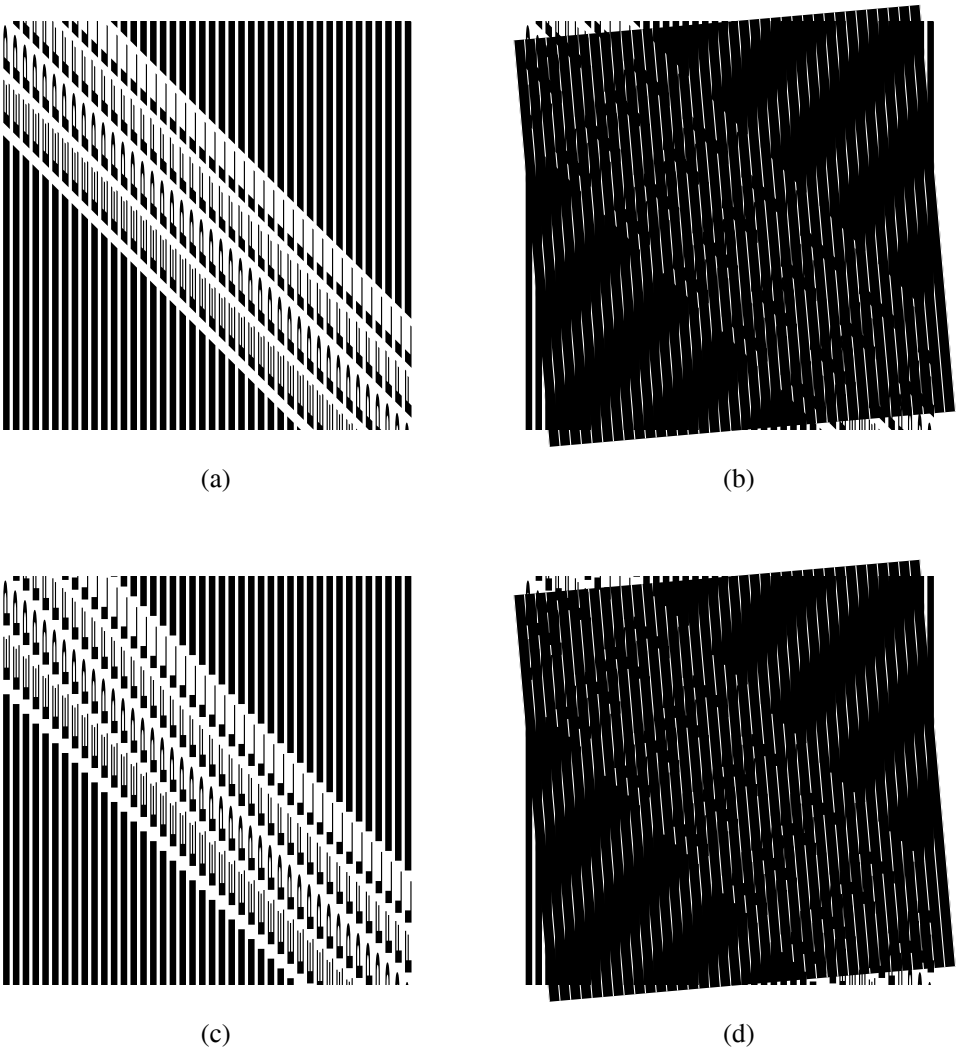

(a) (b)

(c) (d)

Figure C.17: Rectification of the slanted text within the moiré bands can be obtained in two different ways (compare with Fig. C.7(a),(b)): By applying to the original modulated grating a shearing transformation, as shown in (a) and (b); or by staggering, i.e. by gradually shifting (advancing or retracting) the text periods within the original modulated grating without slanting the letters themselves, as shown in (c) and (d). In the latter case the resulting moiré periods are both slanted and shifted with respect to each other (staggered). The slit grating used in (b) and (d) is identical to the one used in Fig. C.7(b). Note that in both (b) and (d) the non-modulated parts of the moiré bands remain identical to those of Fig. C.7(b), and only the text within the bands is affected. (The quality of the resulting moiré letters can be significantly improved by increasing the resolution and the frequency of the original layers or by modifying their rotation angles.)

$r(x,y)$ $\mathrm{Re}[R(u,v)]$ $\mathrm{Im}[R(u,v)]$

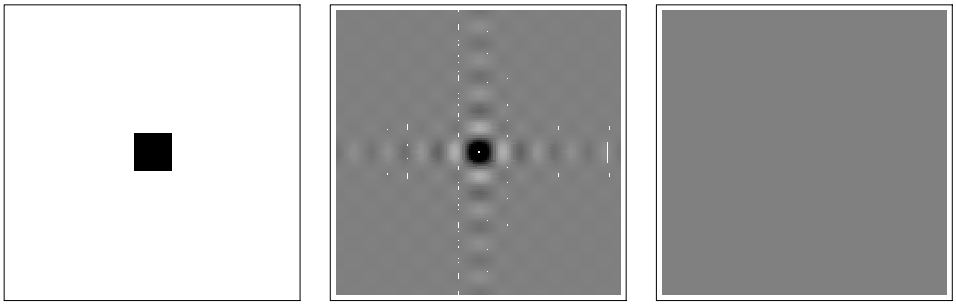

(a)

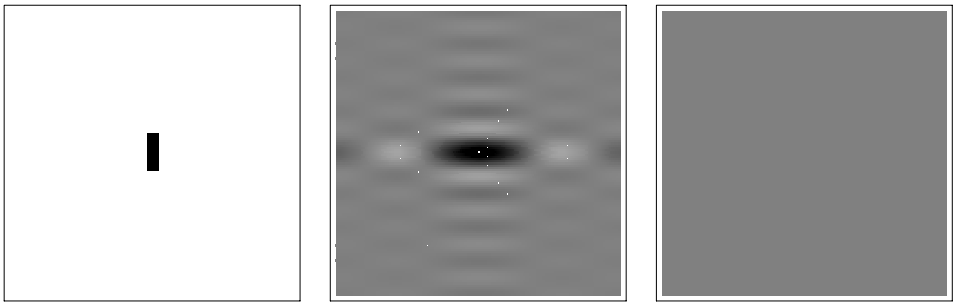

(b)

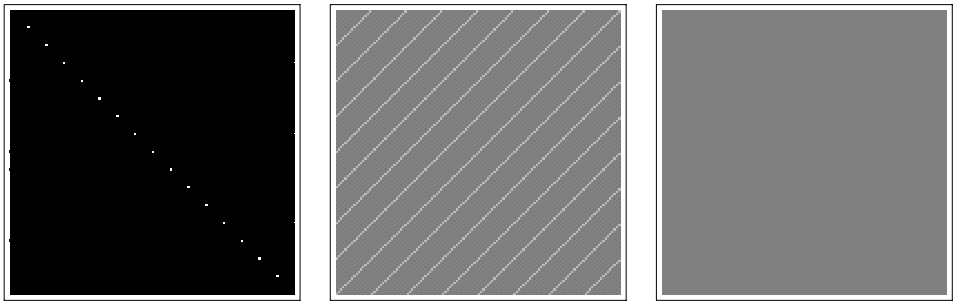

(c)

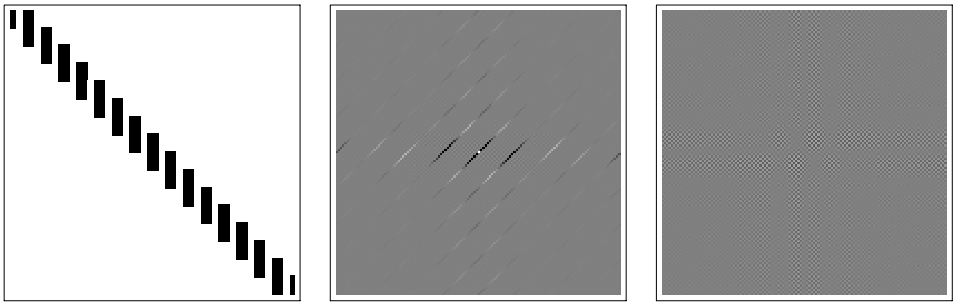

(d)

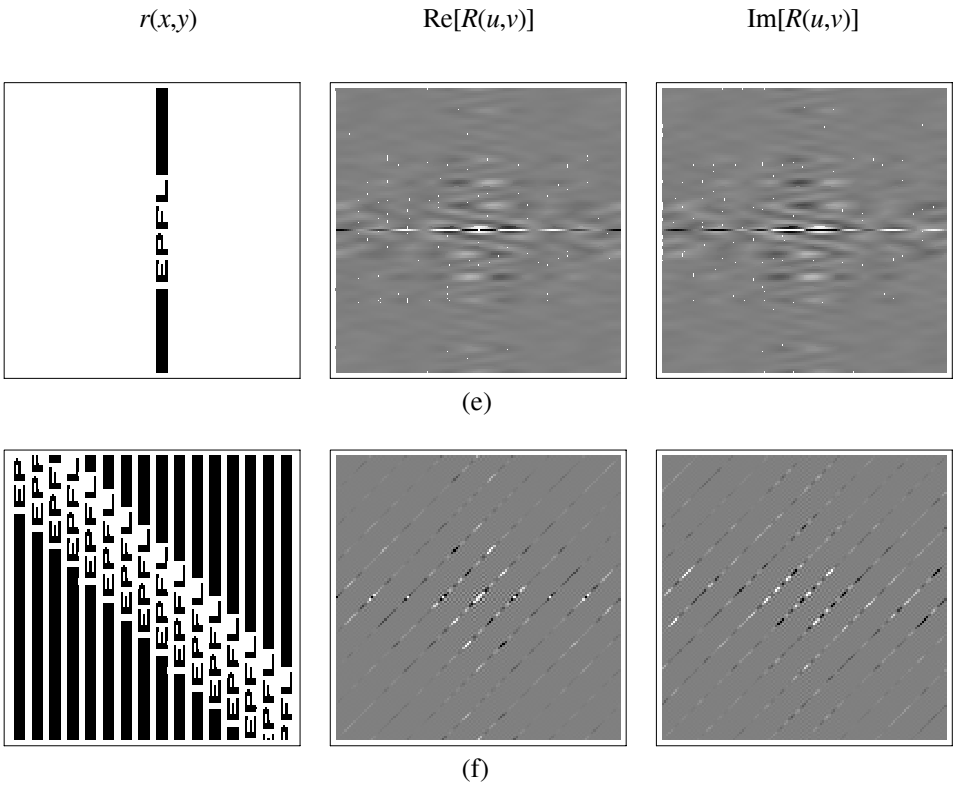

Figure C.18: Explanation of the spectrum of a staggered line grating whose individual modulated lines are gradually shifted along the line direction; two simple examples are shown in (d) and (f). The explanation here is the same as in Fig. C.11, except that this time the single modulated lines, (b) or (e), are convolved with a *slanted* impulse comb (c). In the resulting line gratings, shown respectively in (d) and (f), the modulated periods are gradually shifted along the lines of the grating. The spectrum of such staggered gratings consists of slanted (rather than vertical) blades that sample the same spectrum as in Fig. C.11, i.e. the spectrum of the corresponding single line, (b) or (e). Note that according to the shearing theorem the spectrum of a vertically *sheared* version of the gratings of Figs. C.11(d) and C.11(f) would consist of similar slanted blades, but these blades would sample the horizontally sheared spectra that correspond to the vertically sheared version of the single lines (b) and (e). In other words, in both cases the sampling blades are the same, and the difference is only in the *envelope* of the sampled spectra, i.e. in the amplitude of the resulting line impulses.

If we were using here the (1,0,-1,0)-moiré between two dot screens we could have distributed this transformation between the two layer transformations $\mathbf{g}_1(x,y)$ and $\mathbf{g}_2(x,y)$ at will, provided that their difference gives $\mathbf{g}(x,y)$ (see Eq. (C.16)). However, because we are using here the hybrid (1,-1)-moiré we are slightly more limited, since the second component of $\mathbf{g}_2(x,y)$ has no influence and is set to zero (see Eq. (C.21)). This means that

the *second* component of $\mathbf{g}(x,y)$ must be entirely taken care of by $\mathbf{g}_1(x,y)$, although the *first* component of $\mathbf{g}(x,y)$ can be distributed between $\mathbf{g}_1(x,y)$ and $\mathbf{g}_2(x,y)$ at will. In other words, using the hybrid (1,-1)-moiré the only way to expand our resulting moiré text *vertically* is by applying this vertical expansion to the first layer (the modulated grating). For example, we may choose the layer transformations:

$$\mathbf{g}_1\begin{pmatrix} x \\ y \end{pmatrix} = \begin{pmatrix} x - \varepsilon\cos(2\pi f y) \\ y/2 \end{pmatrix}, \qquad \mathbf{g}_2\begin{pmatrix} x \\ y \end{pmatrix} = \begin{pmatrix} (1 - 1/T_x)x - \varepsilon\cos(2\pi f y) \\ 0 \end{pmatrix}$$

But if we insist on using the same modulated grating as before (namely, Eq. (C.27); see Fig. C.16(c)), then no transformation $\mathbf{g}_2(x,y)$ to be applied to the slit grating will be able to provide a vertical magnification of the resulting moiré bands. ■

Remark C.4: Due to the shearing effect that is inherent to the hybrid (1,-1)-moiré the resulting text in the moiré bands may sometimes appear too slanted and therefore hardly recognizable (see, for example, Fig. C.8). In such cases it may be advantageous, in order to straighten up the text which appears within the resulting moiré bands, to design the original, modulated grating with already back-slanted (or over-slanted) text. This initial slanting of the text can be seen mathematically as a vertical shearing transformation that has been applied beforehand to the first, modulated grating (see Fig. C.17(a)):

$$\mathbf{v}\begin{pmatrix} x \\ y \end{pmatrix} = \begin{pmatrix} x \\ y + ax \end{pmatrix} \tag{C.28}$$

To see the effect of this layer transformation on the resulting moiré bands compare Figs. C.17(a),(b) with Figs. C.7(a),(b); note that in both cases the same slit grating is being used. As we can see in Fig. C.17(b), this straightening method only affects the text slanting within the moiré bands, but the moiré bands themselves remain unchanged, as in Fig. C.7(b). This shearing effect can be easily explained by applying the shear theorem to Figs. C.9(a),(d) and observing its effects on Figs. C.9(c),(f) and C.10.

If, in addition to the shearing $\mathbf{v}(x,y)$, we wish to distort our modulated grating by a geometric transformation:

$$\mathbf{f}\begin{pmatrix} x \\ y \end{pmatrix} = \begin{pmatrix} f_1(x,y) \\ f_2(x,y) \end{pmatrix} \tag{C.29}$$

then we have to apply this transformation to the already sheared (back-slanted or over-slanted) layer, meaning that the global transformation undergone by the original, modulated layer is given by $\mathbf{g}_1(x,y) = \mathbf{f}(\mathbf{v}(x,y))$, namely:

$$\mathbf{g}_1\begin{pmatrix} x \\ y \end{pmatrix} = \mathbf{f}\begin{pmatrix} x \\ y + ax \end{pmatrix} = \begin{pmatrix} f_1(x,\, y + ax) \\ f_2(x,\, y + ax) \end{pmatrix}$$

The resulting transformation of the moiré bands can be obtained, as usual, using Eq. (C.21).

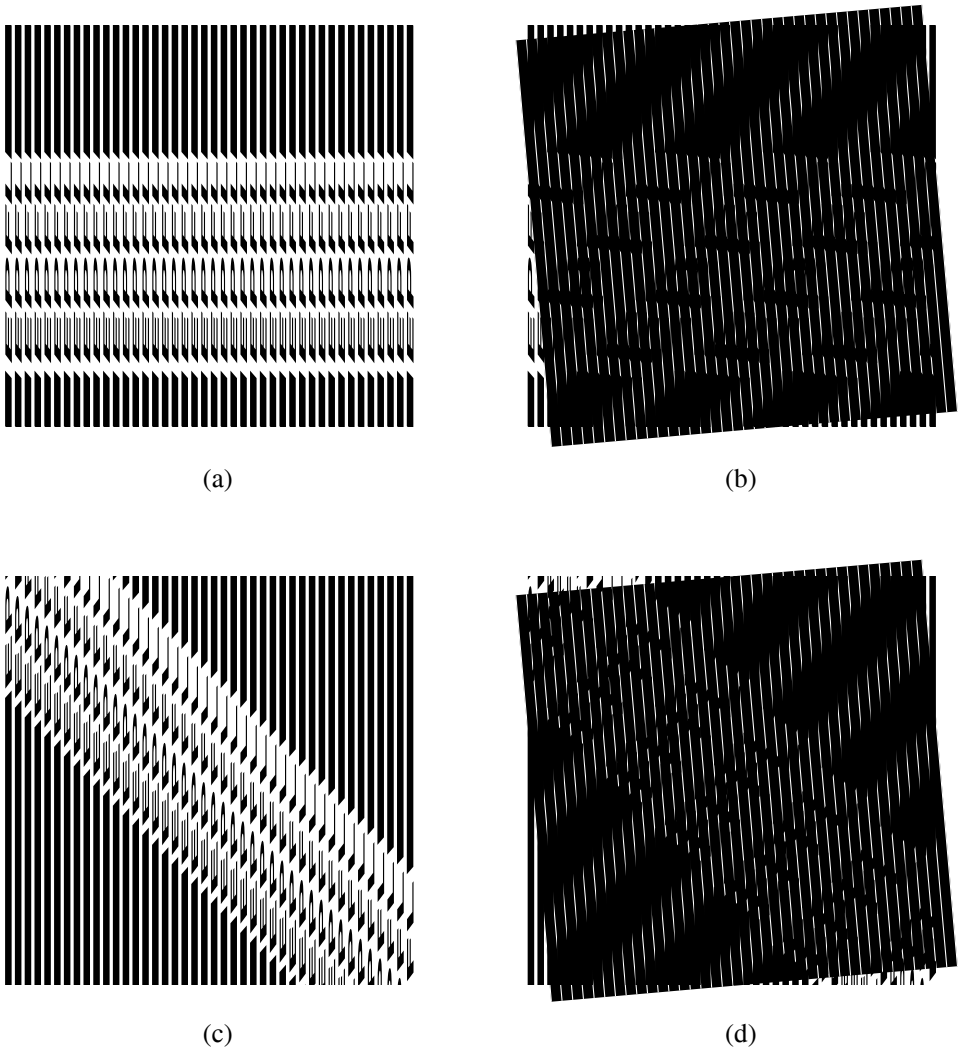

(a) (b)

(c) (d)

Figure C.19: The effect of combined shearing and staggering in the first, modulated grating on the resulting moiré bands. (a),(b) Vertical shearing like in Fig. C.17(a) which is compensated by staggering in the opposite direction. (c),(d) Vertical shearing in the opposite direction followed by staggering; compare with Figs. C.17(c),(d). The slit grating used in (b) and (d) is identical to the one used in Fig. C.7(b) and in Figs. C.17(b),(d).

Another straightening effect can be also obtained by gradually shifting (advancing or retracting) the text positioning along consecutive lines of the first grating, without slanting the letters themselves (see Fig. C.17(c)). In this case the period of the first, modulated grating is no longer a scalar T_1, as in Fig. C.7(a), but rather a vector $\mathbf{T}_1 = (T_x, T_y)$, where

$T_x = T_1$ and T_y is the new vertical shift increment between two consecutive periods of the first, modulated grating (Fig. C.17(c)). To see how this staggering effect affects the resulting moiré bands, compare Figs. C.17(c),(d) with Figs. C.7(a),(b); note that in both cases the same slit grating is being used. As we can see in Fig. C.17(d), this staggering in the first, modulated grating results in a shearing of the moiré text of Fig. C.7(b), which is also accompanied by staggering. But here, too, the non-modulated parts of the moiré bands remain unchanged, as they were in Fig. C.7(b). This effect can be explained once we understand the spectrum of the staggered grating, which is explained in detail in Fig. C.18. As we can see, the spectrum of a staggered grating is similar to the spectrum of a vertically sheared grating that is obtained by the application of the shear theorem, and both consist of slanted line impulses that sample the spectrum of a single modulated line. The difference between these spectra is only in their envelopes (i.e. in the amplitudes of the continuous spectra that are being sampled by the line impulses): In the case of a sheared grating the spectrum of the single modulated line that is being sampled is sheared, too, while in the case of a staggered grating the spectrum of the single modulated line is *not* sheared. Now, if the staggering effect and its spectral counterpart are applied to Figs. C.9(a),(d), they also influence accordingly Figs. C.9(c),(f) and the extracted moiré in Fig. C.10. Note, in particular, that the resulting moiré periods are not only staggered, but also sheared. The *shearing* effect in the resulting moiré is due to the slanting of the line impulses in the spectrum of the staggered grating (see Figs. C.18(d) and (f)), which also affects the slanting of the line impulses in the spectrum convolution (Fig. C.9(f)) and in the spectrum of the resulting moiré (Fig. C.10(b)). The *staggering* effect in the resulting moiré is due to the difference, in the spectrum of the resulting moiré, between the shearing that applies to the sampling blades and the shearing that applies to the underlying continuous spectrum of a single moiré period. This can be best understood by considering a version of Fig. C.18 in which the single period element, (b) or (e), is in itself vertically sheared, independently of the staggering effect.

Obviously, the two straightening effects mentioned above (shearing and staggering) can be also used together in various different combinations, as shown, for example, in Figs. 19(a),(b) and in Figs. 19(c),(d).

A detailed formulation of the effects of shearing, staggering and geometric transformations on the resulting moiré periods (using a different approach that is based on geometric considerations and indicial equations) can be found in [Hersch04] and in [Chosson06]. ■

C.15 Moiré effects between general 2-fold periodic layers

Moiré effects that are generated between 2-fold periodic layers such as line grids or dot screens have a particular importance in the moiré theory and in many applications. Such moiré effects have been discussed in the second part of Chapter 4 (in Secs. 4.3–4.5), following the discussion on the moiré effect between 1-fold periodic line gratings in Sec.

4.2. But although the results obtained in Chapter 4 are fully general, we have only illustrated them there for the particular case in which each of the given 2-fold periodic layers (line grid or dot screen) is *regular*, i.e. periodic in two orthogonal directions with an identical period length to both directions. This simple 2-fold periodic case is, indeed, a rather straightforward generalization of the 1-fold periodic case, because each regular grid (or screen) can be considered as a composition of two orthogonal gratings (or virtual gratings), who generate in the superposition the two orthogonal directions of the resulting 2-fold periodic moiré (see Secs. 2.11, 2.12 and Fig. 2.10).

However, while the simple case consisting of regular layers is certainly the most basic 2-fold periodic case, both for didactic reasons and for many practical purposes, it is not yet sufficiently general. For example, it does not include the moiré effects that are generated between oblique screens or between hexagonal screens (see Fig. 2.13(b)), cases which may turn to be quite advantageous in certain applications.[25] Although such cases are covered by our results in Chapter 4, their particular behaviour is not explicitly obvious from these general results.

In the present section we provide an alternative, yet completely equivalent approach that more explicitly illustrates all of the 2-fold periodic cases, either regular or not. This approach is based on results that we obtained in Chapter 10 for the superposition of curved screens (see Sec. 10.9.2); but instead of considering general non-linear layer transformations $\mathbf{g}_1(\mathbf{x})$ and $\mathbf{g}_2(\mathbf{x})$, that yield curved layers, we will limit ourselves here to the case where the layer transformations $\mathbf{g}_1(\mathbf{x})$ and $\mathbf{g}_2(\mathbf{x})$ are *linear* (scalings, rotations, shearings, combinations thereof, or any other non-degenerate linear transformations[26]).

C.15.1 Examples of general 2-fold periodic layers

As we have seen in Chapter 10, any curved dot screen or line grid $r(x,y)$ can be obtained by applying a certain transformation $(x',y') = \mathbf{g}(x,y)$ to $p(x',y')$, the original uncurved regular counterpart of $r(x,y)$ having a unit period to both directions:

$$r(x,y) = p(\mathbf{g}(x,y)) = p(g_1(x,y),g_2(x,y)) \tag{C.30}$$

The general 2-fold periodic layer (dot screen or line grid) can be seen as a particular case of Eq. (C.30) in which $\mathbf{g}(x,y)$ is a *linear* transformation:

$$(x',y') = \mathbf{g}(x,y) = \begin{pmatrix} g_1(x,y) \\ g_2(x,y) \end{pmatrix} = \begin{pmatrix} u_1x + v_1y \\ u_2x + v_2y \end{pmatrix} = \begin{pmatrix} u_1 & v_1 \\ u_2 & v_2 \end{pmatrix} \begin{pmatrix} x \\ y \end{pmatrix} = \begin{pmatrix} \mathbf{f}_1 \\ \mathbf{f}_2 \end{pmatrix} \begin{pmatrix} x \\ y \end{pmatrix} \tag{C.31}$$

namely:

$$r(x,y) = p(\mathbf{g}(x,y)) = p(u_1x + v_1y,\, u_2x + v_2y) = p(\mathbf{f}_1 \cdot \mathbf{x},\, \mathbf{f}_2 \cdot \mathbf{x}) \tag{C.32}$$

---

[25] For instance, hexagonal microlens arrays have the advantage of better filling the plane than their orthogonal counterparts, and consequently they may let more light pass through. Indeed, a hexagonal pattern is known to be the most effective way to pack the largest number of similar objects (circles, etc.) in a minimum area [Weisstein99 pp. 254–255].

[26] Degenerate linear transformations, such as the null transformation $\mathbf{g}(\mathbf{x}) = \mathbf{0}$ or transformations that project the entire 2D plane onto a 1D line, will obviously not interest us here.

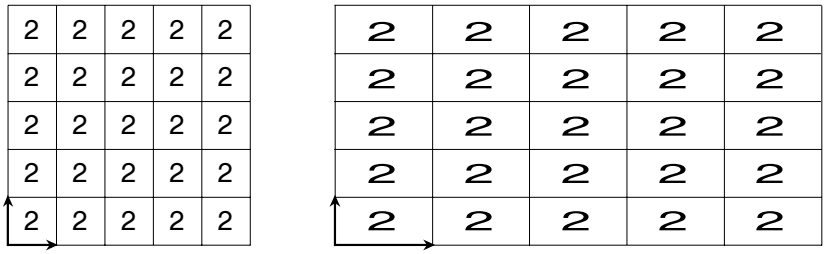

(a) (b)

Figure C.20: (a) A regular dot screen $p(x',y')$ having a unit period to both directions. (b) Its horizontally stretched version $r(x,y) = p(x/2,y)$ is a non-regular 2-fold periodic dot screen. See Example C.4.

where $\mathbf{x} = (x,y)$. Note that $\mathbf{f}_1 = (u_1,v_1)$ and $\mathbf{f}_2 = (u_2,v_2)$ are the frequency vectors of the 2-fold periodic layer $r(x,y)$; in the general case these two vectors are not necessarily orthogonal, and their lengths may be different. As we have seen in Secs. A.4 and A.5 of Appendix A, the frequency vectors $\mathbf{f}_1$ and $\mathbf{f}_2$ are related to the period vectors $\mathbf{P}_1 = (x_1,y_1)$ and $\mathbf{P}_2 = (x_2,y_2)$ of the same layer by Eq. (A.33), meaning that these two vector pairs are reciprocal to each other. According to Eq. (A.36) this also means that the two matrices

$$\mathrm{F} = \begin{pmatrix} \mathbf{f}_1 \\ \mathbf{f}_2 \end{pmatrix} = \begin{pmatrix} u_1 & v_1 \\ u_2 & v_2 \end{pmatrix} \quad \text{and} \quad \mathrm{P} = \begin{pmatrix} \mathbf{P}_1 \\ \mathbf{P}_2 \end{pmatrix} = \begin{pmatrix} x_1 & y_1 \\ x_2 & y_2 \end{pmatrix}$$

are the transpose inverse of each other: $\mathrm{F} = \mathrm{P}^{-\mathrm{T}}$.

Remark C.5: As shown above, the linear transformation $\mathbf{g}(x,y)$ is always expressed in terms of the *frequencies* of the 2-fold periodic layer $r(x,y)$ in the spectral domain, and not in terms of its *periodicities* in the image domain.[27] This fact will accompany us throughout our discussion below. ■

Let us now see a few concrete examples of 2-fold periodic layers that are not regular:

Example C.4: Consider the horizontally stretched dot screen $r(x,y)$ shown in Fig. C.20(b). The period vectors of this screen are $\mathbf{P}_1 = (2,0)$ and $\mathbf{P}_2 = (0,1)$, and its frequency vectors are therefore, according to Eq. (A.33), $\mathbf{f}_1 = (\frac{1}{2},0)$ and $\mathbf{f}_2 = (0,1)$. This horizontally stretched dot screen is obtained from its normalized, regular counterpart $p(x',y')$ (see Fig. C.20(a)) by applying to $p(x',y')$ the linear domain transformation:

$$(x',y') = \mathbf{g}(x,y) = \begin{pmatrix} \mathbf{f}_1 \\ \mathbf{f}_2 \end{pmatrix} \begin{pmatrix} x \\ y \end{pmatrix} = \begin{pmatrix} \frac{1}{2} & 0 \\ 0 & 1 \end{pmatrix} \begin{pmatrix} x \\ y \end{pmatrix} = \begin{pmatrix} \frac{1}{2}x \\ y \end{pmatrix}$$

---

[27] This follows from the fact that the transformation $(x',y') = \mathbf{g}(x,y)$ is applied to $p(x',y')$ as a *domain transformation*, and thus its effect on $p(x',y')$ is indeed that of the inverse transformation. For example, applying the transformation $(x',y') = (x/2,y/2)$ gives $p(x/2,y/2)$, a two-fold *magnification* of $p(x',y')$, and applying the transformation $(x',y') = (x\cos\theta + y\sin\theta, -x\sin\theta + y\cos\theta)$ gives a *counterclockwise* rotation of $p(x',y')$ by the angle θ. This is explained in more detail in Sec. D.6 of *Vol. II*.

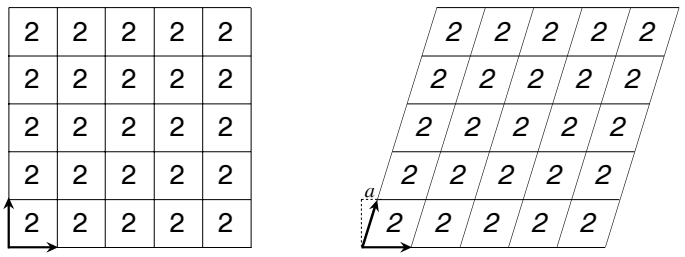

Figure C.21: (a) A regular dot screen $p(x',y')$ having a unit period to both directions. (b) Its horizontally slanted version $r(x,y) = p(x-ay,y)$ is a non-regular 2-fold periodic dot screen. See Example C.5.

And indeed, it is easy to see that the resulting transformed screen:

$$r(x,y) = p(\mathbf{g}(x,y)) = p(x/2,y)$$

is a horizontally stretched version of the original screen $p(x',y')$. Note that, in accordance with Remark C.5, $\mathbf{g}(x,y)$ expresses the *frequencies* of $r(x,y)$ in the spectral domain, and not its *periodicities* in the image domain. ■

Example C.5: An *oblique* (also called *slanted* or *skew-periodic*) dot screen is obtained from a regular dot screen by a shearing transformation. Consider, for example, the horizontally sheared dot screen $r(x,y)$ shown in Fig. C.21(b). The period vectors of this screen are $\mathbf{P}_1 = (1,0)$ and $\mathbf{P}_2 = (a,1)$, and its frequency vectors are therefore, according to Eq. (A.33), $\mathbf{f}_1 = (1,-a)$ and $\mathbf{f}_2 = (0,1)$. This horizontally slanted dot screen is obtained from its normalized, regular counterpart $p(x',y')$ (see Fig. C.21(a)) by applying to $p(x',y')$ the linear domain transformation:

$$(x',y') = \mathbf{g}(x,y) = \begin{pmatrix} \mathbf{f}_1 \\ \mathbf{f}_2 \end{pmatrix} \begin{pmatrix} x \\ y \end{pmatrix} = \begin{pmatrix} 1 & -a \\ 0 & 1 \end{pmatrix} \begin{pmatrix} x \\ y \end{pmatrix} = \begin{pmatrix} x-ay \\ y \end{pmatrix}$$

And indeed, it is easy to see that the resulting transformed screen:

$$r(x,y) = p(\mathbf{g}(x,y)) = p(x-ay,y)$$

is a horizontally slanted version of the original screen $p(x',y')$. ■

Example C.6: A *hexagonal* dot screen. Consider the hexagonal screen shown in Fig. C.22(b). The period vectors of this screen are $\mathbf{P}_1 = (1,0)$ and $\mathbf{P}_2 = (\frac{1}{2}, \sin 60°) = (\frac{1}{2}, \frac{\sqrt{3}}{2})$, and its frequency vectors are therefore, according to Eq. (A.33), $\mathbf{f}_1 = (1,-\frac{1}{\sqrt{3}})$ and $\mathbf{f}_2 = (0, \frac{2}{\sqrt{3}})$. This hexagonal dot screen is obtained from its normalized, regular counterpart $p(x',y')$ (see Fig. C.22(a)) by applying to $p(x',y')$ the linear domain transformation:

$$(x',y') = \mathbf{g}(x,y) = \begin{pmatrix} \mathbf{f}_1 \\ \mathbf{f}_2 \end{pmatrix} \begin{pmatrix} x \\ y \end{pmatrix} = \begin{pmatrix} 1 & -\frac{1}{\sqrt{3}} \\ 0 & \frac{2}{\sqrt{3}} \end{pmatrix} \begin{pmatrix} x \\ y \end{pmatrix} = \begin{pmatrix} x-\frac{1}{\sqrt{3}}y \\ \frac{2}{\sqrt{3}}y \end{pmatrix}$$

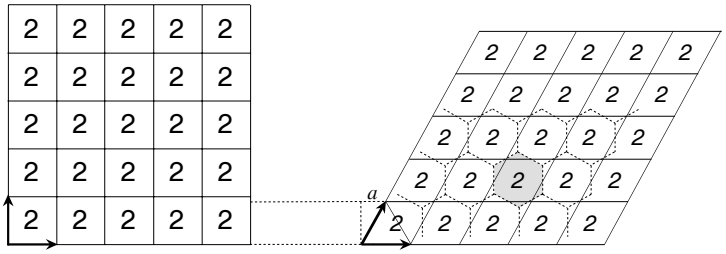

Figure C.22: (a) A regular dot screen $p(x',y')$ having a unit period to both directions. (b) Its hexagonal version $r(x,y) = p(x - \frac{1}{\sqrt{3}}y, \frac{2}{\sqrt{3}}y)$ is a non-regular 2-fold periodic dot screen. Note that in this case the transformation $\mathbf{g}(x,y)$ only modifies the angle between the two period vectors, but not their lengths; consequently, unlike in Fig. C.21, the cell height in (b) is smaller than in (a). See Example C.6.

We will henceforth call this transformation the *hexagonality transformation* and its matrix the *hexagonality matrix*. And indeed, it is easy to see that the resulting transformed screen:

$$r(x,y) = p(\mathbf{g}(x,y)) = p(x - \tfrac{1}{\sqrt{3}}y, \tfrac{2}{\sqrt{3}}y)$$

is the hexagonal version of the original screen $p(x',y')$.

Note that the hexagonal screen can be also seen as a slanted screen with $a = \frac{1}{2}$ and a further vertical scaling of $\sin 60° = \frac{\sqrt{3}}{2}$. Its two vector periods $\mathbf{P}_1$ and $\mathbf{P}_2$ have the same length, and they form an angle of 60°. ■

Remark C.6: A more general form of the hexagonal screen is obtained by applying to the above hexagonal screen a similarity transformation, i.e. a linear transformation that consists of *rotation* and *uniform scaling* (scaling with identical scaling factors to both directions). This more general form of the hexagonal screen is obtained by applying to $p(x',y')$ the linear domain transformation:

$$(x',y') = \mathbf{g}(x,y) = \begin{pmatrix} s & 0 \\ 0 & s \end{pmatrix} \begin{pmatrix} \cos\theta & \sin\theta \\ -\sin\theta & \cos\theta \end{pmatrix} \begin{pmatrix} 1 & -\frac{1}{\sqrt{3}} \\ 0 & \frac{2}{\sqrt{3}} \end{pmatrix} \begin{pmatrix} x \\ y \end{pmatrix} \qquad \text{(C.33)}$$

where the two first matrices represent a similarity transformation: a uniform scaling (magnification by the factor $1/s$) and a counterclockwise rotation by angle θ; see the footnote in Remark C.5 above. ■

Remark C.7: Note that the contents of the period cell in a hexagonal screen is not necessarily slanted as in Fig. C.22(b). If the desired hexagonal cell contains, for example, an upright "2", it simply means that in the original regular screen, before the application of the transformation **g**, we had a back-slanted version of "2", so that after the application of the transformation we obtain, indeed, an upright "2" in each of the period cells. ■

C.15.2 Adaptation of results from Chapter 10 to our particular case

Let us now return to Sec. 10.9.2 and reformulate some of its main results for the particular case in which the layer transformations $\mathbf{g}_1(x,y)$ and $\mathbf{g}_2(x,y)$ are linear.

We start by reformulating Proposition 10.5 for the linear case:

Proposition C.1: The (1,0,-1,0)-moiré $m_{1,0,-1,0}(\mathbf{x})$ in the superposition of the two 2-fold periodic layers $r_1(\mathbf{x}) = p_1(\mathbf{g}_1(\mathbf{x}))$ and $r_2(\mathbf{x}) = p_2(\mathbf{g}_2(\mathbf{x}))$, where $\mathbf{g}_1(\mathbf{x})$ and $\mathbf{g}_2(\mathbf{x})$ are linear transformations, is given by $m_{1,0,-1,0}(\mathbf{x}) = p_{1,0,-1,0}(\mathbf{g}_{1,0,-1,0}(\mathbf{x}))$, where:

(1) $p_{1,0,-1,0}(\mathbf{x}')$, the normalized periodic-profile of the (1,0,-1,0)-moiré, is the T-convolution of the normalized periodic-profiles of the original layers:

$$p_{1,0,-1,0}(\mathbf{x}') = p_1(\mathbf{x}') \ast\ast\ p_2(-\mathbf{x}')$$

(2) $\mathbf{g}_{1,0,-1,0}(\mathbf{x})$, the linear transformation of the (1,0,-1,0)-moiré, is given by:

$$\mathbf{g}_{1,0,-1,0}(\mathbf{x}) = \mathbf{g}_1(\mathbf{x}) - \mathbf{g}_2(\mathbf{x}). \quad \blacksquare$$

Using a less formal language we can now state the counterpart of Proposition 4.5 for the superposition of two 2-fold periodic layers as follows:

Proposition C.2: Let $r_1(x,y)$ and $r_2(x,y)$ be two 2-fold periodic layers, which are obtained from two normalized regular 2-fold periodic layers $p_1(x',y')$ and $p_2(x',y')$ by the linear coordinate transformations $\mathbf{g}_1(x,y)$ and $\mathbf{g}_2(x,y)$, namely:

$$\begin{pmatrix} x' \\ y' \end{pmatrix} = \begin{pmatrix} g_1(x,y) \\ g_2(x,y) \end{pmatrix} \qquad \text{and} \qquad \begin{pmatrix} x' \\ y' \end{pmatrix} = \begin{pmatrix} g_3(x,y) \\ g_4(x,y) \end{pmatrix}$$

respectively. The (1,0,-1,0)-moiré $m_{1,0,-1,0}(x,y)$ generated in the superposition of these 2-fold periodic layers can be seen from the image-domain point of view as the result of a 3-stage process:

(1) Normalization of the original 2-fold periodic layers by, in each of them, replacing $(g_i(x,y)\,,\, g_{i+1}(x,y))$ with (x',y') (i.e., by undoing in each of them the coordinate transformation), in order to straighten them into the normalized regular 2-fold periodic layers $p_1(x',y')$ and $p_2(x',y')$ having unit periods $T_{x'} = T_{y'} = 1$ (see Sec. C.16 below).

(2) T-convolution of these normalized layers. This gives the normalized periodic-profile of the (1,0,-1,0)-moiré, with the same unit periods $T_{x'} = T_{y'} = 1$.

(3) Bending the normalized periodic-profile of the moiré into the actual geometric layout of the moiré, by replacing (x',y') with $\mathbf{g}_1(x,y) - \mathbf{g}_2(x,y)$, i.e., by applying the linear coordinate transformation $\begin{pmatrix} x' \\ y' \end{pmatrix} = \begin{pmatrix} g_1(x,y) - g_3(x,y) \\ g_2(x,y) - g_4(x,y) \end{pmatrix}$. $\blacksquare$

It follows, therefore, that in order to synthesize between two 2-fold periodic layers a (1,0,-1,0)-moiré whose geometric layout is given by the two independent linear functions $g^{(1)}(x,y)$ and $g^{(2)}(x,y)$, all that we have to do is to choose two original 2-fold periodic layers whose linear transformations $\mathbf{g}_1(x,y) = (g_1(x,y),\, g_2(x,y))$ and $\mathbf{g}_2(x,y) = (g_3(x,y),\, g_4(x,y))$ satisfy the condition:

$$g_1(x,y) - g_3(x,y) = g^{(1)}(x,y)$$

$$g_2(x,y) - g_4(x,y) = g^{(2)}(x,y)$$

The periodic-profile of the synthesized moiré will be determined by the periodic-profiles of the superposed layers, in accordance with the first part of Proposition C.1.

Similar results for the general (k_1,k_2,k_3,k_4)-moiré between any two 2-fold periodic layers can be obtained from the fundamental moiré theorem and Proposition 10.7 by restricting them to the particular case in which the layer transformations $\mathbf{g}_1(x,y)$ and $\mathbf{g}_2(x,y)$ are linear.

C.15.3 The (1,0,-1,0)-moiré between two regular screens or grids

In Chapter 4 we have seen that the (1,0,-1,0)-moiré between any two regular screens or grids is itself regular (i.e. orthogonal with identical periods to both directions), and we determined the angle and the period of the resulting (1,0,-1,0)-moiré using the formulas that we have obtained previously for the (1,-1)-moiré between two line gratings (see Sec. 4.4.2).

Let us now show, based on Proposition C.1, how this result can be obtained directly, using a simple 2D matrix formulation, without having to resort to the (1,-1)-moiré between line gratings. The most general case with non-regular layers will be treated in Sec. C.15.5 below.

Because in our present case both of the layers $r_1(x,y)$ and $r_2(x,y)$ are regular, it follows that the linear transformations $\mathbf{g}_1(x,y)$ and $\mathbf{g}_2(x,y)$ that generate these layers from their normalized counterparts $p_1(x',y')$ and $p_2(x',y')$ having a unit period to both directions are similarity transformations, i.e. they only consist of rotations and uniform scalings:

$$\mathbf{g}_1(x,y) = \begin{pmatrix} f_1 & 0 \\ 0 & f_1 \end{pmatrix} \begin{pmatrix} \cos\theta_1 & \sin\theta_1 \\ -\sin\theta_1 & \cos\theta_1 \end{pmatrix} \begin{pmatrix} x \\ y \end{pmatrix} \tag{C.34}$$

$$\mathbf{g}_2(x,y) = \begin{pmatrix} f_2 & 0 \\ 0 & f_2 \end{pmatrix} \begin{pmatrix} \cos\theta_2 & \sin\theta_2 \\ -\sin\theta_2 & \cos\theta_2 \end{pmatrix} \begin{pmatrix} x \\ y \end{pmatrix} \tag{C.35}$$

where θ_i is the rotation angle of the regular layer $r_i(x,y)$ and f_i is its frequency (i.e. the scaling ratio between the frequency of $r_i(x,y)$ and the unit-frequency of its counterpart $p_i(x',y')$). Note that the first matrix in $\mathbf{g}_i(x,y)$ corresponds to a magnification of $p_i(x',y')$ by the factor $T_i = 1/f_i$ and the second matrix corresponds to a rotation by θ_i counterclockwise (see Remark C.5 above and the footnote therein).

Now, according to Proposition C.1, the linear transformation of the (1,0.-1,0)-moiré between two regular layers $r_1(x,y)$ and $r_2(x,y)$ is given by:

$$\mathbf{g}_{1,0,-1,0}(\mathbf{x}) = \mathbf{g}_1(\mathbf{x}) - \mathbf{g}_2(\mathbf{x})$$

$$= \begin{pmatrix} f_1 & 0 \\ 0 & f_1 \end{pmatrix} \begin{pmatrix} \cos\theta_1 & \sin\theta_1 \\ -\sin\theta_1 & \cos\theta_1 \end{pmatrix} \begin{pmatrix} x \\ y \end{pmatrix} - \begin{pmatrix} f_2 & 0 \\ 0 & f_2 \end{pmatrix} \begin{pmatrix} \cos\theta_2 & \sin\theta_2 \\ -\sin\theta_2 & \cos\theta_2 \end{pmatrix} \begin{pmatrix} x \\ y \end{pmatrix}$$

$$= \left[\begin{pmatrix} f_1 & 0 \\ 0 & f_1 \end{pmatrix}\begin{pmatrix} \cos\theta_1 & \sin\theta_1 \\ -\sin\theta_1 & \cos\theta_1 \end{pmatrix} - \begin{pmatrix} f_2 & 0 \\ 0 & f_2 \end{pmatrix}\begin{pmatrix} \cos\theta_2 & \sin\theta_2 \\ -\sin\theta_2 & \cos\theta_2 \end{pmatrix}\right]\begin{pmatrix} x \\ y \end{pmatrix}$$

$$= \begin{pmatrix} f_1\cos\theta_1 - f_2\cos\theta_2 & f_1\sin\theta_1 - f_2\sin\theta_2 \\ -(f_1\sin\theta_1 - f_2\sin\theta_2) & f_1\cos\theta_1 - f_2\cos\theta_2 \end{pmatrix}\begin{pmatrix} x \\ y \end{pmatrix} \tag{C.36}$$

Let us recall at this point the following result from linear algebra (see, for example, [Lay03 p. 339]):

Proposition C.3: Any matrix of the form $\left(\begin{smallmatrix} a & -b \\ b & a \end{smallmatrix}\right)$ represents a similarity transformation, i.e. a linear transformation consisting of rotation by angle θ and uniform scaling by a scaling factor f. Furthermore, the angle and the scaling factor of this similarity transformation are given by:

$$\theta = \arctan(b/a)$$

$$f = \sqrt{a^2 + b^2} \qquad \blacksquare$$

Returning now to Eq. (C.36), we see that the matrix it contains (i.e. the matrix which represents the moiré transformation $\mathbf{g}_{1,0,-1,0}(\mathbf{x})$) has indeed the form $\left(\begin{smallmatrix} a & -b \\ b & a \end{smallmatrix}\right)$, meaning that it represents a similarity transformation. This means in turn that the (1,0,-1,0)-moiré $m_{1,0,-1,0}(\mathbf{x}) = p_{1,0,-1,0}(\mathbf{g}_{1,0,-1,0}(\mathbf{x}))$ is itself regular, since it is obtained by the application of a similarity transformation (rotation and uniform scaling) to its normalized counterpart $p_{1,0,-1,0}(\mathbf{x}')$ which is obviously regular.

Furthermore, the angle φ_M of this (1,0,-1,0)-moiré and its scaling factor f_M are given according to Proposition C.3 by:[28]

$$\varphi_M = \arctan(b/a) = \arctan\left(\frac{f_1\sin\theta_1 - f_2\sin\theta_2}{f_1\cos\theta_1 - f_2\cos\theta_2}\right) \tag{C.37}$$

$$f_M^2 = a^2 + b^2 = (f_1\cos\theta_1 - f_2\cos\theta_2)^2 + (f_1\sin\theta_1 - f_2\sin\theta_2)^2$$

$$= f_1^2(\cos^2\theta_1 + \sin^2\theta_1) - 2f_1f_2(\cos\theta_1\cos\theta_2 + \sin\theta_1\sin\theta_2) + f_2^2(\cos^2\theta_2 + \sin^2\theta_2)$$

$$= f_1^2 - 2f_1f_2\cos(\theta_2 - \theta_1) + f_2^2 \tag{C.38}$$

As we can see, this is precisely the result that we have obtained in Sec. C.1 for the case of the (1,-1)-moiré between two line gratings. Note that in accordance with Remark C.5, all our results are formulated here in terms of the spectral domain, i.e. in terms of *frequencies* rather than in terms of *periods* (see Eqs. (C.34)–(C.38)). We can, however, express Eq. (C.38) in terms of periods by rewriting it as follows (denoting the angle difference between the two layers by $\alpha = \theta_2 - \theta_1$):

---

[28] Note that Proposition C.3 assumes that the transformation belonging to the matrix $\left(\begin{smallmatrix} a & -b \\ b & a \end{smallmatrix}\right)$ is applied as a direct transformation. When it is applied as a domain (and hence inverse) transformation, like in our case (see Remark C.5 and the footnote therein), the rotation is applied to the inverse direction. But since in our case the matrix has the form $\left(\begin{smallmatrix} a & b \\ -b & a \end{smallmatrix}\right)$, i.e. b is negative, the sign inversion in the rotation angle is finally cancelled out.

$$\frac{1}{T_M^2} = \frac{1}{T_1^2} - 2\frac{1}{T_1}\frac{1}{T_2}\cos\alpha + \frac{1}{T_2^2}$$

$$= \frac{T_2^2 - 2T_1T_2\cos\alpha + T_1^2}{(T_1T_2)^2}$$

This finally gives, indeed, the period T_M of the moiré (to both directions) as predicted by Eq. (2.9):

$$T_M = \frac{T_1T_2}{\sqrt{T_1^2 + T_2^2 - 2T_1T_2\cos\alpha}} \tag{C.39}$$

Similarly, we can also express the angle φ_M of the moiré in terms of periods, by rewriting Eq. (C.37) as follows:

$$\varphi_M = \arctan\left(\frac{\frac{\sin\theta_1}{T_1} - \frac{\sin\theta_2}{T_2}}{\frac{\cos\theta_1}{T_1} - \frac{\cos\theta_2}{T_2}}\right) = \arctan\left(\frac{T_2\sin\theta_1 - T_1\sin\theta_2}{T_2\cos\theta_1 - T_1\cos\theta_2}\right) \tag{C.40}$$

As we can see, the period and the angle of the (1,0,-1,0)-moiré between two regular screens or grids are, indeed, identical to those of the (1,-1)-moiré between two line gratings (see Eq. (2.9) and Sec. C.1).

Example C.7: Suppose that we are given two regular dot screens $r_1(x,y)$ and $r_2(x,y)$, the first consisting of tiny "2"-shaped periods and the second consisting of tiny pinholes (see Fig. C.23(a)). Suppose that the period lengths and the orientations of our two regular screens are, respectively, $T_1 = 5$, $\theta_1 = 0°$ and $T_2 = 5.2$, $\theta_2 = 5°$. What are the period and the orientation of the (1,0,-1,0)-moiré in the superposition of these two screens?

According to Proposition C.1 (see also Sec. 4.4), the resulting (1,0,-1,0)-moiré consists of a periodic pattern of magnified "2"-shaped elements. The periodicity of this moiré (in both directions) is given according to Eq. (C.39) by:

$$T_M = \frac{5\cdot 5.2}{\sqrt{5^2 + 5.2^2 - 2\cdot 5\cdot 5.2\cos 5°}} = 53.28$$

meaning that its magnification factor is 53.28/5 = 10.66. The direction of this moiré is given according to Eq. (C.40) by:

$$\varphi_M = \arctan\left(\frac{5.2\sin 0° - 5\sin 5°}{5.2\cos 0° - 5\cos 5°}\right) = \arctan(-1.991) = -63.33°$$

meaning that the "2"-shaped moiré is rotated by 66.77° clockwise with respect to the x axis. Note that the moiré angle φ_M is independent of the length units in which the periods T_1 and T_2 are expressed, since if we express T_1 and T_2 in terms of another length unit we simply multiply their values by a constant factor which is then cancelled out in Eq. (C.40). The moiré period T_M, on its part, is expressed in terms of the same length units as the periods T_1 and T_2. ■

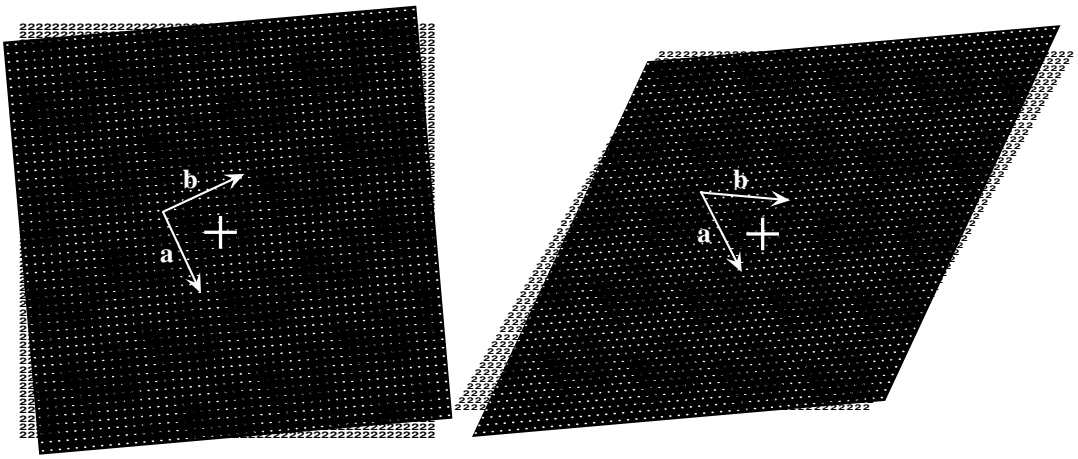

(a) (b)

Figure C.23: (a) The moiré effect between the two regular dot screens of Example C.7. (b) The moiré effect between the two hexagonal dot screens of Example C.8. Each of the two layers in (b) is obtained by applying the hexagonality transformation to the corresponding layer in (a); the resulting moiré in (b) is the hexagonal counterpart of the regular moiré in (a), which is obtained by applying the hexagonality transformation to the regular moiré. Note, however, that for the sake of clarity the symbol "2" within the oblique periods in (b) has been kept upright, as explained in Remark C.7. The two white arrows in (a) and (b) show the period-vectors **a** and **b** of the respective moiré effects.[29] Note that the angle φ_M of the moiré, i.e. the baseline direction of the "2"-shaped moiré,[30] as well as the length T_M of the two moiré period-vectors, are exactly the same in (a) and (b), and only the internal angle between the two period vectors is different (90° in (a) and 60° in (b)). Although hexagonal screens are usually clipped to have square or rectangular external borders, just like their regular counterparts, we have chosen for didactic reasons not to clip them in the present figure, in order to clearly show their oblique nature.

Obviously, these results apply only to the particular case in which both layers are regular grids or screens (note that we have assumed that our original normalized layers $p_1(x',y')$ and $p_2(x',y')$ are regular, and that the linear transformations $\mathbf{g}_1(x,y)$ and $\mathbf{g}_2(x,y)$ that are applied to them consist of rotations and uniform scalings alone, i.e. they are similarity transformations). In the general case $\mathbf{g}_1(x,y)$ and $\mathbf{g}_2(x,y)$ may be any linear transformations, that may include shearing, scalings with different factors to both directions, etc., so that the transformed layers (as well as the resulting moiré) are no longer regular (orthogonal with identical periods to both directions). This general case is treated in Sec. C.15.5 below.

---

[29] The moiré period-vectors **a** and **b** can be found by applying the moiré transformation $\mathbf{g}_{1,0,-1,0}(x,y)$ to the normalized layer period-vectors (1,0) and (0,1), respectively, using Eq. (C.36) in the regular case and Eq. (C.43) in the hexagonal case. Note that the hexagonality matrix in Eq. (C.43) does not modify the vector (1,0), meaning that the vector **a** is precisely the same in (a) and (b).

[30] The baseline direction of the moiré is indicated by the vector **a**.

And yet, interestingly, we can still use the above considerations as a useful basis for some other particular cases, for example, the case in which both layers are hexagonal screens, as shown below.

C.15.4 The (1,0,-1,0)-moiré between two hexagonal screens or grids

In this subsection we discuss the particular case of hexagonal layers, which is probably the most widely used 2-fold periodic case after regular layers. We will show that a (1,0,-1,0)-moiré between two hexagonal layers is always hexagonal, and we will determine the periodicities and the orientation of this moiré.

Because in this case both of the layers $r_1(x,y)$ and $r_2(x,y)$ are hexagonal, it follows from Remark C.6 that the linear transformations $\mathbf{g}_1(x,y)$ and $\mathbf{g}_2(x,y)$ that generate these layers from their normalized counterparts $p_1(x',y')$ and $p_2(x',y')$ having a unit period in both directions are given by:

$$\mathbf{g}_1(x,y) = \begin{pmatrix} f_1 & 0 \\ 0 & f_1 \end{pmatrix} \begin{pmatrix} \cos\theta_1 & \sin\theta_1 \\ -\sin\theta_1 & \cos\theta_1 \end{pmatrix} \begin{pmatrix} 1 & -\frac{1}{\sqrt{3}} \\ 0 & \frac{2}{\sqrt{3}} \end{pmatrix} \begin{pmatrix} x \\ y \end{pmatrix} \tag{C.41}$$

$$\mathbf{g}_2(x,y) = \begin{pmatrix} f_2 & 0 \\ 0 & f_2 \end{pmatrix} \begin{pmatrix} \cos\theta_2 & \sin\theta_2 \\ -\sin\theta_2 & \cos\theta_2 \end{pmatrix} \begin{pmatrix} 1 & -\frac{1}{\sqrt{3}} \\ 0 & \frac{2}{\sqrt{3}} \end{pmatrix} \begin{pmatrix} x \\ y \end{pmatrix} \tag{C.42}$$

Note that Eqs. (C.41) and (C.42) only differ from their counterparts (C.34) and (C.35) of the regular case by the presence of a new, third matrix. This additional matrix is, indeed, the *hexagonality matrix* (see Example C.6), and its corresponding linear transformation is the *hexagonality transformation*.

Now, according to Proposition C.1, the linear transformation of the (1,0.-1,0)-moiré between the two hexagonal layers $r_1(x,y)$ and $r_2(x,y)$ is given by:

$$\begin{aligned}
\mathbf{g}_{1,0,-1,0}(\mathbf{x}) &= \mathbf{g}_1(\mathbf{x}) - \mathbf{g}_2(\mathbf{x}) \\
&= \begin{pmatrix} f_1 & 0 \\ 0 & f_1 \end{pmatrix} \begin{pmatrix} \cos\theta_1 & \sin\theta_1 \\ -\sin\theta_1 & \cos\theta_1 \end{pmatrix} \begin{pmatrix} 1 & -\frac{1}{\sqrt{3}} \\ 0 & \frac{2}{\sqrt{3}} \end{pmatrix} \begin{pmatrix} x \\ y \end{pmatrix} \\
&\qquad - \begin{pmatrix} f_2 & 0 \\ 0 & f_2 \end{pmatrix} \begin{pmatrix} \cos\theta_2 & \sin\theta_2 \\ -\sin\theta_2 & \cos\theta_2 \end{pmatrix} \begin{pmatrix} 1 & -\frac{1}{\sqrt{3}} \\ 0 & \frac{2}{\sqrt{3}} \end{pmatrix} \begin{pmatrix} x \\ y \end{pmatrix} \\
&= \left[\begin{pmatrix} f_1 & 0 \\ 0 & f_1 \end{pmatrix} \begin{pmatrix} \cos\theta_1 & \sin\theta_1 \\ -\sin\theta_1 & \cos\theta_1 \end{pmatrix} - \begin{pmatrix} f_2 & 0 \\ 0 & f_2 \end{pmatrix} \begin{pmatrix} \cos\theta_2 & \sin\theta_2 \\ -\sin\theta_2 & \cos\theta_2 \end{pmatrix} \right] \begin{pmatrix} 1 & -\frac{1}{\sqrt{3}} \\ 0 & \frac{2}{\sqrt{3}} \end{pmatrix} \begin{pmatrix} x \\ y \end{pmatrix} \\
&= \begin{pmatrix} f_1\cos\theta_1 - f_2\cos\theta_2 & f_1\sin\theta_1 - f_2\sin\theta_2 \\ -(f_1\sin\theta_1 - f_2\sin\theta_2) & f_1\cos\theta_1 - f_2\cos\theta_2 \end{pmatrix} \begin{pmatrix} 1 & -\frac{1}{\sqrt{3}} \\ 0 & \frac{2}{\sqrt{3}} \end{pmatrix} \begin{pmatrix} x \\ y \end{pmatrix}
\end{aligned} \tag{C.43}$$

A comparison between Eqs. (C.43) and (C.36) shows that the only difference between the transformations $\mathbf{g}_{1,0,-1,0}(\mathbf{x})$ in the hexagonal case and in the regular case is the presence of the hexagonality matrix in the hexagonal case. And indeed, because the first matrix in

Eq. (C.43) is a similarity matrix, it follows from Remark C.6 that the (1,0,-1,0)-moiré $m_{1,0,-1,0}(\mathbf{x}) = p_{1,0,-1,0}(\mathbf{g}_{1,0,-1,0}(\mathbf{x}))$ in the hexagonal case is hexagonal in itself, since it is obtained by the application of the hexagonality transformation (plus a certain rotation and uniform scaling due to the similarity transformation) to its regular, normalized counterpart $p_{1,0,-1,0}(\mathbf{x}')$.

Furthermore, the additional hexagonality transformation in Eq. (C.43) only modifies the internal angle between the two period vectors of the 2-fold periodic moiré but not the length of these period vectors or the baseline direction of the moiré (see Figs. C.22, C.23). Therefore the periodicity and the rotation angle (i.e. the baseline direction) of the hexagonal moiré are still determined by the same similarity transformation as in the regular case, and hence they are given by the same formulas as in the regular case, i.e. by Eqs. (C.39) and (C.40). And if both layers have the same periods these formulas reduce again into Eqs. (2.10).

Example C.8: Suppose that we are given two hexagonal dot screens $r_1(x,y)$ and $r_2(x,y)$, the first consisting of tiny "2"-shaped periods and the second consisting of tiny pinholes (see Fig. C.23(b)). Suppose that the period lengths and the orientations of our two hexagonal screens are, respectively, $T_1 = 5$, $\theta_1 = 0°$ and $T_2 = 5.2$, $\theta_2 = 5°$, like in Example C.7 with the regular screens. What are the period and the orientation of the (1,0,-1,0)-moiré in the superposition of these two screens?

We note that the period lengths and the rotation angles of the two hexagonal screens in this case are identical to those of the two regular screens in Example C.7, the only difference between the two cases being in the internal angle that is formed between the two period vectors of each layer (90° in a regular screen, and 60° in a hexagonal screen). Therefore, as we have seen above, the period length T_M and the rotation angle φ_M of the moiré in the hexagonal case are identical to those of the regular moiré of Example C.7, the only difference between them being, once again, in the internal angle between the two period vectors of the moiré (see Fig. C.23).

Note, however, that because the two individual layers (as well as the moiré effect) in this hexagonal case have been obtained by applying the hexagonality transformation to their respective counterparts of Example C.7, it follows that the "2"-shaped elements in the hexagonal case (both in the original layer $r_1(x,y)$ and in the moiré effect) are slightly smaller than in the regular case (compare Figs. C.23(a) and C.23(b)), although the period vectors in both cases have the same length. The reason is that the height of the oblique period cell in the hexagonal case is only $T\sin 60° = 0.866T$ rather than T, the height of the square period cell in the corresponding regular case. In principle, the "2"-shaped elements in the hexagonal case should be slanted versions of their counterparts in the regular case; but according to Remark C.7 it is always possible to "rectify" them, if so desired (as we have done, indeed, in Fig. C.23(b)). ■

Similar considerations can be also devised for other layer types, e.g. the hexagonal screen variant obtained by *vertical* rather than horizontal shearing, etc.

C.15.5 The (1,0,-1,0)-moiré between two general 2-fold periodic screens or grids

We now proceed to the case involving general 2-fold periodic layers.

Proposition C.4: Suppose we are given two 2-fold periodic layers $r_1(\mathbf{x}) = p_1(\mathbf{g}_1(\mathbf{x}))$ and $r_2(\mathbf{x}) = p_2(\mathbf{g}_2(\mathbf{x}))$ that are obtained from their original, unit-period normalized counterparts $p_1(\mathbf{x})$ and $p_2(\mathbf{x})$ by the linear transformations:

$$\mathbf{g}_1(\mathbf{x}) = \begin{pmatrix} u_1x + v_1y \\ u_2x + v_2y \end{pmatrix} = \mathrm{F}_1 \cdot \mathbf{x} \quad \text{with} \quad \mathrm{F}_1 = \begin{pmatrix} u_1 & v_1 \\ u_2 & v_2 \end{pmatrix} = \begin{pmatrix} \mathbf{f}_1 \\ \mathbf{f}_2 \end{pmatrix}, \quad \mathbf{x} = (x,y)$$

$$\mathbf{g}_2(\mathbf{x}) = \begin{pmatrix} u_3x + v_3y \\ u_4x + v_4y \end{pmatrix} = \mathrm{F}_2 \cdot \mathbf{x} \quad \text{with} \quad \mathrm{F}_2 = \begin{pmatrix} u_3 & v_3 \\ u_4 & v_4 \end{pmatrix} = \begin{pmatrix} \mathbf{f}_3 \\ \mathbf{f}_4 \end{pmatrix}, \quad \mathbf{x} = (x,y)$$

It therefore follows from Proposition C.1 that the transformation $\mathbf{g}_{1,0,-1,0}(\mathbf{x})$ of the (1,0,-1,0)-moiré between the two layers, i.e. the transformation which brings the unit-period normalized moiré profile $p_{1,0,-1,0}(\mathbf{x})$ into the final (1,0,-1,0)-moiré $p_{1,0,-1,0}(\mathbf{g}_{1,0,-1,0}(\mathbf{x}))$ between the two layers $r_1(\mathbf{x})$ and $r_2(\mathbf{x})$, is given by:

$$\begin{aligned} \mathbf{g}_{1,0,-1,0}(\mathbf{x}) &= \mathbf{g}_1(\mathbf{x}) - \mathbf{g}_2(\mathbf{x}) \\ &= \begin{pmatrix} (u_1-u_3)x + (v_1-v_3)y \\ (u_2-u_4)x + (v_2-v_4)y \end{pmatrix} = \mathrm{F}_M \cdot \mathbf{x} \quad \text{with} \quad \mathrm{F}_M = \begin{pmatrix} u_1-u_3 & v_1-v_3 \\ u_2-u_4 & v_2-v_4 \end{pmatrix} = \begin{pmatrix} \mathbf{a} \\ \mathbf{b} \end{pmatrix} \end{aligned}$$

where $\mathrm{F}_M = \mathrm{F}_1 - \mathrm{F}_2$, namely: $\begin{pmatrix} \mathbf{a} \\ \mathbf{b} \end{pmatrix} = \begin{pmatrix} \mathbf{f}_1 - \mathbf{f}_3 \\ \mathbf{f}_2 - \mathbf{f}_4 \end{pmatrix}$. ■

This gives us the connection between the frequency vectors of the two individual layers ($\mathbf{f}_1$, $\mathbf{f}_2$ and $\mathbf{f}_3$, $\mathbf{f}_4$) and the frequency vectors $\mathbf{a}$ and $\mathbf{b}$ of the resulting (1,0,-1,0)-moiré. This result is, indeed, identical to the result that we have already obtained in Chapter 4 (see Eq. (4.17)).

Note that the explicit results that we have obtained in the previous subsections for the cases of regular or hexagonal screens are simply particular cases of this general result, although their particularities are not explicitly obvious from the general result.

C.15.6 Allowing for layer shifts

So far we have considered here the (1,0,-1,0)-moiré effects between 2-fold periodic layers $r_1(\mathbf{x})$ and $r_2(\mathbf{x})$ that were obtained from their original, unit-period normalized counterparts $p_1(\mathbf{x})$ and $p_2(\mathbf{x})$ by purely linear transformations such as rotations, scalings, shearings, or any combinations thereof. Note, however, that all linear transformations leave the layer's origin at the point (0,0). Therefore, if we want to take into consideration layer shifts as well, we must consider rather than purely linear transformations the slightly larger family of *affine* transformations. The general 1D affine transformation has the form:

$$x' = ax + x_0$$

and the general 2D affine transformation has the form:

$$x' = a_1 x + b_1 y + x_0$$

$$y' = a_2 x + b_2 y + y_0$$

or in vector notation, denoting $\mathbf{x} = (x,y)$, $\mathbf{x}' = (x',y')$, $\mathbf{x}_0 = (x_0,y_0)$ and $\mathrm{A} = \begin{pmatrix} a_1 & b_1 \\ a_2 & b_2 \end{pmatrix}$:

$$\mathbf{x}' = \mathrm{A}\cdot\mathbf{x} + \mathbf{x}_0$$

where x_0, y_0 and $\mathbf{x}_0 = (x_0,y_0)$ are arbitrary constants that represent a given displacement. Note that linear transformations are a particular case of affine transformations in which $x_0 = 0$ and $y_0 = 0$.

Now, in order to be able to consider layer shifts, as we already did in Chapter 7, we must use here a slightly wider variant of Proposition C.1 in which the transformations $\mathbf{g}_1(\mathbf{x})$, $\mathbf{g}_2(\mathbf{x})$ and hence $\mathbf{g}_{1,0,-1,0}(\mathbf{x}) = \mathbf{g}_1(\mathbf{x}) - \mathbf{g}_2(\mathbf{x})$ are *affine* rather than *linear*. We thus obtain the following generalization of Proposition C.4:

Proposition C.5: Suppose we are given two 2-fold periodic layers $r_1(\mathbf{x}) = p_1(\mathbf{g}_1(\mathbf{x}))$ and $r_2(\mathbf{x}) = p_2(\mathbf{g}_2(\mathbf{x}))$ that are obtained from their original, unit-period normalized counterparts $p_1(\mathbf{x})$ and $p_2(\mathbf{x})$ by the affine transformations $\mathbf{g}_1(\mathbf{x})$ and $\mathbf{g}_2(\mathbf{x})$:

$$\mathbf{g}_1(\mathbf{x}) = \begin{pmatrix} u_1 x + v_1 y + x_1 \\ u_2 x + v_2 y + y_1 \end{pmatrix} = \mathrm{F}_1\cdot\mathbf{x} + \mathbf{x}_1 \quad \text{with} \quad \mathrm{F}_1 = \begin{pmatrix} u_1 & v_1 \\ u_2 & v_2 \end{pmatrix} = \begin{pmatrix} \mathbf{f}_1 \\ \mathbf{f}_2 \end{pmatrix},\ \mathbf{x} = (x,y),\ \mathbf{x}_1 = (x_1,y_1)$$

$$\mathbf{g}_2(\mathbf{x}) = \begin{pmatrix} u_3 x + v_3 y + x_2 \\ u_4 x + v_4 y + y_2 \end{pmatrix} = \mathrm{F}_2\cdot\mathbf{x} + \mathbf{x}_2 \quad \text{with} \quad \mathrm{F}_2 = \begin{pmatrix} u_3 & v_3 \\ u_4 & v_4 \end{pmatrix} = \begin{pmatrix} \mathbf{f}_3 \\ \mathbf{f}_4 \end{pmatrix},\ \mathbf{x} = (x,y),\ \mathbf{x}_2 = (x_2,y_2)$$

It follows, therefore, from the affine variant of Proposition C.1, that the transformation $\mathbf{g}_{1,0,-1,0}(\mathbf{x})$ which brings the unit-period normalized moiré profile $p_{1,0,-1,0}(\mathbf{x})$ into the final (1,0,-1,0)-moiré $p_{1,0,-1,0}(\mathbf{g}_{1,0,-1,0}(\mathbf{x}))$ between the two layers $r_1(\mathbf{x})$ and $r_2(\mathbf{x})$ is given by:

$$\mathbf{g}_{1,0,-1,0}(\mathbf{x}) = \mathbf{g}_1(\mathbf{x}) - \mathbf{g}_2(\mathbf{x})$$
$$= \begin{pmatrix} (u_1-u_3)x + (v_1-v_3)y + (x_1-x_2) \\ (u_2-u_4)x + (v_2-v_4)y + (y_1-y_2) \end{pmatrix} = \mathrm{F}_M\cdot\mathbf{x} + (\mathbf{x}_1 - \mathbf{x}_2) \quad \text{with} \quad \mathrm{F}_M = \begin{pmatrix} u_1-u_3 & v_1-v_3 \\ u_2-u_4 & v_2-v_4 \end{pmatrix} = \begin{pmatrix} \mathbf{a} \\ \mathbf{b} \end{pmatrix}$$

where $\mathrm{F}_M = \mathrm{F}_1 - \mathrm{F}_2$, namely: $\begin{pmatrix} \mathbf{a} \\ \mathbf{b} \end{pmatrix} = \begin{pmatrix} \mathbf{f}_1 - \mathbf{f}_3 \\ \mathbf{f}_2 - \mathbf{f}_4 \end{pmatrix}$. ■

This slight generalization of Proposition C.4 allows us now to consider the most general case of the (1,0,-1,0)-moiré between periodic layers, in which the individual layers are also shifted by $\mathbf{x}_1 = (x_1,y_1)$ and $\mathbf{x}_2 = (x_2,y_2)$, respectively.

Remark C.8: Obviously, the behaviour of the 2-fold periodic (1,0,-1,0)-moiré effect under layer shifts, as predicted by Proposition C.5, must be consistent with the results that we have already obtained in Chapter 7. Therefore, the following interesting question may be asked at this point: We already know from Chapter 7 that when the original periodic layers undergo slight layer shifts, the resulting periodic moiré usually undergoes a much larger shift (see, for example, Fig. 7.6). How is this fact reflected in Proposition C.5, given that the resulting shift $\mathbf{x}_1 - \mathbf{x}_2$ in $\mathbf{g}_{1,0,-1,0}(\mathbf{x})$ is not necessarily greater than the individual

layer shifts $\mathbf{x}_1$ and $\mathbf{x}_2$?

To answer this question we must remember, once again, that the layer transformations $(x',y') = \mathbf{g}_1(x,y)$, $(x',y') = \mathbf{g}_2(x,y)$ as well as the resulting moiré transformation $(x',y') = \mathbf{g}_{1,0,-1,0}(x,y)$ are applied to the respective unit-period normalized layers $p_1(x',y')$, $p_2(x',y')$ and $p_{1,0,-1,0}(x',y')$ as *domain* transformations, and thus their effects are indeed those of the *inverse* transformations (see Remark C.5 above and the footnote therein). To better illustrate this point, consider the simple 1-fold periodic (1,-1)-moiré that is obtained in the superposition of two parallel periodic line gratings, one of which has been slightly shifted to the *right* while the other has been slightly *scaled up* (see Fig. 7.9 and Problem 7-18 in Chapter 7). In this case the layer transformations with respect to the original unit-period normalized layers are given by:

$$g_1(x) = x - x_0$$

$$g_2(x) = 0.9x$$

and therefore the moiré transformation with respect to the unit-period normalized layer is:

$$g_{1,-1}(x) = g_1(x) - g_2(x) = 0.1x - x_0 \tag{C.44}$$

At first sight this seems to indicate that the moiré effect is shifted by the same amount x_0 as the first layer. But if we remember that the actual effect of the domain transformation $x' = g_{1,-1}(x)$ is expressed by the *inverse* transformation, $x = g^{-1}{}_{1,-1}(x')$:[31]

$$x = 10x' + 10x_0 \tag{C.45}$$

we see immediately that Eq. (C.44) represents, in fact, a 10-fold magnification and a shift that is 10 times bigger than the shift x_0 in $g_1(x)$ (in the same direction). ■

Example C.9: As a further example, let us consider here the case illustrated in Fig. 7.6 of Chapter 7. This figure shows the superposition of two regular line grids, one of which is simply shifted by (x_1,y_1):

$$\mathbf{g}_1(x,y) = \begin{pmatrix} 1 & 0 \\ 0 & 1 \end{pmatrix}\begin{pmatrix} x \\ y \end{pmatrix} - \begin{pmatrix} x_1 \\ y_1 \end{pmatrix}$$

while the second is rotated by angle α counterclockwise:

$$\mathbf{g}_2(x,y) = \begin{pmatrix} \cos\alpha & \sin\alpha \\ -\sin\alpha & \cos\alpha \end{pmatrix}\begin{pmatrix} x \\ y \end{pmatrix}$$

It follows, therefore, that the transformation undergone by the moiré effect is given by:

$$\mathbf{g}_{1,0,-1,0}(x,y) = \mathbf{g}_1(x,y) - \mathbf{g}_2(x,y)$$

$$= \begin{pmatrix} 1 & 0 \\ 0 & 1 \end{pmatrix}\begin{pmatrix} x \\ y \end{pmatrix} - \begin{pmatrix} x_1 \\ y_1 \end{pmatrix} - \begin{pmatrix} \cos\alpha & \sin\alpha \\ -\sin\alpha & \cos\alpha \end{pmatrix}\begin{pmatrix} x \\ y \end{pmatrix}$$

[31] Note that being the inverse of $g_{1,-1}(x)$, Eq. (C.45) expresses the transformation undergone by the moiré effect in terms of a *direct* transformation. Similarly, the transformations undergone by the two original layers can be expressed as direct transformations by $x = x' + x_0$ and $x = \frac{10}{9}x'$, respectively. But the relationship $g_{1,-1}(x) = g_1(x) - g_2(x)$ is only valid for the domain (and hence, inverse) transformations.

$$= \begin{pmatrix} 1-\cos\alpha & -\sin\alpha \\ \sin\alpha & 1-\cos\alpha \end{pmatrix} \begin{pmatrix} x \\ y \end{pmatrix} - \begin{pmatrix} x_1 \\ y_1 \end{pmatrix}$$

Note, again, that the layer transdormations $(x',y') = \mathbf{g}_1(x,y)$, $(x',y') = \mathbf{g}_2(x,y)$ as well as the resulting moiré transformation $(x',y') = \mathbf{g}_{1,0,-1,0}(x,y)$ are applied to the respective unit-period normalized layers $p_1(x',y')$, $p_2(x',y')$ and $p_{1,0,-1,0}(x',y')$ as *domain* transformations, and hence their effects are indeed those of the *inverse* transformations. Thus, the effect of $\mathbf{g}_1(x,y)$ is a shift of the first layer by (x_1,y_1) to the *right*, and the effect of $\mathbf{g}_2(x,y)$ is a rotation of the second layer by angle α *counterclockwise*. In order to see the actual effect of the transformation $(x',y') = \mathbf{g}_{1,0,-1,0}(x,y)$, namely, how it transforms the unit-period normalized moiré profile $p_{1,0,-1,0}(x',y')$ into the final (1,0,-1,0)-moiré $p_{1,0,-1,0}(\mathbf{g}_{1,0,-1,0}(x,y))$ between the two given layers $r_1(x',y')$ and $r_2(x',y')$, let us find the inverse transformation $(x,y) = \mathbf{g}^{-1}{}_{1,0,-1,0}(x',y')$:

$$\begin{pmatrix} x \\ y \end{pmatrix} = \begin{pmatrix} 1-\cos\alpha & -\sin\alpha \\ \sin\alpha & 1-\cos\alpha \end{pmatrix}^{-1} \left[\begin{pmatrix} x' \\ y' \end{pmatrix} + \begin{pmatrix} x_1 \\ y_1 \end{pmatrix} \right]$$

$$= \frac{1}{(1-\cos\alpha)^2 + (\sin\alpha)^2} \begin{pmatrix} 1-\cos\alpha & \sin\alpha \\ -\sin\alpha & 1-\cos\alpha \end{pmatrix} \left[\begin{pmatrix} x' \\ y' \end{pmatrix} + \begin{pmatrix} x_1 \\ y_1 \end{pmatrix} \right]$$

$$= \tfrac{1}{2} \begin{pmatrix} 1 & \frac{\sin\alpha}{1-\cos\alpha} \\ -\frac{\sin\alpha}{1-\cos\alpha} & 1 \end{pmatrix} \begin{pmatrix} x' \\ y' \end{pmatrix} + \tfrac{1}{2} \begin{pmatrix} 1 & \frac{\sin\alpha}{1-\cos\alpha} \\ -\frac{\sin\alpha}{1-\cos\alpha} & 1 \end{pmatrix} \begin{pmatrix} x_1 \\ y_1 \end{pmatrix}$$

$$= \tfrac{1}{2} \begin{pmatrix} 1 & \cot(\alpha/2) \\ -\cot(\alpha/2) & 1 \end{pmatrix} \begin{pmatrix} x' \\ y' \end{pmatrix} + \tfrac{1}{2} \begin{pmatrix} 1 & \cot(\alpha/2) \\ -\cot(\alpha/2) & 1 \end{pmatrix} \begin{pmatrix} x_1 \\ y_1 \end{pmatrix} \qquad \text{(C.46)}$$

We note that the matrix in this transformation has the form $\frac{1}{2}\left(\begin{smallmatrix} 1 & -b \\ b & 1 \end{smallmatrix}\right)$ with $b = -\cot(\alpha/2)$. This matrix is therefore a particular case of the similarity matrix $\left(\begin{smallmatrix} a & -b \\ b & a \end{smallmatrix}\right)$. As we know from Proposition C.3 this matrix corresponds to a linear transformation that is composed of:

- a rotation by angle θ, where: $\theta = \arctan(b/a)$
- and a scaling by: $s = \sqrt{a^2 + b^2}$

By inserting here $a = \frac{1}{2}$ and $b = -\frac{1}{2}\cot(\alpha/2)$ (taking into account the factor $\frac{1}{2}$ before the matrix) and using the identities $\arctan x = \frac{\pi}{2} - \operatorname{arccot} x$ [Bronstein90 p. 280] and $1/\sqrt{1+\cot^2 x} = \sin x$ [Spiegel68 p. 15] we see from Eq. (C.46) that the moiré shift is obtained from the layer shift (x_1,y_1) by:

- a rotation by angle θ: $\theta = \arctan(-\cot\frac{\alpha}{2}) = -\arctan(\cot\frac{\alpha}{2}) = \operatorname{arccot}(\cot\frac{\alpha}{2}) - \frac{\pi}{2}$

  namely: $\theta = \frac{\alpha}{2} - \frac{\pi}{2}$ (C.47)
- and a scaling by: $s = \frac{1}{2}\sqrt{1+\cot^2(\alpha/2)} = \frac{1}{2\sin(\alpha/2)}$ (C.48)

And indeed, as expected, this result fully agrees with the moiré shift as explained in Chapter 7, which is obtained as follows:

(a) As predicted by proposition 7.2, the moiré effect is shifted in its own direction, which is, as shown in Fig. 4.8, exactly $\frac{\alpha}{2} - \frac{\pi}{2}$.

(b) Furthermore, the extent of the shift of the moiré effect is given, in terms of periods, by Eqs. (7.26) and (2.10), namely:

$$b_M = T_M(\phi_1 - \phi_2) = \frac{T}{2\sin(\alpha/2)}(\phi_1 - \phi_2) \tag{C.49}$$

where b_M is the resulting shift of the moiré, T_M is the period length of the moiré, T is the period length of the two individual layers, and ϕ_1 and ϕ_2 are the shifts of the individual layers in terms of the period T. Noting that in our case $\phi_2 = 0$ (the second layer is not shifted), we see that for a shift of d in the first layer (i.e., $\phi_1 = d/T$ periods), the extent of the resulting shift of the moiré is:

$$b_M = \frac{1}{2\sin(\alpha/2)}\, d \tag{C.50}$$

Hence, the shift of the periodic moiré is obtained by scaling up the shift d of the first layer by the factor $s = \frac{1}{2\sin(\alpha/2)}$, exactly as predicted by Eq. (C.48) above.

This shows us, indeed, that the moiré shifts obtained by Proposition C.5 are in full agreement with our previous results from Chapter 7. ■

Example C.10: Finally, returning to the general case of Proposition C.5, what is the actual shift undergone by the moiré effect in the superposition?

According to Proposition C.5, the moiré transformation $\mathbf{g}_{1,0,-1,0}(\mathbf{x})$ is expressed by:

$$\mathbf{x}' = \mathrm{F}_M \cdot \mathbf{x} + (\mathbf{x}_1 - \mathbf{x}_2)$$

where $\mathrm{F}_M = \mathrm{F}_1 - \mathrm{F}_2$. Remembering that the actual effect of the domain transformation $\mathbf{x}' = \mathbf{g}_{1,0,-1,0}(\mathbf{x})$ is expressed by its *inverse*, $\mathbf{x} = \mathbf{g}^{-1}{}_{1,0,-1,0}(\mathbf{x}')$:

$$\mathbf{x} = \mathrm{F}_M^{-1} \cdot (\mathbf{x}' - (\mathbf{x}_1 - \mathbf{x}_2)) = \mathrm{F}_M^{-1} \cdot \mathbf{x}' - \mathrm{F}_M^{-1} \cdot (\mathbf{x}_1 - \mathbf{x}_2)$$

we see that the actual shift of the moiré effect in the superposition is given here by the second term, $-\mathrm{F}_M^{-1} \cdot (\mathbf{x}_1 - \mathbf{x}_2)$. Denoting this vector by $\mathbf{x}_M = (x_M, y_M)$, it follows that the direction and the extent of the moiré shift are given by $\arctan(y_M/x_M)$ and $\sqrt{x_M^2 + y_M^2}$, respectively. ■

C.15.7 The order of the superposed layers

At this point, the following interesting question may be asked: Suppose that we change the numbering of the superposed layers, so that the layer transformations $\mathbf{g}_1$ and $\mathbf{g}_2$ are interchanged. Physically, this may correspond to changing the order of the superposed layers, such that the top layer in the original superposition becomes now the bottom layer and vice versa. Clearly, this has no influence whatsoever on the resulting moiré effect. And yet, because $\mathbf{g}_1$ and $\mathbf{g}_2$ have been interchanged, it turns out that the sign of the resulting moiré transformation $\mathbf{g}_{1,0,-1,0}$ has been inverted (since $\mathbf{g}_{1,0,-1,0}$ is the difference between the two individual layer transformations). This should mean that the resulting moiré effect has

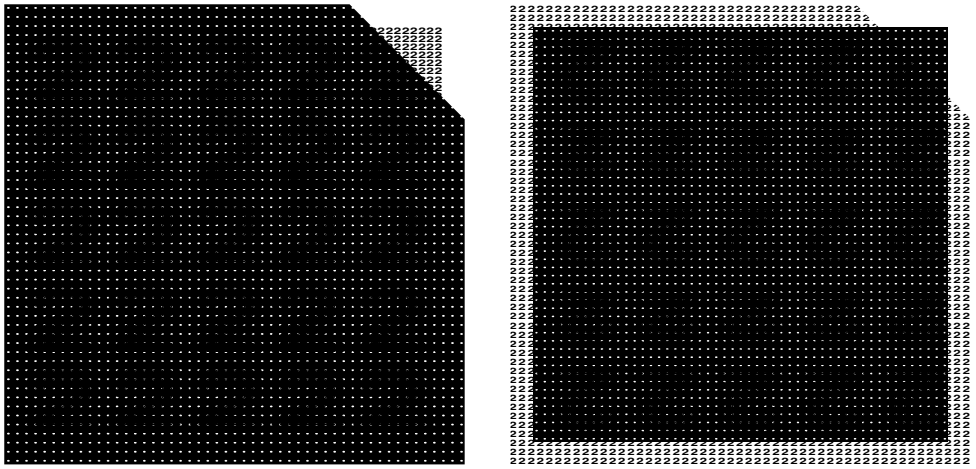

(a) (b)

Figure C.24: (a) The superposition of two regular dot screens $r_1(x,y)$ and $r_2(x,y)$, the first consisting of tiny "2"-shaped periods and the second consisting of tiny pinholes, where the first layer has been slightly scaled down: $\mathbf{g}_1(\mathbf{x}) = 1.1\mathbf{x}$, $\mathbf{g}_2(\mathbf{x}) = \mathbf{x}$. (b) The superposition of the same dot screens, but this time it is the second layer (the pinhole screen) that has been slightly scaled down: $\mathbf{g}_1(\mathbf{x}) = \mathbf{x}$, $\mathbf{g}_2(\mathbf{x}) = 1.1\mathbf{x}$. Note that the multiplication of a layer transformation by 1.1 corresponds, indeed, to a scale *down* effect in that layer (see Remark C.5 and the footnote therein).

been rotated by 180° — but as mentioned above, we know that the moiré effect does not depend on the order in which the two layers are superposed (or on the way we choose to number the layers). How can we explain this contradiction? The same question applies also to the sign of the frequency or the period of the moiré effect in Eqs. (2.11), (4.17), etc. The answer is, of course, that the orientation of the moiré is not only determined by the moiré transformation $\mathbf{g}_{1,0,-1,0}$, but also by its intensity profile $p_{1,0,-1,0}$, as clearly indicated by the two parts of Proposition C.1 (see also Propositions 10.2 and 10.5). Indeed, Propositions C.4 and C.5 only concentrate on the second part of Proposition C.1, the geometric transformations, but we should never forget that the first part of Proposition C.1 is also involved in the determination of the orientation of the moiré. To illustrate this more clearly, consider the following example.

Example C.11: Fig. C.24(a) shows a superposition of two regular dot screens, the first consisting of tiny "2"-shaped periods and the second consisting of tiny pinholes, where the first layer has been slightly scaled down: $\mathbf{g}_1(\mathbf{x}) = 1.1\mathbf{x}$, $\mathbf{g}_2(\mathbf{x}) = \mathbf{x}$, so that the layer frequencies (to both directions) are $f_1 = 1.1$, $f_2 = 1$ units. In this case we have, therefore:

$$\mathbf{g}_{1,0,-1,0}(\mathbf{x}) = 1.1\mathbf{x} - \mathbf{x} = 0.1\mathbf{x} \qquad \text{(or: } f_M = f_1 - f_2 = 0.1\text{)}$$

$$p_{1,0,-1,0}(\mathbf{x}') = p_1(\mathbf{x}') \ast\ast\, p_2(-\mathbf{x}') = \text{"2"} \ast\ast\, \text{"pinhole"} = \text{"2"}$$

Note that in this case the sign inversion in the second term of the convolution has no effect, since a pinhole is invariant under a 180° rotation.

What happens, now, if we change the order of the layers? In this case we obtain:

$$\mathbf{g}_{1,0,-1,0}(\mathbf{x}) = \mathbf{x} - 1.1\mathbf{x} = -0.1\mathbf{x} \qquad \text{(or: } f_M = 1 - 1.1 = -0.1\text{)}$$

which may lead us to the conclusion that the moiré effect has been inverted (rotated by 180°). But if we also consider the intensity profiles, we see that in this case the moiré profile $p_{1,0,-1,0}(\mathbf{x}')$ itself has been inverted, due to the sign inversion in the second term of the convolution:

$$p_{1,0,-1,0}(\mathbf{x}') = \text{“pinhole”} \ast\ast \text{“inverted 2”} = \text{“inverted 2”}$$

This means that the inversion in the moiré transformation rectifies the inversion in the moiré intensity profile, so that both inversions are cancelled out.

Consider now Fig. C.24(b). In this case, it is the second layer (the pinhole screen) that has been slightly scaled down: $\mathbf{g}_1(\mathbf{x}) = \mathbf{x}$, $\mathbf{g}_2(\mathbf{x}) = 1.1\mathbf{x}$, so that the layer frequencies are $f_1 = 1$, $f_2 = 1.1$ frequency units. As we can see in the figure, in this case the moiré effect is indeed rotated by 180°. To understand this, we note that in the present case we have:

$$\mathbf{g}_{1,0,-1,0}(\mathbf{x}) = \mathbf{x} - 1.1\mathbf{x} = -0.1\mathbf{x} \qquad \text{(or: } f_M = 1 - 1.1 = -0.1\text{)}$$

$$p_{1,0,-1,0}(\mathbf{x}') = p_1(\mathbf{x}') \ast\ast p_2(-\mathbf{x}') = \text{“2”} \ast\ast \text{“pinhole”} = \text{“2”}$$

This means that unlike in the previous case, the moiré profile itself has not been rotated by 180°, so that the sign inversion in the moiré transformation is not cancelled out, and it does, indeed, cause an inversion in the resulting moiré effect.

Now, if we change the order of the layers we obtain:

$$\mathbf{g}_{1,0,-1,0}(\mathbf{x}) = 1.1\mathbf{x} - \mathbf{x} = 0.1\mathbf{x} \qquad \text{(or: } f_M = 1.1 - 1 = 0.1\text{)}$$

$$p_{1,0,-1,0}(\mathbf{x}') = \text{“pinhole”} \ast\ast \text{“inverted 2”} = \text{“inverted 2”}$$

meaning that the moiré profile has been rotated by 180°, but the moiré transformation is not sign-inverted, and hence it does not rectify this inversion. The resulting moiré remains, therefore, rotated by 180°, as expected. ■

Remark C.9: The 1D counterpart of the explanation above gives a more precise formulation for the orientation of the 1D moiré in Eq. (2.11), which is no longer dependent on the order of the layers or on their numbering. This formulation could not be given in Chapter 2 since it depends on notions from Chapter 10. Indeed, the orientation of the moiré — just like its intensity profile — cannot be deduced from geometric considerations only. ■

C.16 Layer normalization issues

As we have seen in Chapter 4, the T-convolution of the two given periodic layers (or, equivalently, the multiplication of their impulse combs or nailbeds in the spectral domain)

requires that the two layers be first *normalized* (see the explanation preceding Proposition 4.2 in Sec. 4.2, as well as Propositions 4.2, 4.3 and 4.5). This normalization is required in order that the periods of the two layers to be convolved coincide (or, equivalently, in terms of the spectral domain, in order that the two combs or nailbeds to be multiplied have a common support). This normalization allows us, therefore, to apply the *T*-convolution theorem even though the two original layers do not necessarily have the same period sizes and orientations.

A similar consideration is also used in Chapter 10, which deals with the more general case in which the superposed layers are *repetitive* (i.e. non-linear transformations of periodic layers); see, for example, the explanation that precedes Proposition 10.2, as well as Propositions 10.3, 10.4, 10.5 and 10.7 in Sec. 10.9.

However, as the reader may have noticed, the normalizations being used in Chapter 4 and in Chapter 10 are not the same: In Chapter 4 the original layers are normalized to the period size and orientation of the final moiré; but in Chapter 10 the original curvilinear layers are normalized to their straight (uncurved) periodic counterparts having a unit period and angle 0° (i.e. the unit grid), and after the *T*-convolution the resulting normalized moiré is then transformed back into its actual geometric layout.

The reason for this difference is as follows. In fact, in order to perform the *T*-convolution of the two given layers (or, equivalently, the multiplication of their respective spectra in the Fourier domain), it is enough to normalize both of the layers into *any* common periodicity and orientation, be it the periodicity of the final moiré, a unit-grid periodicity, or any other arbitrary periodicity. In the case of Chapter 4, the moiré layout considerations are only *qualitative*,[32] and therefore it is more natural there to normalize the two original layers directly into the geometric layout of the final moiré, rather than to make first a normalization of the original layers into a unit-period structure and then transform the resulting unit-period moiré back into its actual geometric layout. But in Chapter 10, where we provide the full *quantitative* moiré layout considerarions (such as $g_{1,-1}(x,y) = g_1(x,y) - g_2(x,y)$, etc.), it is most natural to use a unit-period normalization, since here $g_1(x,y)$, $g_2(x,y)$ and $g_{1,-1}(x,y)$ express, indeed, the transformations undergone by the two original layers and by the resulting moiré, respectively, *with respect to this underlying unit-period grid or coordinate system*. Any other choice would imply a more complex interpretation of the transformations $g_1(x,y)$, $g_2(x,y)$ and $g_{1,-1}(x,y)$, which would be less intuitive and less useful. For example, if we choose to normalize our layers with respect to a two-units grid, or with respect to the final moiré layout (as we did in Chapter 4), the intuitive meaning of $g_1(x,y)$, $g_2(x,y)$ and $g_{1,-1}(x,y)$ would be lost.

Remark C.10: Note that in terms of the moiré layout relationships ($g_{1,-1}(x,y) = g_1(x,y) - g_2(x,y)$, $\mathbf{g}_{1,0,-1,0}(x,y) = \mathbf{g}_1(x,y) - \mathbf{g}_2(x,y)$, etc.) choosing a different normalization simply means a coordinate change in the already unit-period normalized layers. For example, if we choose to normalize our layers with respect to the coordinate grid having a

[32] In the sense that they do not yet explicitly provide the quantitative moiré layout relationships $g_{1,-1}(x,y) = g_1(x,y) - g_2(x,y)$, $\mathbf{g}_{1,0,-1,0}(x,y) = \mathbf{g}_1(x,y) - \mathbf{g}_2(x,y)$, etc. that are given later in Chapter 10.

two units periodicity, it simply means that we now use the new s,t coordinate system with $s = 2x$, $t = 2y$, i.e. $x = s/2$, $y = t/2$, and our layout relationship then becomes $g_{1,-1}(s/2,t/2) = g_1(s/2,t/2) - g_2(s/2,t/2)$. In the general case, if $(s,t) = \mathbf{h}(x,y)$, and the inverse coordinate transformation is given by $(x,y) = \mathbf{h}^{-1}(s,t)$, then our layout relationship becomes $g_{1,-1}(\mathbf{h}^{-1}(s,t)) = g_1(\mathbf{h}^{-1}(s,t)) - g_2(\mathbf{h}^{-1}(s,t))$. Similar considerations can be devised for all the other moiré layout relationships, such as the (1,0,-1,0)-moiré between two dot screens $\mathbf{g}_{1,0,-1,0}(x,y) = \mathbf{g}_1(x,y) - \mathbf{g}_2(x,y)$, or any higher order moirés. This simply reflects the fact that the function identities expressing the moiré layout relationships are invariant under coordinate changes in the plane. ■

Example C.12: Let us see what happens to the layout relationship of the (1,0,-1,0)-moiré between two periodic dot screens, $\mathbf{g}_{1,0,-1,0}(x,y) = \mathbf{g}_1(x,y) - \mathbf{g}_2(x,y)$, if we choose to normalize our layers with respect to the final moiré layout, as we did in Chapter 4. As shown in Remark C.10, this normalization is obtained, in fact, by applying the coordinate change $(x,y) = \mathbf{g}^{-1}{}_{1,0,-1,0}(s,t)$ to the layers that are already normalized with respect to the unit grid.

Suppose that we are given two periodic dot screens $r_1(x,y)$ and $r_2(x,y)$ that have been obtained from their respective unit-period normalized counterparts $p_1(x',y')$ and $p_2(x',y')$ by the linear transformations $(x',y') = \mathbf{g}_1(x,y)$ and $(x',y') = \mathbf{g}_2(x,y)$, respectively. The periodic (1,0,-1,0)-moiré between these layers has, therefore, the geometric layout $\mathbf{g}_{1,0,-1,0}(x,y) = \mathbf{g}_1(x,y) - \mathbf{g}_2(x,y)$, where $\mathbf{g}_1$, $\mathbf{g}_2$ and $\mathbf{g}_{1,0,-1,0}$ are expressed with respect to the unit grid. Now, if we apply to the unit-period normalized layers the coordinate change $(x,y) = \mathbf{g}^{-1}{}_{1,0,-1,0}(s,t)$, the layout relationship of the moiré becomes, in terms of this new coordinate system:

$$\mathbf{g}_{1,0,-1,0}(\mathbf{g}^{-1}{}_{1,0,-1,0}(s,t)) = \mathbf{g}_1(\mathbf{g}^{-1}{}_{1,0,-1,0}(s,t)) - \mathbf{g}_2(\mathbf{g}^{-1}{}_{1,0,-1,0}(s,t))$$

namely:

$$(s,t) = \mathbf{g}_1(\mathbf{g}^{-1}{}_{1,0,-1,0}(s,t)) - \mathbf{g}_2(\mathbf{g}^{-1}{}_{1,0,-1,0}(s,t))$$

As we can see, under this normalization (coordinate change) the moiré layout is simply $(x',y') = (s,t)$ (i.e. it coincides with the new coordinate lines), and the layouts of the two dot screens become, respectively, $(x',y') = \mathbf{g}_1(\mathbf{g}^{-1}{}_{1,0,-1,0}(s,t))$ and $(x',y') = \mathbf{g}_2(\mathbf{g}^{-1}{}_{1,0,-1,0}(s,t))$. But this result is obviously less useful for quantitative calculations than its counterpart that is normalized with respect to the unit grid, $\mathbf{g}_{1,0,-1,0}(x,y) = \mathbf{g}_1(x,y) - \mathbf{g}_2(x,y)$. ■

Example C.13: Suppose that we are given two periodic gratings $r_1(x,y)$ and $r_2(x,y)$ that have been obtained from their respective unit-period normalized counterparts $p_1(x')$ and $p_2(x')$ by the linear bending transformations $x' = g_1(x,y)$ and $x' = g_2(x,y)$, respectively. The periodic (1,-1)-moiré between these layers has, therefore, the geometric layout $g_{1,-1}(x,y) = g_1(x,y) - g_2(x,y)$. Now, if we apply to the two given non-normalized gratings new layer transformations $(x,y) = \mathbf{h}_1(s,t)$ and $(x,y) = \mathbf{h}_2(s,t)$, respectively, the geometric layout of the (1,-1)-moiré becomes $g_1(\mathbf{h}_1(s,t)) - g_2(\mathbf{h}_2(s,t))$, because now the transformations of the individual gratings with respect to their unit-period normalized counterparts are $g_1(\mathbf{h}_1(s,t))$ and $g_2(\mathbf{h}_2(s,t))$, respectively. Note that this moiré layout is *not* obtained by applying the transformation $(x,y) = \mathbf{h}_{1,-1}(s,t) = \mathbf{h}_1(s,t) - \mathbf{h}_2(s,t)$ to the original moiré layout $g_{1,-1}(x,y) = g_1(x,y) - g_2(x,y)$. The counterpart of this example for the case of the (1,0,-1,0)-moiré between two dot screens can be obtained in a similar way; its generalization to the (k_1,k_2,k_3,k_4)-moiré is given in Chapter 10 in Proposition 10.8. ■

Appendix D

Glossary of the main terms

D.1 About the glossary

Several thousands of publications on the moiré phenomenon have appeared during the last decades, in many different fields and applications. However, the terminology used in this vast literature is very far from being consistent and uniform. Different authors use different terms for the same entities, and what is even worse, the same terms are often used in different meanings by different authors. As a few examples among many others, let us cite here some of the many terms used in literature for what we call here *gratings*: line gratings, rulings [Nishijima64], sets of parallel lines [Fink92 p. 44], grids [Jarić89 pp. 29–31], parallel-line grids [Stecher64], grilles [Post67], and even line-screens [Tollenaar64]. For what we call here *screens* one can find the terms: lattices, grids (again!), meshes, masks, etc. Even the moiré patterns are often called fringes, beats, interferences, aliasing effects, and so forth.

Obviously, in such an interdisciplinary domain as the moiré theory it would be quite impossible to adopt a universally acceptable standardization of the terms, because of the different needs and traditions in the various fields involved (optics, mechanics, mathematics, printing, etc.).[1] Nevertheless, even without having any far-reaching pretensions, we were obliged to make our own terminological choices in a systematic and coherent way, in order to prevent confusion and ambiguity in our own work. We tried to be consistent in our terminology throughout this work, even if it forced us to assign to some terms a somewhat different meaning than one would expect (depending on his own background, of course).

In the present glossary we included all the terms for which we felt a clear definition was desirable to avoid any risk of ambiguity. Note, however, that this glossary is not ordered alphabetically; rather, we preferred to group the various terms according to subjects. We hope this should help the reader not only to clearly see the meaning of each individual term by itself, but also to put it in relation with other closely related terms (which would be completely dispersed throughout the glossary if an alphabetical order were preferred). Note that terms in the glossary can be found alphabetically through the general index at the end of the book.

---

[1] For example, the term *density* has very different meanings in almost any imaginable field of science or technology. A non-exhaustive list, just for the sake of illustration, may include: density of matter (in physics), density of population (in statistics), probability density (in probability), spectral density (in spectral analysis), density of a set (in mathematic topology), ink or colour density (in printing and colorimetry), etc. Another similar example is the term *phase*. It should be also noted that terminology sometimes tends to change over the years or according to fashions. As an example, the term *function convolution* in modern literature appears in older publications as *function composition* [Zygmund68 p. 36], the *resultant* of two functions, or even using the German term *Faltung* [Hardy68 p. 10].

D.2 Terms in the image domain

grating (or *line-grating*) —
A pattern consisting of parallel lines. Unless otherwise mentioned it will be assumed that a grating is periodic and consists of equally wide parallel, straight lines that are separated by equal spaces. For example, a *binary grating* is a grating with a square-wave intensity profile consisting of white lines (with a constant value of 1) on a black background (whose value is 0).

curvilinear grating —
A repetitive pattern consisting of parallel curvilinear lines. A curvilinear grating can be seen as a non-linear transformation of an initial uncurved periodic grating of straight lines (see Sec. 10.2). Examples of curvilinear gratings with a cosinusoidal periodic profile are shown in Fig. 10.1; examples with a square-wave periodic profile are shown in the left side of Fig. 10.8.

cosinusoidal grating (not to be confused with *cosine-shaped grating*) —
A grating with a cosinusoidal periodic-profile; for example, a cosinusoidal circular grating is a circular grating with a cosinusoidal periodic-profile. Note, however, that since reflectance and transmittance functions always take values ranging between 0 and 1, the cosinusoidal grating is normally "raised" and rescaled into this range of values. For example, a reflectance function in the form of a vertical straight cosinusoidal grating is expressed by: $r(x,y) = \frac{1}{2}\cos(2\pi fx) + \frac{1}{2}$.

cosine-shaped grating (not to be confused with *cosinusoidal grating*) —
A grating (with any periodic-profile form) whose corrugations in the x,y plane are bent into a cosinusoidal shape, like in Fig. 10.1(l).

grid (or *line-grid*; also called in literature *cross-line grating*) —
A pattern consisting of two superposed line-gratings, crossing each other at a non-zero angle. Unless otherwise mentioned it will be assumed that a grid is 2-fold periodic, and consists of two binary straight line gratings. Note that every grid can be also seen as a screen (whose dot-elements are the spaces left between the lines of the grid).

regular grid (or *square grid*) —
A 2-fold periodic grid composed of two superposed straight line-gratings that are identical but perpendicular to each other.

curved grid —
A repetitive pattern obtained by applying a non-linear transformation on a periodic grid (see Sec. 10.2). An example of a curved grid is shown in Fig. 10.2(b).

screen (or *dot-screen*; not to be confused with *lattice* or *dot-lattice*) —
A pattern consisting of dots. In most cases it will be assumed that a screen is 2-fold periodic, with a parallel, equally spaced arrangement of identical dots.

regular screen —
A 2-fold periodic screen whose dot arrangement is orthogonal and whose periods (or frequencies) to both orthogonal directions are equal.

curved screen —
A repetitive pattern obtained by applying a non-linear transformation on a periodic screen (see Sec. 10.2). An example of a curved screen is shown in Fig. 10.2(b).

halftone screen —
A more relaxed case of a binary screen in which the size (and the shape) of the screen dots may vary (typically, according to the gray level of a given original continuous-tone image), while its frequency and direction remain fixed throughout. Halftone screens are used in the printing world for the reproduction of continuous-tone images on bilevel printing devices.

screen gradation (or *wedge*) —
A halftone screen whose screen dots vary gradually (in their size and possibly also in their shape) across the image, generating a halftoned image with a smooth and uniform tone gradation.

image (has nothing to do with the image of a transformation) —
The most general term we use to cover "anything" in the image domain. It may be periodic or not, binary or continuous, etc. In principle, a monochrome (black-and-white) image has reflectance (or transmittance) values that vary between 0 (black) and 1 (white); similarly, a colour image has reflectance (or transmittance) values varying between 0 and 1 for each wavelength λ of its colour spectrum.

opening (of a periodic binary grating or square wave) —
The length of the white span within the period of a periodic binary grating or square wave (see Fig. 2.4).

opening ratio (of a periodic binary grating or square wave) —
The ratio τ/T between the opening τ and the period T of a periodic binary grating or square wave (see Fig. 2.9(a)–(c)). Note that the opening ratio remains fixed even when the periodic binary grating undergoes a non-linear coordinate transformation.

spot function —
A function which defines the way the size and the shape of the dots in a given halftone screen change as they grow from 0 to 100 percent coverage.

period (or *repetition-period* of a function p) —
A number $T \neq 0$ such that for any $x \in \mathbb{R}$, $p(x+T) = p(x)$. Note that the set of all the periods of $p(x)$ forms a lattice in $\mathbb{R}$. In the case of a 2-fold periodic function $p(x,y)$, a double period (or period parallelogram) of $p(x,y)$ is any parallelogram A which

tiles the x,y plane so that $p(x,y)$ repeats itself identically on any of these tiles (see also Sec. A.3.4 in Appendix A).

period-vector (of a periodic function $p(x,y)$) —
A non-zero vector $\mathbf{P} = (x_0,y_0)$ such that for any $(x,y)\in\mathbb{R}^2$, $p(x+x_0,y+y_0) = p(x,y)$. The set $L_\mathbf{P}$ of all the period-vectors of $p(x,y)$ forms a lattice in the x,y plane, which is 2D if $p(x,y)$ is 2-fold periodic, 1D if $p(x,y)$ is 1-fold periodic, and 0D, i.e., $L_\mathbf{P} = \{(0,0)\}$, if $p(x,y)$ is not periodic. If $\mathbf{P}_1$, $\mathbf{P}_2$ are two non-collinear period-vectors of a 2-fold periodic function $p(x,y)$, then for any point $\mathbf{x}\in\mathbb{R}^2$ the points $\mathbf{x}$, $\mathbf{x}+\mathbf{P}_1$, $\mathbf{x}+\mathbf{P}_2$, $\mathbf{x}+\mathbf{P}_1+\mathbf{P}_2$ define a period parallelogram of $p(x,y)$.

period-lattice (of a periodic function) —
The lattice formed by the set of all periods (or period-vectors) of the periodic function (see Secs. A.2, A.3.4 in Appendix A).

step-vector (of a periodic function $p(x,y)$) —
See Sec. A.6 in Appendix A, and the use of step-vectors in Sec. 7.5.2.

periodic function —
A function having a period. Note that a 2D function $p(x,y)$ can be 2-fold periodic (such as $p(x,y) = \cos x + \cos y$) or only 1-fold periodic (such as $p(x,y) = \cos x$).

almost-periodic function —
See Secs. B.3, B.5 in Appendix B.

aperiodic function (not to be confused with *non-periodic function*) —
A function which is not included in the class of almost-periodic functions. See Fig. B.3 in Appendix B.

non-periodic function (not to be confused with *aperiodic function*) —
A function which is not included in the class of periodic functions. See Fig. B.3 in Appendix B.

repetitive structure (or *repetitive function*) —
A structure (or a function) which is repetitive according to a certain rule, but which is not necessarily periodic (or almost-periodic). For example: concentric circles; gratings with logarithmic line-distances; screen gradations; etc. Note that such structures are sometimes called in literature *quasi-periodic* (like in [Bryngdahl74 p. 1290]); however, we reserve the term quasi-periodic only to its meaning in the context of the theory of almost-periodic functions (see Sec. B.5 in Appendix B).

coordinate-transformed structure —
A repetitive structure $r(x,y)$ which is obtained by the application of a non-linear coordinate transformation $\mathbf{g}(x,y)$ on a certain initial periodic structure $p(x,y)$. More formally, using vector notation: $r(\mathbf{x}) = p(\mathbf{g}(\mathbf{x}))$. Curvilinear gratings (such as parabolic or circular gratings) and gratings with a varying frequency (such as a

grating with logarithmic line-distances) are examples of coordinate-transformed structures.

profile-transformed structure —
A repetitive structure $r(x,y)$ which is obtained by the application of a non-linear transformation $t(z)$ on the profile of a certain initial periodic structure $p(x,y)$. More formally, using vector notation: $r(\mathbf{x}) = t(p(\mathbf{x}))$. Screen gradations are an example of profile-transformed structures.

coordinate-and-profile transformed structure —
A repetitive structure $r(x,y)$ which is obtained from a certain initial periodic structure $p(x,y)$ by the application of both a non-linear coordinate-transformation $\mathbf{g}(x,y)$ and a non-linear profile-transformation $t(z)$. More formally, using vector notation: $r(\mathbf{x}) = t(p(\mathbf{g}(\mathbf{x})))$. An example of a coordinate-and-profile-transformed structure is given in Remark 2 of Sec. 10.2.

intensity profile (of a structure $r(x,y)$) —
A function (surface) over the x,y plane that gives at any point (x,y) the intensity of the structure $r(x,y)$.

periodic profile (of a curvilinear grating, curved grid, etc.) —
The periodic profile of a curvilinear grating or a curved screen $r(x,y)$ is defined as the intensity profile of the original, uncurved periodic grating (or screen), before the non-linear transformation has been applied to it (see Sec. 10.2). Examples of curvilinear gratings with a cosinusoidal periodic profile are shown in Fig. 10.1; examples with a square-wave periodic profile are shown in Fig. 10.8(left). Note that in periodic structures the periodic profile coincides with the intensity profile.

normalized periodic profile (of a curvilinear grating, curved grid, etc.) —
See Sec. 10.2.

geometric layout (of a curvilinear grating, curved grid, etc.) —
The geometric layout of a curvilinear grating $r(x,y)$ is the locus of the centers of its curvilinear corrugations in the x,y plane; it is defined by the bending function of the curvilinear grating (see Sec. 10.2). Similarly, the geometric layout of a curved grid or a curved screen is defined by its two bending functions. Fig. 10.1 shows curvilinear gratings with various geometric layouts; Fig. 10.2(b) shows a curved screen whose geometric layout is given by two inverse hyperbolic sine functions.

bending function (of a curvilinear grating, curved grid, etc.) —
The bending function of a curvilinear grating $r(x,y) = p(g(x,y))$ is the non-linear function $x' = g(x,y)$ which bends the original, uncurved periodic grating $p(x')$ into the curvilinear grating $r(x,y)$. The bending functions of a curved grid or a curved screen $r(x,y) = p(g_1(x,y),g_2(x,y))$ are the two components $x' = g_1(x,y)$, $y' = g_2(x,y)$ of the non-linear coordinate transformation $\mathbf{g}(x,y) = (g_1(x,y),g_2(x,y))$ which bends the original, uncurved periodic grid or screen $p(x',y')$ into the curved structure $r(x,y)$.

We usually assume that the bending transformation is smooth (a diffeomorphism), so that it has no abrupt jumps or other troublesome singularities.

local period (of a curvilinear grating, curved grid, etc.) —

The local period of a curvilinear grating (or curved grid) at a point (x,y) is the period of the straight, periodic grating (or grid) which is defined by the tangents to the curvilinear grating (or curved grid) at a small neighbourhood around the point (x,y). In a periodic structure the local period is constant throughout the x,y plane, and it equals the period of the structure.

zone grating (or *zone plate*) —

According to the classical definition, a zone grating is a circularly symmetric grating which is obtained by drawing a family of concentric circles $x^2+y^2 = nr_1^2$, $n = 1,2,...$ (where the radius of the n-th circle is proportional to $\sqrt{n}$: $r_n = r_1\sqrt{n}$, r_1 being the radius of the central circle), and blackening alternate rings (zones) between these circles. This construction implies that the surface areas of the central circle and of each of the black or white rings which surround it are all equal. According to this classical definition the periodic-profile of a zone grating is a binary (black-and-white) square wave with opening ratio $\tau/T = 1/2$. Such classical zone gratings are called *Fresnel zone plates*, and they are often used in optics as focusing devices which are based on diffraction [Baez61, Myers51] (just like focusing lenses, that are based on refraction, or focusing mirrors, that are based on reflectance). However, we prefer to use the term zone grating in a wider sense, where the periodic-profile may have an opening ratio other than 1/2, or even where the periodic-profile is not at all a binary square wave. For example, a zone grating may have a cosinusoidal periodic-profile; such a zone grating is sometimes called a *Gabor zone plate* [Chau69]. In fact, we extend the definition of a zone grating even further, allowing also elliptic, hyperbolic and linear zone gratings [Welberry76]; see Example 10.7 in Sec. 10.3.

D.3 Terms in the spectral domain

spectrum (or *frequency spectrum*; not to be confused with *colour spectrum*) —

The frequency decomposition of a given function, which specifies the contribution of each frequency to the function in question. The frequency spectrum is obtained by taking the Fourier transform of the given function.

visibility circle —

A circle around the spectrum origin whose radius represents the cutoff frequency, i.e., the threshold frequency beyond which fine detail is no longer detected by the eye. Obviously, its radius depends on several factors such as the viewing distance, the light conditions, etc. It should be noted that the visibility circle is just a first-order approximation. In fact, the sensitivity of the human eye is a continuous 2D

bell-shaped function [Daly92 p. 6], with a steep "crater" in its center (representing frequencies which are too small to be perceived), and "notches" in the diagonal directions (owing to the drop in the eye sensibility in the diagonal directions [Ulichney88 pp.79–84]).

frequency vector —
A vector in the *u*,*v* plane of the spectrum which represents the geometric location of an impulse in the spectrum (see Sec. 2.2 and Fig. 2.1).

DC impulse —
The impulse that is located on the spectrum origin. This impulse represents the frequency of zero, which corresponds to the constant component in the Fourier series decomposition of the periodic image; the amplitude of the DC impulse corresponds to the intensity of this constant component. This impulse is traditionally called the *DC impulse* because it represents in electrical transmission theory the direct current component, i.e., the constant term in the frequency decomposition of an electric wave; we are following here this naming convention.

comb (or *impulse-comb*, *Dirac-comb*, *impulse-train*) **—**
An infinite train of equally spaced impulses located on a straight line in the spectrum. Any 1-fold periodic function is represented in the spectrum by a comb centered on the spectrum origin. The step and the direction of this comb represent the frequency and the orientation of the periodic function; its impulse amplitudes, which are given by the Fourier series development of the periodic function, determine its intensity profile.

nailbed (or *impulse-nailbed*) **—**
An infinite 2D train of equally spaced impulses located in the spectrum on a dot-lattice (either square-angled or skewed). Any 2-fold periodic function is represented in the spectrum by an impulse nailbed centered on the spectrum origin. The steps and the two main directions of this nailbed represent the frequency and the orientation of the two main directions of the function's 2D periodicity; the impulse amplitudes, which are given by the 2D Fourier series development of the periodic function, determine its intensity profile.

compound impulse —
An impulse in the spectrum which is composed of several distinct impulses that happen to fall on the same location and hence "fuse down" into a single impulse. The amplitude of a compound impulse is the sum of the amplitudes (real or complex) of the individual impulses from which it is composed. See Sec. 6.4 in Chapter 6.

compound comb —
A comb of compound impulses.

compound nailbed —
A nailbed of compound impulses.

support (of a *comb*, a *nailbed*, a *spectrum*, etc.) —
The set of the geometric locations on the u,v plane of all the impulses of the specified comb, nailbed, or spectrum.

lattice (or *dot-lattice*; not to be confused with *screen* or *dot-screen*) —
An algebraic structure, subset of $\mathbb{R}^n$; see definition 5.1 in Sec. 5.2.1. Note that our definition is narrower than the classical definition of a lattice in algebra textbooks such as [Jacobson85 pp. 457–459]; it rather corresponds to a lattice (or a lattice of points) in geometry of numbers [Cassels71 p. 9], or a lattice in crystallography. However, any lattice by our definition is indeed a lattice also in the larger sense.

frequency lattice (of a periodic function) —
The lattice formed by the set of all the integer linear combinations of the fundamental frequency(ies) of a periodic function, in the spectral domain. It is the reciprocal lattice of the period-lattice in the image domain (see Sec. A.4 in Appendix A).

reciprocal lattice (or *dual lattice*) —
See Appendix A, Sec. A.4.

module (or $\mathbb{Z}$-*module*; has nothing to do with the module of a complex number) —
An algebraic structure, subset of $\mathbb{R}^n$; see definition 5.2 in Sec. 5.2.1. Note that our definition is narrower than the classical definition of a module in algebra textbooks such as [Lang78 pp. 127–128]; however, any module by our definition is indeed a module also in the larger sense.

cluster (or *impulse-cluster*; has nothing to do with clusters in halftoning) —
A subset (either a lattice or a module) of impulse-locations in the spectrum support which collapse down, at a given singular state, into a single point in the spectrum. Algebraically, each cluster contains all points (impulses) which belong to one equivalence class in the singular state, and to each equivalence class there corresponds a cluster in the spectrum (see Chapter 5). As the superposed layers move away from the singular state, each cluster spreads-out in the spectrum. The impulse cluster which is generated around the spectrum origin (which belongs to the equivalence class of $\mathbf{0}$) has a particular significance, since it represents the spectrum of the isolated (extracted) moiré in question.

line-impulse —
A generalized function which is impulsive along a 1D line through the plane, and null everywhere else. A line-impulse can be graphically illustrated as a "blade" whose behaviour is continuous along its 1D line support but impulsive in the perpendicular direction. As an example, the spectrum of a parabolic cosinusoidal grating consists of two parallel line-impulses (see Example 10.5 in Sec. 10.3).

Note that the amplitude of a line-impulse does not necessarily die out away from its center, and it may even rapidly oscillate between two constant values.

compound line-impulse —
A line-impulse in the spectrum which is composed of several distinct line-impulses that happen to fall on the same 1D line and hence "fuse down" into a single line-impulse. Note that the center (skeleton location) of each of the individual line-impulses may be found in a different point along their common support. The amplitude of a compound line-impulse is the sum of the amplitudes (real or complex) of the individual line-impulses from which it is composed.

curvilinear impulse —
A generalized function which is impulsive along a 1D curvilinear path through the plane, and null everywhere else. A curvilinear impulse can be graphically illustrated as a curvilinear "blade" whose behaviour is continuous along its 1D curvilinear support but impulsive in the perpendicular direction.

hump —
A 2D continuous surface, often bell-shaped, elliptic or hyperbolic, which is defined around a given center on the plane. For example, the convolution of two non-parallel line-impulses gives a hump (see Sec. 10.7.3 and Fig. 10.13). Note that the amplitude of a hump does not necessarily die out away from its center, and in some cases it may even rapidly oscillate between two constant values.

wake —
A 2D continuous surface which trails off from an impulsive element (line-impulse, curvilinear impulse, etc.), gradually dying out as it goes away from the impulsive element in question. The amplitude of the wake may be considered as negligible with respect to that of its generating impulsive element. As an example, the spectrum of the cosinusoidal circular grating $\cos(2\pi f\sqrt{x^2+y^2})$ is a circular impulse ring of radius f, with a particular dipole-like impulsive behaviour on the perimeter of the circle and a negative, continuous wake which gradually trails off toward the center (see Example 10.6 in Sec. 10.3 and Fig. 10.4(d)).

local frequency (of a curvilinear grating, curved grid, etc.) **—**
The local frequency of a curvilinear grating (or curved grid) at a point (x,y) is the frequency of the straight, periodic grating (or grid) which is defined by the tangents to the curvilinear grating (or curved grid) at a small neighbourhood around the point (x,y). In a periodic structure the local frequency is constant throughout the x,y plane, and it equals the frequency of the structure. See also Remark 10.4 in Sec. 10.2, and Sec. 11.4.

internal discrepancy —
The distance between the centers (skeleton locations) of two consecutive line-impulses in a cluster of line-impulses which has collapsed on a common line to

form a compound line-impulse; see Sec. C.8 in Appendix C. If all the individual line-impulses are collapsed with a common center, the internal discrepancy of the compound line-impulse is zero. One may also define by analogy the internal discrepancy of a cluster of humps as the distance between the centers (skeleton locations) of two consecutive humps of the cluster.

skeleton —

According to the gradual transition approach (see Sec. 10.4.1) we may often think of a line-impulse cluster, a hump-cluster etc. as originating from an impulse-cluster whose impulses have "leaked out" or "melted down" to form the line-impulses or humps in question. This impulse-cluster is called the *skeleton* of the line-impulse cluster (or of the hump cluster). See, for example, Sec. 10.7.3.

skeleton location (or *center* of a line-impulse, a hump, etc.) —

The location in the spectrum of the skeleton-impulse which "leaked out" to give the line-impulse or hump in question.

impulsive spectrum —

A spectrum which only consists of impulses, i.e., whose support consists of a finite or at most denumerably infinite number of points. All periodic and almost-periodic functions have impulsive spectra.

line-spectrum —

A spectrum which consists of line impulses (see, for example, Fig. 10.11).

hybrid spectrum —

A spectrum which contains any combination of impulses, line-impulses and continuous humps (as opposed to a purely impulsive spectrum, a purely line-spectrum or a purely continuous spectrum). See, for instance, Example 10.14 of Sec. 10.7.4 and Fig. 10.13.

singular support (of a *spectrum*, etc.; distinguish from a *singular locus of a moiré*) —

The subset of the spectrum support over which the spectrum is impulsive. The singular support of a given spectrum includes the support of all the impulsive elements which are included in the spectrum (impulses, line-impulses, etc.), but not the support of continuous elements such as humps or wakes.

D.4 Terms related to moiré

moiré effect (or *moiré phenomenon*) —

A visible phenomenon which occurs when repetitive structures (such as line-gratings, dot-screens, etc.) are superposed. It consists of a new pattern which is clearly observed in the superposition, although it does not appear in any of the original structures.

(k_1,...,k_m)-moiré —

The 1-fold periodic structure in the image domain which corresponds to the (k_1,...,k_m)-comb in the spectrum convolution (the spectrum of the superposition); see Sec. 2.8. In other words, this is the moiré which is generated due to the interaction between the k_i harmonic frequencies of the respective layers in the superposition. This moiré may be visible if at least its fundamental impulse, the (k_1,...,k_m)-impulse, is located inside the visibility circle.

singular moiré (or *singular state, singular superposition*) —

A configuration of the superposed layers in which the period of the moiré in question becomes infinitely large (i.e., its frequency becomes 0), and hence it can no longer be seen in the superposition. Singular moirés are unstable moiré-free states, since any slight deviation in the angle or frequency of any of the superposed layers may cause the moiré in question to "come back from infinity" and to reappear with a large, visible period. Formally, we say that a (k_1,...,k_m)-moiré reaches a singular state whenever the geometric location of its fundamental impulse, the (k_1,...,k_m)-impulse in the spectrum convolution, falls on the spectrum origin (0,0) (i.e., whenever the frequency vectors $\mathbf{f}_1$,...,$\mathbf{f}_m$ which define the superposed layers are linearly dependent over $\mathbb{Z}$: $\sum k_i\mathbf{f}_i = \mathbf{0}$). Note that every ($k_1$,...,$k_m$)-moiré can be made singular by sliding the vector-sum $\sum k_i\mathbf{f}_i$ to the spectrum origin, namely: by appropriately modifying the vectors $\mathbf{f}_1$,...,$\mathbf{f}_m$ (or the frequencies and angles of the superposed layers).

stable moiré-free state —

A moiré-free configuration of the superposed layers in which no moiré becomes visible even when small deviations occur in the angle or frequency of any of the layers (see Fig. 2.8).

unstable moiré-free state —

A moiré-free configuration of the superposed layers in which any slight deviation in the angle or frequency of any of the layers causes the reappearance of a moiré with a large, visible period (see Fig. 2.8). Any singular state is an unstable moiré-free state.

combined-moiré (or *composite-moiré*) —

A 2D moiré which is combined of two or more (k_1,...,k_m)-moirés. See Sec. 2.8.

moiré profile (or *moiré intensity profile*; *moiré intensity surface*) —

A function (surface) which defines the intensity level of the moiré at any point of the image (see Secs. 2.10 and 4.1).

macrostructure, microstructure (within a superposition) —

The superposition of two or more layers (gratings, screens, etc.) may generate new structures which appear in the superposition but not in the original layers. These new structures can be classified into two categories: the *macrostructures*, i.e., the

moiré effects proper, which are much coarser than the detail of the original layers; and the *microstructures*, i.e., the tiny geometric forms which are almost as small as the periods of the original layers, and are normally visible only from a close distance or through a magnifying glass (see Chapter 8).

rosettes —
The various tiny flower-like shapes which are often present in the microstructure of dot-screen or grid superpositions.

singular locus of a moiré (not to be confused with *singular support* in the spectrum) —
The locus in the image domain (a point, a straight line, a curve etc.) along which a moiré between curved, repetitive layers is singular. Along this singular locus the moiré locally disappears to the eye, its local period there being infinitely large. But at any other point of the x,y plane outside this singular locus the moiré in question has a finite local period, which gradually decreases as one moves away from the singular locus. For example, the singular locus of the moiré shown in Fig. 10.18(c) is a straight line which coincides with the x axis. Note that the singular locus of any moiré between periodic layers consists of the entire x,y plane.

moiré eyelet (or *eye-shaped moiré*) —
A moiré effect whose singular locus consists of a single point. The moiré eyelet is centered on its singular locus point, where its local period is infinitely large, and around this point its frequency gradually increases in all directions until it exceeds the resolving power of the eye and disappears. See, for example, the moiré eyelets in Fig. 10.14(a).

additive / subtractive moiré (not to be confused with *additive superposition*) —
Classical terms often used in literature to designate moirés which are generated by frequency sums or frequency differences, respectively, in the spectrum. For example, the (1,-1)-moiré is subtractive, while the (1,1)-moiré is additive. Note, however, that these terms cannot be generalized to more complex cases such as the (1,1,-1)-moiré between three gratings. These terms are mostly useful in the superposition of two curvilinear gratings, where both the additive and the subtractive moiré are often observed simultaneously, each of them having a different shape and location (see, for example, Fig. 10.31). In this case the most convenient way to define them is based on their indicial equations (see Sec. 11.2): the additive moiré is the system of moiré fringes which corresponds to the indicial equation $m+n=p$, while the subtractive moiré is the system of moiré fringes which is selected by the indicial equation $m-n=p$.

D.5 Terms related to light and colour

colour spectrum (not to be confused with *frequency spectrum*) —
The wavelength decomposition of a given light, which specifies the contribution of

each visible light wavelength λ (approximately between $\lambda = 380$ nm for violet and $\lambda = 750$ nm for red) to the given light. The colour spectrum determines the visible colour of the light in question.

monochrome (or *black-and-white*; not to be confused with *monochromatic*) —
Achromatic light, image, etc. involving only black, white and all the intermediate gray levels. The colour spectrum of an ideal monochrome light is flat, i.e., it has a constant value (between 0 and 1) for all wavelengths λ of the visible light.

monochromatic (not to be confused with *monochrome*) —
Chromatic light, image, etc. involving only a single pure wavelength λ of the visible light. The colour spectrum of an ideal monochromatic light consists of a single impulse of intensity 1 at the wavelength λ.

reflectance (or *reflectance function*) —
A function $r(x,y)$ which assigns to any point (x,y) of a monochrome image viewed by reflection a value between 0 and 1 representing its light reflection: 0 for black (or no reflected light), 1 for white (or full light reflection), and intermediate values for in-between shades. More formally, reflectance is defined at any point (x,y) as the ratio of reflected to incident radiant power [Wyszecki82 p. 463].

transmittance (or *transmittance function*) —
A function $r(x,y)$ which assigns to any point (x,y) of a monochrome image viewed by transmission (such as a transparency, a film, etc.) a value between 0 and 1 representing its light transmission: 0 for black (or no transmitted light), 1 for white (or full light transmission), and intermediate values for in-between shades. More formally, transmittance is defined at any point (x,y) as the ratio of transmitted to incident radiant power [Wyszecki82 p. 463].

chromatic reflectance (or *chromatic reflectance function*) —
A function $r(x,y;\lambda)$ which assigns to any point (x,y) of a colour image viewed by reflection its full colour spectrum. In other words, it gives for every wavelength λ of the visible light (approximately between $\lambda = 380$ nm and $\lambda = 750$ nm) a value between 0 and 1, which represents the reflectance of light of wavelength λ at the point (x,y) of the image. This is a straightforward generalization of the reflectance function $r(x,y)$ in the monochrome case.

chromatic transmittance (or *chromatic transmittance function*) —
A function $r(x,y;\lambda)$ which assigns to any point (x,y) of a colour image viewed by transmission its full colour spectrum. In other words, it gives for every wavelength λ of the visible light (approximately between $\lambda = 380$ nm and $\lambda = 750$ nm) a value between 0 and 1, which represents the transmittance of light of wavelength λ at the point (x,y) of the image. This is a straightforward generalization of the transmittance function $r(x,y)$ in the monochrome case.

D.6 Miscellaneous terms

binary (grating, etc.) —
A structure which contains only two transmittance (or reflectance) levels: 0 and 1.

discrete —
A subset D of $\mathbb{R}^n$ is called *discrete* if there exists a number $d > 0$ so that for any points $a,b \in D$ the distance between a and b is larger than d. Note, however, that the term *discrete* is also used (often carelessly) as the opposite of *continuous*. For example: *discrete spectra* (including everywhere dense spectra of almost-periodic functions!) vs. *continuous spectra* in [Champeney87 pp. 109–114]; or in our own case, the *discrete* mapping Ψ vs. the *continuous* mapping Φ, in Sec. 5.5.

dense (or *everywhere dense*; has nothing to do with the term *density* below) —
A subset S of $\mathbb{R}^n$ is called *dense* or *everywhere dense* in $\mathbb{R}^n$ if $[S] = \mathbb{R}^n$, where $[S]$ denotes the closure of S, i.e., the set containing S and all its limit points [EncMath88 Vol. 3 p. 434]. Note that a dense subset of $\mathbb{R}^n$ is not necessarily continuous; for example, the set $\mathbb{Q}$ of all rational numbers is everywhere dense in $\mathbb{R}$ but nowhere continuous.

density (has nothing to do with the term *dense* above) —
A representation of reflectance (or transmittance) values in logarithmic terms (see Fig. 2.9). This representation corresponds better to human visual perception due to the rather logarithmic nature of the eye's sensibility to light intensity [Pratt91 pp. 27–29]. Also called *reflection density* (or *transmission density*), or more generally: *optical density* [Rosenfeld82 p. 4].

scaling (of a *comb*, *nailbed*, etc.; not to be confused with *spreading-out* / *squeezing*) —
We distinguish between *amplitude* scalings, and *period* or *frequency* scalings (in which the expansion or contraction occurs along the x,y axes in the image, or the u,v axes in the spectrum).

squeezing / spreading-out (of an *impulse cluster*; not to be confused with *scaling*) —
We reserve these terms only to lateral (or spatial) contractions or expansions in the geometric locations of the cluster impulses when the superposed layers approach or move away from a singular state (see Sec. 5.6.3). A cluster can be squeezed towards its "center", or spread-out from the "center" outwards.

commensurable (or *commensurate*) —
Two vectors $\mathbf{v}_1,\mathbf{v}_2 \in \mathbb{R}^n$ (or real numbers in $\mathbb{R}$) are called *commensurable* if there exist non-zero integers m,n for which $\mathbf{v}_2 = \frac{m}{n}\mathbf{v}_1$ (so that both $\mathbf{v}_1$ and $\mathbf{v}_2$ can be measured as integer multiples of the same length unit, say $\frac{1}{n}\mathbf{v}_1$). Note that two numbers $x,y \in \mathbb{R}$ are commensurable *iff* their ratio x/y is rational. More generally, k vectors $\mathbf{v}_1,...,\mathbf{v}_k \in \mathbb{R}^n$ (or real numbers in $\mathbb{R}$) are called commensurable if they are linearly dependent over $\mathbb{Q}$ (which is identical to linear dependence over $\mathbb{Z}$).

incommensurable (or *incommensurate*) —

Two vectors $\mathbf{v}_1,\mathbf{v}_2 \in \mathbb{R}^n$ (or real numbers in $\mathbb{R}$) are called *incommensurable* if there do not exist non-zero integers m,n so that $\mathbf{v}_2 = \frac{m}{n}\mathbf{v}_1$. Note that two numbers $x,y \in \mathbb{R}$ are incommensurable *iff* their ratio x/y is irrational. More generally, k vectors $\mathbf{v}_1,...,\mathbf{v}_k \in \mathbb{R}^n$ (or real numbers in $\mathbb{R}$) are called incommensurable if they are linearly independent over $\mathbb{Q}$ (which is identical to linear independence over $\mathbb{Z}$).

vector (or *point* in a vector space) —

An element of the vector space in question ($\mathbb{R}^n$, the u,v plane, etc.). We always consider vectors as radius-vectors attached to the origin, and we do not distinguish between a *vector* and a *point* in the vector space (= the end point or the head of the vector).

phase (of a periodic function, a moiré, etc.) —

See Appendix C Sec. C.4 and Chapter 7 Secs. 7.1–7.5.

geometry of numbers (or *geometric number theory*) —

A branch of number theory, initiated by Minkowski in 1896, that studies number-theoretical problems by the use of geometric methods [EncMath88 Vol. 4 pp. 267–271]. One of the distinctive characteristics of geometry of numbers is that it combines concepts from both continuous and discrete mathematics: it studies properties which come from the realm of continuous mathematics (like volume, area, etc.) in relation to lattices, which are discrete objects [Kannan87 p. 2]. A typical task of this theory is the problem of finding the minimum of some real function $f(x_1,...,x_m)$ where $(x_1,...,x_m)$ are restricted to integral points (i.e., to points of the lattice $\mathbb{Z}^m$), normally with some supplementary condition, such as $(x_1,...,x_m) \neq \mathbf{0}$. The main concepts we use from the theory of geometry of numbers (see Chapter 5) are the restriction of the continuous linear mapping Φ (which is defined on $\mathbb{R}^m$) into its counterpart Ψ which is only defined on integral points, i.e., on $\mathbb{Z}^m$ (see Secs. 5.3–5.5); the investigation of their kernels and images and the interrelations between their ranks over $\mathbb{R}$ and over $\mathbb{Z}$; and the notions of lattice and module (which are already bordering on algebra).

diffeomorphism —

A diffeomorphism (in our case, on $\mathbb{R}^2$) is a one-to-one continuously differentiable mapping of $\mathbb{R}^2$ onto itself whose inverse mapping is also continuously differentiable.

chirp (or *chirp signal*) —

An oscillatory signal with an increasing (or decreasing) oscillation rate. For example, $\cos(ax^2)$ is a 1D chirp signal, and $\cos(ax^2 + by^2)$ is a 2D chirp signal.

equivalent grating number —

The number m of virtual gratings in a given superposition (where each 2D dot-screen or line-grid contributes two virtual gratings). See Sec. 2.12 in Chapter 2.

virtual gratings (or *grating equivalents*) —
See Sec. 2.12 and Sec. 7.5.2.

separable function (of two variables) —
A function $f(x,y)$ is said to be *separable* if it can be presented as (or separated into) a product of a function of x and a function of y: $f(x,y) = g(x)\cdot h(y)$ [Gaskill78 pp. 16–17; Cartwright90 p. 117]. Note, however, that we use this term in a slightly larger sense: A 2D function $f(x,y)$ is separable if it can be presented as a product of two independent 1D functions. Therefore, although $f(x,y) = g(x)\cdot h(y)$ may no longer be separable (in the narrower sense) after it has undergone a rotation or a skewing transformation, we will still consider it as separable (with respect to the rotated or skewed axes x' and y': $f(x',y') = g(x')\cdot h(y')$).

inseparable function (of two variables) —
A function that is not *separable*. For example, the function representing a square white dot is separable: $\text{rect}(x,y) = \text{rect}(x)\cdot\text{rect}(y)$, while the function representing a circular white dot is inseparable. See also Sec. 2.12.

spatially separable (not to be confused with a *separable function*) —
Two functions $F(u,v)$ and $G(u,v)$ in the spectrum are called spatially separable if their supports in the u,v plane are not overlapping. Spatially separable elements in the spectrum can be separated and extracted by means of filtering, i.e., by multiplying the spectrum with an appropriate 2D low-pass or band-pass filter (see, for example, Fig 10.22).

spatially inseparable (not to be confused with an *inseparable function*) —
Two functions $F(u,v)$ and $G(u,v)$ in the spectrum are called spatially inseparable if their supports in the u,v plane are at least partially overlapping. Spatially inseparable elements in the spectrum cannot be separated or extracted by multiplying the spectrum with 2D low-pass or band-pass filters (see, for example, Fig 10.27).

dots per inch (dpi) (or *dots per centimeter*; not to be confused with *lines per inch*) —
A term used to specify the resolution of a digital device such as a printer, a scanner, etc. For example, a device whose resolution is 300 dpi can only address points on an underlying pixel-grid whose period is 1/300 of an inch, and no in-between points or pixel-fractions can be addressed. Some devices have different resolutions in the horizontal and in the vertical directions.

lines per inch (lpi) (or *lines per centimeter*; not to be confused with *dots per inch*) —
A term used to specify the frequency of gratings, dot-screens, etc. This term specifies the number of periods per inch. For example: the finest grating that can be produced on a 300 dpi device, namely: a sequence of alternating one-pixel wide black and white lines, is a grating of 150 lpi (since one period consists here of two device pixels).

1D —

One dimensional (layer, periodicity, spectrum, impulse comb, etc.). Strictly, a one dimensional entity is an entity that has only one dimension (such as a straight line). However, by abuse of language we often use this term to designate a 2D entity that only varies along one dimension, while its other dimension is constant. For example, we say that an impulse comb such as in Fig. 2.5(d) or 2.5(e) is 1D, even though it subsists in the 2D u,v spectrum, because it varies only in one dimension, while in the orthogonal direction it remains constantly zero. Similarly, we often say that a 1-fold periodic structure such as a line grating (see, for example, Fig. 2.5(a) or 2.5(b)) is a 1D structure, even though it actually spreads in the 2D x,y space, because it only varies along one dimension but remains constant along the orthogonal direction (i.e. along the individual grating lines). Such a 1D periodic layer is, in fact, a constant extension of a really one-dimensional structure (such as a square wave) into the second dimension. Note that we sometimes use the terms "1D periodic" and "1-fold periodic" interchangeably as synonyms.

2D —

Two dimensional (layer, periodicity, spectrum, impulse nailbed, etc.). Strictly, any entity that has two dimensions, including a 1-fold periodic structure such as a line grating, is a 2D layer. However, by abuse of language we often use this term to designate a 2D entity that indeed varies along two dimensions. For example, we say that a structure such as a line grid or a dot screen is a 2D layer, because it varies along two dimensions. Note that we sometimes use the terms "2D periodic" and "2-fold periodic" interchangeably as synonyms.

domain / range transformation —

Any image $r(x,y)$ (or function r: $\mathbb{R}^2 \to \mathbb{R}$) can undergo two types of coordinate transformations: Either a transformation of its *domain*, $r(x,y) \mapsto r(\mathbf{g}(x,y))$, or a transformation of its *range*, $r(x,y) \mapsto t(r(x,y))$. As explained in Sec. D.6 of Appendix D in *Vol. II*, in the first case $\mathbf{g}(x,y)$ is applied as an inverse transformation, while in the second case $t(x)$ is used as a direct transformation. Similarly, any mapping $\mathbf{f}(x,y)$, $\mathbf{f}$: $\mathbb{R}^2 \to \mathbb{R}^2$, can undergo two types of coordinate transformations: Either a transformation of its *domain*, $\mathbf{f}(x,y) \mapsto \mathbf{f}(\mathbf{g}(x,y))$, or a transformation of its *range*, $\mathbf{f}(x,y) \mapsto \mathbf{g}(\mathbf{f}(x,y))$. Again, in the first case $\mathbf{g}(x,y)$ is applied as an inverse transformation, while in the second case it is used as a direct transformation.

direct / inverse transformation (or *direct / inverse mapping*) **—**

The mathematical terms used to designate a mapping (geometric transformation) $\mathbf{g}$ and its inverse $\mathbf{g}^{-1}$. We have, therefore, $\mathbf{g}(\mathbf{g}^{-1}(x,y)) = \mathbf{g}^{-1}(\mathbf{g}(x,y)) = (x,y)$. Note that the designations *direct* and *inverse* are interchangeable, and they depend on our point of view; thus, if we focus our attention to the mapping $\mathbf{h} = \mathbf{g}^{-1}$, we may consider $\mathbf{h}$ as the direct mapping and $\mathbf{h}^{-1} = (\mathbf{g}^{-1})^{-1} = \mathbf{g}$ as its inverse. For example, if $\mathbf{g}(x,y) = (2x,2y)$ then $\mathbf{g}^{-1}(x,y) = (x/2,y/2)$; and if $\mathbf{g}(x,y) = (x/2,y/2)$ then

$\mathbf{g}^{-1}(x,y) = (2x,2y)$. Note that the similar terms *direct / inverse transforms* are reserved to operators that act on functions, such as the Fourier transform.

List of notations and symbols

This list consists of the main symbols used in the text. They appear with a very brief description and a reference to the page in which they are first used or defined. Obvious symbols such as '+', '–', etc. have not been included.

Symbol	Short description	Page
x, y	The coordinates (axes) of the image plane	10
u, v	The coordinates (axes) of the spectral plane	10
x', y'	Rotated coordinates (axes) in the image plane	380
$p(x)$	A 1D periodic function	375
$p(x,y)$	A 2D periodic function	378
$p(\mathbf{x})$	The vector notation for $p(x,y)$	379
$P(u)$	The spectrum of $p(x)$	377
$P(u,v)$	The spectrum of $p(x,y)$	379
$P(\mathbf{u})$, $P(\mathbf{f})$	The vector notation for $P(u,v)$	380
$r(x)$	A 1D reflectance (or transmittance) function	21
$r(x,y)$	A 2D reflectance (or transmittance) function	10
$R(u)$	The spectrum of $r(x)$	22
$R(u,v)$	The spectrum of $r(x,y)$	11
$d(x,y)$	A single dot (of a dot-screen)	44
$D(u,v)$	The spectrum of $d(x,y)$	44
$*$	1D convolution (or T-convolution)	86
$**$	2D convolution (or T-convolution)	11, 95
$\theta, \theta_1, \ldots$	Angles of superposed layers	12, 18
α, β, γ	Angle differences between superposed layers	20, 68–69

φ_M	Angle of a moiré effect	18, 20
$\alpha \to 0°$	The angle difference α tends to 0°	156
f, f_1, ...	Frequencies of 1D periodic functions $p(x)$, $p_1(x)$, ...	12
f_M	Frequency of a moiré effect	20
T, T_1, ...	Periods of 1D periodic functions $p(x)$, $p_1(x)$, ...	18
T_M	Period of a moiré effect	20
$\mathbf{P}_1$, $\mathbf{P}_2$	Period-vectors	381
$\mathbf{T}_1$, $\mathbf{T}_2$	Step-vectors	393
P, F	Matrices	390
$\mathrm{P}^{-\mathrm{T}}$	The inverse transpose of matrix P	390
a, b, r, s, t	Real numbers (sometimes also used as integer numbers)	169
a, **b**, **r**, **t**, **w**	Vectors	171
i, j, k, l, m, n	Integer numbers	33
i	(In complex numbers): the imaginary unit, $\sqrt{-1}$	10
a_n, b_n, c_n, d_n	Fourier series coefficients; impulse amplitudes	21, 23, 376
$\mathbb{Z}$	The set of all integer numbers (positive, negative, and 0)	110
$\mathbb{Q}$	The set of all rational numbers	113
$\mathbb{R}$	The set of all real numbers	110
$\mathbb{C}$	The set of all complex numbers	412
$\mathbb{Z}^n$	The n-dimensional integer lattice	110
$\mathbb{R}^n$	The n-dimensional Euclidean space	110
L	A lattice	110
M	A module	110
$\mathrm{rank}_{\mathbb{R}} M$	The rank of M (also denoted: rank M)	111
$\mathrm{rank}_{\mathbb{Z}} M$	The integral rank of M	111
$\mathbf{f}_1,\ldots,\mathbf{f}_m$	Frequency vectors in the u,v plane of the spectrum	12, 28

$\mathbf{v}_1,...,\mathbf{v}_m$	Vectors in $\mathbb{R}^n$	110
$\mathrm{Sp}(\mathbf{v}_1,...,\mathbf{v}_m)$	The set of all linear combinations of $\mathbf{v}_1,...,\mathbf{v}_m$	112
$\mathrm{Md}(\mathbf{v}_1,...,\mathbf{v}_m)$	The set of all integral linear combinations of $\mathbf{v}_1,...,\mathbf{v}_m$	112
V, W	Vector spaces	115
$\dim V$	Dimension of vector space V	117
$\Phi : V \to W$	A linear transformation from vector space V to vector space W	115
$\mathrm{Im}\Phi$	The image of transformation Φ	115
$\mathrm{Ker}\Phi$	The kernel of transformation Φ	115
$\Psi_{\mathbf{f}_1,...,\mathbf{f}_m}$	The discrete linear transformation from $\mathbb{Z}^m$ to $\mathrm{Md}(\mathbf{f}_1,...,\mathbf{f}_m)$	114–115
$\Phi_{\mathbf{f}_1,...,\mathbf{f}_m}$	The continuous extension of $\Psi_{\mathbf{f}_1,...,\mathbf{f}_m}$	115
Re[ ]	The real-valued part of a complex entity	253, 412
Im[ ]	The imaginary-valued part of a complex entity	253, 412
Abs[ ]	The magnitude of a complex entity	412
Arg[ ]	The phase of a complex entity	412
U	A subspace of the vector space V	116
V/U	The quotient space of V modulo U	117
0	The number zero	37
$\mathbf{0}$	The zero vector	37
(u,v)	The Cartesian coordinates of the frequency vector $\mathbf{f}$	12
(f,θ)	The polar coordinates of the frequency vector $\mathbf{f}$	12
$a \cdot b$	Multiplication	20
$\mathbf{v} \cdot \mathbf{w}$	Scalar product of two vectors	181
$\mathbf{v} \times \mathbf{w}$	Vector product of two vectors	387–388
$\mathbf{v}^{-1}$	The reciprocal vector of $\mathbf{v}$	393
τ	Opening (white width) of a binary grating or a square wave	21
τ/T	Opening ratio of a binary grating or a square wave	23

τ_ε	ε-almost-period of an almost-periodic function	396
ε	An arbitrarily small, positive real number	396
$\lvert a\rvert$	The absolute value of the number a (real or complex)	21
$\lvert\mathbf{v}\rvert$	The length (=Euclidean norm) of the vector $\mathbf{v}$	388
$\mathbf{v}\|\|\mathbf{w}$	$\mathbf{v}$ is parallel to $\mathbf{w}$	384
$\mathbf{v}\perp\mathbf{w}$	$\mathbf{v}$ is perpendicular to $\mathbf{w}$	384
$\text{proj}(\mathbf{v})_{\mathbf{w}}$	The projection of $\mathbf{v}$ on $\mathbf{w}$	389
$\inf_{a<x<b} f(x)$	Infimum (greatest lower bound) of $f(x)$ within $(a,b)\subset\mathbb{R}$	399
$F(u,v)=\mathcal{F}[f(x,y)]$	$F(u,v)$ is the Fourier transform of $f(x,y)$	17
$f(x,y)=\mathcal{F}^{-1}[F(u,v)]$	$f(x,y)$ is the inverse Fourier transform of $F(u,v)$	91
$f(x,y)\leftrightarrow F(u,v)$	$f(x,y)$ and $F(u,v)$ are a Fourier pair	259
$\sim$	Is Fourier series of ...	429
$\approx$	Approximately equal	29
m	The number of superposed gratings (or grating equivalents)	26, 46
$(k_1,...,k_m)$	An index-vector: an m-tuple of integers (=a point in $\mathbb{Z}^m$)	30
$\mathbf{f}_{k_1,...,k_m}$	The frequency-vector of the $(k_1,...,k_m)$-impulse	32
$a_{k_1,...,k_m}$	The amplitude of the $(k_1,...,k_m)$-impulse	32
$(k_1,...,k_m)$-moiré	The 1D moiré corresponding to the $(k_1,...,k_m)$-comb	34
$\{k_1,...,k_m\}$-moiré	A family of moirés	35
$m_{k_1,...,k_m}(\mathbf{x})$	The isolated (extracted) $(k_1,...,k_m)$-moiré	91, 162
$M_{k_1,...,k_m}(\mathbf{u})$	The spectrum of the isolated $(k_1,...,k_m)$-moiré	91, 94
$\delta(u)$	The impulse symbol	23
$\delta(u,v)$	The 2D impulse symbol	379
$\text{rect}(x)$	A square pulse: 1 in the range $-0.5\le x\le 0.5$, and 0 elsewhere	21
$\text{rect}(x,y)$	A 2D square pulse: 1 in the range $-0.5\le x,y\le 0.5$, and 0 elsewhere	44
$\text{sinc}(x)$	$\frac{\sin(\pi x)}{\pi x}$ for $x\neq 0$, and 1 for $x=0$	22

a mod b	The remainder of the integer division of a by b	169
ϕ	The period-shift of $p(x)$	169
$\boldsymbol{\phi}$	The period-shift of $p(\mathbf{x})$	172
φ	Phase increment (in the sense of complex numbers)	413–417
ξ	Period-coordinate	211
$\Xi(x,y)$	Period-coordinate function	215
$\mathbf{g}(x,y)$	A 2D coordinate transformation	256
$\mathbf{f}(x,y)$	Local frequency vector	364
$\forall$	For all ...	21
■	End of example, proof, etc.	22

List of abbreviations

Symbol	Short description	Page
1D	1-dimensional	123
2D	2-dimensional	10, 123
1D-L	A 1D lattice	122–123
1D-M	A 1D module	122–123
2D-L	A 2D lattice	122–123
2D-M	A 2D module	122–123
CMYK	The four process ink colours: Cyan, Magenta, Yellow, blacK	60
RGB	The three colour display primaries: Red, Green, Blue	235, 243
DC	The impulse at the spectrum origin (i.e., at frequency zero)	12

DFT	Discrete Fourier transform	99
FFT	Fast Fourier transform	84, 100
dpi	Dots per inch (printer resolution)	448
lpi	Lines per inch (frequency of a grating or a screen)	448
iff	If and only if	111

References

[Adkins92] W. A. Adkins and S. H. Weintraub, *Algebra, an Approach via Module Theory*. Springer-Verlag, NY, 1992.

[Adobe90] Adobe Systems Inc., *PostScript language Reference Manual*. Addison-Wesely, Reading, Massachusetts, 1990 (second edition).

[Ahumada83] A. J. Ahumada, Jr., D. C. Nagel and A. B. Watson, "Reduction of display artifacts by random sampling," in *Applications of Digital Image Processing VI*, Proceedings of the SPIE, Vol. 432, 1983, pp. 216–221.

[Alasia98] A. Alasia, "Digital anti-counterfeiting software methos and apparatus," US Patent No. 5,708,717, 1998.

[Allebach78] J. P. Allebach, "Random nucleated halftone screen," *Photographic Science and Engineering*, Vol. 22, No. 2, 1978, pp. 89–91.

[Allebach79] J. P. Allebach, "Aliasing and quantization in the efficient display of images," *Jour. of the Optical Society of America*, Vol. 69, June 1979, pp. 869–877.

[Amidror91] I. Amidror, "The moiré phenomenon in colour separation," in *Raster Imaging and Digital Typography II*, Proceedings of the 2nd International Conference on Raster Imaging and Digital Typography, R. A. Morris and J. André (Eds.), Cambridge University Press, 1991, pp. 98–119.

[Amidror94] I. Amidror, R. D. Hersch and V. Ostromoukhov, "Spectral analysis and minimization of moiré patterns in colour separation," *Journal of Electronic Imaging*, Vol. 3, No. 3, July 1994, pp. 295–317.

[Amidror94a] I. Amidror, "A generalized Fourier-based method for the analysis of 2D moiré envelope forms in screen superpositions," *Journal of Modern Optics*, Vol. 41, No. 9, September 1994, pp. 1837–1862.

[Amidror95] I. Amidror, *Analysis of Moiré Patterns in Multi-Layer Superpositions*. Ph.D. Thesis No. 1341, EPFL, Lausanne, 1995.

[Amidror96] I. Amidror, "Fourier-based analysis of phase shifts in the superposition of periodic layers and their moiré effects," *Jour. of the Optical Society of America A*, Vol. 13, No. 5, 1996, pp. 974–987.

[Amidror97] I. Amidror, "Fourier spectrum of radially periodic images," *Jour. of the Optical Society of America A*, Vol. 14, No. 4, 1997, pp. 816–826.

[Amidror97a] I. Amidror and R. D. Hersch, "Quantitative analysis of multichromatic moiré effects in the superposition of coloured periodic layers," *Jour. of Modern Optics*, Vol. 44, No. 5, 1997, pp. 883–899.

[Amidror98] I. Amidror and R. D. Hersch, "Analysis of the superposition of periodic layers and their moiré effects through the algebraic structure of their Fourier spectrum," *Jour. of Mathematical Imaging and Vision*, Vol. 8, 1998, pp. 99–130.

[Amidror98a] I. Amidror, "Fourier spectrum of curvilinear gratings of the second order," *Jour. of the Optical Society of America A*, Vol. 15, No. 4, 1998, pp. 900–913.

[Amidror98b] I. Amidror and R. D. Hersch, "Fourier-based analysis and synthesis of moirés in the superposition of geometrically transformed periodic structures," *Jour. of the Optical Society of America A*, Vol. 15, No. 5, 1998, pp. 1100–1113.

[Amidror98c] I. Amidror, "The Fourier-spectrum of circular sine and cosine gratings with arbitrary radial phases," *Optics Communications*, Vol. 149, 1998, pp. 127–134.

[Amidror99] I. Amidror and R. D. Hersch, "Methods and apparatus for authentication of documents by using the intensity profile of moire patterns," US Patent No. 5,995,638, 1999.

[Amidror01] I. Amidror and R. D. Hersch, "Method and apparatus for authentication of documents by using the intensity profile of moire patterns," US Patent No. 6,249,588, 2001.

[Amidror02] I. Amidror, "A new print-based security strategy for the protection of valuable documents and products using moiré intensity profiles," in *Optical Security and Counterfeit Deterrence Techniques IV*, R. L. Van Renesse (Ed.), Proceedings of SPIE Vol. 4677, SPIE, Bellingham, 2002, pp. 89–100.

[Amidror04] I. Amidror and R. D. Hersch, "Authentication of documents and valuable articles by using moire intensity profiles," US Patent No. 6,819,775, 2004.

[Artin91] M. Artin, *Algebra*. Prentice Hall, NJ, 1991.

[Asundi93] A. K. Asundi, "Moiré methods using computer-generated gratings," *Optical Engineering*, Vol. 32, No. 1, January 1993, pp. 107–116.

[Badcock85] D. R. Badcock and A. M. Derrington, "Detecting the displacement of periodic patterns," *Vision Research*, Vol. 25, No. 9, 1985, pp. 1253–1258.

[Badcock89] D. R. Badcock and A. M. Derrington, "Detecting the displacement of spacial beats: no role for distortion products," *Vision Research*, Vol. 29, No. 6, 1989, pp. 731–739.

[Baez61] A. V. Baez, "Fresnel zone plate for optical image formation using extreme ultraviolet and soft X radiation," *Jour. of the Optical Society of America*, Vol. 51, No. 4, April 1961, pp. 405–412.

[Bann90] D. Bann and J. Gargan, *How to Check and Correct Colour Proofs*. North Light Books, USA, 1990.

[Bass71] J. Bass, *Cours de Mathématiques (Tome 3)*. Masson, Paris, 1971 (in French).

[Baudoin38] P. Baudoin, *Les Ovales de Descartes et le Limaçon de Pascal*. Librairie Vuibert, Paris, 1938 (In French).

[Besicovitch32] A. S. Besicovitch, *Almost Periodic Functions*. Cambridge University Press, Cambridge, 1932.

[Birkhoff77] G. Birkhoff and S. Mac Lane, *A Survey of Modern Algebra*. Macmillan Publishing, NY, 1977 (fourth edition).

[Black53] H. S. Black, *Modulation Theory.* D. van Nostrand, NY, 1953.

[Blatner98] D. Blatner, G. Fleishman and S. Roth, *Real World Scanning and Halftones.* Peachpit Press, Berkeley, 1998 (second edition).

[Boff86] K. R. Boff, L. Kaufman and J. P. Thomas, *Handbook of Perception and Human Performance (Vol. 2)*, John Wiley & sons, NY, 1986.

[Bohr23] H. Bohr, "Sur les fonctions presque périodiques," *Comptes Rendus Hebd. de L'academie des Sciences*, Paris, Vol. 177, 1923, pp. 737–739; "Sur l'approximation des fonctions presque périodiques par des sommes trigonométriques," *ibid.*, pp. 1090–1092 (in French).

[Bohr51] H. Bohr, *Almost Periodic Functions*. Chelsea Publishing Company, NY, 1951.

[Bracewell86] R. N. Bracewell, *The Fourier Transform and its Applications.* McGraw-Hill Publishing Company, Reading, NY, 1986 (second edition).

[Bracewell95] R. N. Bracewell, *Two Dimensional Imaging.* Prentice Hall, NJ, 1995.

[Brigham88] E. O. Brigham, *The Fast Fourier Transform and Its Applications.* Prentice-Hall, NJ, 1988.

[Bronshtein97] I. N. Bronshtein and K. A. Semendyayev, *Handbook of Mathematics*. Springer, Berlin, 1997 (Reprint of the third edition; English translation).

[Bronstein90] I. N. Bronstein and K. A. Semendiaev, *Aide-Mémoire de Mathématiques.* Eyrolles, Paris, 1990 (9th edition; French translation).

[Bryngdahl74] O. Bryngdahl, "Moiré: formation and interpretation," *Jour. of the Optical Society of America,* Vol. 64, No. 10, 1974, pp. 1287–1294.

[Bryngdahl75] O. Bryngdahl, "Moiré and higher grating harmonics," *Jour. of the Optical Society of America,* Vol. 65, No. 6, 1975, pp. 685–694.

[Bryngdahl76] O. Bryngdahl, "Characteristics of superposed patterns in optics," *Jour. of the Optical Society of America,* Vol. 66, No. 2, 1976, pp. 87–94.

[Bryngdahl81] O. Bryngdahl, "Beat pattern selection — multi-color-grating moiré," *Optics Communications,* Vol. 39, No. 3, 1981, pp. 127–131.

[Burch77] J. M. Burch and D. C. Williams, "Varifocal moiré zone plates for straightness measurement," *Applied Optics*, Vol. 16, No. 9, September 1977, pp. 2445–2450.

[CanadianBank68] Canadian Bank Note Company Ltd., "Improvements in printed matter for the purpose of rendering counterfeiting more difficult," UK Patent No. 1,138,011, 1968.

[Cartwright90] M. Cartwright, *Fourier Methods for Mathematicians, Scientists and Engineers*. Ellis Horwood, UK, 1990.

[Cassels71] J. W. S. Cassels, *An Introduction to the Geometry of Numbers*. Springer-Verlag, NY, 1971 (second printing, corrected).

[Champeney73] D. C. Champeney, *Fourier Transforms and their Physical Applications.* Academic Press, London, 1973.

[Champeney87] D. C. Champeney, *Fourier Theorems.* Cambridge University Press, UK, 1987.

[Chau69] H. H. M. Chau, "Zone plates produced optically," *Applied Optics*, Vol. 8, No. 6, June 1969, pp. 1209–1211.

[Chosson06] S. Chosson, *Synthèse d'Images Moiré*. Ph.D. Thesis No. 3434, EPFL, Lausanne, 2006 (in French).

[Corduneanu68] C. Corduneanu, *Almost Periodic Functions.* Interscience Publishers, US, 1968.

[Cornsweet70] T. N. Cornsweet, *Visual Perception.* Harcourt Brace Jovanovich, Florida, 1970.

[Coudray91] M. A. Coudray, "Understanding halftone moiré," *Screen Printing,* Vol. 81, No. 11, 1991, pp. 142–147, 212.

[Courant88] R. Courant, *Differential and Integral Calculus (Vol. II).* Wiley-Interscience, USA, 1988.

[Daels94] K. Daels and P. Delabastita, "Color balance in conventional halftoning," Proceedings of the TAGA Conference, Baltimore, May 1994, pp. 1–18.

[Daly92] S. Daly, "The visible differences predictor: an algorithm for the assessment of image fidelity," *Human Vision, Visual Processing and Digital Display III*, SPIE proceedings, Vol. 1666, USA, 1992, pp. 2–15.

[Delabastita92] P. A. Delabastita, "Screening techniques, moiré in four color printing," Proceedings of the TAGA Conference, Vancouver, April 1992, pp. 44–65.

[Durelli70] A. J. Durelli and V. J. Parks, *Moiré Analysis of strain.* Prentice-Hall, Englewood Cliffs, New Jersey, 1970.

[Ebbeni70] J. Ebbeni, "Nouvaux aspects du phénomène de moiré," *Nouvelle Revue d'Optique Appliquée*, Vol. 1, 1970, pp. 333–342, 353–358 (in French).

[Egorov93] Yu. V. Egorov and M. A. Shubin (Eds.), *Partial Differential Equations IV: Microlocal Analysis and Hyperbolic Equations*. Springer Verlag, Berlin, 1993.

[EncMath88] *Encyclopaedia of Mathematics,* Vols. 1–10. Kluwer Academic Publishers, Dordrecht, 1988–1994.

[Erdélyi54] A. Erdélyi (Ed.), *Tables of Integral Transforms (Vol. 1)*. McGraw-Hill, NY, 1954.

[Eschbach88] R. Eschbach, "Generation of moiré by nonlinear transfer characteristics," *Jour. of the Optical Society of America A,* Vol. 5, No. 11, 1988, pp. 1828–1835.

[Fink92] P. Fink, *PostScript Screening: Adobe Accurate Screens.* Adobe Press, California, 1992.

[Firby84] P. A. Firby and D. J. Stone, "Interference patterns and two-dimensional potential theory," *IMA Journal of Applied Mathematics*, Vol. 33, 1984, pp. 291–301.

[Foley90] J. D. Foley, A. van Dam, S. K. Feiner and J. F. Hughes, *Computer Graphics: Principles and Practice.* Addison-Wesely, Reading, Massachusetts, 1990 (second edition).

[Foster72] A. M. Foster, "The moiré interference in digital halftone generation," Proceedings of the TAGA Conference, 1972, pp. 130–143.

[Gaskill78] J. D. Gaskill, *Linear Systems, Fourier Transforms, and Optics*. John Wiley & Sons, NY, 1978.

[Gåsvik95] K. J. Gåsvik, *Optical Metrology*. John Wiley & Sons, NY, 1995 (second edition).

[Gelfand64] I. M. Gelfand and G. E. Shilov, *Generalized Functions (Vol. 1).* Academic Press, CA, 1964.

[Giger86] H. Giger, "Moirés," *Computers & Mathematics with Applications*, Vol. 12B, No. 1/2, 1986, pp. 329–361.

[Glass73] L. Glass and R. Pérez, "Perception of random dot interference patterns," *Nature*, Vol. 246, December 1973, pp. 360–362.

[Gradshteyn94] I. S. Gradshteyn and I. M. Ryzhik, *Table of Integrals, Series, and Products.* Academic Press, Boston, 1994 (fifth edition).

[Gruber93] P. M. Gruber and J. M. Wills (Eds.), *Handbook of Convex Geometry (Vol. B)*. North-Holland, Amsterdam, 1993.

[Hahn96] S. L. Hahn, *Hilbert Transforms in Signal Processing*. Artech House, Norwood, MA, 1996.

[Harburn75] G. Harburn, T. R. Welberry and R. P. Williams, "A Fourier-series approach to moiré patterns with special reference to those produced by overlapping zone plates," *Optica Acta*, Vol. 22, No. 5, 1975, pp. 409–420.

[Harding83] K. G. Harding and J. S. Harris, "Projection moiré interferometer for vibration analysis," *Applied Optics*, Vol. 22, No. 6, March 1983, pp. 856–861; reprinted in [Indebetouw92, pp. 269–274].

[Hardy68] G. H. Hardy and W. W. Rogosinski, *Fourier Series*. Cambridge University Press, London, 1968 (reprint of third edition of 1956).

[Hardy73] G. H. Hardy, *Divergent Series*. University Press, Oxford, 1973 (corrected reprint of first edition of 1949).

[Harthong81] J. Harthong, "Le Moiré," *Advances in Applied Mathematics,* Vol. 2, 1981, pp. 24–75 (in French).

[Heaviside71] O. Heaviside, *Electromagnetic Theory (Vol. II)*. Chelsea, NY, 1971 (third edition).

[Hersch04] R. D. Hersch and S. Chosson, "Band moiré images," Proceedings of SIGGRAPH 2004, *ACM Transactions on Graphics*, Vol. 23, No. 3, 2004, pp. 239–248.

[Hersch04a] R. D. Hersch and S. Chosson, "Authentication of documents and articles by moire patterns," Published US Patent Application No. 2004/0076310, 2004.

[Hersch06] R. D. Hersch and S. Chosson, "Model-based synthesis of band moire images for authenticating security documents and valuable products," Published US Patent Application No. 2006/0003295, 2006.

[Hersch06a] R. D. Hersch and S. Chosson, "Model-based synthesis of band moire images for authentication purposes," Published US Patent Application No. 2006/0129489, 2006.

[Hoy92] D. E. P. Hoy, "Color digital imaging system for bicolor moiré analysis," *Experimental Techniques,* Vol. 16, No. 3, 1992, pp. 25–27.

[Huang74] T. S. Huang, "Digital transmission of halftone pictures," *Computer Graphics and Image Processing,* Vol. 3, 1974, pp. 195–202.

[Huck03] J. Huck, *Mastering Moirés: Investigating Some of the Fascinating Properties of Interference Patterns*. Private publication by J. Huck, 2003. `http://pages.sbcglobal.net/joehuck`

[Huck04] J. Huck, "Moiré patterns and the illusion of depth," Proceedings of the fifth Interdisciplinary Conference of the International Society of the Arts, Mathematics and Architecture (ISAMA 2004), Chicago, June 2004.

[Hunt87] R. W. G. Hunt, *The Reproduction of Colour in Photography, Printing and Television.* Fountain Press, England, 1987 (fourth edition).

[Hutley91] M. Hutley, R. Stevens and D. Daly, "Microlens arrays," *Physics World,* Vol. 4, July 1991, pp. 27–32.

[Indebetouw92] G. Indebetouw and R. Czarnek (Eds.), *Selected Papers on Optical Moiré and Applications.* SPIE Milestone Series, Vol. MS64, SPIE Optical Engineering Press, Washington, 1992.

[Jacobson85] N. Jacobson, *Basic Algebra (Vol. 1).* W. H. Freeman and Co., NY, 1985 (second edition).

[Jansson97] P. A. Jansson (Ed.), *Deconvolution of Images and Spectra.* Academic Press, US, 1997 (second edition).

[Jarić89] M. V. Jarić (Ed.), *Introduction to the Mathematics of Quasicrystals (Vol. 2).* Academic Press, US, 1989.

[Jones94] P. R. Jones, "Evolution of halftoning technology in the United States patent literature," *Journal of Electronic Imaging,* Vol. 3, No. 3, July 1994, pp. 257–275.

[Kafri89] O. Kafri and I. Glatt, *The Physics of Moiré Metrology*. John Wiley & Sons, NY, 1989.

[Kang97] H. R. Kang, *Color Technology for Electronic Imaging Devices*. SPIE Optical Engineering Press, Bellingham, Washington, 1997.

[Kannan87] R. Kannan, *Algorithmic Geometry of Numbers.* Report No. 87453-OR, Rheinische Friedrich-Wilhelm Universität, Bonn, 1987.

[Katz86] A. Katz and M. Duneau, "Quasiperiodic patterns and icosahedral symmetry," *Journal de Physique*, Vol. 47, 1986, pp. 181–196.

[Katzenelson68] Y. Katzenelson, *An Introduction to Harmonic Analysis.* John Wiley & Sons, US, 1968.

[Kendig80] K. M. Kendig, "Moiré phenomena in algebraic geometry: polynomial alterations in $\mathbb{R}^n$," *Pacific Journal of Mathematics*, Vol. 89, No. 2, 1980, pp. 327–349.

[Kermisch75] D. Kermisch and P. G. Roetling, "Fourier spectrum of halftone images," *Jour. of the Optical Society of America*, Vol. 65, June 1975, pp. 716–723.

[King72] M. C. King and D. H. Berry, "Photolithographic mask alignment using moiré techniques," *Applied Optics*, Vol. 11, No. 11, November 1972, pp. 2455–2459.

[Kipphan01] H. Kipphan, *Handbook of Print Media.* Springer, Berlin, 2001.

[Konno94] H. Konno, H. Ohara, K. Murata and Y. Nakano, "Measurement of focusing properties of axially asymmetric lenses using moiré technique," *Optical Review*, Vol. 1, No. 1, 1994, pp. 107–109.

[Korn68] G. A. Korn and T. M. Korn, *Mathematical Handbook for Scientific and Engineers.* McGraw-Hill, NY, 1968 (second edition).

[Kumar83] R. Kumar and M. M. Bindal, "Measurement of small angles and small angular rotations by moiré method," *Atti della Fondazione Giorgio Ronchi*, Vol. 38, No. 4, July-August 1983, pp. 399–410.

[Kunt86] M. Kunt, *Digital Signal Processing.* Artech House, MA, 1986.

[Lang78] S. Lang, *Undergraduate Algebra.* Springer-Verlag, NY, 1978.

[Latimer93] P. Latimer, "Talbot plane patterns: grating images or interference effects?" *Applied Optics*, Vol. 32, No. 7, March 1993, pp. 1078–1083.

[Lay03] D. C. Lay, *Linear Algebra and its Applications.* Addison-Wesley, Boston, 2003 (third edition).

[Legault73] R. Legault, "The aliasing problems in two-dimensional sampled imagery," in *Perception of Displayed Information*, L. M. Biberman (Ed.), Plenum Press, NY, 1973, pp. 279–312.

[Leifer73] I. Leifer, J. M. Walls and H. N. Southworth, "The moiré pattern produced by overlapping zone plates," *Optica Acta*, Vol. 20, No. 1, 1973, pp. 33–47.

[Levien93] R. Levien, "Well tempered screening technology," IS&T Third Technical Symposium on Prepress, Proofing and Printing, Chicago, 1993, pp. 98–101; also reprinted in *Recent Progress in Digital Halftoning,* R. Eschbach (Ed.), IS&T, 1994, pp. 83–86.

[Levitan82] B. M. Levitan and V. V. Zhikov, *Almost Periodic Functions and Differential Equations*. Cambridge University Press, Cambridge, 1982.

[Lipschutz91] S. Lipschutz, *Linear Algebra*. Schaum's Outline Series, McGraw-Hill, NY, 1991 (second edition).

[Lockwood61] E. H. Lockwood, *A Book of Curves*. Cambridge University Press, Cambridge, 1961.

[Lohmann67] A. W. Lohmann and D. P. Paris, "Variable Fresnel zone pattern," *Applied Optics*, Vol. 6, September 1967, pp. 1567–1570.

[Luo98] J. Luo, R. de Queiroz and Z. Fan, "Robust technique for image descreening based on the wavelet transform," *IEEE Transactions on Signal Processing*, Vol. 46, No. 4, April 1998, pp. 1179–1184.

[Marsh80] J. S. Marsh, "Contour plots using a moiré technique," *American Jour. of Physics*, Vol. 48, January 1980, pp. 39–40.

[Matteson04] R. Matteson, *Scanning for the SOHO — Small Office and Home Office*. Virtualbookworm Publishing, Texas, 2004.

[McDonald97] R. McDonald (Ed.), *Colour Physics for Industry*. Society of Dyers and Colourists, Bradford, England, 1997 (second edition).

[Meadows70] D. M. Meadows, W. O. Johnson and J. B. Allen, "Generation of surface contours by moiré patterns," *Applied Optics*, Vol. 9, No. 4, April 1970, pp. 942–947.

[Miceli92] C. M. Miceli and K. J. Parker, "Inverse Halftoning," *Journal of Electronic Imaging*, Vol. 1, No. 2, April 1992, pp. 143–151.

[Morimoto88] Y. Morimoto, Y. Seguchi and T. Higashi, "Application of moiré analysis of strain using Fourier transform," *Optical Engineering*, Vol. 27, No. 8, 1988, pp. 650–656.

[Morimoto90] Y. Morimoto, Y. Seguchi and M. Okada, "Screening and moiré suppression in printing and its analysis by Fourier transform," *Systems and Computers in Japan*, Vol. 21, No. 2, 1990, pp. 98–106.

[Morimura75] M. Morimura and K. Nakagawa, "Small-angle measuring device utilizing moiré fringe," *Japan Journal of Applied Physics*, Vol. 14, Supplement 14-1, 1975, pp. 461–464.

[Myers51] O. E. Myers, Jr., "Studies of transmission zone plates," *American Journal of Physics*, Vol. 19, No. 6, 1951, pp. 359–365.

[Nakano85] Y. Nakano and K. Murata, "Talbot interferometry for measuring the focal length of a lens," *Applied Optics*, Vol. 24, No. 19, October 1985, pp. 3162–3166.

[Nelson86] R. D. Nelson, "Quasicrystals," *Scientific American*, Vol. 255, August 1986, pp. 33–41.

[Nishijima64] Y. Nishijima and G. Oster, "Moiré patterns: their application to refractive index and refractive index gradient measurements," *Jour. of the Optical Society of America,* Vol. 54, No. 1, January 1964, pp. 1–5.

[Ohyama86] N. Ohyama, M. Yamaguchi, J. Tsujiuchi, T. Honda and S. Hiratsuka, "Suppression of moiré fringes due to sampling of halftone screened images," *Optics Communications*, Vol. 60, No. 6, December 1986, pp. 364–368.

[Oster63] G. Oster and Y. Nishijima, "Moiré patterns," *Scientific American,* Vol. 208, May 1963, pp. 54–63.

[Oster64] G. Oster, M. Wasserman and C. Zwerling, "Theoretical interpretation of moiré patterns," *Jour. of the Optical Society of America,* Vol. 54, No. 2, 1964, pp. 169–175.

[Oster65] G. Oster, "Optical art," *Applied Optics,* Vol. 4, No. 11, 1965, pp. 1359–1369.

[Oster69] G. Oster, *The Science of Moiré Patterns.* Edmund Scientific Co., Barrington, NJ, 1969 (second edition).

[Ostromoukhov93] V. Ostromoukhov, "Pseudo-random halftone screening for color and black&white printing," Proceedings of the 9-th International Congress on Advances in Non-impact Printing Technologies, Yokohama, October 1993, pp. 579–582; also reprinted in *Recent Progress in Digital Halftoning,* R. Eschbach (Ed.), IS&T, 1994, pp. 130–134.

[Ostromoukhov95] V. Ostromoukhov and R. D. Hersch, "Artistic screening," Proceedings SIGGRAPH 95, Computer Graphics Proceedings, Annual Conference Series, 1995, pp. 219–228.

[Papoulis68] A. Papoulis, *Systems and Transforms with Applications in Optics*. McGraw-Hill, NY, 1968.

[Patorski76] K. Patorski, S. Yokozeki and T. Suzuki, "Moiré profile prediction by using Fourier series formalism," *Japanese Jour. of Applied Physics,* Vol. 15, No. 3, 1976, pp. 443–456.

[Patorski93] K. Patorski, *Handbook of the Moiré Fringe Technique*. Elsevier, Amsterdam, 1993.

[Post67] D. Post, "Sharpening and multiplication of moiré fringes," *Experimental Mechanics,* Vol. 7, April 1967, pp. 154–159.

[Post94] D. Post, B. Han and P. Ifju, *High Sensitivity Moiré: Experimental Analysis for Mechanics and Materials*. Springer-Verlag, NY, 1994.

[Pratt91] W. K. Pratt, *Digital Image Processing*. John Wiley & Sons, NY, 1991 (second edition).

[Pssc65] Physical Science Study Committee, *Physics*. D.C. Heath and Company, Boston, 1965 (second edition).

[Rayleigh74] Lord Rayleigh, "On the manufacture and theory of diffraction-gratings," *London, Edinburgh, and Dublin Philosophical Magazine*, Series 4, Vol. 47, 1874, pp. 81–93 and 193–205.

[Renesse05] R. L. van Renesse, *Optical Document Security*. Artech House, Boston, 2005 (third edition).

[Réveillès91] J.-P. Réveillès, *Géométrie Discrète, Calcul en Nombres Entiers et Algorithmique*. Thèse d'Etat, Université Louis-Pasteur, Strasbourg, 1991 (in French).

[Righi87] A. Righi, "Sui fenomeni che si producono colla sovrapposizione di due reticoli e sopra alcune loro applicazioni," *Il Nuovo Cimento*, Series 3, Vol. 21, 1887, pp. 203–229 (in Italian).

[Rodriguez94] M. Rodriguez, "Promises and pitfalls of stochastic screening in the graphics arts industry," Proceedings of the 47th Annual Conference of the IS&T, May 1994; also reprinted in *Recent Progress in Digital Halftoning,* R. Eschbach (Ed.), IS&T, 1994, pp. 34–37.

[Rogers77] G. L. Rogers, "A geometrical approach to moiré pattern calculations," *Optica Acta*, Vol. 24, No. 1, 1977, pp. 1–13.

[Rosenfeld82] A. Rosenfeld and A. C. Kak, *Digital Picture Processing (Vol.1)*. Academic Press, Florida, USA, 1982 (second edition).

[Russ95] J. C. Russ, *The Image Processing Handbook*. CRC Press, Florida, 1995 (second edition).

[Saichev97] A. I. Saichev and W. A. Woyczyński, *Distributions in the Physical and Engineering Sciences (Vol. 1)*. Birkhäuser, Boston, 1997.

[Scantips97] `http://www.scantips.com/basics06.html`

[Schilling06] A. Schilling, W. R. Tompkin, R. Staub, R. D. Hersch, S. Chosson and I. Amidror, "Diffractive moiré features for optically variable devices," in *Optical Security and Counterfeit Deterrence Techniques VI*, R. L. Van Renesse (Ed.), Proceedings of SPIE Vol. 6075, SPIE, Bellingham, 2006, pp. 60750V-1– 60750V-12.

[Schoppmeyer85] J. Schoppmeyer, "Screen systems for multicolor printing," US Patent No. 4,537,470, 1985.

[Schreiber93] W. F. Schreiber, *Fundamentals of Electronic Imaging Systems*. Springer-Verlag, Berlin, 1993 (third edition).

[Shamir73] J. Shamir, "Moiré gauging by projected interference fringes," *Optics and Laser Technology*, Vol. 5, April 1973, pp. 78–86.

[Shechtman84] D. Shechtman, I. Blech, D. Gratias and J. W. Cahn, "Metallic phase with long-range orientational order and no translational symmetry," *Physical Review Letters*, Vol. 53, 1984, pp. 1951–1954.

[Shepherd79] A. T. Shepherd, "25 years of moiré fringe measurement," *Precision Engineering*, Vol. 1, No. 2, 1979, pp. 61–69.

[Shikin95] E. V. Shikin, *Handbook and Atlas of Curves*. CRC Press, Boca Raton, 1995.

[Shu89] J. S. Shu, R. Springer and C. L. Yeh, "Moiré factors and visibility in scanned and printed halftone images," *Optical Engineering*, Vol. 28, No. 7, July 1989, pp. 805–812.

[Siegel89] C. L. Siegel, *Lectures on the Geometry of Numbers*. Springer-Verlag, Berlin, 1989.

[Spiegel68] M. R. Spiegel, *Mathematical Handbook of Formulas and Tables*. Schaum's Outline Series, McGraw-Hill, NY, 1968.

[Stecher64] M. Stecher, "The moiré phenomenon," *American Journal of Physics*, Vol. 32, No. 4, 1964, pp. 247–257.

[Steinbach82] A. Steinbach and K. Y. Wong, "Moiré patterns in scanned halftone pictures," *Journal of the Optical Society of America*, Vol. 72, No. 9, 1982, pp. 1190–1198.

[Steinhardt90] P. J. Steinhardt and P. Taylor, "Methods and apparatus for eliminating moiré interference using quasiperiodic patterns," US Patent No. 4,894,726, 1990.

[Stevenson97] R. L. Stevenson, "Inverse halftoning via MAP estimation," *IEEE Transactions on Image Processing*, Vol. 6, No. 4, April 1997, pp. 574–583.

[Swift74] D. W. Swift, "A simple moiré fringe technique for magnification checking," *Journal of Physics E*, Vol. 7, No. 3, 1974, pp. 164–166.

[Takasaki70] H. Takasaki, "Moiré topography," *Applied Optics*, Vol. 9, No. 6, 1970, pp. 1467–1472.

[Takeda82] M. Takeda, H. Ina and S. Kobayahi, "Fourier-transform method of fringe-pattern analysis for computer-based topography and interferometry," *Journal of the Optical Society of America*, Vol. 72, No. 1, 1982, pp. 156–160.

[Taub86] H. Taub and D. L. Schilling, *Principles of Communication Systems*. McGraw-Hill, NY, 1986 (second edition).

[Theocaris69] P. S. Theocaris, *Moiré Fringes in Strain Analysis*. Pergamon Press, UK, 1969.

[Theocaris73] P. S. Theocaris and S. A. Paipetis, "Plane kinematics of moiré fringes," *Journal of Physics E*, Vol. 6, 1973, pp. 987–990.

[Theocaris75] P. S. Theocaris, S. A. Paipetis, and C. Liakopoulos, "Some aspects on the formation of spatial moiré fringes," *Optik*, Vol. 42, No. 3, 1975, pp. 269–286.

[Tollenaar64] D. Tollenaar, "Moiré in halftone printing interference phenomena." English translation published in 1964; reprinted in [Indebetouw92, pp. 618–633].

[Tolstov62] G. P. Tolstov, *Fourier Series.* Prentice-Hall, New Jersey, 1962.

[Ulichney88] R. Ulichney, *Digital Halftoning.* MIT Press, USA, 1988.

[Vygodski73] M. Vygodski, *Aide-Mémoire de Mathématiques Supérieures.* Mir, Moscow, 1973 (French translation).

[Walls75] J. M. Walls and H. N. Southworth, "The moiré pattern formed on superposing a zone plate with a grating or grid," *Optica Acta*, Vol. 22, No. 7, 1975, pp. 591–601.

[Wandell95] B. A. Wandell, *Foundations of Vision.* Sinauer, Massachusetts, 1995.

[Weber73] R. L. Weber, *A Random Walk in Science*. The Institute of Physics, London, 1973, pp. 199–200. Also published in *Applied Optics*, Vol. 7, No. 4, 1968, p. 625.

[Weisstein99] E. W. Weisstein, *CRC Concise Encyclopedia of Mathematics*. CRC, Boca Raton, 1999.

[Welberry76] T. R. Welberry and R. P. Williams, "On certain non-circular zone plates," *Optica Acta*, Vol. 23, No. 3, 1976, pp. 237–244.

[Widmer92] E. Widmer, K. Schläpfer, V. Humbel and S. Persiev, "The benefits of frequency modulation screening," Proceedings of the TAGA Conference, Vancouver, April 1992, pp. 28–43.

[Witschi86] W. Witschi, "Moirés," *Computers & Mathematics with Applications*, Vol. 12B, Nos. 1/2, 1986, pp. 363–378.

[Wurzburg61] F. L. Wurzburg, Jr., "Understanding moiré screen pattern," *Gravure*, Vol. 7, 1961, pp. 17–21.

[Wyszecki82] G. Wyszecki and W. S. Stiles, *Color Science: Concepts and Methods, Quantitative Data and Formulae*. John Wiley & Sons, NY, 1982 (second edition).

[Yokozeki70] S. Yokozeki and T. Suzuki, "Theoretical interpretation of moiré pattern for two grids of parallel lines," *Japan Jour. of Applied Physics*, Vol. 9, 1970, pp. 1011–1012.

[Yokozeki74] S. Yokozeki, "Theoretical interpretation of the moiré pattern," *Optics Communications*, Vol. 11, No. 4, August 1974, pp. 378–381.

[Yule67] J. A. C. Yule, *Principles of Color Reproduction*. John Wiley & Sons, NY, 1967, Chapter 13: "Moiré Patterns and Screen Angles", pp. 328–345.

[Zunino03] L. Zunino and M. Garavaglia, "Moiré by fractal structures," *Jour. of Modern Optics*, Vol. 50, No. 9, 2003, pp. 1477–1486.

[Zygmund68] A. Zygmund, *Trigonometric Series (Vol. 1).* Cambridge University Press, US, 1968 (corrected reprint of second edition of 1959).

Index

Page numbers followed by the letter "g" indicate entries in the glossary (Appendix D).